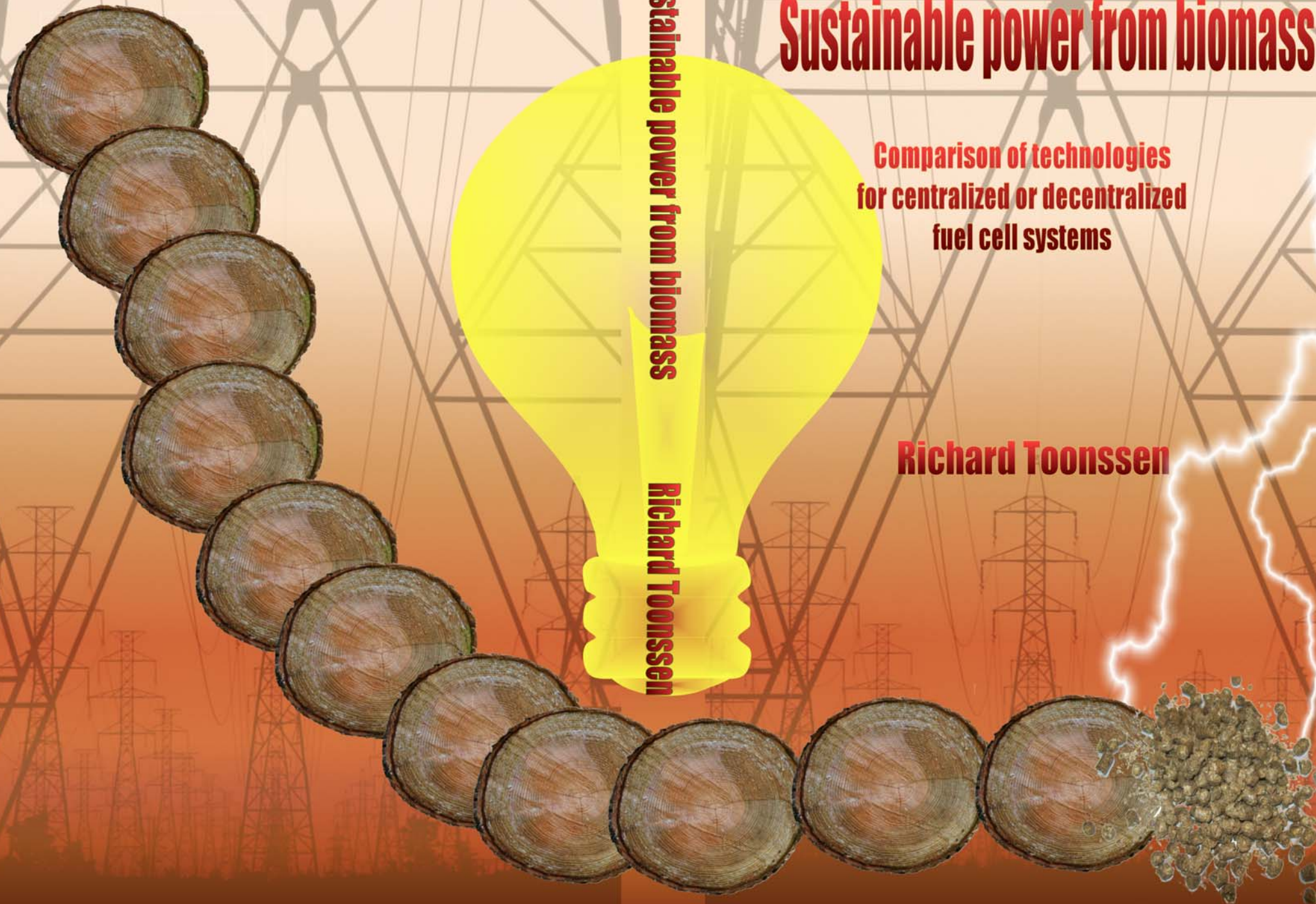# Sustainable power from biomass

Comparison of technologies for centralized or decentralized fuel cell systems

Richard Toonssen

Sustainable power from biomass — Richard Toonssen

Sustainable Power from Biomass:
Comparison of technologies for centralized or de-centralized fuel cell systems

Proefschrift

ter verkrijging van de graad van doctor
aan de Technische Universiteit Delft,
op gezag van de Rector Magnificus prof. ir. K. C. A. M. Luyben,
voorzitter van het College voor Promoties
in het openbaar te verdedigen op donderdag 8 juli 2010 om 12.30 uur

door

Richard TOONSSEN

scheikundig ingenieur
geboren te Den Haag

Dit proefschrift is goedgekeurd door de promotor(en):

Prof. dr. ir. A. H. M. Verkooijen

Samenstelling promotiecommissie:

Rector Magnificus,	Voorzitter
Prof. dr. ir. A. H. M. Verkooijen,	Technische Universiteit Delft, promotor
Prof. dr. ir. B. J. Boersma,	Technische Universiteit Delft
Prof. ir. J. P. van Buijtenen,	Technische Universiteit Delft
Prof. dr. ir. G. Brem,	Universiteit Twente
Prof. dr. W. Prins,	Universiteit Gent
Dr. K. Hemmes,	Technische Universiteit Delft
Dr. ir. J. Kiel,	ECN

ir. N. Woudstra heeft als begeleider in belangrijke mate aan de totstandkoming van het proefschrift bijgedragen.

Summary

Sustainable Power from Biomas:
Comparison of technologies for centralized and de-centralized fuel cell systems

Biomass is considered as a sustainable source of energy for the production of electricity and heat. Gasification is a technology for the conversion of biomass into a gas mixture also known as (bio-)syngas. This syngas consists mainly of hydrogen, carbon monoxide, methane, carbon dioxide and water. Besides these components, the gas also contains several contaminants, like tars, alkali compounds, nitrogen compounds, chlorine compounds and sulphur compounds. These contaminants need to be removed from the gas before it can be used in fuel production or fuel cells.

Fuel cells, especially the proton exchanger membrane (PEM) fuel cell and solid oxide fuel cell (SOFC), are expected to play an important role in the energy production in the future. The PEM fuel cell operates at a temperature of approximately 80°C and produces electricity and low temperature heat. This low operating temperature makes it suitable for the application in a micro combined and power system.

The SOFC operates higher temperatures between 600°C and 1000°C producing electricity and high temperature heat. This makes the fuel cell suitable to combine it with a gas turbine, which results result in highly efficient energy conversion devices.

The objective of the thesis is the comparison and selection of suitable conversion technologies for biomass gasification applied in hydrogen based energy systems with fuel cells. For the combination of biomass gasification and fuel cells, various systems configurations can be proposed. In this thesis, two different conversion chains are considered. The first conversion chain is centrally converting biomass into syngas, which is directly used in a SOFC combined with a gas turbine for the production of electricity. The produced electricity is distributed via the grid and is finally used in households. The households use some of the electricity in a heat pump for heating purposes.

In the second chain, biomass is centrally converted into syngas. This syngas is further processed into a gaseous fuel (clean dry syngas, or hydrogen, or synthetic natural gas). The gaseous fuel is distributed via a grid to the customers. The customers are households, which use the fuel in micro combined heat and power (μ-CHP) units. These μ-CHP units consist of a fuel cell system and a heat pump, in order to meet the electricity and heat demand of the household.

Each energy conversion chain starts at the biomass gasification process and ends at a single household. A single household is assumed to have an electricity demand of 1 kW and a heat demand of 3kW. Fluctuations in the heat and power demand in a domestic setting are beyond the scope of this thesis.

Different process and system designs are created in the flow sheeting program Cycle-Tempo. With Cycle-Tempo, the system and process designs are analysed thermodynamically. The results from the energy and exergy analysis form the basis for the system comparison and selection. The main used criteria are the overall and electrical exergy efficiency of the process chain.

In chapter 2, an overview is given of the different technologies and future developments involved in the systems of the two different chains. This chapter includes technology discussions about biomass gasification, gas cleaning, gas processing, PEM and solid oxide

fuel cells. For biomass gasification, the emphasis is on fluidized bed gasification technologies. This chapter forms the basis for every systems design in this thesis.

Chapter 3 presents a study on the influence of gasification technology and gas cleaning technology on performance of a biomass based hydrogen production plant. Ten different models of hydrogen production plants are created. These models are based on five different commercial or pilot scale gasification systems. For each gasification techniques two different gas cleaning techniques are used, namely low temperature gas cleaning and high temperature gas cleaning. The thermal input of every plant is 10 MW$_{th}$ of biomass with the same dry composition. The goal of each hydrogen plants is the production of 99.99% pure hydrogen. It is found that the output of the gasifier is important. Large amount of carbon dioxide or nitrogen complicated the gas processing. Air gasification results in a nitrogen diluted gas; this nitrogen is hard to remove from the gas. In oxygen gasification, this complication of nitrogen dilution can be avoided. But the air separation process is a very energy intensive process. The air separation results in additional losses, which reduces the overall performance. The processes based on indirect steam gasification and staged reforming showed the best performance. These gasification technologies produce a syngas with relatively high hydrogen content, which is important when producing hydrogen. The exergy losses in the high temperature gas cleaning are lower than for the low temperature gas cleaning. This effect does not result in a better overall performance of the hydrogen plant.

Chapter 4 shows a system design of a power plant based on biomass gasification and a solid oxide fuel cell gas turbine hybrid system. In this design, biomass is gasified in a fast internal circulating fluidized bed gasifier. This is an indirect steam gasification unit. The raw syngas from the gasifier is cooled, filtered, scrubbed, compressed and finally passed through a sulphur guard. This clean and compressed gas enters the solid oxide fuel cell gas turbine hybrid system for the production of electricity. The heat from the syngas cooling and from the flue gas leaving the system is used to produce steam in a heat recovery steam generator. The generated steam in used in a Rankine cycle for the production of additional electricity. The power output of the complete system is 34 MW and the electrical exergy efficiency is 48.9%. This design is intended as a reference system.

Chapter 5 shows a feasibility study of the combination of hydrothermal biomass gasification and a hybrid SOFC gas turbine. In this study three cases are evaluated. The difference between the cases is the gasification temperature. In case 1, the gasification temperature is 400°C, in case 2 it is 500°C and in case 3 it is 700°C. The different gasification temperatures result in different gas compositions. In case 1, the gas has a relative high methane content, in case 3 the gas has a relative high hydrogen content and in case 2 both the methane and hydrogen content in high. The produced syngas is used in a solid oxide fuel cell gas turbine hybrid system for the production of electricity. The power output of the systems is approximately 550 kW. The electrical exergy efficiency of the three cases is around 50%. Case 2 has the highest electrical exergy, which is 51.8%.

In chapter 6, the influence of the gasification technology, gas cleaning technology and system scale on the overall system performance of power production plants based on biomass gasification and hybrid SOFC gas turbines is studied. In this study four different systems have been created: the first system is a large scale system (30MW$_e$) based on indirect steam gasification and low temperature gas cleaning, the second system is a large

scale system based on pressurized air gasification and low temperature gas cleaning, the third system is a large scale system based on pressurized air gasification and high temperature gas cleaning, the fourth and last system is at small scale (100 kW$_e$) based on pressurized air gasification and high temperature gas cleaning. It is found that the gasification technology has hardly any influence on the electrical exergy efficiency of the system. High temperature gas cleaning results in a higher electrical exergy efficiency. The performance of the small scale system is lower than the performance of the large scale systems.

Chapter 7 shows a study on the central production of hydrogen from biomass. The hydrogen is distributed and eventually used in a μ-CHP system based on a PEM fuel cell. In this study two different purities of hydrogen are produced, namely pure hydrogen and 60% hydrogen. The influence of the hydrogen purity on the overall chain performance is evaluated. Besides this, also two techniques for additional heat production in the μ-CHP are evaluated. The first technique uses a fuel by-pass to a combustor for additional heat production; the second technique uses a ground coupled compression heat pump. It is found that the chain in which 60% hydrogen is used as a fuel for the μ-CHP system has a higher overall exergy efficiency then the chain in which pure hydrogen is used as a fuel. The μ-CHP system including heat pump is more efficient then the one with the fuel by-pass to the combustor.

Chapter 8 shows a study on the central production of gaseous fuel from biomass. The fuel is distributed and used in a μ-CHP system based on a SOFC combined with a ground coupled compression heat pump. Three different fuels have been evaluated: hydrogen, synthetic natural gas (SNG) and clean syngas. It is found that the overall exergy efficiency of the chain in which syngas is distributed is the highest, closely followed by the chain in which SNG is distributed. The chain in hydrogen is distributed has the lowest exergy efficiency.

In chapter 9, the results of chapters 4 to 8 are evaluated. The results from chapters 4, 5 & 6 are used and expanded, so the results for the whole chain from biomass to heat and power at a household can be obtained. The expanded results can be compared with the results of chapter 7 & 8. It is preferred to centrally produce power from biomass instead of centralized fuel production and de-centralized power production from that fuel. Also, hydrogen is not a suitable energy carrier when considering chain efficiencies. Electricity is more suitable. It is also found that SOFC's are preferred for both centralized and de-centralized power production.

Richard Toonssen

Samenvatting

Duurzame Electriciteit uit Biomassa:
Vergelijking van technologieën voor centrale of de-centrale brandstofcelsystemen

Biomassa wordt beschouwd als een duurzame bron van energie voor de productie van elektriciteit en warmte. Vergassing is een technologie voor de omzetting van biomassa in een gasmengsel bekend onder naam (bio-)syngas. Dit syngas bestaat uit hoofdzakelijk waterstof, koolstof monoxide, methaan, koolstof dioxide en water. Naast deze componenten bevat het gas verontreinigingen, zoals teren, alkaliverbindingen, stikstofverbindingen, chloorverbindingen en zwavelverbindingen. Deze verontreinigingen moeten worden verwijderd uit het gas voordat het kan worden gebruikt in brandstof productie of brandstofcellen.

Van brandstofcellen, in het bijzonder de proton exchange membrane (PEM) brandstofcel en de vaste oxide brandstofcel (solid oxide fuel cell (SOFC)), wordt verwacht dat ze in de toekomst een belangrijke rol gaan spelen in de energie productie. De PEM brandstofcel werkt op een temperatuur van ongeveer 80°C en produceert elektriciteit en lage temperatuur warmte. Deze lage werkingstemperatuur maakt het geschikt voor de toepassing in micro warmte kracht koppeling systemen.

De SOFC werkt op hogere temperaturen tussen de 600°C en 1000°C en produceert elektriciteit en hoge temperatuur warmte. Hierdoor is de brandstofcel om te combineren met een gas turbine, wat resulteert in een zeer efficiënte energie omzetting apparaat.

Het doel van dit proefschrift is de vergelijking en selectie van geschikte omzettingssystemen voor biomassa vergassing toegepast in waterstof gebaseerde energie systemen met brandstofcellen. Voor de combinatie van biomassa vergassing en brandstofcellen kunnen verschillende system worden voorgesteld. In het proefschrift worden twee verschillen omzettingsketens beschouwd. In de eerste omzettingsketen wordt biomassa centraal omgezet in syngas, welke direct gebruikt wordt in een SOFC gecombineerd met een gas turbine voor de productie van elektriciteit. De geproduceerde elektriciteit wordt gedistribueerd via het elektriciteitsnet en wordt uiteindelijke gebruikt in een huishouden. In het huishouden wordt een deel van de elektriciteit gebruikt door een warmtepomp voor verwarmingsdoeleinden.

In de tweede omzettingsketen wordt biomassa centraal omgezet in syngas. Dit syngas wordt verder opgewerkt in een gasvormige brandstof (schoon en droog syngas, of waterstof, of synthetisch aardgas). De gasvormige brandstof wordt gedistribueerd via een netwerk naar de klanten. De klanten zijn huishoudens, die de brandstof gebruiken in een micro warmte kracht koppelingssysteem (μ-WKK). Deze μ–WKK systemen bestaan uit een brandstofcelsysteem en een warmtepomp, zodat aan de warmte- en elektriciteitsvraag van het huishouden kan worden voldaan.

Elke energie omzettingsketen begint bij het biomassa vergassingsproces en eindigt bij een enkel huishouden. Voor het enkele huishouden is aan genomen dat het een elektriciteitsvraag heeft van 1 kW en een warmtevraag van 3 kW. Fluctuaties in de warmte- en elektriciteitsvraag binnen een huishouden vallen buiten het blikveld van dit proefschrift. Verschillende proces- en systeemontwerpen zijn gemaakt in het computer programma Cycle-Tempo. Met Cycle-Tempo zijn de proces- en systeemontwerpen thermodynamisch geanalyseerd. De resultaten van de energie en exergie analyse vormen de basis voor de

systeemvergelijking en selectie. De belangrijkste criteria die zijn gebruikt zijn de totale en elektrische exergie efficiëntie van de procesketen.

In hoofdstuk 2 wordt een overzicht gegeven van de verschillende technologieën en toekomstige ontwikkelingen met betrekking tot de systemen in de twee verschillende ketens. Dit hoofdstuk bevat technologische beschrijvingen over biomassa vergassing, gas reiniging, gas bewerking, PEM en vaste oxide brandstofcellen. Bij biomassa vergassing ligt de nadruk op fluïde bed vergassingstechnologieën. Dit hoofdstuk vormt de basis voor elk systeemontwerp in dit proefschrift.

Hoofdstuk 3 presenteert een studie over de invloed van vergassingstechnologie en gas reinigingstechnologie op de prestaties van een op biomassa gebaseerde waterstof productie fabriek. Tien verschillende modellen van waterstof productie fabrieken zijn er gemaakt. Deze modellen zijn gebaseerd op vijf verschillende commerciële of proefschaal vergassingssystemen. Voor elke vergassingstechniek zijn twee gasreinigingstechnieken gebruikt, namelijk lage temperatuur gasreiniging en hoge temperatuur gasreiniging. De thermische input voor elke fabriek is 10 MW_{th} aan biomassa met dezelfde droge compositie. Het doel van elke waterstoffabriek is de productie van 99.99% pure waterstof. Er is gevonden dat de output van de vergasser erg belangrijk is. Grote hoeveelheden van koolstof dioxide of stikstof maken de gasbewerking moeilijk. Luchtvergassing resulteert in een gas dat is verdund met stikstof; dit stikstof is lastig uit het gas te verwijderen. In zuurstof vergassing kan de verdunning door stikstof worden vermeden. Maar het scheiden van lucht is een erg energie intensief proces. De scheiding van lucht resulteert in additionele verliezen, welke de totale prestatie reduceren. De processen gebaseerd op indirecte stoom vergassing en staged reforming laten de beste prestaties zien. Deze vergassings- technologieën produceren een syngas met een relatief hoog waterstofgehalte, wat belangrijk is bij waterstof productie. De exergie verliezen in de hoge temperatuur gas reiniging zijn lager dan voor de lage temperatuur gasreiniging. Dit effect resulteert niet in een beter totaal prestatie van de waterstoffabriek.

Hoofdstuk 4 laat een systeem ontwerp van een energiecentrale gebaseerd op biomassa vergassing en een vaste oxide brandstofcel gas turbine hybride systeem zien. In dit ontwerp wordt biomassa vergast in een intern circulerend fluide bed vergasser. Dit is een indirecte stoom vergassingseenheid. Het ruwe syngas van de vergasser wordt gekoeld, gefiltreerd, gewassen, gecomprimeerd en gaat uiteindelijk door een zwavel verwijdering. Het schone en gecomprimeerde gas gaat naar de vaste oxide brandstofcel gas turbine hybride systeem voor de productie van elektriciteit. De warmte, afkomstig van de syngas koeling en van het rookgas wat het systeem verlaat, wordt gebruikt voor de productie van stoom in een warmte terugwinning stoom generator. De geproduceerde stoom wordt gebruikt in een Rankine cycle voor de productie van extra elektriciteit. De elektrische output van het complete systeem is 34 MW en de elektrische exergie efficiëntie is 48.9%. Dit systeemontwerp is bedoeld als een referentie systeem.

Hoofdstuk 5 is een haalbaarheidsstudie van de combinatie van hydrothermisch vergassen en een hybride SOFC gas turbine. In deze studie zijn drie opties bekeken. Het verschil tussen de opties is de vergassingstemperatuur. In optie 1 is de vergassingstemperatuur 400°C, in optie 2 is het 500°C en in optie 3 is het 700°C. De verschillende vergassingstemperaturen resulteren in verschillende gascomposities. In optie 1 is het gas relatief rijk aan methaan, in optie 3 is het gas relatief rijk aan waterstof, en in optie 2 zijn de hoeveelheden van zowel

methaan als waterstof hoog. Het geproduceerde syngas wordt gebruikt in en vaste oxide brandstofcel gas turbine hybride systeem voor de productie van elektriciteit. Het vermogen van de systemen is ongeveer 550 kW. Het elektrische exergie rendement van de drie opties ligt rond de 50%. Optie 2 heeft het hoogste elektrische exergie rendement, namelijk 51.8%.

In hoofdstuk 6 wordt de invloed van de vergassingstechnologie, gas reinigingstechnologie en systeemschaal op de totale systeemprestaties van elektriciteitscentrales gebaseerd op biomassa vergassing en SOFC gas turbines bestudeerd. In deze studie zijn vier verschillende systemen gemaakt: het eerste systeem is een grootschalig systeem (30 MW$_e$) gebaseerd op indirecte stoom vergassing en lage temperatuur gasreiniging, het tweede systeem is een grootschalig systeem gebaseerd op hoge druk luchtvergassing en lage temperatuur gasreiniging, het derde systeem is een grootschalig systeem op basis van hoge druk luchtvergassing en hoge temperatuur gasreiniging, het vierde en laatste systeem is een kleinschalig systeem (100 kW$_e$) gebaseerd op hoge druk luchtvergassing en hoge temperatuur gas-reiniging. Er is gevonden dat de vergassingstechnologie nauwelijks een invloed heeft op het elektrische rendement van het systeem. Hoge temperatuur gasreiniging resulteert in een hoger elektrisch exergie rendement. De prestaties van het kleinschalige systeem zijn lager dan voor de grootschalige systemen.

Hoofdstuk 7 geeft een studie weer over de centrale productie van waterstof vanuit biomassa. Het waterstof wordt gedistribueerd en uiteindelijke gebruikt in een μ-WKK systeem gebaseerd op een PEM brandstofcel. In deze studie worden twee verschillende zuiverheden waterstof geproduceerd, namelijk puur waterstof en 60% waterstof. De invloed van de waterstof zuiverheid op de totale keten prestaties is beschouwd. Daarnaast zijn ook twee technieken voor de productie van extra warmte in de μ-WKK beschouwd. De eerste techniek gebruikt een omleiding van brandstof naar een verbrander voor de extra warmte productie; de tweede techniek maakt gebruik van een grond gekoppelde compressie warmtepomp. Er is gevonden dat de keten welke 60% waterstof gebruikt als een brandstof voor de μ-WKK een hoger totaal exergy rendement heeft dan de keten welke puur waterstof als brandstof gebruikt. Het μ-WKK systeem inclusief warmtepomp heeft een hoger rendement dan het systeem met de brandstof omleiding naar de verbrander.

Hoofdstuk 8 laat een studie zien over de centrale productie van gasvormige brandstof van biomassa. Deze brandstof wordt gedistribueerd en gebruikt in een μ-WKK systeem op basis van een SOFC gecombineerd met een grond gekoppelde compressie warmtepomp. Drie verschillende brandstoffen zijn beschouwd: waterstof, synthetisch aardgas en schoon syngas. Er is gevonden dat het totale exergie rendement van de keten waarin syngas wordt gedistribueerd het hoogst is, op de voet gevolgd door de keten waarin synthetisch aardgas wordt gedistribueerd. De keten waarin watersof wordt gedistribueerd heeft het laagste exergie rendement.

In hoofdstuk 9 worden de resultaten van hoofdstukken 4 tot en met 8 beschouwd. De resultaten van hoofdstukken 4, 5 & 6 worden gebruikt en uitgebreid, op een manier dat er resultaten van een keten van biomassa naar warmte en elektriciteit in een huishouden kunnen worden verkregen. De uitgebreide resultaten kunnen worden vergeleken met de resultaten van hoofdstukken 7 & 8. Er wordt de voorkeur gegeven aan de centrale productie van elektriciteit uit biomassa in plaats van de centrale brandstof productie en de decentrale elektriciteitsproductie uit deze brandstof. Waterstof is een ongeschikte energie drager wanneer men naar ketenrendementen kijkt. Elektriciteit is beter geschikt. Er is ook

gevonden dat SOFC's de voorkeur hebben voor zowel centrale als decentrale elektriciteitsproductie.

Richard Toonssen

Table of Contents

Appendices

1. Introduction

The energy demand is rising; in 2030 the world's energy consumption is expected to rise by 50% [1]. Demand will reach over 17.7 billions tons of oil equivalents [1]. The source of energy is for the largest part fossil fuels. The fossil fuel reserves are diminishing, leading to an increase in the price for fossil fuels. The impact on the environment is starting to have its effect on human life. There is a general consensus that the release of greenhouse gasses, as carbon dioxide, lead to global warming and to climate changes. In 2005, the carbon dioxide concentration in the atmosphere was 379 ppm, approximately 180-300 ppm more than the equilibrium concentration for the past 650 000 years [2]. A greater environmental awareness accelerates the research into alternative and more sustainable ways to produce energy and energy carriers.

'Decarbonising' energy supply is a technological solution, which addresses global CO_2 emissions [3]. One of the options is the 'hydrogen energy economy'. An idyllic vision of a 'hydrogen energy economy' is one in which hydrogen and electricity are the sole energy carriers and are both produced from renewable resources [3].

Renewable energy sources are constantly replenished on consumption and can never run out. One of those renewable sources is biomass. Biomass is the combination of the energy from the sun with the absorbed carbon dioxide from the atmosphere through photosynthesis. In the photosynthesis carbohydrates are produced, which are building block for biomass. Because of this, biomass is considered carbon dioxide neutral.

Biomass comes in a wide variety of compositions and moisture contents (See Appendix A). For the conversion of biomass into either fuel or energy, many different processes are available. Each process has its own requirements, products and applications.

In general, there are three product groups to be considered: heat, electricity and secondary fuel. After the conversion of the biomass, the products need further processing. The products are combusted in one way or another for the production of heat and electricity. In Figure 1-1, an overview is given of the different pathways from biomass towards heat, electricity and fuel.

The consideration of a certain biomass conversion technique depends on several factors. The most important factors are: type of biomass to be converted, the required end-product and conversion efficiency. More information about biomass, biomass pre-treatment and the different conversion techniques can be found in Appendix A, B & C. In Table 1-1 an overview is given of the different conversion techniques, their feedstock, efficiency and final product.

Table 1-1 overview of the different biomass conversion techniques

Conversion method	Feed stock	Efficiency	Final product
Combustion	Ligno-cellulosic biomass	30-40%[4]	Electricity
Pyrolysis	Ligno-cellulosic biomass	<80%[5]	Pyrolysis oil
Gasification	Ligno-cellulosic biomass	63-85%[6]	Syn-gas
SCW Gasification	Wet biomass	44-65%[7]	Syn-gas/methane rich gas
Liquefaction	Ligno-cellulosic biomass	55-79% [8, 9]	Sugars/Oil
Anaerobic digestion	Wet biomass	20-40%[5]	Methane rich gas
Dark fermentation	Wet biomass	-	Hydrogen
Photolysis	Wet biomass	-	Hydrogen
Bio-WGS	Carbon monoxide	-	Hydrogen
Light (photo) fermentation	Sugar- and starch crops	43%[4]	Ethanol
Light (photo) fermentation	Ligno-cellulosic biomass	46%[4]	Ethanol
Mechanical extraction	Oilseed rape, cotton, nuts	88%[4]	Vegetable oil
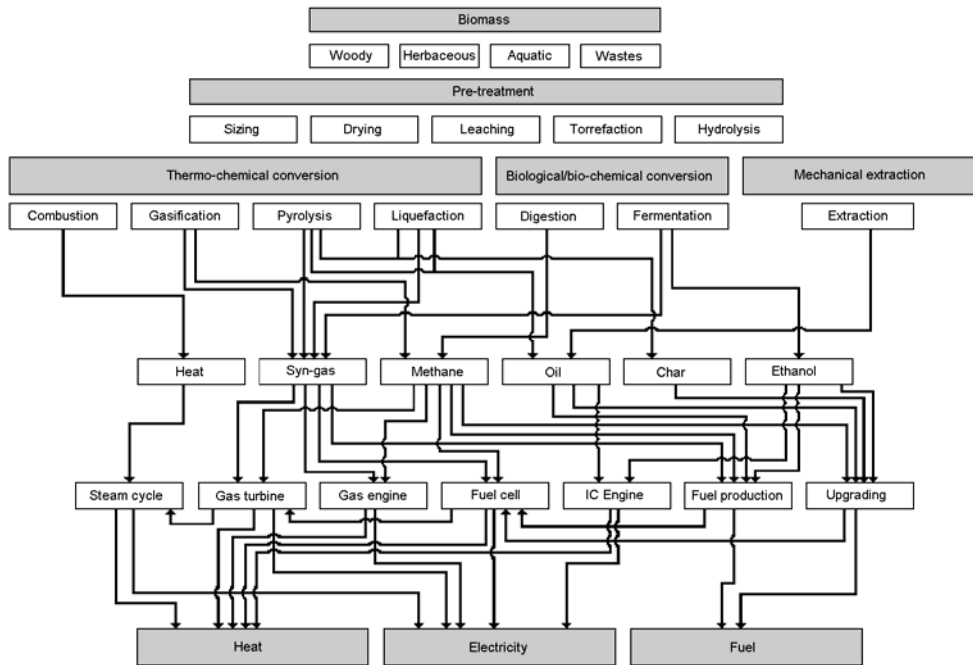
Figure 1-1 overview of biomass conversion pathways towards heat, electricity and fuel

1.1. Motivation

For the future, the application of biomass for energy conversion is important to reduce the emission of carbon dioxide and to contribute to the prevention of climate change. These energy conversion systems need to be efficient to get the most energy out of the biomass and assure a CO_2 emission reduction.

Biomass gasification is an efficient way to convert biomass into a secondary energy carrier, as can be seen from Table 1-1. In the biomass gasification process, biomass is converted into a hydrogen rich gas, called (bio-)syngas. This syngas consist mainly of hydrogen, carbon monoxide, methane, carbon dioxide and water. Besides the main components the produced syngas also contains several impurities, e.g. tars, alkalis, particulates, sulphur compounds and halogen compounds. These compounds can have a deteriorating effect on all kinds of processes and downstream equipment. Before the gas can be used it needs to be purified in a gas cleaning system. The clean syngas can be used, either directly or can be further processed, into a fuel, like hydrogen or synthetic natural gas (SNG).

Fuel cells are electrochemical devices, which convert gaseous fuels into electricity. There are different kinds of fuel cells each with their own operating window and gas composition requirements. Low temperature fuel cells, like the proton exchange membrane (PEM) fuel cell, require highly pure hydrogen as a fuel. On the other hand, high temperature fuel cells, like the solid oxide fuel cell (SOFC), require less pure fuel and can even operate on light hydrocarbons instead of pure hydrogen.

The coupling of fuel cells with biomass gasification could result in highly efficient energy conversion systems.

The objective of this thesis is the comparison and selection of suitable conversion technologies for biomass gasification applied in hydrogen based energy systems with fuel

cells. For the combination of biomass gasification and fuel cells, various system configurations and conversion chains can be proposed.

In the application of the biomass gasification and fuel cells two different pathways will be considered. The first one is the central biomass gasification and production of power with fuel cells. The second one is the central gasification of biomass and processing of the gas, followed by the application of gas in a fuel distribution system, in combination with the de-central production of power and heat. In Figure 1-2, a schematic overview of the two different pathways is given.
There are a few different types of gasifiers, which have their own scale of operation. The type of gasifier selected is a fluidized bed gasifier. Because the biomass gasification plant is supposed to be at a large scale, the only realistic gasifier concept is the fluidized bed gasifier [10-12].
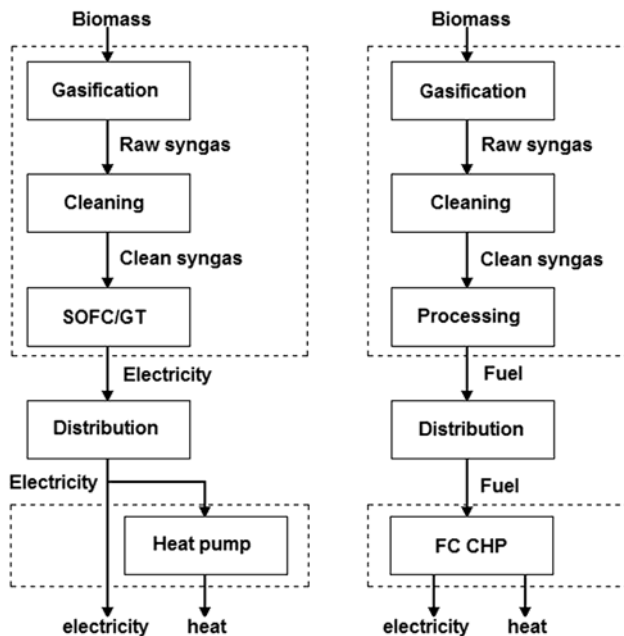
Figure 1-2 two pathways from biomass to heat and power

In the central power production pathway, biomass is gasified and after gas cleaning the hydrogen rich gas is directly used to produce electricity. For the energy conversion, a fuel cell will be used. There are different kinds of fuel cells each with their own operating window, and gas demands. High temperature fuel cells are especially interesting, because of their high efficiency and their low sensitivity to contaminants [13, 14]. Also the high quality heat produced by the fuel cell is an advantage [15-17]. There are two types of high temperature fuel cells; the molten carbonate fuel cell and the solid oxide fuel cell. The solid oxide fuel cell is selected for the central power production pathway, because of the solid state design [14, 18, 19]. This means no electrolyte management system is needed. Other reasons to select the solid oxide fuel cell are: the possibility for hybridization with a gas turbine [20, 21], the ability to convert methane and carbon monoxide [16-19, 22, 23], and the high exergy efficiency.

The main purpose of the central power production pathway is the production of electricity. In order to increase the efficiency of the total system any residual heat is to be utilized as much as possible by e.g. a heat recovery steam generator and steam turbine.

In the decentralized power production pathway, the cleaned hydrogen rich gas is centrally processed and purified. Four different fuels have been considered: pure hydrogen, 60% hydrogen, synthetic natural gas and syngas. The production of hydrogen involves steam reforming, water gas shift and further purification. The production of SNG involves a methanation process and further purification through CO_2 removal. Syngas is already available, it only needs drying. Each fuel is assumed to be distributed with the help of a distribution grid, which supplies it to dwellings for the production of heat and power.
The hydrogen distribution and syngas distribution can be comparable to the natural gas distribution grid.
For the production of heat and power in a decentralized setting, two fuel cell types are selected. The first type is the proton exchange membrane (PEM) fuel cell, which is fuelled with either pure hydrogen or 60% hydrogen. This type of fuel cell is selected because of its low operation temperature, which has several benefits. These benefits are fast start-up [19, 24, 25], fast response to load changes [25], and good on/off cycling characteristics [24]. The fuel cell produces heat at a relative low temperature (±80°C); this heat can be applied e.g. for space heating. A disadvantage of this fuel cell is that the gas needs to be virtually free from carbon monoxide, as it has an adverse effect on the operation of the PEM fuel cell. The hydrogen produced centrally is used de-centrally in a combined heat and power (CHP) unit based on a PEM fuel cell.
The second fuel cell type selected is the solid oxide fuel cell, which is fuelled with pure hydrogen, SNG or syngas. This fuel cell is selected because of its high fuel flexibility and high efficiency. The fuel produced centrally is used de-centrally in a CHP unit based on a SOFC.

Some key questions could be asked:
1. Centralized or de-centralized power generation?
2. What energy carrier should be distributed? (Hydrogen, SNG, syngas, electricity)
3. What type of gasification?
4. What type of gas cleaning?
5. What type of fuel cell?

This thesis attempts to answer these questions.

1.2. Research scope

The research starts with the evaluation of the different basic technologies involved in the conversion of biomass into either fuel or electricity. The next step is the process and system design, which is preformed in the flow sheeting program Cycle-Tempo [26]. Cycle-Tempo can analyse the process and systems designs thermodynamically. The results from the system energy and exergy analysis form the basis for the process selection. The main criteria in the selection process are the overall and electrical exergy efficiency of the process chain.
The chains, which are being evaluated, start at the biomass gasification process. The feed for every system is A-quality wood (clean wood), except for the hydrothermal gasification system, where the feed is manure. A-quality wood is selected as feed, because it is relatively well defined and therefore easy to apply. In an actual system, the biomass would come from waste streams. The problem with these waste streams is that the composition is

not uniform and is hard to define. The conversion technologies applied should be robust in order to cope with the fluctuating composition.

It is assumed that the feed does not require any pre-treatment and that it has the right size, moisture content to be fed to the conversion process. This assumption is made, because the collection and transport of the biomass is not included in the research. Often, it is better to do the pre-treatment, like sizing and drying, before the biomass is transported.

In order to model the systems a lot of parameters are required. Most of the parameters are extracted from the literature, for instance steam to biomass ratios and oxygen to biomass ratios in biomass gasification processes. Process conditions for al kinds of reactions are also adopted from literature. Since some of the system components are still in a development stage, estimations have to be made with respect to the process conditions. The literature involving these technologies often provides help in the selection of proper values.

Some parameters, like system size, are more arbitrarily chosen. The system size of approximately 30 MW_e is chosen, because this is the size appropriate for a small town. The size 100 kW_e is more appropriate for block of houses.

The chains end at a single household, which is assumed to have an electricity demand of 1 kW and a heat demand of 3 kW. Fluctuations of the heat and power demand in a domestic setting are beyond the scope of this study.

In some chains a CHP unit is used. This CHP unit is designed on the basis of an average heat and power demand and is assumed to be connected to the electricity grid in order to smooth out the peaks in the electricity demand and production. It is also assumed that heat buffers are applied to smooth out the peaks in the heat demand and production. In this way, it is also possible to decouple the electricity and heat supply. The design point of the CHP units is 1 kW_e and 3 kW_{th}.

1.3. Thesis outline

In this PhD thesis, several pathways from biomass to electricity via gasification and fuel cells are considered. Each chapter in this thesis forms a part of a bigger picture. This work leads to the evaluation of the proposed chains. The thesis consists of one conference paper and 5 journal papers. Some of the papers are already accepted and published others are submitted and being reviewed.

Chapter 2 gives an overview of the different technologies and future developments involved in systems based on biomass gasification and fuel cells. Chapter 2 consists of four parts. Part one is a discussion about the different gasification technologies. There is an emphasis on the fluidized bed gasification technologies. In the second part, the gas cleaning steps are being treated, subdivided into the different types of contaminants. Part three is about different gas processing technologies. Among these technologies are steam reforming, water gas shift, preferential oxidation, methanation, CO_2 removal and hydrogen purification. The last and fourth part is about fuel cell technology. In this part, the PEM-FC and SOFC are being discussed. This chapter forms the basis for every system design given in this thesis.

Chapter 3 evaluates different gasification systems in hydrogen production plants. In this chapter, five different gasification technologies are evaluated, with two different types of gas cleaning each. This results in ten different systems. The thermodynamic performance and hydrogen production of each system is evaluated and all the systems are compared. On

the basis of this study, a gasification technology is selected for the production of gaseous fuels from biomass.

In **Chapter 4** a system design for a system of biomass gasification coupled with a solid oxide fuel cell gas turbine hybrid is given. This system also includes a heat recovery system for the production of additional electricity. The created system sets a benchmark for all the following systems designed in this study.

In **Chapter 5**, a system study is performed on a system with super critical water gasification combined with a solid oxide fuel cell gas turbine hybrid system. This study is performed to check whether this combination of technologies is feasible. Three different cases are studied. The difference between the cases is the temperature of super critical water gasification, which results in different compositions of the fuel for the solid oxide fuel cell gas turbine hybrid system. The thermodynamic performance of the three cases is compared.

In **Chapter 6**, the influence of gasification agent, gas cleaning technology, and process scale on the overall performance of a biomass integrated SOFC/GT plant is evaluated. Four different systems are evaluated. The first system is based on large scale steam gasification with low temperature gas cleaning. The second system is based on large scale pressurized air gasification with low temperature gas cleaning. The third system is based large scale pressurized air gasification with high temperature gas cleaning. The last and fourth system is based on small scale pressurized air gasification combined with high temperature gas cleaning.

Chapter 7 contains a study considering centralized hydrogen production and decentralized application of the produced hydrogen in a, PEM fuel cell based, micro combined heat and power system. In order to investigate the influence of the hydrogen purity on the performance of the whole chain, two hydrogen production plants have been designed. One plant produces pure hydrogen; the other plant produces 60% hydrogen. The produced hydrogen is assumed to be distributed through a distribution grid to households. Here, a micro-combined heat and power system uses the fuel.

In **Chapter 8** is also the centralized production of gas considered. In this chapter, three different gas production plants are evaluated: a hydrogen plant, a synthetic natural gas plant and a syngas plant. The produced gas is also distributed through gas distribution network to households. The fuel is still used de-centrally, but is now in micro combined heat and power systems, based on solid oxide fuel cells.

Chapter 9 gives an overall evaluation of the systems discussed in this thesis. The results of the different chapters are combined and placed in a broader perspective. The questions raised are answered.

Finally, in **Chapter 10** conclusions are drawn based on the previously given evaluation. Furthermore, some recommendations for future research are given.

1.4. References

1. IEA. World Energy Outlook 2007. International Energy Agency, 2007.
2. IPCC. Climate Change 2007: Physical Science Basis. 2007; Report, Intergovernmental Panel on Climate Change.
3. Florin N. H., Harris A. T. Enhanced hydrogen production from biomass with in situ carbon dioxide capture using calcium oxide sorbents. Chem Eng Sci 2008; 63(2): 287-316.
4. Faaij A. P. C. Bio-energy in Europe: changing technology choices. Energy Policy 2006; 34(3): 322-342.
5. McKendry P. Energy production from biomass (part 2): conversion technologies. Bioresource Technol 2002; 83(1): 47-54.
6. van der Nat K. V., Woudstra N., Spliethoff H. Evaluation of several biomass gasification processes for the production of a hydrogen rich synthesis gas In: International Hydrogen Energy Congress and Exhibition IHEC 2005, Istanbul, 2005.
7. Kruse A. Supercritical water gasification. Biofuels, Bioprod Biorefin 2008; 2(5): 415-437.
8. Feng W., van der Kooi H. J., de Swaan Arons J. Biomass conversions in subcritical and supercritical water: driving force, phase equilibria, and thermodynamic analysis. Chem Eng Process 2004; 43(12): 1459-1467.
9. Behrendt F., Neubauer Y., Oevermann M., Wilmes B., Zobel N. Direct Liquefaction of Biomass. Chem Eng Technol 2008; 31(5): 667-677.
10. Kivisaari T., Bjornbom P., Sylwan C. Studies of biomass fuelled MCFC systems. J Power Sources 2002; 104(1): 115-124.
11. Kurkela E., Stahlberg P., Laatikainen J., Simell P. Development of simplified IGCC-processes for biofuels: Supporting gasification research at VTT. Bioresource Technol 1993; 46(1-2): 37-47.
12. Bridgwater A. V. The technical and economic feasibility of biomass gasification for power generation. Fuel 1995; 74(5): 631-653.
13. Tomasi C., Baratieri M., Bosio B., Arato E., Baggio P. Process analysis of a molten carbonate fuel cell power plant fed with a biomass syngas. J Power Sources 2006; 157(2): 765-774.
14. Dayton D., Ratcliff M., Bain R. Fuel Cell Integration: A Study of the Impacts of Gas Quality and Impurities. 2001; Report, NREL, National Renewable Energy Laboratory.
15. Wang L., Weller C. L., Jones D. D., Hanna M. A. Contemporary issues in thermal gasification of biomass and its application to electricity and fuel production. Biomass Bioenergy 2008; 32(7): 573-581.
16. Hofmann P., Schweiger A., Fryda L., Panopoulos K. D., Hohenwarter U., Bentzen J. D., Ouweltjes J. P., Ahrenfeldt J., Henriksen U., Kakaras E. High temperature electrolyte supported Ni-GDC/YSZ/LSM SOFC operation on two-stage Viking gasifier product gas. J Power Sources 2007; 173(1): 357-366.
17. Singh D., Hernandez-Pacheco E., Hutton P. N., Patel N., Mann M. D. Carbon deposition in an SOFC fueled by tar-laden biomass gas: a thermodynamic analysis. J Power Sources 2005; 142(1-2): 194-199.
18. Ghosh S., De S. Energy analysis of a cogeneration plant using coal gasification and solid oxide fuel cell. Energy 2006; 31(2-3): 345-363.

19.   Song C. Fuel processing for low-temperature and high-temperature fuel cells:
        Challenges, and opportunities for sustainable development in the 21st century.
        Catal Today 2002; 77(1-2): 17-49.
20.   Park S. K., Kim T. S. Comparison between pressurized design and ambient
        pressure design of hybrid solid oxide fuel cell-gas turbine systems. J Power
        Sources 2006; 163(1):
21.   Aravind P. V. Studies on High Efficiency Energy Systems Based on Biomass
        Gasifiers and Solid Oxide Fuel Cells with Ni/GDC Anodes. PhD Thesis,
        University of Technology Delft, 2007.
22.   Jansen D., van der Laag P. C., Oudhuis A. B. J., Ribberink J. S. Prospects for
        advanced coal-fuelled fuel cell power plants. J Power Sources 1994; 49(1-3): 151-
        165.
23.   Baron S., Brandon N., Atkinson A., Steele B., Rudkin R. The impact of wood-
        derived gasification gases on Ni-CGO anodes in intermediate temperature solid
        oxide fuel cells. J Power Sources 2004; 126(1-2): 58-66.
24.   O'Hayre R. P. Fuel Cell Fundamentals. Hoboken: Wiley, 2006.
25.   EG&G Techincal Services. Fuel Cell Handbook. Morgantown: Nation Energy
        Technology Laboratory, 2004.
26.   Cycle-Tempo, 5.0. TU Delft, 2009. www.cycle-tempo.nl

2. Background and technology

The combination of biomass gasification and fuel cells involves many different types of technologies, varying with the goal and size of the system designed. Systems combining biomass gasification and fuel cells contain, besides biomass gasification technology, also gas cleaning technology, gas processing technologies and of course fuel cell technology. In this chapter most of the technologies in a fuel cell system, based on biomass gasification can be found.

In the first section, the biomass gasification technologies are discussed. The second section describes the gas cleaning and processing of the bio-syngas. The third and last section involves the SOFC and PEM fuel cell technologies.

2.1. Biomass gasification

Biomass gasification is a complex thermo-chemical process involving, numerous different reactions. Biomass is mainly converted into a mixture of hydrogen, carbon monoxide, carbon dioxide, methane and water. This mixture is also known as bio syn-gas. The biomass gasification process can be divided into two parts, pyrolysis and gasification [1-3]. Pyrolysis is discussed in Appendix C. In the gasification part the gasses, bio-liquid and char react further. During the gasification hundreds of different reactions take place. The most important of these reactions are given in equations (2.1)-(2.7) [3-5]. In these equations, char has the molecular formula of carbon ($C_{(s)}$), and equation (2.7) shows the stoichiometric values a, b and c, which depend on the composition of the tar.

$$C_{(s)} + O_2 \rightleftarrows CO_2 \qquad \Delta H^0_{298} = -394\,\text{kJ}\,\text{mol}^{-1} \tag{2.1}$$

$$C_{(s)} + H_2O \rightleftarrows CO + H_2 \qquad \Delta H^0_{298} = 131\,\text{kJ}\,\text{mol}^{-1} \tag{2.2}$$

$$C_{(s)} + CO_2 \rightleftarrows 2CO \qquad \Delta H^0_{298} = 173\,\text{kJ}\,\text{mol}^{-1} \tag{2.3}$$

$$C_{(s)} + 2H_2 \rightleftarrows CH_4 \qquad \Delta H^0_{298} = -75\,\text{kJ}\,\text{mol}^{-1} \tag{2.4}$$

$$CO + H_2O \rightleftarrows CO_2 + H_2 \qquad \Delta H^0_{298} = -41\,\text{kJ}\,\text{mol}^{-1} \tag{2.5}$$

$$CH_4 + H_2O \rightleftarrows CO + 3H_2 \qquad \Delta H^0_{298} = 206\,\text{kJ}\,\text{mol}^{-1} \tag{2.6}$$

$$\text{Tar} \rightarrow aCO + bCH_4 + cC \tag{2.7}$$
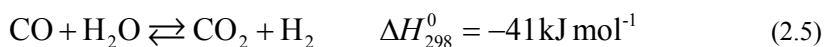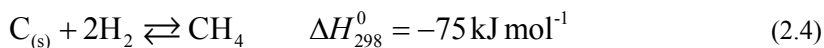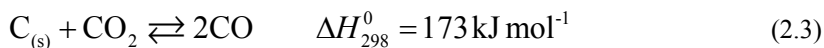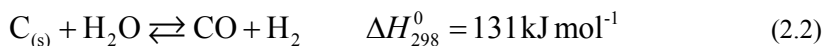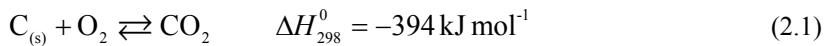
The gasification process is usually performed with aid of a gasification agent. The gasification agent can be steam, or air, or enriched air, or oxygen, or a combination of steam and an oxygen source, or carbon dioxide. The process is performed at relative high temperature 873-1773K and the pressure can range from atmospheric pressure up to 7 MPa. There are also small amounts of impurities in the gas: particulates, tars, alkalis, nitrogen compounds, sulphur compounds, and chlorine compounds.

For biomass gasification, many different reactor designs are available. The type of design depends on the required throughput of biomass, as well as on the type of biomass. For instance, if the throughput of biomass is below 1MW_{th}, then a downdraft fixed bed design is preferred. If the throughput is higher, then a fluidized bed type of gasifier is preferred. High moisture content contributes to low exergy efficiency due to the latent heat of evaporation. The demand of mechanical dewatering techniques is extremely high. Recently,

the development of super critical water gasification seems to open new, efficient gasification results. When the biomass is very wet, with moisture contents above 80%, supercritical water gasification seems to be a more suitable option [6].
The commonly used types of biomass used in gasification processes are woody plants and herbaceous plants. The moisture content should usually be low, around 10-15 wt%. The efficiency of the process is around 63-85% [7]. This efficiency is based on the LHV of the produced gas divided by the LHV of the biomass feed.

For super critical water gasification, the biomass needs to have high moisture contents and the amount of fibrous content should be low. Manures and sewage sludge are possible feed stocks for this gasification process. The water in the biomass is used as reaction medium. Therefore, it is also called hydrothermal gasification. Water gets some special properties when it approaches near- and supercritical conditions. It provides a relatively fast hydrolysis, which leads to the rapid degradation of the polymeric structure of the biomass [8]. Tar and coke formation are inhibited by the high solubility of the intermediates in the reaction medium at supercritical conditions [8]. Since a lot of water has to be heated for hydrothermal gasification, the amount of heat required for heating may exceed the energy content of the biomass [8]. Therefore, heat recovery from the process is very important. It is a determining factor in the system efficiency.
The efficiency of the current designs of super critical water gasification is 44% to 65% [6].

In the following sections, the different technologies for biomass gasification are described. First, the fixed bed systems are discussed. This is followed by the fluidized bed technologies. After that, the entrained flow gasifiers will be discussed. Finally, some hydrothermal gasification options will be discussed.

2.1.1. Fixed bed gasification

Fixed bed gasification units are usually used for small scale applications of a few MW$_{th}$. Air is often the gasification agent. Three general kinds of fixed bed gasifiers can be distinguished; the downdraft gasifier, the updraft gasifier and the cross-current gasifier. In the following sections the different types will be further discussed starting with the downdraft gasifier, followed by the updraft gasifer and finally the cross-current gasifier.

Downdraft gasifiers

The downdraft gasifier is a co-current reactor, where the fuel and the gasification agent move in the same direction. In Figure 2-1, a schematic representation is given of a downdraft gasifier.
As can be seen in Figure 2-1, the down draft gasifier has different reaction zones. In the drying zone the moisture is evaporated from the biomass as it slowly descents towards the pyrolysis zone. In the pyrolysis zone the biomass is split into char, tars and gasses. Some of the pyrolysis products are combusted in the combustion zone. Due to the high temperature in this combustion zone, tars are cracked. As a result, the produced gas is relatively clean and low on tars.
The downdraft gasifier is simple, reliable and proven for certain fuels, such as relatively dry blocks or lumps with a low ash content and containing a low portion of fine and coarse particles [10]. The physical limitations of the diameter and the particle size relation means that there is a upper limit to the capacity of this configuration of around 500 kg h^{-1} [10].
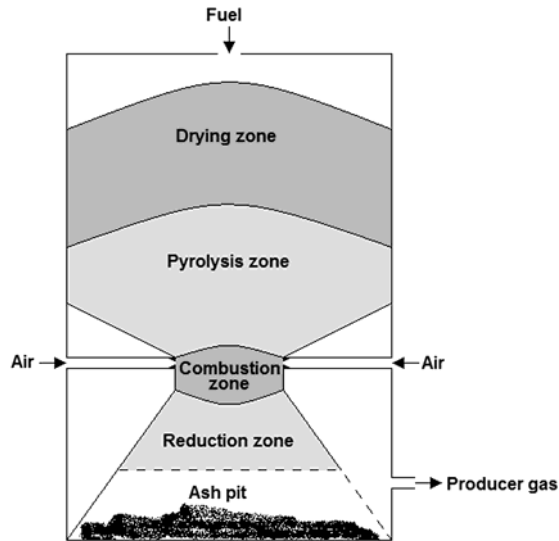
Figure 2-1 schematic representation of a downdraft gasifier [9]

Updraft gasifiers

The updraft gasifier is a counter-current reactor, where the fuel and the gasification agent move in opposite directions. In Figure 2-2, a schematic representation of an updraft gasifier is given.
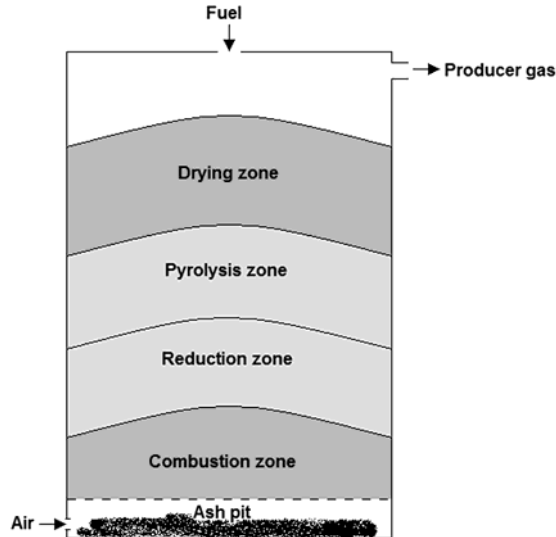
Figure 2-2 schematic representation of a updraft gasifier [9]

In the updraft gasifier, the biomass is dried by the hot producer gas, in the drying zone. Further down in the bed the biomass is pyrolyzed, the resulting char moves further down in the bed. The tars and gasses follow the updraft in the reactor. Part of the tars will condense

on the solid particles in the bed; the residual tars will remain in the gas and leave the reactor. The char slowly descent down towards the combustion zone where it will be gasified. The gas produced in an updraft gasifier has relatively high tar content and hydro-carbon content, which leads to relatively high heating value of the gas. This producer gas needs significant cleaning before it can be processed further.

Cross-draft gasifiers

In a cross-draft gasifier the fuel and gasification agent move perpendicular of each other. In Figure 2-3, a schematic representation of a cross-draft gasifier is given.
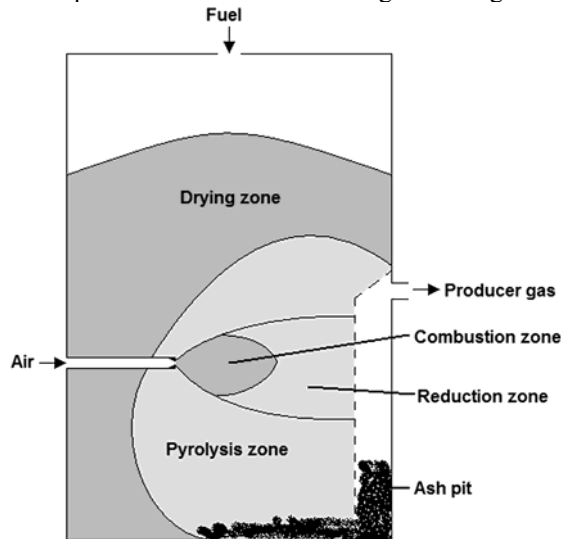
Figure 2-3 schematic representation of a cross-draft gasifier [9]

The cross-draft gasifer is only suitable for the gasification of charcoal. The temperatures in the combustion zone can rise to 1500°C. The construction material of the reactor has to withstand the high temperature in the reactor. As the updraft gasifier, the cross-draft gasifier has a low tar conversion. Therefore, a high quality charcoal has to be used.

2.1.2. Fluidized bed gasification

Fluidized bed gasifiers come in many forms. In general, fluidized bed gasifiers are designed for mid-scale thermal capacities of 10 MW_{th} to large scale capacities of 100 MW_{th} and higher. A inert or catalytic bed material is used to transport heat and mass through the reactor. The bed is fluidized by blowing the gasification agent through the bed, which lifts the bed against gravity. As a results, the turbulence in the bed creates an even temperature distribution in the bed. Therefore, there are no different reaction zones in the bed as in the fixed bed gasifiers. The operating window of a fluidized bed is usually at a temperature of 700-900°C and at an over pressure between 0 and 70 bar. Due to the operating temperature, bed sintering is common problem when a biomass with a high ash content is used. The alkali components in the ash have the tendency to form low-melting eutectics with silica being the most common bed material. These eutectics cause bed agglomeration and bed sintering, which can lead to loss of fluidization. The most common types of fluidized beds are the bubbling fluidized bed (BFB) and the circulating fluidized bed (CFB).

Bubbling fluidized bed

In a bubbling fluidized bed, the gasification agent is blown through the bed in such a way that it forms bubbles in the bed. The gas velocity is above the minimal fluidization velocity and below the maximal settling velocity. Therefore, the bed material remains in the reactor. In Figure 2-4, a schematic representation of a BFB is given.

In the BFB, most of the gasification reactions take place in the fluidized bed. Some reactions, especially, the thermal cracking reactions and the gasification of entrained small particles continue in the freeboard. The carbon conversion in the process is nearly 100%, due to the high residence time of the biomass particles and the residual conversion when entrained to the freeboard. The tar content of the gas is in between the tar content of the downdraft and updraft gasifiers.
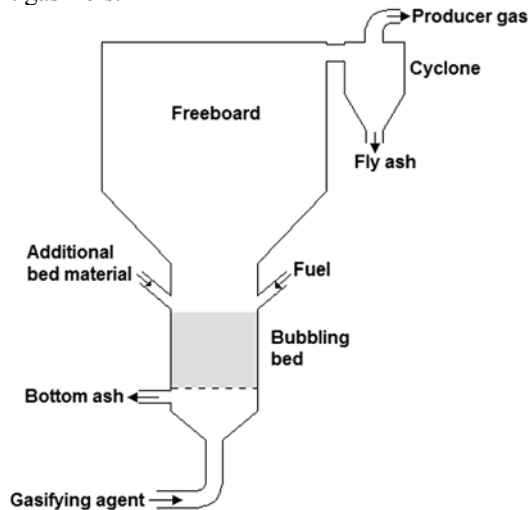
Figure 2-4 schematic representation of a BFB

An example of a BFB, is a gasification process, developed by the Institute of Gas Technology (IGT). This is a pressurized direct oxygen fired gasifier, operating at a temperature of 920°C and a pressure of 25 bar. The gasification agent in this process is a mixture of steam and oxygen entering the process at a temperature of 240°C and a pressure of 25 bar. The used bed material is aluminia (Al_2O_3). In Table 2-1, the dry composition of the producer gas is given. The producer gas leaves the reactor at approximately at 920°C.

Circulating fluidized bed

In a circulating fluidized bed, the gasification agent is blown with such a velocity that large amounts of the solids are entrained with the product gas. The entrained solids are separated from the gas in a cyclone and recycled back to the gasifier. In Figure 2-5, a schematic representation of a CFB is given.

The CFB has a high carbon conversion efficiency, because of the recycling of the bed material. The producer gas coming from a CFB has a relatively high dust content. Some examples of CFB's are the gasifier located at Värnamo (Sweden) [11] and the gasifier at the Amer power plant in Geertruidenberg (The Netherlands) [12].

The Värnamo gasifier is a pressurized air blown gasifier, with a capacity of 18 MW$_{th}$. Wood is used as the fuel for this process. The gasifier is developed in cooperation of Sydkraft AB and Foster Wheeler Energy International Inc. This gasifier is used in an

integrated gasification combined cycle (IGCC). The whole plant produces 6 MW_e and 9 MW_{th}, the latter is supplied to a district heating system. The district heating system supplies the produced heat to the city of Värnamo.
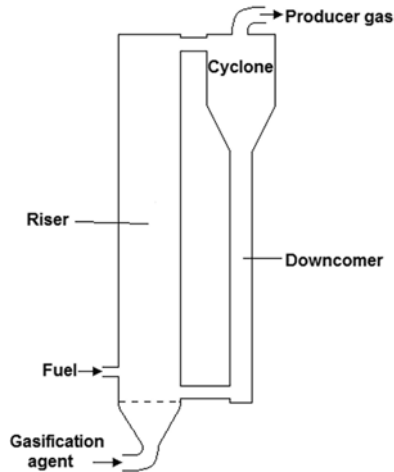
Figure 2-5 schematic representation of a CFB

The wood entering the gasifier, is already dried in a fuel processing plant. The resulting moisture content of the wood is between 5 and 20 %. Fuel is fed to the gasifier via a lock hopper system, which makes it possible to feed the fuel at the operating pressure. The gasifier operates at a temperature of around 950-1000°C and a pressure of 18 bar. All the parts of the gasifier are refractory lined. Air is used as gasification agent; this air is extracted from the air compressor of the gas turbine system of the plant. In Table 2-1, the dry composition of the producer gas is given. The tar level in the producer gas is below 5 mg Nm^{-3} [11]. The alkali levels are found to be below 0.1 ppm on weight basis [11]. Different bed materials have been investigated. Most of the time, the used bed material was magnecite [13].
This gasifier is also used as a pressurized oxygen blown gasifier. In this way the produced gas is virtually nitrogen free.

The gasifier at the Amer power plant is an air blown atmospheric gasifier. This design is originated from the Lurgi gasifier. It is completely refractory lined. The capacity of the biomass feed is approximately 84 MW_{th} (6 kg s^{-1}) and the fuel is demolition wood with a moisture content of less than 20 %. This gasifier operates at a temperature of 820-880°C and atmospheric pressure. The bed material is quartz sand. The produced gas is cleaned and then used as fuel for the coal fired boiler (Amer 9) of the power plant [14]. In Table 2-1, the dry composition of the producer is given.

Other fluidized beds

Besides the BFB and the CFB there are also designs of gasification installations which uses multiple coupled beds. Examples of these processes are the Battelle gasification process and the Fast Internal Circulating Fluidized Bed (FICFB). These processes are also known as indirect gasification processes, because the heat required for the gasification reactions is produced in a separate reactor.

The Battelle gasification process is developed by Battelle's Columbus Laboratory and is owned by Future Energy Resources Corporation (FERCO). The process consists of two coupled CFBs. In Figure 2-6, a schematic drawing is given of the Battelle gasifier.
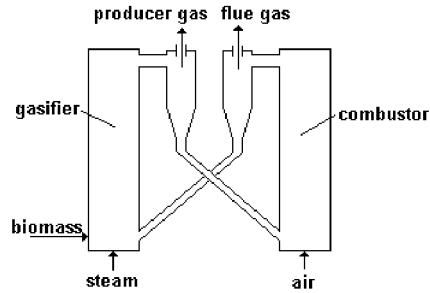
Figure 2-6 schematic drawing of the Battelle gasifier

The biomass is gasified in the gasifier part of the reactor with steam. The char formed in the gasification process is separated together with the bed material in a cyclone. These solids are led to the second CFB which functions as a combustor. The heat produced during the combustion of the char is transported to the gasifier with the bed material. The gasification section of the process operates at a temperature of 820°C; the combustor operates at a temperature of 1050°C. The whole system operates at atmospheric pressure. The bed material used in this process is sand. Extra fuel is added to the combustor to maintain the high operating temperature. By separating the heat production from the gasification, air can be used for the combustion reactions without having a nitrogen diluted producer gas. The dry composition of the producer gas for the Battelle gasifier is given in Table 2-1. The tar concentrations in the producer gas are around the 16 g m^{-3} [15].
A demonstration plant of this gasification technology is build at the Burlington Electric Department's McNiel power station. The capacity of the gasifier is 182 dry tonnes of wood per day [16].

The FICFB is also a combination of two fluidized beds. A BFB is coupled with a CFB, as indicated in Figure 2-7.
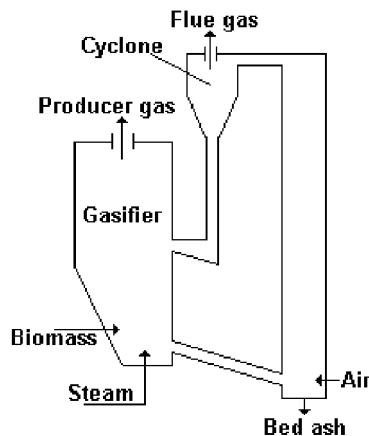
Figure 2-7 schematic representation of the FICFB gasifier

The BFB is used for the gasification process and the CFB is used for the combustion of the char and heat supply to the process. The gasification agent in this process is steam; air is used for the combustion part of the process. The biomass enters the BFB and is gasified with steam. The char which is formed during the gasification process moves together with the bed material to the combustion section. In combustion section the char is combusted with air. The hot flue gas is separated from the hot bed material in cyclone. This hot bed material is recycled to the gasification section of the process.

In Güssing (Austria) is a demonstration plant of 8 MW_{th} based on this technology. The process is fuelled with wood. The dry composition of the producer gas of this plant is given in Table 2-1. The operating temperature of gasification section is around 800-900°C and the operating temperature of the combustor around 1050°C. The operating pressure is atmospheric. As bed material, olivine $((MgFe)_2SiO_4)$, is used. The tar content of the producer gas is around 0.5-15 g Nm^{-3}; the sulphur content is around 20-50 ppm and the amount of particles in the gas is 10-20 g Nm^{-3} [17].

The gasifier in Güssing is coupled to a gas engine, for the cogeneration of heat and power. The overall system produces 2 MW of electricity and 4.5 MW of heat for district heating [17].

Table 2-1 dry composition of producer gas from different fluidized bed gasifiers in vol%

Component	IGT [18]	Värnamo [11]	Battelle [19]	FICFB [17]	Amer [12]
Hydrogen (H_2)	46.2	9.5-12	16.7	30-40	15
Carbon monoxide (CO)	22.1	16-19	37.1	20-30	18
Methane (CH_4)	0.9	5.8-7.5	12.6	8-12	5
Carbon dioxide (CO_2)	30.8	14.4-17.5	8.9	15-25	20
Nitrogen (N_2)	0.0	48-52	0.0	1-5	41

2.1.3. Entrained flow gasification

Entrained flow gasifiers are, in general, for thermal capacities of 100 MW_{th} up to 1000MW_{th}. In these type of gasifiers, the fuel is gasified at high temperatures ranging between 1300°C and 1500°C and pressures ranging from 20 bar to 50 bar. The high temperatures result in a producer gas which is low on tars and hydrocarbons, but also require oxygen as an oxidant. In an entrained flow gasifier is the fuel transported into the reactor by entrainment in a gasification medium. Therefore, the entrained flow gasifier can only handle liquid fuels or solid fuels with sizes typically smaller than 100 μm. Pre-treatment of the fuel is therefore always necessary. Pre-treatment can be extremely difficult with biomass, due to its fibrous nature.

The fuel and gasification agent are fed to the burner of the gasifier. The burners of an entrained flow gasifier are designed to create strong mixing of reactants, in order to achieve high temperatures and fast gasification. In Figure 2-8, a schematic representation is given for an entrained flow gasifier.

Two different types of entrained flow gasifiers can be distinguished; the slagging gasifier and the non-slagging gasifier.
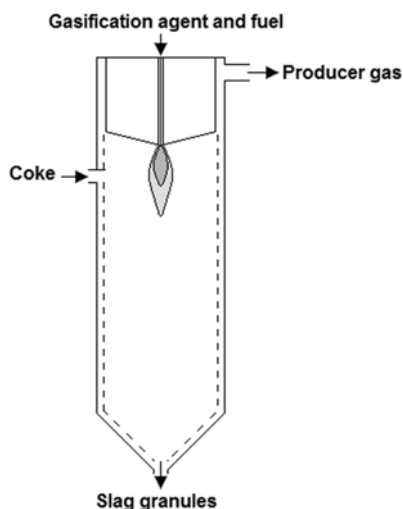
Figure 2-8 schematic representation of an entrained flow gasifier

In a slagging entrained flow gasifier, the minerals and ash components of the fuel melt inside the reactor. The molten ash and mineral condense on the relative cold reactor wall and create a layer of liquid-solid ash. The ash layer at the wall side is solid and at the gasification side liquid. This forms a protective layer for the reactor between the wall and the hot reaction zone. The layer slowly flows down to the bottom of the reactor where it is removed. To ensure the ash layer has the right properties, like viscosity, mineral additives are added to the fuel.

Non-slagging entrained flow gasifiers do not form such an ash layer. This type of reactor requires fuels with a low ash and mineral content. The maximal ash content is then usually around 1 wt%.

2.1.4. Hydrothermal gasification

Hydrothermal gasification is a promising new gasification technology, but it is still under development. Some small demonstration setups have been built, but large scale systems still have to be developed. The reactions take place at temperatures of 400-700°C and a pressure above 25 MPa. Because of these conditions, the demands on the materials and reactor design are high. There are also other difficulties which have to be overcome, like reactor blockage, catalytic poisoning and corrosion. These difficulties are due to nature of the reaction products in super critical water.

Several different reactor designs have been suggested. Elliott and co-workers [20] demonstrated successfully the continuous gasification of biomass to methane rich product gas in a catalyst packed bed. Initially problems occurred by blockage of the packed catalyst bed during the process. This is solved by adding a liquefaction reactor before the gasifier [20, 21]. This system worked well but poisoning of the catalyst was observed.

Nakamura et al. [22] gasified chicken manure in an experimental pilot plant. They used suspended carbon catalyst in the chicken manure instead of a packed bed of catalyst which could get plugged. In this plant (see Figure 2-9), the chicken manure and catalyst mixture is heated in a heat exchanger. Then the mixture enters the heated "liquidizing reactor", in which the biomass is converted into oil. After the reactor, the liquid is cooled in a heat exchanger and then pressurized to 25 MPa. The pressurized mixture is further heated in heat exchanger and a heater before it enters the gasification reactor. The reaction

temperature is 600°C. The product mixture is cooled to normal conditions in a heat exchanger and a cooler. After the cooling, the pressure is released and the mixture is separated in a gas phase and a liquid phase. Heat is supplied to the heater and the gasifier by propane burners.
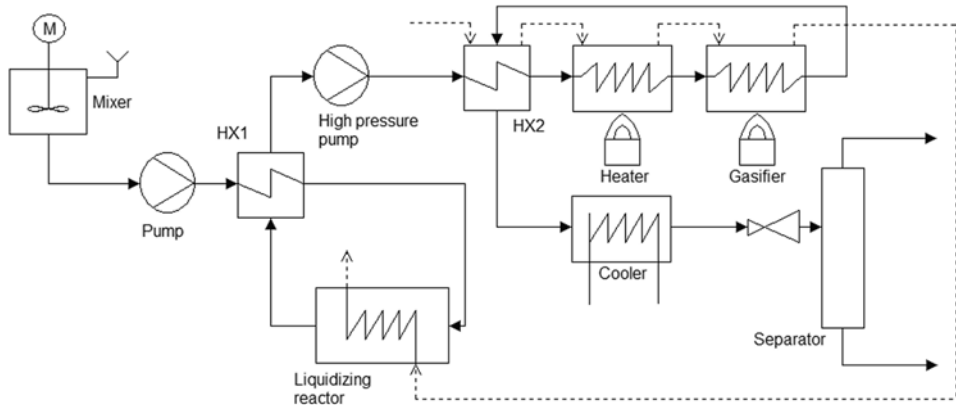
Figure 2-9 scheme of the pilot plant for the gasification of a biomass catalyst suspension (Adapted from [22])

At the Karlsruhe Research Centre, Germany, the largest plant for hydrothermal biomass gasification was build [8]. This test facility is called VERENA and is designed for 700°C and a maximum pressure of 35 MPa [8]. In this system the biomass is crushed and then mixed with water to adjust the water content of the mixture. Next, the mixture is pressurized. After pressurization, the mixture is heated in a heat exchanger and in a so-called pre-heater. This pre-heater uses hot flue gasses from a propane burner. Then the mixture is fed to the gasifier, which is also heated with hot flue gasses coming form a propane burner. The gasifier is a vessel where the reaction takes place. After the gasification the product mixture is cooled in the heat exchanger and a subsequent cooler. Large part of the gas is separated from the liquid under pressure. In order to keep the carbon dioxide dissolved in the aqueous phase. After that, the product gas is scrubbed in order to remove even more CO_2. This system does not use any catalyst. In Figure 2-10, a scheme of the VERENA pilot plant is given.

Matsumura and Minowa [23] suggested a fluidized bed design for supercritical water gasification of biomass. In their fundamental study they found that bubbling fluidized bed is the best option for supercritical water gasification of biomass. In this design it was possible to obtain long enough residence time for the conversion of biomass.
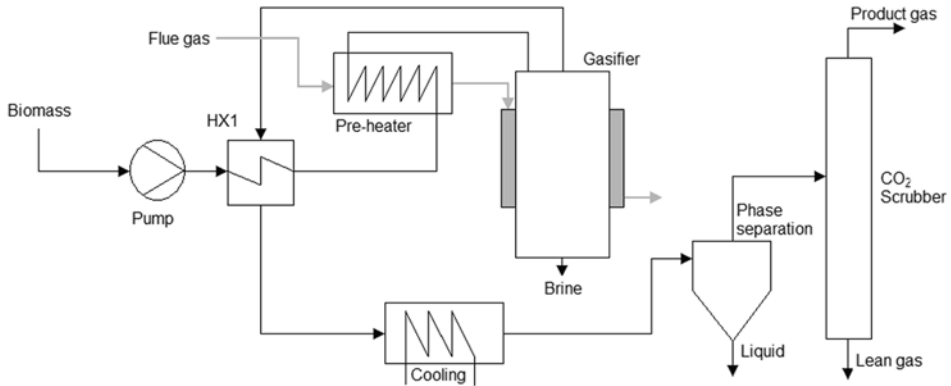
Figure 2-10 scheme of VERENA demonstration plant[8]

2.1.5. Biomass gasification modelling

In system studies it is important to have a model which predicts the reaction products and thermodynamic performance. This model should be relatively simple, since little information is available. To types of models are available for biomass gasification: thermodynamic equilibrium and kinetic rate models. Kinetic rate models are based on the conversion rates of the different reactions occurring in the process. In biomass gasification, the number of reactions taking place is very large. Most kinetic rate models contain design specific parameters or relations, which makes them hardly applicable for different gasification process designs [24]. Usually the number of required input parameters is large. Thermodynamic equilibrium models are design independent and therefore more convenient in system studies.

When calculating the synthesis gas composition from a fluidized bed with an equilibrium model, the amounts of hydrogen, carbon monoxide and water are overestimated, while the amount of methane is underestimated [25]. By using a correction method on the equilibrium model, a "quasi"-equilibrium model is created. In literature, several different approaches are indicated. One method is to introduce a correction factor in the equilibrium calculations, as indicated in the work of Li et al [26]. This method is usually only possible when the source code is accessible or when user defined functions can be applied. This is often not the case when using commercial flow sheeting programs like Aspen Plus[27] or Cycle-Tempo[28]. Then another method has to be used, which corrects the equilibrium model. One of those methods is the use of multiple reactor units to create a "quasi'-equilibrium model. Panopoulos [29] indicates a method for quasi equilibrium modelling of catalytic FB biomass gasification in Aspen Plus using three different reactors and a by-pass. The first reactor is to split the biomass into its elements. The second reactor is used to convert some of the carbon and hydrogen into methane and tars. In this case tar is modelled as naphthalene. The unconverted elements are led to an equilibrium reactor where the other gas compounds are formed. There is also a carbon by-pass to simulate the char formation. Altafini et al. [30] demonstrates that complicated systems of equilibrium models are required for the modelling of the non-equilibrium process of biomass gasification. Several models are shown for the calculation of the final composition and heating value of the syn-gas produced in a gasifier. All the models use multiple equilibrium gasifier models with by-

passes of gasses between the two gasifier models. A basis for the Cycle-Tempo models of Altafini et al. [30] is the work of Elmegaard and Korving [31].
In this thesis, the fluidized bed gasification is modelled as a system of equilibrium models. The models consists two equilibrium models in series with a bypass over the second equilibrium model. The equilibrium conditions and by-pass are set in such way that the output composition of the model matches the composition of the gasifer found in literature. In this way the mass and energy balances can be closed and the thermodynamic performance of the gasifier can be determined. An example of the system of the two equilibrium models is indicated in Figure 2-11.
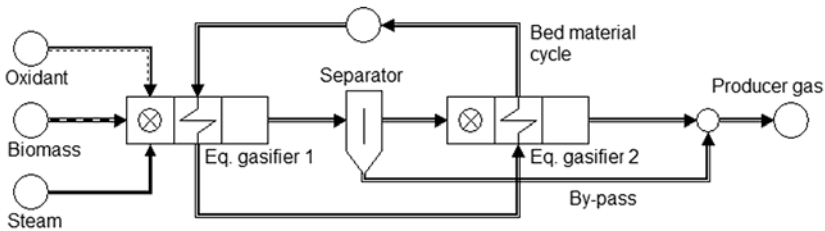
Figure 2-11 example of a fluidized bed gasifier model in Cycle-Tempo

Most of the impurities formed during the gasification, like tars and alkali metal compounds, are not modelled in these equilibrium models. Since the amount of these compounds is relatively low, these compounds are negligible in most cases and hardly influence the thermodynamic performance of the process. In this thesis, mostly wood is used as a fuel. For this fuel, the concentrations of formed tars and alkali metal compounds are very low and are therefore neglected.
The modelling of hydrothermal gasification on the other hand is performed by thermodynamic equilibrium calculations. In hydrothermal gasification, the products are close to chemical equilibrium and the model gives good overall predictions for the gas composition [32, 33].

2.2. Gas cleaning and processing

As indicated in the previous section, hydrogen rich gas is produced in the biomass gasification process. The gas also contains several impurities, like: particulates, tars, sulphur compounds, halogen compounds, and alkali metal compounds. These impurities need to be removed before the gas can be used or further processed, since these impurities have a deteriorating effect on all kinds of processes and systems, in particular on fuel cells. The systems which remove these impurities are called gas cleaning systems.
If hydrogen should be the final product, the required hydrogen quality is determining the necessary processing. The different gas processing steps are methane reforming, water gas shift, methanation, and preferred oxidation. Several processes to purify the hydrogen are possible. The latter are processes for the production of pure hydrogen.
In this section different systems are discussed for the gas cleaning, gas processing, and hydrogen purification. All these processes can be applied in biomass gasification systems, depending on the gas requirements.
First the different gas cleaning systems are being discussed, which are divided into different steps. The discussed steps are particles removal, tar removal, halides removal, alkali removal, and sulphur removal. Then the gas upgrading processes are discussed, starting with steam reforming followed by the water gas shift process. Then the preferential

oxidation process and the methanation process are discussed. The final processing systems are carbon capture processes. After the gas processing systems, the processes of hydrogen purification are being discussed. This involves adsorption processes, cryogenic separation processes, and membrane separation processes.

2.2.1. Gas cleaning

In this section, several gas cleaning techniques are discussed. Gas cleaning involves the removal of particulates, tars, alkali compounds, halides and sulphur compounds. The different techniques are categorized by impurity, starting with particulates. Following the particle removal techniques, subsequently tar, halide, alkali and sulphur removal techniques are discussed. Finally, some general considerations are given.

Particulate removal

The particulates coming from the gasification process are materials coming from the bed material, unconverted biomass, ashes, char, solidified substances or impurities in the feed stock. These solids need to be removed from the producer gas, because the solids can have an adverse effect on the down stream equipment, by deposition, blocking or agglomeration. In the following sections different pieces of equipment will be discussed for the removal of particulates from the producer gas.

Cyclones

Cyclones are designed for the removal of solids from liquids or gasses. In Figure 2-12, schematic drawings of cyclones are given.
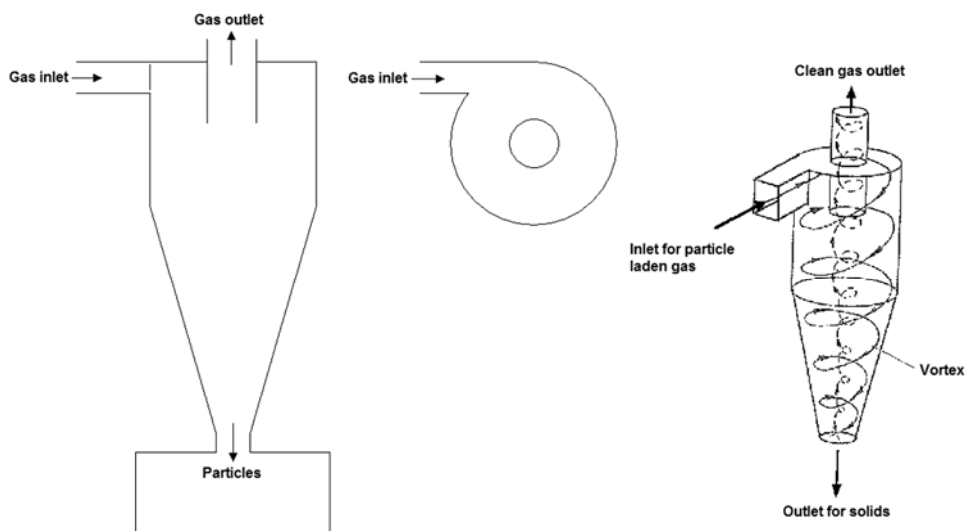
Figure 2-12 schematic drawings of a cyclone [34]

The working principle is based on centrifugal forces. The gas entering the cyclone is transformed into a confined vortex. The centrifugal forces from this vortex tend to force suspended particles towards the wall of the cyclone. The particles leave the cyclone at the bottom and the gas leaves the cyclone at the top. Cyclones are most often used to remove the bulk of the solids from the producer gas [35, 36]. Particles from gas as small as 1 μm can be removed by cyclones [37]. These kinds of cyclones, so-called high efficiency

cyclones, can remove more then 99% of the dust and 95% of the particle >10 μm [35]. The residual particulate levels in the gas are around 5-30 g/m^3 [10]. The smaller particles (< 5-10 μm) can still have an adverse effect on the down stream equipment.

Cyclones have a simple design, and they do not contain any moving parts. The cyclones can be used continuously and over a wide range of temperatures. These separators are often used in combination with other particle separation techniques.

Barrier filters

The working principle of a barrier filter is simple. A porous material allows the passage of gasses but it prevents the passage of particulates. The major separation effect comes from the filter cake. These types of filters can effectively remove particulates in the range of 0.5-100 μm in diameter from a gas stream [36]. There are a few different types of barrier filters, like: the rigid cross flow filter, the bag filter, and the packed bed filter. All these different types will be discussed separately in the following paragraphs.

The rigid cross flow filter is often also referred to as hot gas filter (works also well at low temperatures). The pressure drop across such a filter is not constant. The thickness of the filter cake plays an important role in the pressure drop. Such filters can have an efficiency of >99.8% [10]. Clogging due to soot formation and tar adhesion to the ash/char particle is a problem [38]. This type of filter can be operated continuously by removing the filter cake by back pulsing. Back pulsing is the method which uses a high pressure gas to dislodge the ash cake from the filter surface [39]. The gas used for this purpose is often nitrogen. The rigid barrier filters consists of arrays of candle shaped elements.

There are two main material types used to construct these filters. The first material is sintered ceramics and the second is sintered metal.

The ceramic filters are usually constructed from clay bonded silicon carbide (SiC) [37]. The main body of the filter is made of course ground silicon carbide, while the outside is surrounded by a thin layer of either fine-ground silicon carbide or alumino-silicate. This outer layer performs the filtering duties [37]. These filters are capable of operating at high temperatures (up to 1000°C). Ceramic filters are brittle and susceptible to breaking due to (thermal) stresses. This was experienced during operation of the biomass integrated gasification combined cycle (BIGCC) in Värnamo [13].

The metal filters are constructed of sintered metal particles. These metal filters have a good mechanical strength under constant and transient load; they perform well at high temperatures up to 1000°C. Metal filters are resistant to the corrosion under typical gasification conditions [37].

Bagfilters are made from a woven material; there is a wide range of materials available. Bagfilters have a maximum operation temperature of about 250°C depending on the material of the bag. This low operation temperature can lead to problems when combined with a gasification system, due to tar and alkali condensation on the filter. These tars and alkalis can form a sticky layer on the filter, resulting in clogging of the filter. These filters can also be cleaned by pack-pulsing. It is also possible to clean the filter by vibrating it [40].

Packed bed filters are also known as granular bed filters. These type of filters are basically large bins containing a granular material through which a gas stream is forced [37]. The bed material is often limestone or alumina. These beds can either be static or moving.

In static beds the particles impact and adhere to the granules, leading to eventual clogging of the void spaces in the bed. The pressure drop increases over the bed and the bed needs to

be cleaned. The cleaning is done by reversing the flow through the bed. The filtering process is interrupted during the cleaning process.

Moving bed filters do not have to be interrupted for cleaning. In this filter the filtering granules move downwards, while the dirty gas stream is moving upwards or in cross flow. The collection efficiency can be greater than 99% for particles greater than 4 μm. The granular bed filter can operate at a wide range of temperatures. It can also be possible to combine the filtering with chemical processing, by adding a catalyst to the granules. Hustad et al. [41] proposed a new design for a granular bed filter in the form of a granular panel bed filter. This filter could be cleaned by back pulse cleaning. Hustad et al. [41] tested also the application of tar cracking catalyst as bed medium, which was successful.

Quench/Scrubber

Quenching or scrubbing can also contribute to the removal of particulates from a gas stream. This removal of particulates is often not primary goal of such a type of system. Usually these systems are used to remove tars, alkalis and halogens. Water condenses on the particulates, which results in an increase in size. This size increase makes the particles more susceptible to agglomeration and coalescence. In this way the particle can easily be removed from the gas stream. The operation temperature is usually low, it depends on the pressure. Usually particles down to 0.5 μm can be removed [40].

Venturi and orifice scrubbers are simple devices. The turbulence created by the venturi or orifice is used to atomise water sprays and promote contact between the liquid droplets and dust particles. The agglomerated particles of dust and liquid are then collected in a centrifugal separator, usually a cyclone [40].

Electrostatic precipitator (ESP)

The gas entering the ESP is ionised by a corona discharge. This is created by a high voltage electrode. The dust particles in the gas become charged and are attracted to the grounded electrode. The collected dust is often removed by vibrating or by washing.

Electrostatic precipitators are capable of collecting very fine particles, < 2 μm, at high efficiencies [40]. The capital and operating costs of the EPS are high.

In Table 2-2 an overview of the different particle removal systems is given together with some typical operation values.

Table 2-2 overview of particle removal systems

Technique	Efficiency	Pressure drop	Operation temperature	Power consumption
Cyclone (high eff.)	95-99%	500-2000 Pa	<1200	low
Rigid backflow filter	>99.8%	20 kPa	<1000	low
Bagfilter	>99%	20 kPa	<250	low
Packed bed filter	99%	500-1500 Pa	<1000	low
Scrubber	95%	0.2-20 kPa	<100	0.2-6 kWh 1000m^{-3}
ESP	>99%	<500 Pa	<1200	high

Tar removal

Tar is a wide variety of organic compounds resulting from the pyrolysis of biomass during the gasification process. All the organic compounds heavier than benzene are referred to as tars. The tars, in gaseous or aerosol form in the producer gas, are coming from the gasifier. These substances will condense and deposit on all kinds of surfaces when the gas is cooled.

The composition of the tars depends on the conditions in the gasifier and on the residence time of the gasses in the reactor, also known as reaction severity [42]. In general there are four types of tars distinguished [36, 43, 44]:

1. Primary tars: characterized by cellulose derived products, hemi-cellulose derived products and lignin derived products.
2. Secondary tars: characterized by phenolics and olefins.
3. Alkyl tertiary tars: include methyl derivatives of aromatics.
4. Condensed tertiary tars: poly aromatic hydrocarbons without substituents.

The more severe the reaction, the more tertiary tars are formed, but the total amount of tars reduces. Some of these tars may partly react to give soot which can have a negative effect on some pieces of equipment [10].

There are three main types of removal available: physical removal, thermal cracking, and catalytic cracking [37].

Physical removal

In physical removal the tars are removed from the gas by either cooling and scrubbing or absorption. In cooling, the tars condense and are then collected. Several techniques are available for these methods of removal. These techniques are discussed in the following sections.

Cooling/Scrubbing towers

Before the gas can be scrubbed with water, it needs to be cooled to approximately 120°C. The cooling results in the condensation of the alkali compounds and tars. This condensation will be mainly on the solid particles in gas and on the cool surfaces, if available [10]. After cooling, the gas enters the scrubber. In the scrubber, water is sprayed in the continuous gas phase. The water condenses on the particles and droplets in the gas, which results in an increase of size of the particles and droplets. This makes the particles and droplets more susceptible for coalescence and agglomeration. The large particles and droplets are collected in centrifugal separator [40].

Besides water also other scrubbing fluids are possible, like organic compounds. For instance, the biomass gasification plant in Güssing is using rape oil methyl ester as a scrubbing fluid [45]. The organic compounds in the tars easily dissolve in the scrubbing fluid, which makes the removal of tars very effective.

Demisters

This type of equipment is specially designed for the coalescence of mist droplets in gas streams. They usually resemble packets of woven wire, cyclones and hydro-cyclones. This type of equipment is commonly used after the cooling of the bio syn-gas or after a scrubber. Or it is already included in a scrubber. The cooling of bio syn-gas results in the condensation of the tars, which forms a mist. This mist consists of small droplets of tars entrained in the gas. Centrifugal forces are used to coalescence the droplet entrained in the gas. The droplets are separated in a similar way as the solids in a normal cyclone.

There is a new type of cyclone being developed, called the condensing cyclone. This type of cyclone can be used as a condenser in a steam cycle [46]. The wall of the cyclone is cooled, which causes the condensation of gasses at the wall of the cyclone. This liquid is collected in the same way as the solids. This could be a promising option for the removal of tars and alkalis from producer gas. But further research is necessary, since the fouling effects are not known.

Wet electrostatic precipitator

In a wet electrostatic precipitator the gas is ionised upon passing between a high voltage electrode and an earthed (grounded) electrode. The ions are formed in a corona discharge and attach themselves to dust particles or droplets of tar and water. Particles and droplets become charged and are attracted to the grounded electrode due to the electric field. The precipitated dust and droplets flow to the bottom of the ESP where they are removed. The gas needs to be quenched, before a wet ESP is able to remove the tars from the gas. A wet ESP is similar to a dry ESP, but the collection plates are being flushed with a liquid, usually water. In Figure 2-13, the working principle of the ESP is given.

A dry ESP cannot be used for this purpose, because the tars droplets will then form a sticky layer on the collector plate, which is very hard to remove and prohibits the removal of particles [43]. The removal of tar mist can be done with efficiencies of 99% with a wet ESP in spite of the fact that a substantial amount of the tar mist exists as sub-μm particles [35].
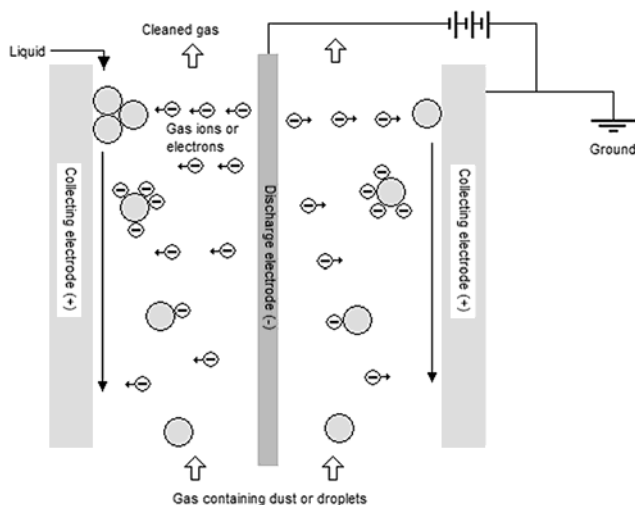
Figure 2-13 working principle of the ESP

Granular beds

Granular bed filters can either be used at high or low temperature. High temperature filtration has the disadvantage the tars stay in the gas phase, so very little tars will be removed. By using activated carbon some of the tars can be absorbed. This principle operates at a temperature of <300°C.

The use of filters is preferred at low temperature, because of the condensation of tars leading to an easier separation by means of a granular filter. The following materials commonly used are: silica, alumina, and sawdust. An advantage of using sawdust is that it can be gasified. The efficiency for the separation of tar with a granular bed filter is found to be 60%-95% [43].

Thermal cracking

In the thermal cracking process, tars are decomposed at a high temperature (>>1000°C). Because of refractory nature of the tars from biomass, high temperatures and high residence times are necessary. The temperature required, depends on the nature of the tars.

Oxygenated tars may require 900°C as more refractory tars need temperatures above 1200°C [36]. During the decomposition, not only gaseous products are formed, but also soot. Soot can have a deteriorating effect on down stream equipment and processes, because of fouling. The high temperatures can cause melting and creep problems. Therefore, more expensive construction materials for the reactor are needed. To improve the thermal cracking process air or oxygen can be added to the gas stream in order to promote partial oxidation of the tars. This will increase the CO_2 level of the gas.

Catalytic cracking

Catalytic cracking of tars can be done in the gasifier (primary removal) or in a separate reactor (secondary removal). This separate reactor could also be a hot gas filter, which is coated with a catalytic layer. Two different types of catalyst are being used, metallic catalysts and non-metallic catalysts. The metal catalyst are usually nickel-based, the non-metallic catalysts are often based on dolomite. The reactions take place at a temperature of about 800-900°C. The tar cracking in the separate reactor is more effective than the in-situ tar cracking. In in-situ tar cracking, the catalyst gets easily deactivated by coking and it is susceptible for attrition [43]. The conversion efficiency of the separate tar cracker can be as high as 99% [10]. This results in additional production of hydrogen and other gaseous components. The catalysts, especially the metal catalysts, are susceptible to poisons, like sulphur. Also deactivation by carbon formation is possible.

Table 2-3 overview of tar removal processes

Technique	Efficiency	Pressure drop	Operation temperature	Power consumption
Scrubber + demister	90%	0.2-20 kPa	60°C	0.2-6 kWh 1000m^{-3}
ESP	99%	<500 Pa	<1200°C	high
Granular bed	60-95%	500-1500 Pa	<1200°C	unknown
Thermal cracking	>50%	500-1500 Pa	>1200°C	unknown
Catalytic cracking	99%	500-1500 Pa	800-900°C	unknown

Halides removal

Halide compounds, like HCl & HF, form during the gasification process. These compounds are acidic, which can cause corrosion in the downstream equipment. They can also act as a poison for some catalysts and sorbents, for instance ZnO. The amount of halide compounds released depends on the type of biomass used, is usually in small quantities. There are typically three ways to remove halide compounds from the gas, i.e.
- Wet scrubbing
- Injection of a sorbent into the gasifier to form salts that can be removed by the particulate removal
- Removal by sorbents in a separate reactor

The wet scrubbing is discussed in the sections about particle removal and tar removal.

Sorbent injection can be done, either in the gasifier, or just after the gasifier. The halide compounds react with the sorbent compound to form a salt, which can be separated from the system by the particle removal system. Common sorbents used for this purpose are: Na_2CO_3, $CaCO_3$, $Ca(OH)_2$, and CaO. Some of these sorbents can lead to an increase of alkalis in the producer gas, which is undesirable.

Halide compounds can alternatively be removed by a separate reactor packed with a sorbent.

Several sorbents are possibly interesting: Na_2CO_3, $NaHCO_3$, $NaOH$, KOH, K_2CO_3, and $Ca(OH)_2$. Most of the sorbents are used at intermediate temperature (400-600°C).

Table 2-4 overview of halide compounds removal processes

Technique	Efficiency	Pressure drop	Operation temperature	Power consumption
Scrubber	99%	0.2-20 kPa	60°C	0.2-6 kWh 1000m^{-3}
Sorbent injection	99%	0	>500°C	Unknown
Adsorption	99%	500-1500 Pa	400-600°C	Unknown

Alkali removal

Biomass feed stocks may contain significant amounts of alkali compounds, mainly potassium and to a lesser extent sodium [44]. Although present at minor levels these compounds vaporize in most gasification processes, if the temperature is higher then 700°C. The alkali compounds also react with other inorganic constituents, like silica, sulphur and chlorine [47]. This results in unwanted deposits and corrosion. The alkali compounds also contribute to the formation of fluidized bed agglomerates.
There are several ways to remove the alkali compounds from the gas.
The easiest way to reduce the amount of alkali compounds in the producer gas is by temperature reduction. By lowering the temperature below 600°C most of the alkali compounds will condense on entrained particles [10]. The particles can than be removed by a particles removal system. The alkali compounds can also deposit on process equipment during cooling, which can lead to corrosion and fouling.
Another way to remove the alkali compounds from the producer gas is by water scrubbing, because the alkali compounds dissolve in water. The scrubbing process is already discussed in the sections about particle removal and tar removal.

It is also possible to use porous sorbents for the removal of alkali compounds from the producer gas, namely alkali getters. There are two ways of adsorption chemi-sorption and physi-sorption, both having their own advantages and disadvantages. In physi-sorption molecules are attracted by weak Van der Waal's forces. Molecules adsorbed in this way can relatively easily be desorbed or removed. In chemi-sorption the molecule is chemically bonded to the sorbent. This makes desorption or removal more difficult, because the bonding to the sorbent is much stronger. Irreversible chemi-sorption is sometimes preferable since it is less likely to release alkali if a gasifier is not at steady state, which results in transients in temperature or pressure [47]. Adsorption can occur either in the gasifier itself, if the sorbent is mixed with the bed material of the gasifier, or it can take place in a separate post-gasifier sorbent bed [37]. Several materials have been tested as alkali getters: activated bauxite, diatomaceous earth, kaoline, emanthlite [48], activated alumina, silica gel, and dolomite. Activated bauxite and activated alumina adsorb the alkalis via physi-sorption, the other adsorb the alkalis via chemi-sorption. Bauxite showed most promise [37]. Bauxite is composed of 80% Al_2O_3 and 10% SiO_2 along with a few impurities [49]. The regeneration of bauxite is relatively simple due to the physical adsorption of the alkalis. By applying boiling water to the bauxite it can be regenerated. The Al_2O_3 in the bauxite mainly causes the adsorption. Dou et al. [50] found that activated Al_2O_3 was the most effective alkali getter.

Sulphur removal

Biomass contains small amounts of sulphur, which are released in the producer gas, mainly in the form of hydrogen sulphide (H_2S). This sulphur compound can have an adverse effect

on downstream equipment, because of its corrosive effect on materials and poisonous effect on catalysts. The amount of hydrogen sulphide is low in the producer gas from biomass gasification, below 100 ppmv [51]. For most applications this amount is still too high, for instance (PEM) fuel cells and turbines have sulphur specifications of ca. 1 ppm [52]. Therefore, the removal of the hydrogen sulphide is necessary.

Hydrogen sulphide is soluble in water, so a large part can be removed during wet scrubbing of the producer gas. The wet scrubbing process is described in the particle removal section, as well as in the tar removal section.

A packed bed packed with a metal oxide, also known as a sulphur guard, is in most cases seen as sufficient for the removal of the hydrogen sulphide [52]. Most of these metal oxides are reusable. The following reactions are involved in the adsorption and regeneration:

$$MO_x + xH_2S \rightarrow MS_x + xH_2O \tag{2.8}$$

$$MS_x + \frac{3x}{2}O_2 \rightarrow MO_x + xSO_2 \tag{2.9}$$

Removal of hydrogen sulphide at elevated temperatures can be carried out by oxides of Fe, Zn, Mo, V, Ca, Sr, Ba, Co, Cu and W. [53]. ZnO is one of the most commonly used adsorbent in a sulphur guard, the operational temperature is around 400°C. Higher temperatures can cause the volatilization of the zinc [52, 53]. One promising sorbent is $(ZnO)_{0.8}TiO_2$, also known as zinc titanate, for application at temperatures above 500°C [52, 54]. Halogens should be removed from the gas, since they have an adverse effect on the sorbent.

Large scale hydrogen sulphide removal needs another process type. Most of these processes are solvent based. In general there are three types of systems: chemical systems, physical systems and a combination of chemical/physical systems. In most of these systems is also carbon dioxide absorbed by the solvent. These techniques based on solvents will be discussed in the section about carbon capture.

General considerations

If high temperature is not required, it is easier to use wet (low temperature) gas cleaning equipment, since this is based on proven concepts. If a high temperature is required then a high temperature system would reduce thermal losses, compared to a low temperature system. Also the sequence of the different cleaning steps is important. For instance, the chlorine removal has to be done before the sulphur removal to make sure the systems function correctly.

2.2.2.Gas processing

Gas processing involves the removal of CO or CO_2 and the conversion of CO or CH_4 into hydrogen and CO_2. Most processing systems increase the hydrogen content of the gas, for instance by steam reforming. Some systems are for the removal of a specific compound, for instance carbon capture for the removal of CO_2. In this chapter, the following processes are discussed: First steam reforming is treated followed by the water gas shift processes. Third and fourth the preferential oxidation and methanation processes are discussed. Finally carbon capture is treated.

Steam reforming

The producer gas coming from biomass gasification contains small amounts of light hydrocarbons, like methane and ethane. Steam reforming is the process to convert small

hydrocarbons into carbon monoxide and hydrogen as the following reactions indicate for methane:

$$CH_4 + H_2O \rightleftarrows CO + 3H_2 \qquad \Delta H_{298}^0 = 206 \text{ kJ mol}^{-1} \qquad\qquad (2.10)$$

$$CO + H_2O \rightleftarrows CO_2 + H_2 \qquad \Delta H_{298}^0 = -41 \text{ kJ mol}^{-1} \qquad\qquad (2.11)$$

$$CH_4 + 2H_2O \rightleftarrows CO_2 + 4H_2 \qquad \Delta H_{298}^0 = 165 \text{ kJ mol}^{-1} \qquad\qquad (2.12)$$
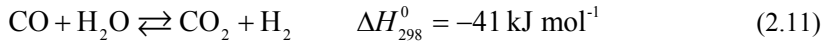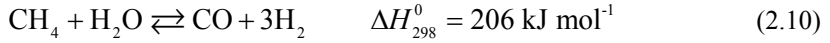
The water gas shift (reaction (2.11)) is also taking place during the reforming process. As can be seen from the reaction enthalpies given with the reactions (2.10) & (2.12), the steam reforming reaction is highly endothermic. The reforming reactions favour a high temperature and a low pressure. The water gas shift reaction (reaction (2.11)) on the other hand favours a low temperature and is unaffected by the pressure [55]. Reaction (2.12) is actually the sum of reactions (2.10) and (2.11). In Figure 2-14, the equilibrium composition for methane reforming is given for different temperatures and pressures.

For the steam reforming, a catalyst is used to enhance the reforming reaction. This catalyst is usually a group VIII metal, because methane is easily activated and oxidized by metals from this group. The most commonly used metal is nickel. In large industrial reforming processes the nickel is impregnated on a carrier, usually α-alumina. This catalyst is very sensitive to sulphur and chlorine poisoning. Therefore the gas needs to be virtually free from sulphur and chlorine. The catalyst also promotes coke formation, which has also an adverse effect on the process.

Coking is one of the processes, which can occur during the steam reforming process. The following reactions cause the coke formation, which is represented by carbon in the reactions.

$$CH_4 \rightleftarrows C + 2H_2 \qquad \Delta H_{298}^0 = 75 \text{ kJ mol}^{-1} \qquad\qquad (2.13)$$

$$2CO \rightleftarrows C + CO_2 \qquad \Delta H_{298}^0 = -173 \text{ kJ mol}^{-1} \qquad\qquad (2.14)$$

$$C_nH_m \rightleftarrows nC + \left(\frac{m}{2}\right)H_2 \qquad\qquad (2.15)$$
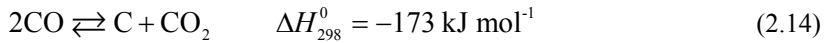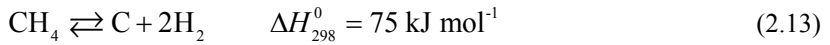
This coke formation can occur in two different ways; the first is the formation of an encapsulating layer of carbon around the catalyst. The second way is the formation of filaments or so-called whiskers. At temperature above 650°C, higher hydrocarbon may react in parallel with reaction (2.14) by thermal cracking into olefins, which form polymers and react further to form coke [57].

$$C_nH_m \rightarrow \text{olefins} \rightarrow \text{polymers} \rightarrow \text{coke} \qquad\qquad (2.16)$$
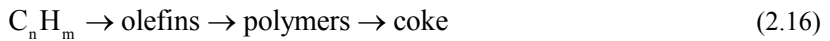
Reaction (2.16) results in pyrolytic carbon, which encapsulates the catalyst particle. This can cause catalyst deactivation, blockages in the reactor or hot spots [57].
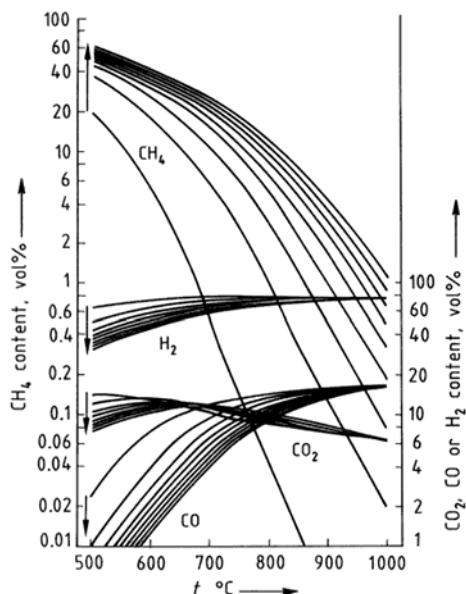
Figure 2-14 Equilibrium composition for methane reforming at 500-1000ºC and pressure (in the direction of the arrows) of 0.1, 0.5, 1, 1.5, 2, 2.5, 3, 3.5, 4 MPa. Molar steam:methane ratio 3.333. Adapted from Ullmann[56]

Reactions (2.13), (2.14) & (2.15) are catalysed by nickel. The carbon formed in these reactions grows as filaments. The carbon diffuses through the nickel particle and settles between the support and the nickel particle. This leads to the lifting of the nickel particle from the support [57, 58]. In order to reduce the coke formation steam needs to be added in excess. The minimum steam to carbon ratio is around 1.7 [55]. The addition of an excess amount of steam has also an advantage; steam promotes the steam reforming reaction.

It is also possible to reform methane with carbon dioxide. This process is often referred to as dry reforming. The reaction is given in reaction (2.17) [4].

$$CH_4 + CO_2 \rightleftarrows 2CO + 2H_2 \qquad \Delta H_{298}^0 = 247 \text{ kJ mol}^{-1} \tag{2.17}$$

Two types of steam reformer, autothermal steam reformers and allothermal steam reformers exist. In autothermal steam reformers air, enriched air or oxygen is added to partially oxidize the gas. This partial oxidation provides the energy needed for the endothermic steam reforming reactions. The following reactions occur during the partial oxidation:

$$CH_4 + 1/2\,O_2 \rightarrow CO + 2H_2 \qquad \Delta H_{298}^0 = -36 \text{ kJ mol}^{-1} \tag{2.18}$$

$$CH_4 + 2O_2 \rightarrow CO_2 + 2H_2O \qquad \Delta H_{298}^0 = -803 \text{ kJ mol}^{-1} \tag{2.19}$$

$$CO + 1/2\,O_2 \rightarrow CO_2 \qquad \Delta H_{298}^0 = -284 \text{ kJ mol}^{-1} \tag{2.20}$$

$$H_2 + 1/2\,O_2 \rightarrow H_2O \qquad \Delta H_{298}^0 = -242 \text{ kJ mol}^{-1} \tag{2.21}$$
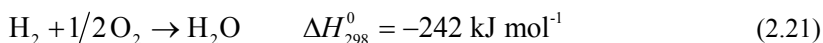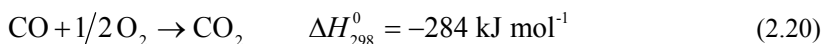
In allothermal steam reforming the energy needed for the endothermic reactions is supplied externally. This means an external heat source supplies the required heat e.g. burner.

The allothermal steam reformer is usually designed as a furnace in which tubes are placed. In the tubes the actual reforming takes place. The tubes are filled with catalyst and the heat required for the reaction is supplied through the wall of the tubes. In most cases, the tubes are placed in a furnace where burners are supplying heat to the tubes. [56]

Autothermal steam reformer is designed differently. Partial oxidation is used to supply heat for the endothermic reactions. There are two designs generally used. In the first design, the reactants are mixed and discharged into a fixed or fluidized bed. The second design has a burner, which mixes the reactants and discharges above a fixed catalyst bed. [56]

There are developments towards new reactor designs; one promising design is the fluidized bed membrane reactor. This reactor is packed with a standard reforming catalyst, where the reaction takes place. In the reactor, also membrane tubes are placed. These tubes are constructed of a composite material. On the wall of the tubes is a thin layer of palladium-iron. The hydrogen produced during the reforming diffuses through the membrane, and is removed from the reactor with a sweep gas. The removal of hydrogen shifts the reaction towards complete conversion. By applying two catalysts in the bed the hydrogen production can even be improved: a catalyst for dry reforming and a catalyst for steam reforming. [59]

Water gas shift

To increase the amount of hydrogen in the producer gas, the carbon monoxide is converted with water into carbon dioxide and hydrogen (See reaction (2.11)). This reaction is an exothermal equilibrium reaction, which favours a low temperature and is independent of pressure. There are three type of water gas shift (WGS): the high temperature WGS, the low temperature WGS and the raw gas WGS [56].

The high temperature water gas shift is performed at a temperature of about 350°C. For this process, an iron-chrome catalyst is used [35, 60]. The low temperature water gas shift is performed at a temperature of about 220°C, and for this process a copper-zinc oxides catalyst is used [35, 60]. This catalyst is very sensitive for sulphur poisoning, <1 ppm. The raw gas WGS is used for gasses containing appreciable amount of sulphur or hydrocarbons. For this type of water gas shift, cobalt and molybdenum catalysts are used. This catalyst needs some sulphur in the gas to be active [56].

It depends on the application of the producer gas, which type of water gas shift will be chosen. When the gas needs to be virtually carbon monoxide free, then the combination of the high temperature shift and the low temperature shift is used. The gas leaving this system contains about 0.2 vol% carbon monoxide [61].

An excess of steam should be used in the process to prevent coke formation. The H_2O:CO ratio should be >3 [18].

The reactor design is usually a packed bed. There are developments towards membrane reactors. These reactors are also packed beds, but membrane tubes are placed in the reactor for the removal of hydrogen during operation. This will lead to a shift of the equilibrium towards complete reaction. Instead of hydrogen separating membranes, also carbon dioxide separating membranes, could be used [62].

Preferential oxidation

Preferential oxidation is a process to remove small amounts of carbon monoxide from a gas stream. The process is usually after a water gas shift system to remove the last 0.2 vol% carbon monoxide. This process is often used in systems for supplying fuel to PEM fuel cells, which required virtually CO free gas. The following reactions occur during the preferential oxidation process.

$$CO + \frac{1}{2}O_2 \rightarrow CO_2 \qquad \Delta H^0_{298} = -283 \ \text{kJ mol}^{-1} \qquad (2.22)$$

$$H_2 + \frac{1}{2}O_2 \rightarrow H_2O \qquad \Delta H^0_{298} = 242 \ \text{kJ mol}^{-1} \qquad (2.23)$$
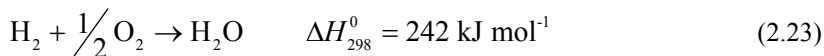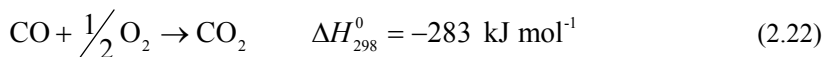
Also the reversed water gas shift reaction (reaction (2.11)) occurs, which is an undesired reaction just like reaction (2.23). The preferential oxidation process is a catalyzed process. In general three types of catalyst are used. The first are platinum or other precious metal catalysts on alumina. The second are gold based catalysts, which show good performance at lower temperatures (around 100°C). The last are catalysts based on several common transition metals. [63]

The operation temperature depends on the catalyst, but the temperature range is in between 100°C and 250°C. For the oxidation, an oxygen source is required, which can be air, enriched air, or pure oxygen. The O_2/CO ratio for this process is about $1.0 - 1.2$. The undesired oxidation of hydrogen depends on the partial pressure of oxygen [63]. The oxygen feed should be limited to prevent the oxidation of precious hydrogen.

Methanation

Another technique for the removal of small amounts of carbon monoxide or carbon dioxide from a gas stream is methanation. The methanation are as follows:

$$CO + 3H_2 \rightleftharpoons CH_4 + H_2O \qquad \Delta H^0_{298} = -205.9 \ \text{kJ mol}^{-1} \qquad (2.24)$$

$$CO_2 + 4H_2 \rightleftharpoons CH_4 + 2H_2O \qquad \Delta H^0_{298} = -164.7 \ \text{kJ mol}^{-1} \qquad (2.25)$$
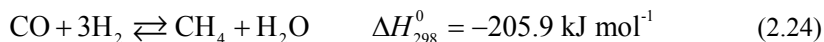
It is often observed that reaction (2.25) is actually a combination of reaction (2.24) and the water gas shift (reaction (2.11)) [56]. The reactions are both highly exothermic; this means the formation of methane is favoured at low temperature. A high pressure is favoured by the methanation reactions. These methanation reactions are catalyzed by nickel based catalysts. The gas needs to be virtually clean of sulphur, to avoid catalyst deactivation. Also low temperature (<200°C) should be avoided, because nickel has the tendency to form carbonyls at lower temperatures. The reactor design is often a packed bed, but other designs are possible. The operation point is around the 300°C and pressure is >1 MPa.

Carbon capture

Carbon capture is interesting technique, due to the link between the carbon dioxide emissions and the global climate changes and greenhouse effect. When carbon dioxide is captured from gasses, which originate from biomass, the involved process becomes carbon dioxide negative. Carbon dioxide is thus extracted from the atmosphere. There are various techniques available for the removal of carbon dioxide from syn-gas, which are discussed in the following sections.

Absorption

Absorption is the process where liquid is used to remove some components from a gas stream. Many techniques have been developed for the removal of sulphur compounds from gas. These techniques are mainly applied for the removal of significant amounts of sulphur. Since the bio syngas is relatively low on sulphur compounds, it is not useful to apply these processes. On the other hand, most of these processes also remove carbon dioxide besides sulphur compounds. The separated carbon dioxide can then be stored or used in greenhouses.

There are three main types of absorption; physical absorption, chemical absorption and a combination of physical and chemical absorption. Physical absorption means the absorbed compounds dissolves in the liquid. In chemical absorption the compounds are chemically bonded to the solvent. When the physical and chemical absorption are combined then a mixture of solvents is used, some dissolve the components and some chemically bind the components. The absorption capacity of chemical solvent is better for low partial pressures than that for physical absorption. On the other hand when the partial pressures are high then the physical absorption is more effective.

In Table 2-5 an overview is given of the different processes and which type of absorption is used.

Table 2-5 overview of solvents [35, 56]

Chemical absorption	
Trade name	*Solvent*
MEA	1-3 N monoethanolamine
DEA	2-4 N diethanolamine
DGA	4-6 N Glycolamine
Econamine	(2-(2-aminoethoxy)ethanol)
DIPA	2N diisopropanolamine
MDEA	2-5 N methyldiethanolamine
ADIP	DIPA or MDEA
Amine Guard/Ucarsol	Formulated MDEA
aMDEA	MDEA + activator (Enhanced CO_2 absorption)
Gas Spec	Formulated MDEA
Flexsorb	Hindered amine
Benfield	K_2CO_3 + activator (DEA)
Catacarb	K_2CO_3 + catalyst
Giammarco-Vetrocoke	K_2CO_3 + activator (arsenic trioxide)
Vacasulf	K_2CO_3 + NaOH
Physical absorption	
Rectisol	Methanol
Selexol	Polyethylene glycol dimethyl ether (DMPEG)
Purisol	N-methyl-2-pyrrolydone (NMP)
Morphysorb	N-formylmorpholine (NFM)
Physical-chemical absorption	
Sulfinol D/M	Sulfolane (tetrahydrothiopheneoxide)+DIPA or MDEA
Amisol	Methanol+MEA, DEA or DETA

In an absorber, the cooled gas is contacted with the liquid sorbent in counter-current operation. Usually the liquid enters the absorber at the top. The loaded solvent leaves the bottom, which is then going to the regenerator. The gas to be processed enters the absorber at the bottom and leaves the absorber at the top. In the absorber, usually inserts are placed which contribute to the enlargement of the contact area. In the regenerator the solvent is treated in such a way that the solvent is unloaded. The treatment depends on the type of solvent. For instance, physical solvents depend on a high partial pressure for absorption, when the pressure is reduced the solvent will be regenerated. This is not the case for chemical solvent, which often needs heat for regeneration. There are three general methods of solvent regeneration: flashing, stripping and reboiling. During flashing the pressure of the system is decreased, so the solvent releases the absorbed component. During stripping

an inert gas is used to strip the compounds from the solvent. Reboiling uses the phenomenon that the solubility, of gasses in a solvent, reduces at elevated temperatures. The solvent is stripped by its own vapour, which is condensed from the overhead gas and recycled as a reflux [56].

Each solvent has its own operating conditions and selectivity towards the absorption of carbon dioxide. The selection of the right solvent depends on the requirements of the product gas, but also on the utilities on site. Also the partial pressure of the compounds, which needs to be removed, is an important factor in the selection of the right solvent and process.

Impurities, like carbonyl sulphide, carbon disulfide, hydrogen cyanide, ammonia, mercaptans, thiophenes, phenols, heavy hydrocarbons, metal carbonyls, chlorides and inorganic components in the gas can influence the selection of the solvent and process [56]. Some trace component react in such way with the solvent that it cannot be removed during the regeneration step. This unwanted reaction will lead to accumulation of the impurity and can cause problems in the process, like plugging, foaming, corrosion and solvent degradation [56].

A detailed description of the different absorption processes can be found in Ullmann Encyclopaedia of Chemical Industry [56].

The U.S. Department of Energy's National Energy Technology Laboratory (NETL) is conducting research on novel techniques to capture CO_2 [62]. One of those techniques involves physical solvents for the removal of CO_2 at high temperatures. Several candidates have been tested, like perfluorinated compounds, and ionic liquids. The perfluorinated compounds have a significant vapour pressure at elevated temperatures. Ionic liquids have negligible vapour pressure even at elevated temperatures [62]. Further investigation is necessary, but the ionic liquids seem promising. It could be possible to regenerate the solvent by means of a temperature swing process. In temperature swing regeneration process the solvent is cooled, so it will release the dissolved compounds, and then it is heated again. A big advantage is the released gas can remain at elevated pressure, which means recompression is not necessary.

New solvents for carbon capture are being developed like hyper branched polymers and liquid crystal absorbents.

Membranes for CO_2 separation

There are some researches involving membrane separation of carbon dioxide from gas streams. The purpose of the membrane is to selectively separate the carbon dioxide from the producer gas. One of the major problems is the selectivity of the membrane towards carbon dioxide. Solution diffusion membranes seem very promising, especially when ionic liquids are used as the transporting liquid. In a solution diffusion membrane a support is impregnated with a liquid. This liquid is the selective transporting medium. The liquid is often instable at elevated temperature, due to the higher vapour pressure. Ionic liquid have virtually no vapour pressure, so it does not have this instability problem. Also, ionic liquids are more selective towards carbon dioxide then to hydrogen [62]. That is why there is more research towards solution diffusion membranes based on ionic liquids. There are still problems regarding the operation at elevated temperatures, due to membrane failure. But these membranes seem promising.

CO₂ adsorption during gasification / chemical looping

It is also possible to adsorb carbon dioxide directly in the gasifier, by using a catalyst as bed material. The bed material adsorbs the carbon dioxide when it is formed. The most commonly used catalyst is CaO, which reacts according the following reaction.

$$CaO_{(s)} + CO_{2(g)} \rightleftarrows CaCO_{3(s)} \qquad \Delta H^0_{923} = -170.5 \text{ kJ mol}^{-1} \qquad (2.26)$$

As equation (2.26) indicates, the adsorption reaction is exothermic, so it could supply some heat for the endothermic gasification reactions. CaO is capable to capture CO_2 at very low concentrations at temperatures around 450-750°C and atmospheric pressure [64]. The big advantage of carbon capturing inside the gasifier is the enhanced hydrogen output of the gasification process, which is demonstrated by equilibrium calculations of Florin and Harris [65].

The regeneration reaction (backward reaction) is endothermic, and therefore requires a high temperature to be regenerated. Regeneration of the CaO occurs at 700-950°C; the temperature depends on the CO_2 concentration.

Pfeifer et al. [66] had performed some experiments with different materials containing CaO. The experiments were performed in a 100 kW$_{th}$ Fast Internal Circulating Fluidized Bed (FICFB). This gasifier consists of two beds one for the gasification process and one combustor, which supplies the heat for the gasification reactions. In the CaO process, the combustor regenerates the CaO at a temperature of 900°C. In the gasification section the CaO adsorbs the formed carbon dioxide at a temperature of around 600-700°C. Pfeifer et al. [66] found that the hydrogen content of the producer gas was around 66-75 vol%.

Other methods for CO₂ removal

For the removal of CO_2, pressure swing adsorption can be used. This method is explained in the section of hydrogen purification (Section 2.2.3). Another method for CO_2 removal is cryogenic distillation. In this method, the gas is compressed to approximately 30 bar and cooled to a temperature of about -30°C. It is important that the gas is dry, because ice formation can seriously damage the process. The gas is then fed into a distillation column. The liquid CO_2 leaves the column at the bottom and the residual gas leaves at the top.

2.2.3. Hydrogen purification

After gas cleaning and gas processing there are still minor impurities in the gas, for instance small amounts of nitrogen. These impurities need to be removed when high purity hydrogen is required. There are several processes known, which are used for the purification of hydrogen. The different processes will be discussed in the next sections.

Pressure swing adsorption (PSA)

Pressure swing adsorption is used to purify hydrogen towards extremely high purities. A simple pressure swing adsorption system consists of three packed beds. The three packed beds ensure continuous operation, because the beds are operated in swing mode. This means, when the first bed and second bed are regenerated the third bed is used for adsorption. The packed bed contains usually zeolites, activated carbon, activated alumina or silica gel. The packing material depends on the components, which need to be removed from the hydrogen. For instance, activated carbon is often used when hydrocarbon compounds need to be removed. The commonly used sorbents in hydrogen purification are

zeolites. Zeolites are highly structured compounds with narrow distributed micropores, which are ideal for adsorption purposes.

The process is called pressure swing adsorption, because pressure is used as operational variable for the adsorption and regeneration process. The impurities are adsorbed at elevated pressure (3 MPa), and the impurities are released at low pressures (0.1-0.4 MPa). The temperature stays more or less constant during the adsorption and desorption process. There are small changes in the temperature, but they contribute to the mechanisms in the process. The adsorption process is exothermal and the desorption process is endothermic. In the adsorption and desorption processes five different steps can be indentified. The five steps are:

- Adsorption at high pressure
- Co-current depressurization, this provides gas for the purge and repressurization
- Counter current depressurization, production of the waste gas
- Counter current purging, also part of the production of the waste gas
- Counter current pressurization

The cycle times are relatively short, between 3 up to 10 minutes. The hydrogen yield of the PSA system depends on several factors. The first factor is the composition of the gas fed to the process. The hydrogen content of this gas should be at least 50%. The concentration and nature of the impurities with respect to the adsorption and desorption behaviour determine the size of the adsorption vessels. The size of the vessel determines the amount of hydrogen, which is lost during a cycle.

The second factor is the pressure ratio between the feed gas and purge gas. This pressure ratio is also determining for the size of the adsorber. It also determines the extent of effort necessary for regeneration.

The third factor is the purity requirements and the nature of the impurities. The purity of hydrogen is usually above 99.9%. Higher purities are possible, but usually at the expense of the hydrogen yield. This is especially applicable for compounds which are poorly adsorbed like e.g. nitrogen.

The last factor is the temperature of the feed gas. High temperatures lead to a lower capacity of the adsorber and thus to a lower hydrogen yield.

The hydrogen produced with this process leaves the adsorber at adsorption pressure. The tail gas on the other hand fluctuates in pressure, composition, and amount. These fluctuations can be smoothed out with buffer vessels. The separation efficiency of the PSA process varies between 70 and 90%. This depends on the composition of the gas fed to the process and the technical sophistication of the process.

Temperature Swing Adsorption (TSA)

Temperature swing adsorption is actually similar to pressure swing adsorption. The main difference is that not pressure, but changes in temperature are used to adsorb and desorb the impurities. The adsorption takes place at low temperatures, and the desorption process takes place at high temperatures. The adsorption usually takes place at ambient temperatures and elevated pressures (3 MPa). After the bed is switched to desorption mode, first the pressure is reduced to start the initial desorption. Because of pressure reduction the temperature of the bed decreases. This cooling deteriorates the desorption process. To increase desorption of the impurities the temperature of the bed is increased to 200°C or higher, which promotes desorption of the impurities. The bed is usually heated by heating coils or by purging the bed with hot purging gas. After regeneration the bed is cooled and pressurized to adsorption conditions. The feed gas needs to be virtually free of water vapour, because it can condensate during the depressurization. Liquids damage the sorbent irreversibly.

The cycle times for TSA are several hours up to days, which are long times compared with PSA. This is because temperature is harder to change in short times, then to change pressure.

Cryogenic purification

Cryogenic purification is based on the large difference between the boiling point of hydrogen and the boiling points of the impurities. Usually the impurities are condensed or sublimated. When the impurities are also needed to be separated from each other, a rectification process is used. There are two main types of cryogenic hydrogen purification processes; condensation processes and absorption processes.

Condensation processes are often used when the difference between the boiling points of hydrogen and the condensing phase is sufficiently high [67]. This is often the case for hydrocarbons. Pre-purification step is applied to remove impurities which can solidify at the lowest temperature of the condensation process. These compounds are usually water, carbon dioxide and hydrocarbon compounds. Water is often removed by glycol scrubbing. Carbon dioxide is adsorbed on activated carbon or by molecular sieves. The residual gas mixtures are reduced in temperature to condense the impurities. For this usually distillation columns are being used.

Absorption processes can yield greater purities than condensation processes and at higher temperatures than condensation processes. These absorption processes are based on physical absorption, in which the impurities are condensed and completely or partially utilized as scrubbing agent [67]. Some examples of scrubbing liquids are, in this case, nitrogen and methane. These liquids are mainly used for the removal of carbon monoxide.

Membrane purification

Membrane purification can either be applied as a single unit or it can be applied in other processes, like methane reforming or water gas shift systems. Most membranes are based on ceramics with thin coating of a palladium metal or a palladium alloy. The hydrogen permeates through the membrane, whereas the other compound cannot permeate. A high partial hydrogen pressure (2 MPa) is required to get a high throughput. Most systems operate at elevated temperatures (300°C). A problem with the palladium based membranes is their sensitivity to impurities like unsaturated hydrocarbons, halogen compounds and sulphur compounds [67]. The impurities can cause membrane rupturing.
The development of membranes for the purification of hydrogen is still continuing. Polymer membranes and ceramics for hydrogen purification are being developed. Polymer based membranes cannot operate at high temperatures >100°C, on the other hand ceramic membranes can. Purities up to 99% are feasible with membrane separation techniques.

2.2.4. Summary and outlook

In section 2.2, an overview is given of the current and coming technologies for the cleaning and processing of bio syn-gas. The cleaning processes include particulate removal, tar cracking, alkali removal, sulphur and halogen removal. After this, the different gas processing processes have been discussed. Finally, some hydrogen purification processes have been overviewed. Most of these processes have already been applied in industry, only the gas cleaning techniques at elevated temperature are still under development. Research to develop more robust gas processing systems, which are less susceptible to impurities in

the gas is abundant. The kind of systems to use depends mainly on the application of the hydrogen rich gas.

2.3. Solid oxide and proton exchange membrane fuel cells

Energy conversion systems are used to convert the energy contained in a fuel into other forms of energy. These forms of energy can be mechanical energy, electrical energy and heat. Most energy conversion systems convert the energy contained in fuel into mechanical energy and heat. This mechanical energy is then converted with the help of a generator into electricity. There is one energy conversion system which converts fuel directly into electricity. This energy conversion system is the fuel cell.

In a fuel cell the chemical energy of a fuel and an oxidant is converted into electricity and heat. When this is compared to direct irreversible combustion, all the energy would be released in the form of heat. The second law of thermodynamics states that heat is only partially convertible into work, i.e. the so-called Carnot-limitation. The fuel cell prevents the direct irreversible combustion of fuel, which is a huge advantage. In Figure 2-15, the difference in efficiency between a Carnot limited system and a fuel cell is given for reversible conversion processes. The reversible efficiency of the fuel cell is determined by equation (2.27).

$$\eta_{rev,FC} = \frac{\Delta G^0}{\Delta H^0} \tag{2.27}$$
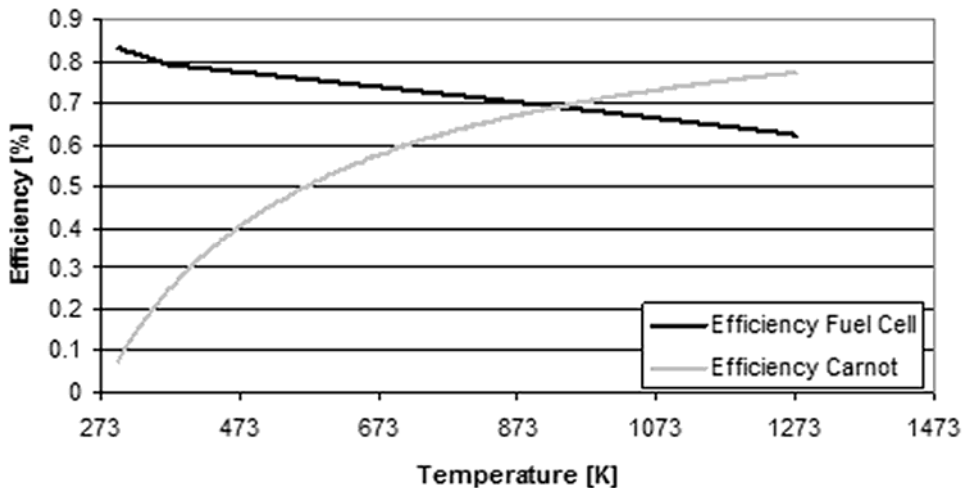
Figure 2-15 different between a Carnot limited system and the fuel cell for reversible conversion processes

During the combustion in a fuel cell electrons move from the high-energy reactant bonds to the low-energy product bonds; the fuel cell uses these electrons to produce an electrical current. This can be performed by spatially separating fuel and the oxygen. The electrons needed for the bonding reconfiguration takes place over a greater distance, so it can be harnessed as an electrical current. For example the normal hydrogen combustion reaction is indicated in equation (2.28).

$$H_2 + \frac{1}{2}O_2 \rightarrow H_2O \qquad \Delta H_r^{298} = -242 \cdot 10^3 \text{ kJ mol}^{-1} \qquad (2.28)$$
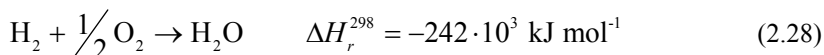
In a fuel cell this reaction is split into two electrochemical half reactions, which have their own standard electrode potential (SEP), as indicated in equations (2.29) & (2.30).

$$H_2 \rightleftarrows 2H^+ + 2e^- \qquad SEP = 0.00V \qquad (2.29)$$

$$\frac{1}{2}O_2 + 2H^+ + 2e^- \rightleftarrows H_2O \qquad SEP = 1.23V \qquad (2.30)$$

By separating these two reactions the electrons from the fuel are forced to flow through an external electrical circuit. To get a good spatial separation an electrolyte is needed. This is a material, which allows ion movement, but does not conduct electrons. So a fuel cell must consist of two electrodes at which the half reactions occur and an electrolyte. The type of electrodes and electrolyte differ per fuel cell type.

There are five mayor fuel cell types:

- Polymer Electrolyte Membrane Fuel Cell (PEMFC) has a polymer membrane as electrolyte. It uses hydrogen or methanol as fuel and air or oxygen as the oxidant.
- Phosphoric Acid Fuel Cell (PAFC) contains liquid phosphoric acid, which is the electrolyte of the fuel cell. It uses hydrogen as fuel and air or oxygen as the oxidant.
- Alkaline Fuel Cell (AFC) employs an aqueous potassium hydroxide electrolyte. Its uses hydrogen as fuel and pure oxygen as oxidant. It is very sensitive towards carbon dioxide.
- Molten Carbonate Fuel Cell (MCFC) uses a molten mixture of alkali carbonates (Li_2CO_3 and K_2CO_3) immobilized in a $LiAlO_2$ matrix as electrolyte. Its fuel is hydrogen or methane and its oxidant is air or oxygen.
- Solid Oxide Fuel Cell (SOFC) employs a solid ceramic electrolyte; it uses hydrogen methane or carbon monoxide as fuel and oxygen as oxidant.

All the fuel cells are based on the same electrochemical principles. But they all operate at different temperature regimes, incorporate different materials, and often differ in their fuel tolerance and performance characteristics. These differences are demonstrated in Table 2-6.

Table 2-6 description of the mayor fuel cell types [68]

	PEM-FC	PAFC	AFC	MCFC	SOFC
Electrolyte	Polymer membrane	Liquid H_3PO_4 [immobilized]	Liquid KOH [immobilized]	Molten Carbonate	Ceramic
Charge carrier	H^+	H^+	OH^-	CO_3^{2-}	O^{2-}
Operating temperature	353 K	473 K	333-493 K	923 K	873-1273 K
Catalyst	Platinum	Platinum	Platinum	Nickel	Perovskites (Ceramic)
Cell components	Carbon based	Carbon based	Carbon based	Stainless steel based	Ceramic based
Fuel compatibility	H_2, Methanol	H_2	H_2	H_2, CH_4, CO	H_2, CH_4, CO

Each fuel cell type has its own requirements concerning fuel purity. The high temperature fuel cells, like the MCFC and the SOFC, are more tolerant towards impurities than the low temperature fuel cells.

The focus in this thesis will be on two promising fuel cell technologies: the PEM-FC and the SOFC. The background of the two fuel cell technologies will be discussed as well as the influence of impurities in the feedstock on the fuel cells. The focus is on the impurities

found in the gas coming from biomass gasification. In appendix D, the thermodynamics of fuel cells and modelling of fuel cells in Cycle-Tempo are being discussed.

2.3.1. Proton Exchange Membrane Fuel Cell

One type of fuel cells is the proton exchange membrane fuel cell, also known as the PEM-fuel cell. Sometimes, it is also called a polymer electrolyte membrane fuel cell. Figure 2-16 is a schematic representation of a PEM-fuel cell.
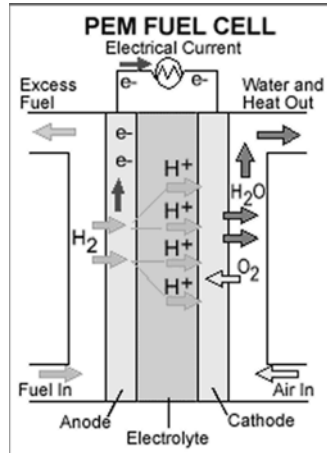
Figure 2-16: Schematic proton exchange membrane fuel cell

In this type of fuel cells the electrolyte is a solid membrane, which exchanges protons (hydrogen ions). The fuel for this fuel cell is pure hydrogen; also methanol can be used as a fuel. When methanol is used it is called a direct methanol fuel cell (DMFC). The PEM fuel cells are preferred for the automotive industry and many other applications, because of their relative low operation temperature (<90°C), their short start-up time, the few restrictions it places on the materials. Therefore, the fuel cell is easier to maintain.

Currently, the high temperature PEM fuel cell, which operates at temperatures up to 200°C, is widely researched. Because the operation at elevated temperatures has several advantages [69]:
- Improvement of the cathode kinetics.
- Improved tolerance of the catalyst to contaminants.
- Improved water management and gas transport.
- More efficient cooling of the fuel cell.
- Easier shutdown procedures and faster cold start-up of a fuel cell stack, since there is no water management system required.

More explanation about these effects will follow in the appropriate sections.

In the following sections the different parts of the PEM fuel cell will be discussed. Starting with the anode, then the electrolyte will be discussed. After that the cathode will be treated followed by the binary plates. Finally, a short summary will be given.

Anode

The PEM fuel cell is generally used to process hydrogen and oxygen into water using the half-reactions mentioned in Equation (2.29) & (2.30). At the anode the hydrogen is split into two protons and two electrons. The protons are then transferred to the electrolyte and the electrons are transferred to the electrical circuit. The anode of a PEM fuel cell consists of at least three layers, which have their own purpose. The first layer is the current collector; this is usually a perforated metal sheet. The second layer is the diffusion layer, and the third layer is the catalyst layer. The diffusion layer is usually a carbon cloth or carbon paper, which acts as carrier for the catalyst layer. This catalyst is usually platinum on carbon, platinum ruthenium on carbon, or palladium on carbon. Carbon is used as a catalyst carrier, because of its good conductivity and also because of its good corrosive resistance and adequate water handling [70].

At the anode, the hydrogen diffuses through the diffusion layer and is split into two protons and two electrons on the catalyst surface. The mechanism is shown in the following reaction equations [71].

$$H_2 + 2Pt \rightleftarrows 2Pt - H_{ads} \qquad\qquad (2.31)$$

$$2Pt - H_{ads} \rightleftarrows 2Pt + 2H^+ + 2e^- \qquad\qquad (2.32)$$

These reactions take place at the interface of the anode and the electrolyte. The hydrogen dissociates at the platinum site and is extracted by the proton accepting group of the electrolyte. In the case of Nafion$^®$ it is the SO_3^- group [72]. The protons go through the PEM and the electrons go through an electrical circuit.

There are several contaminants known for the anode, e.g. carbon oxides, hydrogen sulphide, and ammonia. Most of these contaminants cause kinetic losses due to catalyst poisoning. Both carbon monoxide and carbon dioxide have become a major concern in PEM fuel cells using reformate (hydrogen rich gas) as a fuel [73]. It is well known that carbon monoxide strongly binds to the platinum sites, blocking the reactions sites. This leads to the deactivation of the platinum catalyst. The poisoning effect of carbon monoxide depends on several factors, for instance the CO concentration, the exposure time, the fuel cell operating temperature, and anode catalyst type [73]. When the concentration increases the poisoning effect becomes more severe. The same applies for the exposure time. On the contrary, a higher temperature decreases the poisoning effect of carbon monoxide, as is shown by Jiang et al. and Li et al. [74, 75]. This is one of the major reasons for the increased interest for the high temperature PEM fuel cell, which operates at temperatures up to 200°C. There are catalysts for the anode of the PEM fuel cell, which are more resistant to carbon monoxide poisoning than pure platinum. For instance a Pt/Ru catalyst is more tolerant towards CO than pure Pt [71, 73]. Also Pt/Mo has been proven to be more tolerant towards CO [76, 77]. Pt/Ru catalysts are often used in fuel cells fuelled with reformate.

The presence of carbon monoxide in the fuel could affect the performance of the cathode as a result of CO crossover through pin-holes in the membrane [78, 79].

Carbon dioxide can also cause performance loss in a PEM fuel cell; this is expected to be caused by the reversed water gas shift. The reaction for the reversed water gas shift is given in equation (2.33).

$$CO_2 + H_2 \rightleftarrows CO + H_2O \qquad\qquad (2.33)$$

The performance loss is not as severe as with carbon monoxide, but it can still be significant. The effects are not the same for all the catalysts [80]. For instance Pt/Ru is less

sensitive than pure Pt, and Pt/Mo is even more sensitive than pure Pt [76, 77, 80]. The way the electrode is constructed influences the CO_2 tolerance. If the catalyst is covered by electrolyte material then the reversed water gas shift is suppressed [81].

Some state that carbon dioxide forms a cloud over the catalyst and blocks the hydrogen from reaching the platinum sites [82]. The exposure of the carbon dioxide does not cause permanent damage according to Rajalakshmi et al [82]. The exposure to CO does cause permanent damage.

Sulphur compounds are also known for their poisoning effect to the anode of the PEM fuel cell. Especially, hydrogen sulphide is an even more severe contaminant than carbon monoxide [73]. The sulphur in the hydrogen sulphide strongly adsorbs on platinum, making the sites inaccessible for hydrogen. A suggested reaction mechanism is given in Equation (2.34) and (2.35) [83].

$$H_2S + Pt \rightarrow Pt - S + H_2 \qquad (2.34)$$

$$Pt - H + H_2S \rightarrow Pt - S + \frac{3}{2}H_2 \qquad (2.35)$$

Using platinum alloys has hardly any effect on the poisoning by sulphur. Mohtadi et al. [84] performed some experiments on sulphur poisoning using a Pt/Ru catalyst; it was even faster deactivated than pure platinum. But this could be caused by the smaller amount of platinum sites on the catalyst [84].

Electrolyte

The electrolyte provides the separation between the electrodes and the ion-transport between the electrodes. The most common electrolyte in the PEM fuel is the perfluorosulfonic acid (PFSA) polymer membrane, e.g. Nafion®. Besides this type of membranes there is still a lot of ongoing research to find more suitable membranes, which allow higher operating temperatures of the PEM fuel cell. These membranes should have high proton conductivity, low fuel and oxygen permeability, and high chemical, thermal and mechanical stability [85]. There are mainly three types of membranes [69, 86], which are being researched:

- Modified PFSA membranes, which incorporate hydroscopic oxides and solid inorganic proton conductors.
- Alternative sulfonated polymers and composite membranes, such as PBI.
- Acid-base polymer membranes, such as phosphoric acid-doped PBI.

First the standard PFSA polymer membranes will be discussed then the modified PFSA membranes. After this the sulfonated polyaromatic polymer and composite membranes will be treated. Finally the acid-base polymer membranes will be discussed.

PFSA polymer membrane

Generally one type of membrane is used, the PFSA polymer membranes, e.g. Nafion® (a DuPont trademark) or Flemion membranes. Nafion® is a polymer of perfluorosulphonic acid and has sulphonate side groups at the side chains, which are considered the active groups of the membrane. See Figure 2-17 for an indication of the structure of Nafion®.
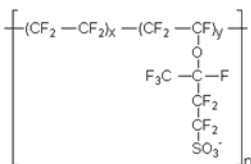
Figure 2-17: Structure of Nafion®

For the transport of protons through the membranes, water is needed. The proton binds from the catalyst site to the sulphonate group at the end of a Nafion® chain [72]. In the structure of the Nafion® pores are present, which could be filled with water. If the pores are filled with water the proton can form hydronium complexes (H_3O^+) as they detach from the sulphonate group [68]. Because of the hydrophobic nature of the Teflon® backbone structure, the transport of water through the membrane is being accelerated [68], and if there are any hydronium complexes, they will also be accelerated. Since the transport of protons is being promoted by the water content of Nafion®, the membrane should be hydrated with liquid all the time. There is a known problem of keeping this membrane hydrated, because during the transport of a proton it drags ±2.5 water molecules along, so the membrane can easily be dehydrated [68, 87]. This effect is called the electro osmotic drag. The electro osmotic drag can cause dehydration of the membrane at the anode side on the membrane, and flooding at the cathode. In the membrane, also some back diffusion of water from the cathode to the anode takes place. In Figure 2-18 a schematic overview is given of the different water transport mechanisms in the Nafion® membrane.
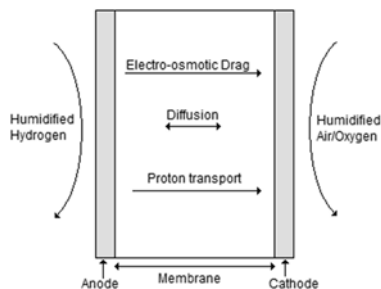
Figure 2-18 Water transport in PEM fuel cell

A good water management is required to keep the membrane fully hydrated. The high water content requirement gives this membrane an upper limit in operating temperature, which is around 80°C [88]. Above this temperature, the evaporation of water is too large, causing drying of the membrane. This can result in increasing resistance, shrinking and or cracking.

The performance of the PEM fuel cell deteriorates in the presence of ammonia [89]. It is believed ammonia reduces the ion conductivity of the membrane at the three phase interface [73, 90]. Ammonia reacts with the protons in the membrane and stays in the membrane as an ammonium ion [90].
Cations are also known to affect the proton conductivity in the proton conducting membrane. Some of those cations (like, Cu^{2+}, Fe^{3+}, Na^+, Ni^{2+}, and Cr^{3+}) have a great affinity for the sulfonic acid groups of the PFSA membrane. This hampers the proton and water transport through and in the membrane, leading to high resistance and possible dehydration of the membrane [73].

Modified PFSA membranes

One of the major drawbacks of the PFSA membranes is their low conductivity at low levels of humidification and at high temperatures (>90°C) [86]. There are several ways to tackle these problems, one of the ways is to modify the PFSA polymer membranes. Four different ways have been found to modify the PFSA polymer membrane. The first way is to replace the water in the membrane by another liquid. For instance, by replacing it by a non-volatile liquid, a higher operation temperature can be achieved. Different liquids have been researched, for instance phosphoric acid, phosphotungstic acid in acetic acid, tetra-n-butylamoniumchloride and ionic liquids.

The second way to improve the PFSA polymer membrane is to make thinner membranes. A thinner membrane will lead to an improvement of the water management within the fuel cell. The back diffusion of the water from the cathode to the anode is in a thin membrane very effective. The thickness has also a positive effect on the internal resistance. In order to make the membranes thinner, the membrane needs to be reinforced. The mechanical strength of the membrane decreases when the membrane becomes thinner. This decrease in mechanical strength occurs especially during swelling and at high temperatures. The reinforcement can be achieved by, for instance a porous sheet of polytetrafluoroethylene (PTFE, also known as Teflon) or by Nafion[®] impregnation of substrates like polypropylene. In this way the thickness of the membranes can be reduced to 5-30 μm.

The third way to improve the PFSA is to recast the PFSA with mixed hygroscopic oxides, like SiO_2 & TiO_2. These hygroscopic oxides improve the water absorption within the membrane, because water absorbs on the oxide surface. This results in an improvement of the back-diffusion of water from the cathode and the electro-osmotic drag of water from anode to cathode is reduced [86]. Because of the improved water retention it is also possible to operate the fuel cell at higher temperatures.

The fourth and last way to improve PFSA is to recast it with solid inorganic proton conductors. These solid inorganic proton conductors are for instance, zirconium phosphates, heteropolyacids, metal hydrogen sulphate and some other materials. The aim of this type of materials is to improve the hydration characteristics of the PFSA membrane [86]. This improvement is realized by decreasing the chemical potential of the water inside the membrane and therefore creating an additional pathway for the proton conduction [86].

The effect of poisons on these improved membranes is not yet known.

Alternative sulfonated polymers and composite membranes

There are two main groups widely investigated for being alternatives of PFSA membranes. The first group is based on polymer containing inorganic elements, like fluorine or silicon. This first group can be divided into two groups; fluoropolymers and polysiloxanes. The second group are aromatic polymers.

Fluoropolymers have an excellent chemical stability and a high melting temperature, which make them very suitable as a backbone of proton conducting membranes. In Nafion[®], polytetrafluoroethylene is the backbone of the polymer. Also other fluor compound have been researched to serve as backbone, like poly(vinylidene fluoride) and poly(tetrafluoroethylene-hexafluoropropylene). The proton conductivity is then introduced to the backbone by linking sulfonated styrene. An example of such a structure is given in Figure 2-19A.
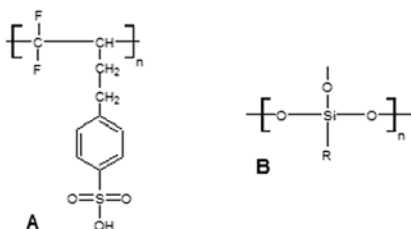
Figure 2-19 example structure of: A) a sulfonated styrene linked to a poly(vinylidene fluoride) backbone; B) example structure of a polysiloxane

Polysiloxanes are also temperature resistant just like the fluoropolymers. An example of the structure of polysiloxanes is given in Figure 2-19B, where R represents methyl or mixed methyl-phenyl groups. The inorganic network of Si-O is developed by the sol-gel process, where it is in an organic or aqueous solution. By adding a functional group, like sulfonate, to the organic group an electrolyte can be created. Electrolytes of this type have been reported to be stable up to 200°C with optical transparency and chemical stability [86].

Aromatic hydrocarbon polymers are relative cheap and are widely commercial available. The aromatics in these polymers have a good oxidation resistance, making them suitable as electrolyte material. In Figure 2-20, several examples are given of such aromatic polymers.
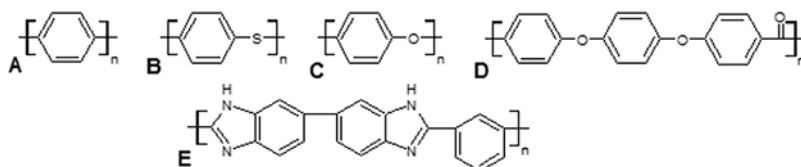
Figure 2-20 examples of the structures of: A) poly-p-phenylene; B) polyphenylene sulphide (PPS); C) polyphenylene oxide (PPO); D)polyetheretherketones (PEEK); E) polybenzimidazole (PBI)

Some of these polymers have already proton conducting properties, like the ketones and imides. These polymers are often sulfonated to create or improve the proton conductivity. The water uptake and the sensitivity to the relative humidity of these types of membranes are less then of PFSA membrane because of their difference in structure. PFSA have a very hydrophobic backbone structure, the backbone structure of aromatic hydrocarbon membrane is less hydrophobic. Also the sulfonic acid groups in aromatic hydrocarbon membranes are less acidic and polar. This leads to a better distribution of water throughout the nanostructure of the membrane.

Acid-base polymer membranes

H_3PO_4-doped polybenzimidazole (PBI) is a membrane of recent interest, which can operate at higher temperatures, because it does not contain as much water as the Nafion® membranes. This is a great advantage when operation above 100°C is desired. It can operate at temperature up to 200°C [91]. Also the drag of water though the membrane is virtually zero [88, 91, 92], because of the different transport method of protons through the membrane and the dense structure of the membrane [93]. The PBI membranes are often doped with acid to improve its conductivity. The conductivity of the proton occurs along different paths depending on the doping level, temperature and relative humidity [91].

Hydrogen bonds immobilize the anions of the acid and form a network for proton transfer via four ways. The first is transfer from one PBI string to another, the second method is along the acid bonded to a PBI string to another acid bonded to a PBI string, the third method is from a bonded acid on a PBI string to the acid groups in the pores, and last is through transport via water molecules in the pores [91]. All four mechanisms are shown in Figure 2-21.
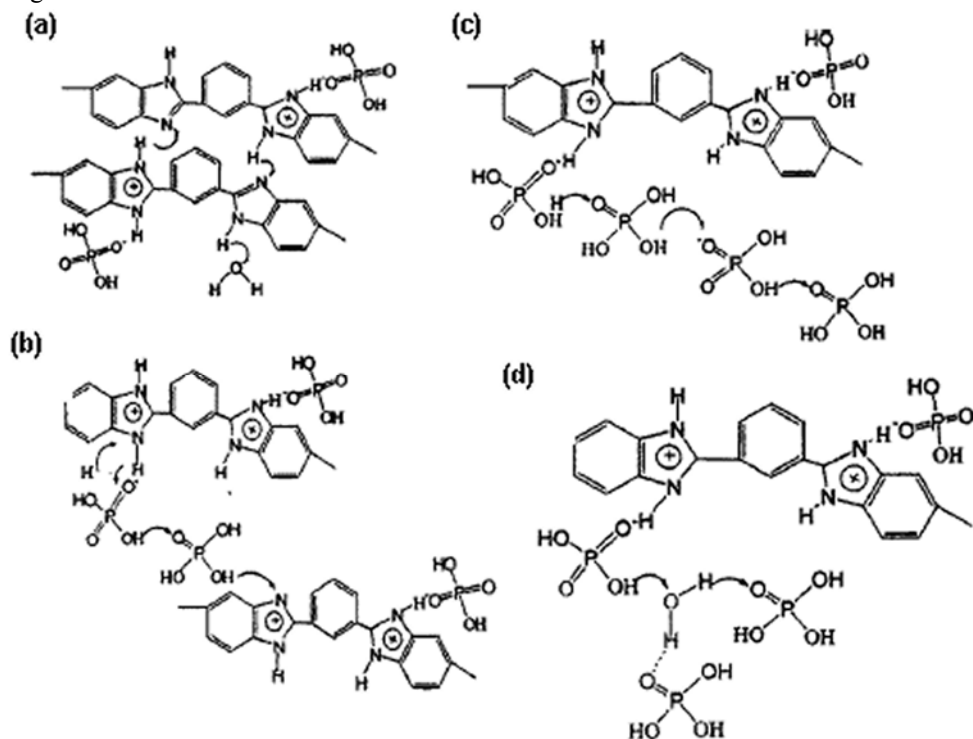
Figure 2-21: (a) H$_3$PO$_4$ protonated PBI, (b) proton transfer acid-BI-acid, (c) proton transfer along acid-acid, (d) proton transfer along acid-water [91]

Acid doping is also performed with other membrane types. But the PBI variant receives the most attention; there are even commercial versions available [94].

The effect of contaminants on the acid doped membranes is not yet known, and further research in this area is required.

Cathode

At the cathode, which also contains a platinum catalyst, the electrons and protons react with oxygen on the catalyst surface to form water, as shown in equations (2.36), (2.37) & (2.38) [95].

$$O_2 + H^+ + 2e^- + Pt \rightleftarrows Pt - (O_2H)_{ads} \qquad (2.36)$$

$$Pt - (O_2H)_{ads} + H_2O + 2Pt \rightleftarrows 3Pt - (OH)_{ads} \qquad (2.37)$$

$$3Pt - (OH)_{ads} + 3H^+ + 3e^- \rightleftarrows 3H_2O + 3Pt \qquad (2.38)$$
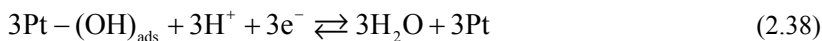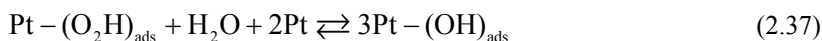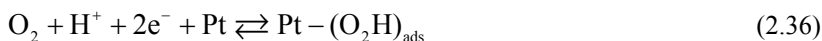
The water formed with this reaction diffuses out of the cathode. Platinum is used because it is the most active electro catalyst for the reduction of oxygen [70]. Like at the anode the catalyst is carried on a carbon carrier.

The search for more active oxygen reduction catalyst is still going on. Again platinum alloys are seen as an alternative. The following alloys have been suggested: Pt/Cr, Pt/Zr, and Pt/Ti. These alloys have a higher activity towards the electrochemical reduction of oxygen.

A recent development is a cathode which does not contain any platinum. The electrode is made of poly(3,4-ethylenedioxythiophene) (PEDOT) [96]. This polymer material is the catalyst for the reduction of oxygen. It is carried on the Goretex porous membrane [96]. The structure of PEDOT is given in Figure 2-22.
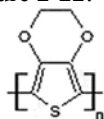
Figure 2-22 structure of poly(3,4-ethylenedioxythiophene)

This material showed similar performance compared to platinum electrodes [96].

The contaminants known for the cathode of PEM fuel cell are: NO, NO_2, SO_2, SO_3, O_3, CO, CO_2, and some organic species usually coming from lubricants of compressors and blowers. In most cases, the amount of contaminants is of such a level that they have hardly any effect on the performance of the fuel cell [97, 98]. Because when ambient air is used, the concentrations of the contaminants are very low. There is no consensus about this. Yang et al.[99] claim that there is an effect of NO_x on the performance of the PEM fuel cell, but that effect is not permanent. The deterioration depends on the concentration of NO_x, and the amount of NO_x in the air, which is in turn dependant on the local environment. For example, the concentration of NO_x will be higher near a highway or factory, then in a rural environment.

The sulphur compounds poison the catalysts in a similar way as hydrogen sulphide does at the anode. The same applies for carbon oxides.

Larger hydrocarbons can also be a source of contamination. These hydrocarbons come from the lubricants and oil used in compressors. Because these hydrocarbons can block the active sites of the catalyst, it is possible that the performance decreases over time. The hydrocarbons can also influence the water management in the cathode, because of their organic nature.

The membrane electrode assembly

A membrane electrode assembly (MEA) is actually, the anode, the membrane and cathode in a single piece. The MEA is constructed by placing an anode and a cathode with the catalytic layer on the membrane. At one side the anode and at the other side of the membrane the cathode. These three elements are usually hot pressed together forming a MEA. The hot pressing is performed to ensure a good contact area and interface between

the catalyst of the electrode and proton conducting membrane. This is the most common way to produce membrane electrode assemblies.

Binary plates

Binary plates have three different functions, to spatially separate two fuel cells, to collect the current produced by the fuel cell, and to distribute the fuel/oxidant. These plates are usually constructed of some kind of alloy; this is to enhance the electrical conductivity and chemical stability. Iron from stainless steel can severely deteriorate the performance of the PEM fuel cell, because iron ions cause leaching of fluorine from the PFSA membrane [100]. Iron free bipolar plates are suggested to be used, like carbon or aluminium alloys. But one has to keep in mind that also other metal ions can leach out the bipolar plate and influence the performance of the fuel cell.

Summary

The PEM fuel cell is a fuel cell especially suitable for small and mobile applications, due to its low operating temperature and fast start-up times. The standard PEM fuel cell operates at a temperature of 80-90°C. This type of fuel cell is very susceptible for contaminations; especially carbon monoxide is very damaging. Therefore a search for a more robust design is ongoing. Most of the research focuses on the increase of the operating temperature of the PEM fuel cell. Since the proton conducting membrane uses water to transport protons from the anode to the cathode, the research focuses on improving or replacing the current membrane materials. The PEM fuel cell is able to operate at higher temperature and is less susceptible to carbon monoxide.

2.3.2.Solid Oxide Fuel Cell

Another type of fuel cells is the solid oxide fuel cell, also known as the SOFC. A schematic representation of a SOFC is given in Figure 2-23.
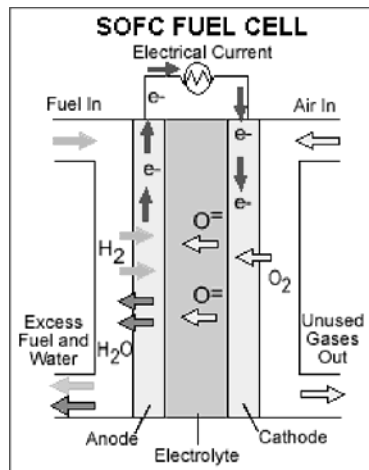
Figure 2-23 schematic representation of a solid oxide fuel cell

In this fuel cell, the electrolyte is a ceramic material, which conducts oxygen ions. The fuel for this type of fuel cell can be hydrogen, carbon monoxide or even light hydrocarbons. It can reform methane into hydrogen and carbon monoxide, since the fuel cell operates at a high temperature (600-1000°C). This type of fuel cells is more applicable in stationary

applications, due to its high operating temperature. This high temperature makes the fuel cell susceptible for thermal stresses; therefore it needs long cold start-up times. In general there are two main designs of SOFC's: the planar design and the tubular design. There are also four different ways to construct these types of fuel cells. The first one uses a thick and strong anode as a support for the electrolyte and cathode, also known as anode supported fuel cells. The second one uses the electrolyte as a support (electrolyte supported fuel cells). The third one is the cathode supported fuel cell. The fourth and last one is the interconnect supported fuel cell. In Figure 2-24, the different construction ways are indicated.The interconnect provides the connection between the cells in stack, to ensure electron transport. This connection can be either in series or parallel.
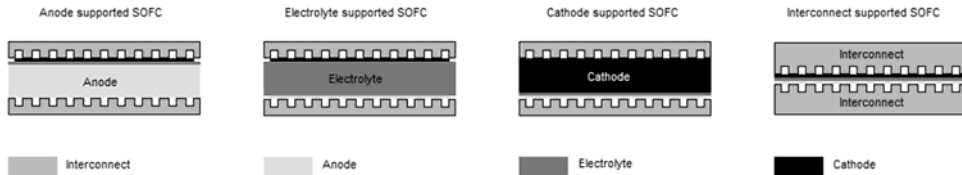
Figure 2-24 different construction methods for the planar SOFC

Currently, most SOFC's operate at a temperature of 900-1000°C. The research focuses on a reduction of this operating temperature to around 600°C, in order to reduce the material costs and thermal stresses within the fuel cell.

In the following sections the different parts of the solid oxide fuel cell will be discussed with a focus on contaminants for these different parts. First the anode of the SOFC will be discussed, followed by the ceramic electrolyte, the cathode and interconnect materials. Finally a summary will be given.

The anode

At the anode of the SOFC the fuel is converted. In contrast with the PEM fuel cell, the reaction products are formed at the anode. This can be a disadvantage, because of the dilution of the fuel by the reaction products. However, when reforming or water gas shift of the fuel is required, it is beneficial. The dilution of the fuel will predominantly occur at high loads of the fuel cell, leading to a drop in the Nernst voltage.
The electrochemical reactions take place at three phase boundary. The three phase boundary is the interface between the catalyst material, the anode material and gas phase, see also Figure 2-25.
Besides hydrogen, also carbon monoxide and small hydrocarbons like methane can be oxidized. As shown in Equation (2.39) & (2.40).

$$CO + O^{2-} \rightleftarrows CO_2 + 2e^- \tag{2.39}$$

$$CH_4 + 4O^{2-} \rightleftarrows CO_2 + 2H_2O + 8e^- \tag{2.40}$$
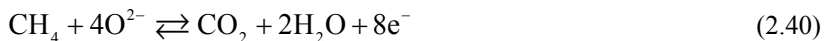
The conversion of carbon monoxide and methane does not only take place at the three phase boundary. The catalyst which is not at the three phase boundary promotes water gas shift and steam reforming processes. Equation (2.41) & (2.42) show the reactions for these processes.

$$CO + H_2O \rightleftarrows CO_2 + H_2 \qquad (2.41)$$

$$CH_4 + H_2O \rightleftarrows CO + 3H_2 \qquad (2.42)$$

The steam reforming reaction is endothermic; when this reaction takes place in the fuel cell the cell requires less cooling.
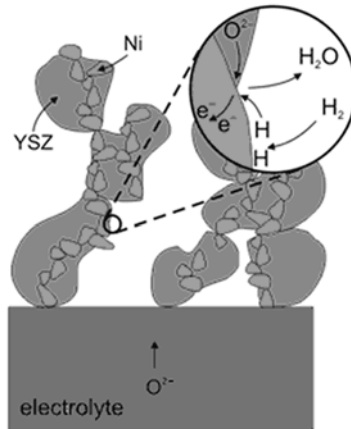
Figure 2-25 three phase boundary of the anode of a SOFC

The anode of a SOFC can be constructed from many different materials, commonly nickel yttria stabilized zirconia (Ni-YSZ) is used as anode material. This material has several drawbacks [101]:

- The material is very sensitive to sulphur poisoning. Also HCl is reported as a strong poison for Ni-YSZ anodes.
- Oxidation reduction intolerance. During the production of the anodes, the nickel is being reduced. When the anode gets into contact with oxygen during operation, the nickel can be oxidized again, leading to changes in the strength and structure of the material.
- Thermal expansion coefficient is considerably higher then of the electrolyte or cathode. This can lead to mechanical and dimensional stresses during thermal cycling.
- The anode material has poor activity towards the conversion of hydrocarbons; there is also the tendency of carbon formation. This carbon can block the pores and catalyst, leading to decreased performance of the fuel cell.

Ni-YSZ is very sensitive to sulphur poisoning (>1 ppm), especially to hydrogen sulphide (H_2S). Concentration into the ppm range can already have a deteriorating effect on the fuel cell performance [102]. If the concentration of H_2S is low, the performance of the fuel cell recovers when the sulphur is removed from the fuel [102]. The sensitivity of the fuel cell towards sulphur depends on the operating temperature and the sulphur concentration. When the operating temperature decreases, the fuel cell becomes more susceptible for sulphur poisoning [102]. The poisoning effect of sulphur at intermediate temperature becomes also irreversible [103, 104]. This means that a high grade desulfurization will be necessary when the operating temperature of the fuel cell is reduced.

The performance loss due to sulphur can be contributed to: (1) Physical absorption and chemisorption of H_2S at the active sites; (2) sulphidation of the anode material due to reaction between sulphur and anode material [103].

Hydrogen chloride is also a poison for the SOFC, but the effects are not as severe as for H_2S [105]. The effects are found to be reversible, but at high concentrations (>1000 ppm) the effect is said to be irreversible [101]. With increasing temperature, the deteriorating effect of the HCl on the SOFC increases [105]. Concentrations below 1 ppm of HCl have no effect on the performance of the fuel cell [106].

The effect of tars on the SOFC is hardly researched. Singh et al. [107] performed a thermodynamic analysis on the effect of tars on the anode of a SOFC. The focus in this research was on the risk of carbon deposition. It is expected that tars cause carbon deposition on the anode of the SOFC. This carbon blocks the active site of the anode, resulting in a deteriorating performance. The study shows that the formation of carbon is determined by the cell temperature, the amount of steam in the fuel, and the current density of the cell [107].

The effects of alkalis on the anode of the SOFC are not studied.

Another material used for anodes is for instance nickel gadolinium doped ceria (Ni-GDC). This material is often used in intermediate temperature solid oxide fuel cells (600-800°C). It has a higher conductivity then Ni-YSZ at intermediate temperatures. The study of Aravind [44] showed Ni-GDC to be more tolerant towards H_2S than Ni-YSZ. The concentration of H_2S in the gas could be as high as 9 ppm without deterioration of the performance of the fuel cell [44, 108]. Also the effects of tars of Ni-GDC anode are researched. Aravind [44] and Aravind et al [108] show that 110 ppm naphthalene has hardly an effect on the performance. Naphthalene is used here as a model compound for tar coming from biomass gasification. Hofman et al [109] also show that the tars have hardly any effect on the performance.

Char particles have a deteriorating effect on the performance of the fuel cell, since it causes carbon formation at the anode [109].

The ceramic electrolyte

The ceramic electrolyte provides the transport of oxygen ions from the cathode to the anode. This is established by doping a crystal lattice; this creates oxygen vacancies in the crystal lattice. The oxygen-ion transport is via a lattice hopping mechanism, where the oxygen moves onto the vacancies in the lattice [110].

The most commonly used material is yttria stabilized zirconia (YSZ), especially when the operating temperature is above 700°C. Other materials have also been suggested like: scandium doped zirconia (SDZ), gadolinium doped ceria (GDC), and lanthanum gallium doped with strontium and magnesium [101].

The cathode

The cathode gives electrons to oxygen molecules, where these oxygen molecules split into oxygen ions (Equation (2.43)).

$$\frac{1}{2}O_2 + 2e^- \rightleftarrows O^{2-} \tag{2.43}$$

The oxygen ions are then transported through the electrolyte. Predominantly, the reduction of oxygen takes place at the three phase boundary. The three phase boundary is where the cathode material, the electrolyte material and the gas phase interact with each other.

The most commonly used materials for the cathode are doped lanthanum-manganites, for instance strontium doped lanthanum manganite (LSM). This material is especially used in SOFC's operating at high temperatures (~1000°C). For lower temperatures other materials

are used, because the conductivity of LSM is low at intermediate temperatures. One of those materials is lanthanum ferrite doped with strontium (LSF).
The influence of contaminants from air is not researched yet.

Interconnects

The interconnect provides the connection between fuel cells in a stack, either in parallel or in series. The materials used for the interconnect depends on the operating temperature. Ceramic materials are used when the operating temperature is above 800°C. Metallic materials are used when the temperature is lower than 800°C. The electrical conductivity of ceramic materials at these lower temperatures is not sufficient.
Due to the high temperature and the oxidizing environment inside the fuel cell the application of metallic interconnects is challenging. The high temperature can cause creep of the metal and the oxidizing environment can cause reduction of conductivity between the electrodes and the interconnect. Also leaching of the metal into the electrode can have a deteriorating effect on the performance of the fuel cell. A commonly used metal for interconnects is Crofer22 APU [101]. In order to prevent the leaching of croma into the fuel cell the interconnect is coated with for instance strontium-doped lanthanum cobaltite or manganite [101].
Research is still ongoing for better and cheaper materials.

Seals

Seals within the SOFC can have a wide range functions, for instance [101]:
- Prevent mixing of fuel and oxidant
- In some configurations, prevent mixing of reactants with the ambient environment
- In some configurations, provide mechanical bonding of components
- In some designs, provide electrical insulation between stack components

Seals are mostly required for planar SOFC fuel cells; some tubular fuel cells do not have any seals.
Fundamentally, there are two types of seals for the SOFC, the bonded seals and the compressive seals.
In bonded seal, a hermetic seal is achieved through adhesive forces between the seal material and the two bonded surfaces. Bonded seals are found in two forms: rigid seals and compliant seals. The rigid seals need to be closely matched to the thermal expansion coefficient of the bonded materials. In the case of a compliant seal the match does not have to be that strict. Bonded seals can be divided into two sub-types: glass-ceramic seals and metal brace seals.

In compressive seals, a hermetic seal is achieved by pressing the seal material between the surfaces to be sealed. Compressive seals offer some advantages [101]:
- Mechanically "de-couple" adjacent stack components, thus reducing thermal stress during cycling
- Thermal expansion matching requirements between cell components may be somewhat relaxed (though electrical contact considerations may still require this)
- Some are easy and inexpensive to fabricate

However, there are also barriers to overcome [101]:
- It is difficult to achieve a hermetic seal with some materials unless "soft seat" interlayer is provided

- Few materials and structures are compliant and provide a hermetic seal at the operating temperatures
- A load frame is required to provide compression to all seals. This type of hardware is potentially bulky and expensive. If (portions of the) load frame must be kept at lower temperatures than the stack itself, packaging and insulation is significantly complicated, especially if multiple stacks are to be combined for larger-capacity systems
- Other stack components must be designed to withstand prolonged pressure. This can be a challenge, given that creep strength of the metals used in the interconnect is typically very low (in the 700 to 800 °C operating temperature range typical for state-of-the-art planar cells)
- To the extent that electrical contact between cell components depends on controlled pressure, balancing these pressure requirements with those of the seal can be a challenge for the cell designer

Mica and hybrid mica are found to be good candidates for these types of seals.

In general, a lot of research still has to be done with respect to sealing materials.

Summary

Solid oxide fuel cells are capable to convert not only hydrogen but also carbon monoxide and small hydrocarbons. The high operating temperature of the fuel cell facilitates the conversion of the small hydrocarbons and a high tolerance towards impurities. The choice of the right anode material is important when considering the application of bio syn-gas. The research focuses on the material, which are able to operate at intermediate temperatures 600-800°C. The lower temperature makes the construction easier. Also the search for more sulphur tolerant materials is ongoing. The planar design of the fuel cell is further researched, since it needs seals to ensure save and good operation of the fuel cell.

2.4. References

1. Dupont C., Boissonnet G., Seiler J.-M., Gauthier P., Schweich D. Study about the kinetic processes of biomass steam gasification. Fuel 2007; 86(1-2): 32-40.
2. Mousques P., Dirion J. L., Grouset D. Modeling of solid particles pyrolysis. J Anal Appl Pyrolysis 2001; 58-59 733-745.
3. de Jong W., Unal O., Andries J., Hein K. R. G., Spliethoff H. Thermochemical conversion of brown coal and biomass in a pressurised fluidised bed gasifier with hot gas filtration using ceramic channel filters: measurements and gasifier modelling. Appl Energy 2003; 74(3-4): 425-437.
4. Moulijn J. A., Makkee M., Van Diepen A. Chemical Process Technology. Chichester: John Wiley and Sons Ltd., 2001.
5. Van den Aarsen F. G. Fluidised Bed Wood Gasifier Performance and Modeling. PhD Thesis, TU Twente, 1985.
6. Kruse A. Supercritical water gasification. Biofuels, Bioprod Biorefin 2008; 2(5): 415-437.
7. van der Nat K. V., Woudstra N., Spliethoff H. Evaluation of several biomass gasification processes for the production of a hydrogen rich synthesis gas In: International Hydrogen Energy Congress and Exhibition IHEC 2005, Istanbul, 2005.
8. Kruse A. Hydrothermal biomass gasification. J Supercrit Fluids 2009; 47(3): 391-399.

9.   Biomass Technology Group B. T. G. Energie uit Biomassa. 2005; Report, BTG
        Biomass Technology Group BV.
10.   Bridgwater A. V. The technical and economic feasibility of biomass gasification
        for power generation. Fuel 1995; 74(5): 631-653.
11.   Stahl K., Neergaard M. IGCC Power Plant for Biomass Utilisation, Värnamo,
        Sweden. Biomass Bioenergy 1998; 15 (3): 205-211.
12.   Essent. Essent biomass conference 2009. In: Mastering biomass, Essent biomass
        conference 2009, 2009.
13.   Stahl K., Waldheim L., Morris M., Johnsson U., Gardmark L. Biomass IGCC at
        Värnamo, Sweden - Past and Future. In: GCEP Energy Workshop, California,
        USA, 2004.
14.   Willeboer W. The amer demolition wood gasification project. Biomass Bioenergy
        1998; 15(3): 245-249.
15.   Paisley M. A., Irving J. M., Overend R. P. A Promising Power Option -- The
        FERCO SILVAGAS Biomass Gasification Process - Operating Experience at the
        Burlington Gasifier In: ASME Turbo Expo, New Orleans, 2001.
16.   Paisley M. A., Farris M. C., Black J. W., Irving J. M., Overend R. P. Preliminary
        Operating Results from the Battell / FERCO Gasification Demonstration Plant in
        Burlington, Vermont, U.S.A. In: 1st World Conference and Exhibition on Biomass
        for Energy and Industry, Sevile, Spain 2000.
17.   Hofbauer H., Rauch R., Loeffler G., Kaiser S., Fercher E., Tremmel H. Six Years
        Experience with the FICFB-Gasification Process. In: 12th European Conference
        and Technology Exhibition on Biomass for Energy, Industry and Climate
        Protection, Amsterdam, The Netherlands, 2002.
18.   Hamelinck C. N., Faaij A. P. C. Future prospects for production of methanol and
        hydrogen from biomass. 2001; Report, Copernicus Institute.
19.   Hamelinck C. N., Faaij A. P. C. Future prospects for production of methanol and
        hydrogen from biomass. J Power Sources 2002; 111(1): 1-22.
20.   Elliott D. C., Neuenschwander G. G., Phelps M. R., Hart T. R., Zacher A. H.,
        Silva L. J. Chemical Processing in High-Pressure Aqueous Environments. 6.
        Demonstration of Catalytic Gasification for Chemical Manufacturing Wastewater
        Cleanup in Industrial Plants. Industrial & Engineering Chemistry Research 1999;
        38(3): 879-883.
21.   Elliott D. C. Catalytic hydrothermal gasification of biomass. Biofuels, Bioprod
        Biorefin 2008; 2(3): 254-265.
22.   Nakamura A., Kiyonaga E., Yamamura Y., Shimizu Y., Minowa T., Noda Y.,
        Matsumura Y. Gasification of Catalyst-Suspended Chicken Manure in
        Supercritical Water. J Chem Eng Jpn 2008; 41(5): 433-440.
23.   Matsumura Y., Minowa T. Fundamental design of a continuous biomass
        gasification process using a supercritical water fluidized bed. Int J Hydrogen
        Energy 2004; 29(7): 701-707.
24.   Schuster G., Loffler G., Weigl K., Hofbauer H. Biomass steam gasification - an
        extensive parametric modeling study. Bioresource Technol 2001; 77(1): 71-79.
25.   Pellegrini L. F., de Oliveira J. S. Exergy analysis of sugarcane bagasse gasification.
        Energy 2007; 32(4): 314-327.
26.   Li X., Grace J. R., Watkinson A. P., Lim C. J., Ergüdenler A. Equilibrium
        modeling of gasification: a free energy minimization approach and its application
        to a circulating fluidized bed coal gasifier. Fuel 2001; 80(2): 195-207.
27.   Aspen Plus, 20.0.3595. Aspen Techechnology Inc., 2006.

28.   Cycle-Tempo, 5.0. TU Delft, 2006. www.cycle-tempo.nl
29.   Panopoulos K. D., Fryda L. E., Karl J., Poulou S., Kakaras E. High temperature solid oxide fuel cell integrated with novel allothermal biomass gasification: Part I: Modelling and feasibility study. J Power Sources 2006; 159(1): 570-585.
30.   Altafini C. R., Wander P. R., Barreto R. M. Prediction of the working parameters of a wood waste gasifier through an equilibrium model. Energy Convers Manage 2003; 44(17): 2763-2777.
31.   Elmegaard B., Korving A. Analysis of an intergrated biomass gasification/combined cycle plant. In: Efficiency, cost, optimization, simulation and environmental aspects of energy systems and processes --ECOS'98, Nancy, France, 1998.
32.   Calzavara Y., Joussot-Dubien C., Boissonnet G., Sarrade S. Evaluation of biomass gasification in supercritical water process for hydrogen production. Energy Convers Manage 2005; 46(4): 615-631.
33.   Tang H., Kitagawa K. Supercritical water gasification of biomass: thermodynamic analysis with direct Gibbs free energy minimization. Chem Eng J 2005; 106(3): 261-267.
34.   Rhodes M. J. Introduction to Particle Technology. Chichester: John Wiley & Sons Ltd., 2000.
35.   Kasper S. Clean-up and processing of coal-derived gas for hydrogen applications. Int J Hydrogen Energy 1983; 8(3): 183-190.
36.   Stevens D. J. Hot Gas Conditioning: Recent Progress with Large-Scale Biomass Gasification Systems. 2001; Report, National Renewable Energy Laboratory (NREL).
37.   Cummer K. R., Brown R. C. Ancillary equipment for biomass gasification. Biomass Bioenergy 2002; 23(2): 113-128.
38.   McKendry P. Energy production from biomass (part 3): gasification technologies. Bioresource Technol 2002; 83(1): 55-63.
39.   Engstrom F. Hot gas clean-up bioflow ceramic filter experience. Biomass Bioenergy 1998; 15(3): 259-262.
40.   Sinnott R. K. Coulson & Richardson's Chemical Engineering. Butterworth-Heinemann, 2000.
41.   Hustad J. E., Hofbauer H., Vik A., Byrknes J. BioSOFC - Technology Development for Integrated SOFC, Biomass Gasification and High Temperature Gas Cleaning. In: Biomass Conference, Biomass for Energy, Industry and Climate Protection, Rome, 2004.
42.   Evans R. J., Milne T. A. Molecular characterization of the pyrolysis of biomass. Energy Fuels 1987; 1(2): 123-137.
43.   Milne T. A., Abatzoglou N., Evans R. J. Biomass Gasifier "Tars": Their Nature, Formation, and Conversion. . 1998; Report, NREL.
44.   Aravind P. V. Studies on High Efficiency Energy Systems Based on Biomass Gasifiers and Solid Oxide Fuel Cells with Ni/GDC Anodes. PhD Thesis, University of Technology Delft, 2007.
45.   Hofbauer H., Rauch R., Bosch K., Kock R., Aichernig C. Biomass CHP Plant Güssing - A Success Story. In: Expert Meeting on Pyrolysis and Gasification of Biomass and Waste, Strasbourg, 2002.
46.   Vittala C. B. V., Ray S., Chaterjee S., Singh T. D., Datta K. Condensing Heat Transfer in Vertical Cyclone. Exp Heat Transfer 2002; 15(4): 221 - 228.

47.   Turn S. Q., Kinoshita C. M., Ishimura D. M., Hiraki T. T., Zhou J., Masutani S. M.
       An Experimental Investigation of Alkali Removal from Biomass Producer Gas
       Using a Fixed Bed of Solid Sorbent. Ind Eng Chem Res 2001; 40(8): 1960-1967.
48.   Ciliberti D. F., Lippert T. E. Filtering system and method of using same. 1985,
       Patent: US4553986
49.   Turn S., Kinoshita C., Zhang Z., Ishimura D., Zhou J. An experimental
       investigation of hydrogen production from biomass gasification. Int J Hydrogen
       Energy 1998; 23(8): 641-648.
50.   Dou B., Shen W., Gao J., Sha X. Adsorption of alkali metal vapor from high-
       temperature coal-derived gas by solid sorbents. Fuel Process Technol 2003; 82(1):
       51-60.
51.   Hepola J., Simell P. Sulphur poisoning of nickel-based hot gas cleaning catalysts
       in synthetic gasification gas: II. Chemisorption of hydrogen sulphide. Appl Catal
       B: Environ 1997; 14(3-4): 305-321.
52.   Torres W., Pansare S. S., Goodwin J. G. Hot Gas Removal of Tars, Ammonia, and
       Hydrogen Sulfide from Biomass Gasification Gas. Catal Rev 2007; 49(4): 407 -
       456.
53.   Westmoreland P. R., Harrison D. P. Evaluation of candidate solids for high-
       temperature desulfurization of low-Btu gases. Environ Sci Technol 1976; 10(7):
       659-661.
54.   Alderliesten P. T., Brunia A., Enoch G. D., Jansen D., Klein Teeselink H.,
       Melman A. G., Raas J. L., Schmal D., Tummers J. F., Verschoor M. J. E., Woudstr
       N. System Study High Temperature Gas Cleaning at IGCC Systems. 1990; Report,
55.   Twigg M. V. Catalyst Handbook. London: Wolfe Publishing Ltd., 1989.
56.   Hiller H., Reimert R., Marschner F., Renner H.-J., Boll W., Supp E., Brejc M.,
       Liebner W., Schaub G., Hochesand G., Higman C., Kalteier P., Muller W.-D.,
       Kriebel M., Schlichting H., Tanz H., Stonner H.-M., Klein H., Hilsebein W.,
       Gronemann V., Zwiefelhofer U., Albrecht J., Cowper C. J., Driesen H. E. Gas
       production.Ullmanns' Encyclopedia of Industrial Chemistry, John Wiley and Sons
       Inc., 2006.
57.   Rostrup-Nielsen J. R. Production of synthesis gas. Catal Today 1993; 18(4): 305-
       324.
58.   Snoeck J. W., Froment G. F., Fowles M. Steam/CO_2 Reforming of Methane.
       Carbon Filament Formation by the Boudouard Reaction and Gasification by CO_2,
       by H_2, and by Steam: Kinetic Study. Ind Eng Chem Res 2002; 41(17): 4252-4265.
59.   Abashar M. E. E. Coupling of steam and dry reforming of methane in catalytic
       fluidized bed membrane reactors. Int J Hydrogen Energy 2004; 29(8): 799-808.
60.   Shoko E., McLellan B., Dicks A. L., da Costa J. C. D. Hydrogen from coal:
       Production and utilisation technologies. Int J Coal Geol 2006; 65(3-4): 213-222.
61.   Balthasar W., Hambleton D. J. Industrial scale production of hydrogen from
       natural gas, naphtha and coal. Int J Hydrogen Energy 1980; 5(1): 21-33.
62.   Pennline H. W., Luebke D. R., Jones K. L., Myers C. R., Morsi B. I., Heintz Y. J.,
       Ilconich J. B. Progress in carbon dioxide capture and separation research for
       gasification-based power generation point sources. Fuel Process Technol 2008;
       89(9): 897-907.
63.   Choi Y., Stenger H. G. Kinetics, simulation and insights for CO selective
       oxidation in fuel cell applications. J Power Sources 2004; 129(2): 246-254.

64.   Florin N. H., Harris A. T. Enhanced hydrogen production from biomass with in situ carbon dioxide capture using calcium oxide sorbents. Chem Eng Sci 2008; 63(2): 287-316.

65.   Florin N. H., Harris A. T. Hydrogen production from biomass coupled with carbon dioxide capture: The implications of thermodynamic equilibrium. Int J Hydrogen Energy 2007; 32(17): 4119-4134.

66.   Pfeifer C., Puchner B., Hofbauer H. In-Situ CO_2-Absorption in a Dual Fluidized Bed Biomass Steam Gasifier to Produce a Hydrogen Rich Syngas. Int J Chem Reactor Eng 2007; 5 A9.

67.   Haussinger P., Lohmuller R., Watson A. M. Hydrogen.Ullmann's Encyclopedia of Industrial Chemistry, John Wiley and Sons Inc., 2000.

68.   O'Hayre R. P. Fuel Cell Fundamentals. Hoboken: Wiley, 2006.

69.   Zhang J., Xie Z., Zhang J., Tang Y., Song C., Navessin T., Shi Z., Song D., Wang H., Wilkinson D. P., Liu Z.-S., Holdcroft S. High temperature PEM fuel cells. J Power Sources 2006; 160(2): 872-891.

70.   Ralph T. R., Hogarth M. P. Catalysis for Low Temerature Fuel Cells. Platinum Met Rev 2002; 46(1): 3-14.

71.   Ralph T. R., Hogarth M. P. Catalysis for Low Temperature Fuel Cells. Platinum Met Rev 2002; 46(3): 117-135.

72.   Tsuda M., Dino W. A., Kasai H. Behavior of hydrogen atom at Nafion-Pt interface. Solid State Commun 2005; 134(9): 601-605.

73.   Cheng X., Shi Z., Glass N., Zhang L., Zhang J., Song D., Liu Z.-S., Wang H., Shen J. A review of PEM hydrogen fuel cell contamination: Impacts, mechanisms, and mitigation. J Power Sources 2007; 165(2): 739-756.

74.   Jiang R., Kunz H. R., Fenton J. M. Electrochemical Oxidation of H_2 and H_2/CO Mixtures in Higher Temperature (T_{cell} > 100°C) Proton Exchange Membrane Fuel Cells: Electrochemical Impedance Spectroscopy. J Electrochem Soc 2005; 152(7): A1329-A1340.

75.   Li Q., He R., Gao J.-A., Jensen J. O., Bjerrum N. J. The CO Poisoning Effect in PEMFCs Operational at Temperatures up to 200°C. J Electrochem Soc 2003; 150(12): A1599-A1605.

76.   Ball S., Hodgkinson A., Hoogers G., Maniguet S., Thompsett D., Wong B. The Proton Exchange Membrane Fuel Cell Performance of a Carbon Supported PtMo Catalyst Operating on Reformate. Electrochem Solid-State Lett 2002; 5(2): A31-A34.

77.   Urian R. C., Gullá A. F., Mukerjee S. Electrocatalysis of reformate tolerance in proton exchange membranes fuel cells: Part I. J Electroanal Chem 2003; 554-555 307-324.

78.   Qi Z., He C., Kaufman A. Effect of CO in the anode fuel on the performance of PEM fuel cell cathode. J Power Sources 2002; 111(2): 239-247.

79.   Qi Z., He C., Kaufman A. Poisoning of Proton Exchange Membrane Fuel Cell Cathode by CO in the Anode Fuel. Electrochem Solid-State Lett 2001; 4(12): A204-A205.

80.   Janssen G. J. M. Modelling study of CO_2 poisoning on PEMFC anodes. J Power Sources 2004; 136(1): 45-54.

81.   de Bruijn F. A., Papageorgopoulos D. C., Sitters E. F., Janssen G. J. M. The influence of carbon dioxide on PEM fuel cell anodes. J Power Sources 2002; 110(1): 117-124.

82.   Rajalakshmi N., Jayanth T. T., Dhathathreyan K. S. Effect of Carbon Dioxide and Ammonia on Polymer Electrolyte Membrane Fuel Cell Stack Performance. Fuel Cells 2003; 3(4): 177-180.

83.   Mathieu M.-V., Primet M. Sulfurization and regeneration of platinum. Appl Catal 1984; 9(3): 361-370.

84.   Mohtadi R., Lee W. k., Cowan S., Van Zee J. W., Murthy M. Effects of Hydrogen Sulfide on the Performance of a PEMFC. Electrochem Solid-State Lett 2003; 6(12): A272-A274.

85.   Jannasch P. Recent developments in high-temperature proton conducting polymer electrolyte membranes. Curr Opin Colloid Interface Sci 2003; 8(1): 96-102.

86.   Li Q., He R., Jensen J. O., Bjerrum N. J. Approaches and Recent Development of Polymer Electrolyte Membranes for Fuel Cells Operating above 100°C. Chem Mater 2003; 15(26): 4896-4915.

87.   Scott K., Taama W., Cruickshank J. Performance and modelling of a direct methanol solid polymer electrolyte fuel cell. J Power Sources 1997; 65(1-2): 159-171.

88.   Jensen J. O., Qingfeng L., He R., Gang X., Gao J., Bjerrum N. High Temperature Polymer Fuel Cells: Heat Utilization and CO Tolerance. In: First European Hydrogen Energy Conference, Grenoble, France, 2003.

89.   Halseid R., Vie P. J. S., Tunold R. Effect of ammonia on the performance of polymer electrolyte membrane fuel cells. J Power Sources 2006; 154(2): 343-350.

90.   Uribe F. A., Gottesfeld S., Zawodzinski J. T. A. Effect of Ammonia as Potential Fuel Impurity on Proton Exchange Membrane Fuel Cell Performance. J Electrochem Soc 2002; 149(3): A293-A296.

91.   Ma Y. L., Wainright J. S., Litt M. H., Savinell R. F. Conductivity of PBI Membranes for High-Temperature Polymer Electrolyte Fuel Cells. J Electrochem Soc 2004; 151(1): A8-A16.

92.   Li Q., Hjuler H. A., Bjerrum N. J. Phosphoric acid doped polybenzimidazole membranes: Physiochemical characterization and fuel cell applications. J Appl Electrochem 2001; 31(7): 773-779.

93.   Weng D., Wainright J. S., Landau U., Savinell R. F. Electro-osmotic Drag Coefficient of Water and Methanol in Polymer Electrolytes at Elevated Temperatures. J Electrochem Soc 1996; 143(4): 1260-1263.

94.   Schmidt T. J., Baurmeister J. Properties of high-temperature PEFC Celtec®-P 1000 MEAs in start/stop operation mode. J Power Sources 2008; 176(2): 428-434.

95.   Antoine O., Bultel Y., Durand R. Oxygen reduction reaction kinetics and mechanism on platinum nanoparticles inside Nafion(R). J Electroanal Chem 2001; 499(1): 85-94.

96.   Winther-Jensen B., Winther-Jensen O., Forsyth M., MacFarlane D. R. High Rates of Oxygen Reduction over a Vapor Phase-Polymerized PEDOT Electrode. Science 2008; 321(5889): 671-674.

97.   Moore J. M., Adcock P. L., Lakeman J. B., Mepsted G. O. The effects of battlefield contaminants on PEMFC performance. J Power Sources 2000; 85(2): 254-260.

98.   Mohtadi R., Lee W. k., Van Zee J. W. Assessing durability of cathodes exposed to common air impurities. J Power Sources 2004; 138(1-2): 216-225.

99.   Yang W. J., Park S. K., Kim T. S., Kim J. H., Sohn J. L., Ro S. T. Design performance analysis of pressurized solid oxide fuel cell/gas turbine hybrid

systems considering temperature constraints. J Power Sources 2006; 160(1): 462-473.

100. Pozio A., Silva R. F., De Francesco M., Giorgi L. Nafion degradation in PEFCs from end plate iron contamination. Electrochim Acta 2003; 48(11): 1543-1549.

101. EG&G Techincal Services. Fuel Cell Handbook. Morgantown: Nation Energy Technology Laboratory, 2004.

102. Matsuzaki Y., Yasuda I. The poisoning effect of sulfur-containing impurity gas on a SOFC anode: Part I. Dependence on temperature, time, and impurity concentration. Solid State Ionics 2000; 132(3-4): 261-269.

103. Gong M., Liu X., Trembly J., Johnson C. Sulfur-tolerant anode materials for solid oxide fuel cell application. J Power Sources 2007; 168(2): 289-298.

104. Zha S., Cheng Z., Liu M. Sulfur Poisoning and Regeneration of Ni-Based Anodes in Solid Oxide Fuel Cells. J Electrochem Soc 2007; 154(2): B201-B206.

105. Trembly J. P., Gemmen R. S., Bayless D. J. The effect of coal syngas containing HCl on the performance of solid oxide fuel cells: Investigations into the effect of operational temperature and HCl concentration. J Power Sources 2007; 169(2): 347-354.

106. Veyo S. E. Evaluation of Fuel Impurity Effects on Solid Oxide Fuel Cel Performance. 1998; Report, Westinghouse Electric Company.

107. Singh D., Hernandez-Pacheco E., Hutton P. N., Patel N., Mann M. D. Carbon deposition in an SOFC fueled by tar-laden biomass gas: a thermodynamic analysis. J Power Sources 2005; 142(1-2): 194-199.

108. Aravind P. V., Ouweltjes J. P., Woudstra N., Rietveld G. Impact of Biomass-Derived Contaminants on SOFCs with Ni/Gadolinia-Doped Ceria Anodes. Electrochem Solid-State Lett 2008; 11(2): B24-B28.

109. Hofmann P., Panopoulos K. D., Fryda L. E., Schweiger A., Ouweltjes J. P., Karl J. Integrating biomass gasification with solid oxide fuel cells: Effect of real product gas tars, fluctuations and particulates on Ni-GDC anode. Int J Hydrogen Energy 2008; 33(11): 2834-2844.

110. Kee R. J., Zhu H., Sukeshini A. M., Jackson G. S. Solid Oxide Fuel Cells: Operating Principles, Current Challenges, and the Role of Syngas. Combust Sci Technol 2008; 180(6): 1207 - 1244.

3. Five Hydrogen production plants based on biomass gasification

Abstract: *Biomass gasification is a promising option for the sustainable production of hydrogen rich gas. Five different commercial or pilot scale gasification systems are considered for the design of a hydrogen production plant that generates almost pure hydrogen. For each of the gasification techniques models of two different hydrogen production plants are developed in Cycle-Tempo: one plant with low temperature gas cleaning (LTGC) and the other with gas cleaning at high temperature (HTGC). The thermal input of all plants is 10 MW of biomass with the same dry composition. An exergy analysis of all processes has been made. The processes are compared on their thermodynamic performance (hydrogen yield and exergy efficiency). Since the heat recovery is not incorporated in the models, two efficiencies are calculated. The first one is calculated for the case that all residual heat can be applied, the case with ideal heat recovery, and the other is calculated for the case without heat recovery. It is expected that in real systems only a part of the residual heat can be used. Therefore, the actual value will be in between these calculated values. It was found that three processes have almost the same performance: The Battelle gasification process with LTGC, the FICFB gasification process with LTGC, and the Blaue Turm gasification process with HTGC. All systems include further processing of the cleaned gas from biomass gasification into almost pure hydrogen. The calculated exergy efficiencies are respectively 50.69%, 45.95%, and 50.52% for the systems without heat recovery. The exergy efficiencies of the systems with heat recovery are respectively 62.79%, 64.41%, and 66.31%. The calculated hydrogen yields of the three processes do not differ very much. The hydrogen yield of the Battelle LTGC process appeared to be 0.097 kg $(kg_{(dry\ biomass)})^{-1}$, for the FICFB LTGC process a yield of 0.096 kg $(kg_{(dry\ biomass)})^{-1}$ was found, and for the Blaue Turm HTGC 0.106 kg $(kg_{(dry\ biomass)})^{-1}$. Since the Blaue Turm gasification process is far behind the technologies of the Battelle and FICFB process it is concluded that further consideration of the Battelle and FICFB processes has to be preferred for the generation of highly pure hydrogen.*

3.1. Introduction

The demand for renewable sources of energy is increasing, due to the increasing concern about global warming and climate changes. Also the fossil fuel reserves are declining. One interesting option is the use of biomass as a renewable source of energy. Due to the short carbon dioxide cycle, biomass is considered CO_2 neutral. Since biomass is a solid fuel, it has to be converted preferably first into a more convenient energy carrier, like hydrogen or bio syn-gas, before it will be converted into power.

A variety of gasification processes is under development to convert biomass in a hydrogen-rich gas. In the gasification process biomass is converted into a mixture of hydrogen, carbon monoxide, carbon dioxide and water using steam, oxygen or a steam/oxygen mixture as a gasifying agent. The oxygen can be fed to the system as air, enriched air or as pure oxygen.

In this chapter, five different gasification processes are considered for hydrogen generation. The five processes are supposed to be the basis for a hydrogen production plant that produces 99.99% pure hydrogen. For each of the gasification processes two different plant configurations are designed, one with high temperature gas cleaning, the other with gas cleaning at low temperature. All the processes have a thermal input of 10 MW. For the thermodynamic evaluation of the alternative systems, system models have been established using the computer program Cycle-Tempo [1], developed at the TU Delft. This program is well suited for exergy analyses. Hydrogen production and exergy losses are considered as the main criteria for the system selection in this study.

3.2. The gasification processes

The following gasification processes are chosen for the system evaluation as presented in this paper:
1. Battelle: Indirect atmospheric steam assisted circulating fluidized bed gasifier;
2. Värnamo: Pressurized air blown circulating fluidized bed gasifier;
3. FICFB: Indirect atmospheric steam assisted fast internal circulating fluidized bed gasifier;
4. IGT: Pressurized oxygen and steam assisted bubbling fluidized bed gasifier;
5. Blaue Turm: Staged reforming process.

These processes have been selected because of their potential use for the production of a hydrogen rich gas mixture. All processes are still under development, but have been successfully operated on a relative scale with a thermal biomass input of 1MW or more.

3.2.1.Battelle gasifier

The Battelle gasification process consists of two circulating fluidized beds as the main reactor: a gasifier (operating at a temperature of 820°C and a pressure of 1.1 bar) and a combustor (operating at: 1050°C and 1.2 bar). Biomass reacts in the gasifier with steam (steam conditions are 150°C and 2 bar); heat for this endothermic gasification reaction is obtained from the hot bed material that is recycled from the combustion reactor. At the outlet of the gasifier the solids in the fluid are separated in a cyclone. These solids still contain an amount of char that is passed to the combustor, where it is burnt with air. The inert bed material is heated in the combustor and separated from the flue gas in a cyclone at the outlet of the combustion reactor. Producer gas and flue gas leave the reactors at the corresponding reactor temperature. The Battelle process has been tested on a large scale with a biomass input of 200 tons day^{-1}. More information on the Battelle process can be found in [2-5].

3.2.2.Värnamo gasifier

The Värnamo gasifier is a pressurized air blown circulating fluidized bed gasifier operating at 950-1000°C and a pressure of 18 bar. Biomass reacts in the gasifier with the air, which enters the gasifier at 220-250°C and 18 bar. The inert bed material with the char is separated from the producer gas in a cyclone and is fed back to the bottom of the gasifier. The char is combusted with the air supplying the energy for the endothermic gasification reactions. The producer gas leaves the reactor at the corresponding reactor temperature. More information about the gasifier can be found here: [6, 7].

3.2.3.FICFB gasifier

The fast internal circulating fluidized bed gasifier is an indirect gasifier where the gasification zone (operating at a temperature of 800°C, and a pressure of 1.1 bar) and the

combustion zone (operating at: 1050°C, 1.1 bar) are separated. In the gasifier, biomass reacts with steam (steam conditions: 400°C and 1.1 bar); the heat for the endothermic reactions is supplied by the hot bed material (Olivine, $(MgFe)_2SiO_4$), which is recycled from the combustor. The gasifier is operated as a bubbling fluidized bed. The bed material and char moves from the bottom of the gasifier to the combustor, which is a circulating fluidized bed. Here, the char is combusted with air to supply heat to the bed material. The hot bed material is separated from the flue gas via a cyclone at the outlet of the combustor. This hot bed material is transported to the gasifier. The producer gas and flue gas leave the reactors at the corresponding reactor temperature. For more information: [8-11]

3.2.4. IGT gasifier

The Institute of Gas Technology has developed a pressurized direct oxygen fired gasifier, operating at a temperature of 920°C and a pressure of 25 bar. In this bubbling fluidized bed gasifier, a fraction of the biomass and char is combusted with oxygen to provide the heat for the endothermic gasification reactions. The gasifying agents in this process are steam and oxygen and they are both entering the reactor at a temperature of 240°C and a pressure of 25 bar. The inert bed material (alumina, Al_2O_3) stays in the reactor. Ashes, which leave the reactor together with the producer gas, are separated via a cyclone. The producer gas leaves the reactor at the reactor temperature. For more information: [12]

3.2.5. Blaue Turm gasifier

The Blaue Turm process is not really a gasification process, but a staged reforming process. It consists of four separate sections: the pyrolyser (operating at a temperature of 500-600°C and a pressure of 1.1 bar), the reformer (operating at: 950°C and 1.1 bar), the combustor (operating at : >1000°C and 1.1 bar), and the heat carrier pre-heater (operating at: 1000°C and 1.1 bar). In the pyrolyser all the volatile content of the biomass (±80%) is released and goes to the reformer. This pyrolysis gas is reformed with steam (steam conditions: 150°C, 2 bar) in order to increase hydrogen formation due to hydrocarbon reforming and shift reactions. Because of the high temperature in the reformer the tars are destroyed and partly converted into hydrogen [13]. The residual 20% of the biomass is separated from the bed material and combusted in the combustor. The flue gasses from the combustor are used to heat the bed material (corundum pebbles) in the heat carrier pre-heater. The hot bed material is used to supply the heat to the endothermic reaction in the reformer, and after being used in the reformer it supplies heat to the pyrolyser. The producer gas and the flue gas leave the process at their corresponding reactor temperatures. More information: [13]

3.3. Gas cleaning and gas processing

In order to produce 99.99% pure hydrogen from the producer gas coming from the gasifier, it needs to be cleaned and processed. The producer gas from the gasifier contains mainly hydrogen, carbon monoxide, carbon dioxide and methane. Besides the main components, the gas contains also minor impurities, like particulates, tar, alkalis, halogens and sulphur compounds. The main components of the producer gas have to be converted into hydrogen as far as possible and the remaining components have to be removed in order get almost pure hydrogen. However, this gas processing is only possible after removing the impurities to sufficiently low levels to enable proper operation of the gas processing reactors. Two methods of gas cleaning are considered for each gasification process: low temperature gas cleaning (LTGC) and high temperature gas cleaning (HTGC).

3.3.1. Low temperature gas cleaning

The gas, which leaves the gasification section, is first cooled to about 120°C. The cooling contributes to the cleaning, because alkalis will probably condense at ±600°C on to the entrained particulates [14]. Then the gas is passed through a bag filter, to remove the particulates together with the condensed alkalis. After the filter the gas is fed to a packed bed containing zinc oxide, which is used to adsorb the hydrogen sulphide in the gas. The amount of sulphur in wood is low, therefore cleaning in a zinc oxide bed is supposed to be sufficient [14]. The final step in the gas cleaning is the water scrubber. In the water are most of the impurities removed, like particles, tars, alkalis, and halogens. The waste water coming from this system needs further treatment before it can be disposed [14, 15].

3.3.2. High temperature gas cleaning

The producer gas is in the high temperature gas cleaning is first passed through a hot gas filter. This filter is constructed from either sintered metal or a ceramic material. Then the gas is passed through the tar cracker, in order to reduce the amount of tars in the gas. This tar cracker is actually a packed bed containing a catalyst like dolomite or a metal based catalyst. The tar cracker operates at 800°C, and a tar conversion of 99% can be achieved [14]. Next, the gas is passed through a reformer, in order to reduce the amount of light hydrocarbons in the gas; this will also increase the amount of hydrogen in the gas. Then the alkalis are absorbed in an absorber, which contains a so-called alkali-getter [15]. In this case bauxite is chosen as alkali-getter, since it can be regenerated [15]. Then the gas is cooled by adding some steam to the gas before it enters the sulphur removal unit. Also in this case the sulphur removal occurs in a packed bed of zinc oxide.

3.3.3. Gas processing

Reforming

Reforming is the process where light hydrocarbons, like methane, are being converted into carbon dioxide and hydrogen in the presence of steam. See for example the following reaction for methane reforming:

$$CH_4 + 2H_2O \rightleftarrows CO_2 + 4H_2 \tag{3.1}$$

Coke formation can occur during reforming; therefore sufficient amounts of steam have to be added. The steam suppresses the coke formation and promotes the reforming reactions [16]. Reforming is a catalyzed process, for the reforming reaction often a nickel catalyst is used. The nickel catalyst is sensitive to sulphur poisoning; therefore the gas needs to be virtually sulphur free.

Water gas shift

In order to produce hydrogen, the carbon monoxide in the product gas of the gasifier can be used to produce even more hydrogen. This can be done by means of the water gas shift reaction:

$$CO + H_2O \rightleftarrows CO_2 + H_2 \tag{3.2}$$

It is often performed in two steps, a high temperature shift and a low temperature shift. Both of these shifts are carried out in a fixed bed reactor, the high temperature bed consists of an iron-chrome catalyst and the low temperature bed consists of a copper and zinc oxides catalyst [17, 18]. The high temperature shift reaction operates at a temperature of about 350°C and the low temperature shift reaction at 220°C [19]. After the low temperature shift the amount of carbon monoxide is about 0.2 vol%. The reaction does not depend on

pressure, so high pressure is not mandatory, although high pressure might be beneficial because it leads to smaller equipment dimensions.

Pressure swing adsorption

For the gas purification a pressure swing adsorption (PSA) system is selected. This process is based on the principle of molecular sieving. The gas is fed to a system of packed beds at elevated pressures (3.1-3.4 MPa) and at ambient temperature (20-30°C). The beds contain zeolites or activated carbon, which absorb all the impurities in the hydrogen. The process works as follows; gas is fed to the first bed until it is almost saturated. Then the gas is fed to a second bed, during that time the first bed is depressurized. During the depressurization the absorbed impurities desorb, after desorption the bed is purged. In the time the first bed is regenerated the second bed becomes saturated, after which the gas feed is switched back to the first bed.

This type of process is usually used with a relatively clean hydrogen stream (e.g. 90% H_2) [18]. It results in hydrogen with a purity of about 99.9% (much higher purities are possible, depending on the number of sorbent beds and sorbents used). When an extremely high purity is required the PSA can be equipped with additional beds.

3.4. Modelling

Modelling of the considered gasification systems is based on literature information. However, the various system descriptions are presented based on different fuel compositions. To enable a correct comparison of the gasification processes all system calculations have been based on the same composition of the dry biomass. Only the moisture content differs depending on the type of gasifier. Drying of the biomass is not taken into account, which can influence the performance of the system. In Table 3-1 is the dry composition of the biomass given.

Table 3-1 Dry composition of biomass used in the models

	Amount	Unit
Carbon (C)	49.97	wt%
Hydrogen (H)	6.12	wt%
Nitrogen (N)	0.55	wt%
Oxygen (O)	42.49	wt%
Sulfur (S)	0.06	wt%
Ash (SiO_2)	0.80	wt%
Lower Heating Value (dry)	18620	kJ/kg
Exergy (dry)	20611	kJ/kg

The environmental conditions in the models are set at a pressure of 1.01325 bar and a temperature of 15°C. The composition of the environment is given in Table 3-2.

Table 3-2 Composition of the environment (for all processes)

Component	Mole fraction [%]	Component	Mole fraction [%]
$Al_2O_{3(s)}$	0.01	O_2	20.60
Ar	0.91	$SiO_{2(s)}$	0.01
CO_2	0.03	SO_2	0.01
H_2O	1.68	Cl_2	0.01
N_2	76.73	F_2	0.01

All hydrogen plant designs are modelled in the program Cycle-Tempo [1], an in-house developed flow sheeting program especially designed for the evaluation of energy conversion systems. The hydrogen produced in this way is 99.99% pure, which can be applied in various applications. The processes are based on a thermal input of 10 MW. For each hydrogen plant a steady state model has been build in Cycle Tempo.

3.4.1. Gasification

The gasification section of the plants in the model are based on equilibrium calculations, the composition of the producer gas is calculated by minimizing the Gibbs energy. These models are valid for coal gasification, in which chemical equilibrium is reached. This is not the case for biomass gasification, because it is a very fast process. This leads to a producer gas, which is not in chemical equilibrium [20]. It was found that by using two equilibrium gasifiers in series, with a selective by-pass over the first gasifier, outlet composition of the modelled gasification processes can be achieved that are sufficiently close to the compositions as known from literature. Pressures and temperatures of the applied gasifier models are chosen to fit the data of the different gasification processes. The validity of the models is determined by comparing the gas composition and the gas flows at the outlet of the gasifier model.

3.4.2. Gas cleaning

The low temperature gas cleaning (LTGC) is mainly modelled as a heat transfer system. The gas cleaning reactors are just considered as a pressure drop, since most of the impurities are not actually modelled. The changes of the chemical exergy of the producer gas are low, since the chemical composition of the gas during the gas cleaning does not change really. Therefore the thermo-mechanical exergy changes are determining. Almost the same applies for the high temperature gas cleaning (HTGC), with an exception for the reformer. The reformer will have an impact on the main chemical composition of the producer gas. These effects have been taken into account in the exergy calculations.

3.4.3. Gas processing

In the systems with gasification processes of Battelle and FICFB with low temperature gas cleaning, a steam methane reformer is included. This is done because the gas contains more than 10 mol% methane, and also because there is sufficient heat available for the reforming reactions from other processes in the system. This was not the case for the systems with the other gasification processes.

Further all processes have the same processing steps, which have similar conditions as far as possible. The water gas shift reactions are performed at 350°C and at 220°C. After shifting the producer gas is compressed to 37 bar; the assumed isentropic efficiency of the compressors is 85%. For the semi-atmospheric processes the compression is done in two steps with inter-cooling. After compression the gas is cooled and fed in to the PSA. This is modelled in two steps. The first step removes CO_2 and water from the gas; the CO_2 is liquefied for storage purposes in order to make the process CO_2 negative. The second part removes the other components from the hydrogen. The separated gas contains also combustible components; therefore the gas is passed to the combustion chamber of a gas turbine to generate some electricity. In Figure 3-1 the flow sheet of the system with FICFB gasifier is shown as an example.

Figure 3-1 Flow sheet of the hydrogen production system based on the FICFB gasifier with low temperature gas cleaning
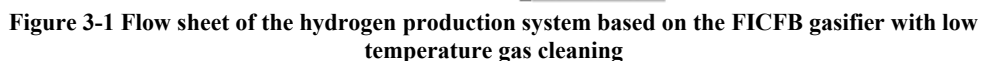
The performance of the processes can be compared by considering the hydrogen yield and exergy efficiency. In this chapter, the hydrogen yield is defined as the ratio of the generated hydrogen mass flow and the mass flow of the dry biomass fed to the process. Further two different exergy efficiencies have been calculated. The first divides the exergy of the produced hydrogen by the exergy of the biomass input and the net consumed electricity by process. The second divides the exergy of the produced hydrogen plus the produced heat by the exergy of the biomass input and the net electricity consumption of the process. The two efficiencies give two extremes of operation, the first is the efficiency where all the heat is

lost and the other gives the efficiency when all the heat in the system is recovered. In reality the efficiency of the process will be in between these two values, since not all the heat can be recovered due to losses.

3.5. Results and discussion

For each gasification process, two alternative systems are developed, distinguished by the applied method of gas cleaning. For instance, the Battelle LTGC is the Battelle gasification system with low temperature gas cleaning, and the Battelle HTGC is the Battelle gasification system with high temperature gas cleaning. All the systems are designed to produce 99.99% pure hydrogen, at a pressure of 30 bar.

3.5.1. The Battelle Processes

A mass flow of 0.645 kg s^{-1} of biomass, with a moisture content of 10%, is supplied to the gasifier. Also 0.049 kg s^{-1} steam (at: 150°C; 2bar) and 1.207 kg s^{-1} air is supplied to the gasifier, resulting in a producer gas composition as given in Table 3-3.

Table 3-3 Composition of the producer gas from the models compared to the literature

Gasifier	Unit	H$_2$	CO	CH$_4$	CO$_2$	N$_2$
Battelle (model)	Mole%	26.06	29.92	13.27	8.59	3.27
Battelle (literature [21])	Mole%	16.7	37.1	12.6	8.9	0.0
Värnamo (model)	Mole%	11.76	17.50	8.12	15.75	46.14
Värnamo (literature [6])	Vol%	9.5-12	16-19	5.8-7.5	14.4-17.5	48-52
FICFB (model)	Mole%	35.22	22.63	17.18	20.86	3.93
FICFB (literature [11])	Vol%	30-40	20-30	8-12	15-25	1-5
IGT (model)	Mole%	48.23	16.85	3.36	30.80	0.46
IGT (literature [12])	Mole%	46.20	22.10	0.90	30.80	0
Blaue Turm (model)	Mole%	52.50	15.28	8.67	23.06	0.43
Blaue Turm (literature [13])	Mole%	55.30	10.20	6.90	26.80	0.20

The composition of the model differs from the composition given in literature this is probably caused by the difference in the used biomass (composition). In literature the composition of the used biomass is not given.

The Battelle LTGC process needs 1.959 kg s^{-1} water for the scrubber and 0.706 kg s^{-1} air for the gas turbine. All the auxiliary equipment in the system consumes 1220.98 kW of electricity. The Battelle HTGC process on the other hand uses 0.150 kg s^{-1} water in a quench and 1.091 kg s^{-1} air for the gas turbine; the auxiliary power consumption is 1159.67 kW electrical. In Table 3-4, the exergy losses for the different process steps of the Battelle LTGC and the Battelle HTGC systems are given.

For both systems exergy flow diagrams are established, which are presented in Figure 3-2.

There are a few differences in the two exergy flow diagrams, for instance in the Battelle HTGC process flue gas leaves the process after the gasifier containing a substantial amount of heat. In the Battelle LTGC process the heat from the gasifier flue gas is used in the gas processing for the reforming, so it leaves the system after the processing. It also becomes clear from Figure 3-2 that the amount of hydrogen produced in the Battelle LTGC process is higher then in the Battelle HTGC process, due to the larger amount exergy.

Table 3-4 Exergy losses in kW for different process steps and performance of the different processes

	Battelle		Värnamo		FICFB	
	LTGC	HTGC	LTGC	HTGC	LTGC	HTGC
Air separation	0.00	0.00	0.00	0.00	0.00	0.00
Gasifier	2372.05	2372.05	2433.82	2433.82	2357.98	2949.20
Gas cleaning	254.51	385.06	1546.21	618.76	343.52	172.74
Gas processing	1808.89	1100.17	2192.27	2179.97	1535.80	830.51
CO_2 liquefaction	68.61	69.83	69.16	75.47	69.07	62.18
Gas turbine	454.23	735.32	1111.25	821.79	348.38	575.00
Total	4958.29	4662.43	7352.71	6129.81	4654.75	4589.63
Performance						
H_2 yield [$kg \cdot kg_{(dry\ biomass)}^{-1}$]	0.097	0.081	0.049	0.067	0.096	0.077
Ex. Eff. without heat recovery [%]	50.69	42.82	24.58	33.19	45.95	39.09
Cold gas efficiency [%]	61.50	51.62	30.66	42.10	57.77	46.19
CO_2 yield [$kg \cdot kg_{(dry\ biomass)}^{-1}$]	1.11	1.02	1.34	1.46	1.11	1.01
Electricity production [kW]	479.69	610.24	1312.42	1172.75	383.56	700.98
Exergy efficiency with heat recovery [%]	62.79	63.72	50.22	52.45	64.41	61.76

Table 3-4 Exergy losses in kW for different process steps and performance of different processes (continued)

	IGT		Blaue Turm	
	LTGC	HTGC	LTGC	HTGC
Air separation	2867.56	2867.56	0.00	0.00
Gasifier	2834.66	2834.45	2693.08	2692.94
Gas cleaning	2107.22	1086.20	836.31	343.45
Gas processing	758.90	1086.20	743.94	765.09
CO_2 liquefaction	104.67	115.26	56.73	66.66
Gas turbine	389.89	272.53	621.25	266.67
Total	9062.90	8262.63	4951.31	4134.81
Performance				
H_2 yield [$kg \cdot kg_{(dry\ biomass)}^{-1}$]	0.080	0.088	0.077	0.106
Ex. Eff. without heat recovery [%]	33.60	36.81	38.76	50.52
Cold gas efficiency [%]	50.51	55.03	45.58	62.31
CO_2 yield [$kg \cdot kg_{(dry\ biomass)}^{-1}$]	1.63	1.79	0.98	1.16
Electricity production [kW]	247.75	311.39	700.33	280.57
Exergy efficiency with heat recovery [%]	55.85	58.55	61.20	66.31

In both the systems heat is lost during the successive cooling steps. Also the heat available from the flue gas is presented as a loss. Some of that heat can be recovered resulting in lower losses and an improvement of the system performance. In Table 3-4 the performance of both the processes can be found. The cold gas efficiency is determined by dividing the product of the mass flow and the lower heating value of hydrogen by the product of mass flow and lower heating value of the biomass.

From Table 3-4 and Figure 3-2 it becomes clear that the Battelle LTGC process is more efficient and has a higher hydrogen yield than the Battelle HTGC process. The lower performance of the Battelle HTGC process is mainly caused by the poor conversion of methane. This leads to more methane going to the gas turbine, resulting in a higher electricity production. The electricity production is not sufficient for the auxiliary power

consumption. Therefore, the auxiliary input at the top of the exergy flow diagrams, in Figure 3-2, is higher than the electricity output at the bottom of the exergy flow diagrams.
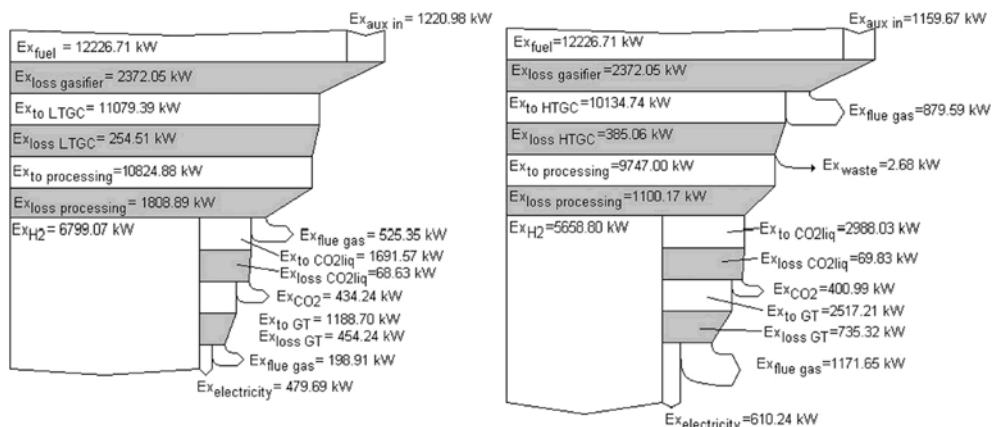
Figure 3-2 exergy flow diagrams for the Battelle LTGC (left) and Battelle HTGC (right)

3.5.2. The Värnamo processes

The biomass fed to the Värnamo gasifier has a moisture content of 15%, the amount fed to the gasifier is 0.645 kg s^{-1}. The gasification process consumes 0.967 kg s^{-1} of air at a pressure of 18 bar and a temperature of 433°C. This results in a producer gas with the dry composition given in Table 3-3.
The mole fraction and the volume fraction would not differ much in this case, so the compositions are comparable.

The Värnamo LTGC process consumes 0.300 kg s^{-1} of water in the scrubber and 1.745 kg s^{-1} of air in the gas turbine. The complete process consumes 2279.77 kW of electricity. The Värnamo HTGC process on the other hand consumes 0.100 kg s^{-1} water in a quench and 1.338 kg s^{-1} of air in the gas turbine. This process consumes 2230.03 kW of electricity. In Table 3-4 the exergy losses for each process step in both processes is determined.
For the Värnamo LTGC process, a exergy flow diagram is created, which can be found in Figure 3-3.

As can be seen from Figure 3-3, the amount of gas to the gas turbine is large, this is caused by the large amounts of nitrogen in the producer gas. These large amounts of nitrogen give problems in the gas processing, since it needs expanding and improving in order to remove all the nitrogen. This would lead to a very complicated and energy consuming gas processing system. It was not possible to remove all the nitrogen for both the processes, so the goal of 99.99% pure hydrogen was not reached. Also the efficiency for these processes is not very high, as can be seen in Table 3-4.

From Table 3-4 it becomes clear the Värnamo HTGC process is more efficient, although the yield and efficiency are not very high.

Ex,aux in=2279.77 kW
Ex,fuel=11762.67 kW
Ex,I gasifier=2433.82 kW
Ex,to LTGC=11600.89 kW
Ex,ashes=7.73 kW
Ex,I LTGC=1546.21 kW
Ex,to processing=10024.44 kW
Ex,sulphur=11.83 kW
Ex,waste water=18.41 kW
Ex,I processing=2192.27 kW
Ex,to CO2liq=4397.02 kW
Ex,I CO2liq=69.16 kW
Ex,CO2=494.78 kW
Ex,to GT=3833.08 kW
Ex,I GT=1111.25 kW
Ex,flue gas=1409.41 kW
Ex,H2=3232.94 kW
Ex,electricity=1312.42 kW
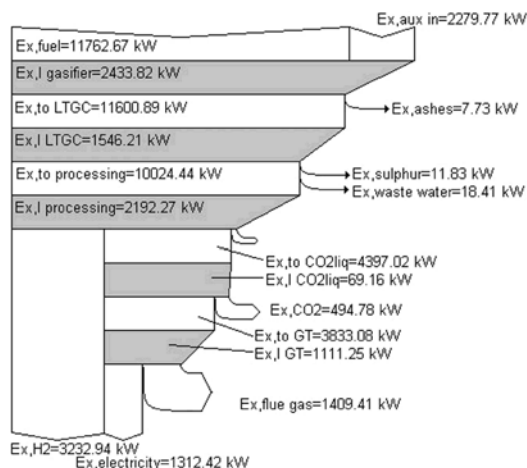
Figure 3-3 Exergy flow diagram of the Värnamo LTGC process

3.5.3. The FICFB processes

These biomass gasification processes are 0.698 kg s^{-1} biomass fed with a moisture content of 25.2%. For the gasification, 1.347 kg s^{-1} air is used at a pressure of 1.5 bar and a temperature of 400°C. There is 0.221 kg s^{-1} steam (at: 1.5 bar; 400°C) needed for the gasification. The resulting dry producer gas composition can be found in Table 3-3. The mole fraction and the volume fraction would not differ much in this case, so the compositions are comparable.

The FICFB LTGC process uses 1.714 kg s^{-1} water for the scrubber and it uses 0.497 kg s^{-1} air for the gas turbine. There is 1388.79 kW of electricity consumed in the auxiliary equipment. The FICFB HTGC process on the other hand uses no additional water and 0.915 kg s^{-1} air for the gas turbine. The electricity consumed by the auxiliary equipment in this process is 917.04 kW. The exergy losses for each process step have been determined and are listed in Table 3-4.

The difference between the losses of the two gasifiers is caused by a slight difference in the models. In the LTGC model, two heat exchangers are replaced by sinks, representing electrical heaters, in order to maintain convergence in the model. So the electrical power demand is higher.
For the FICFB LTGC process, a exergy flow diagram has been created, see Figure 3-4.

In Table 3-4, the performance for both the processes is given.

From Table 3-4, it becomes clear that the FICFB LTGC process is more efficient due to the higher hydrogen yield. Although the exergy losses for the FICFB HTGC process are lower, as shown in Table 3-4, the efficiency is not high due to a poor methane conversion. This unconverted methane ends up in the gas turbine leading to a higher electricity production. The electricity production is not sufficient to supply the whole process.
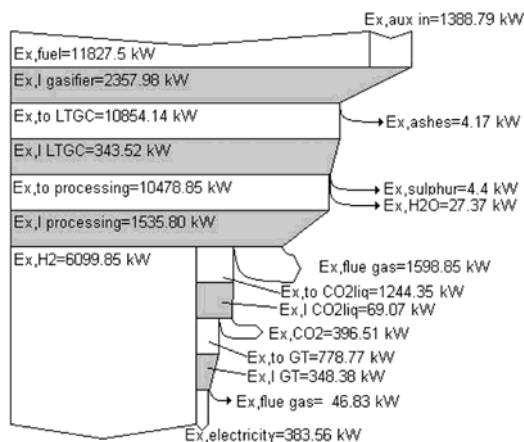
Figure 3-4 Exergy flow diagram plot for the FICFB LTGC process

3.5.4. The IGT processes

The input of the IGT processes is 0.645 kg s^{-1} biomass with a moisture content of 15%. The steam input is 0.581 kg s^{-1} at a pressure of 25 bar and a temperature 240°C. Air is separated in an air separation unit, which consumes 2187.31 kW of electricity, for 1.446 kg s^{-1} of air. This results in a 98% pure oxygen stream of 0.322 kg s^{-1} at 25 bar and a temperature of 50°C. This oxygen is also fed to the gasifier, resulting in the producer gas composition as shown in Table 3-3.

The difference between the compositions of the producer gas in the model and literature are caused by differences in the composition of the used biomass. The biomass used in the literature was not defined.
The IGT LTGC process uses 0.5 kg s^{-1} of water for the scrubber and 0.588 kg s^{-1} of air is used in the gas turbine. The total IGT LTGC process consumes 4098.18 kW of electricity. The IGT HTGC does not use any additional water and it uses 0.434 kg s^{-1} of air for the gas turbine. The whole IGT HTGC process consumes 4052.35 kW of electricity. In Table 3-4 the exergy losses for every process step in both processes are given.

The air separation unit puts a large strain on the process; it consumes a lot of energy and has large exergy losses. This also affects the efficiency of the processes, as can be seen in Table 3-4.

The IGT HTGC is slightly more efficiency then the IGT LTGC process, due to a higher hydrogen production. The water gas shift in the HTGC process is more effective, because of the high water content of the gas entering the WGS. This makes the equilibrium shift to the right site. The water content in gas entering the WGS in the IGT LTGC process is lower, therefore the equilibrium does not shift a far as in the IGT HTGC process.

3.5.5. The Blaue Turm processes

The biomass entering the Blaue Turm gasifier has a moisture content of 30%, and the flow of biomass is 0.698 kg s^{-1}. The gasification process also consumes 0.232 kg s^{-1} of steam (at: 2 bar; 200°C) and 2.284 kg s^{-1} of air. In Table 3-3, the composition of the producer gas is given and compared to the literature.

The differences in the composition of the producer gas are caused by the slight differences in the used biomass.

The Blaue Turm LTGC process uses 1.5 kg s^{-1} water for the scrubber and 0.982 kg s^{-1} air for the gas turbine. The auxiliary equipment consumes 908.97 kW of electricity in the process with LTGC. The process with the HTGC uses only 0.420 kg s^{-1} air for the gas turbine. Here, the auxiliary equipment consumes 929.31 KW. In Table 3-4 the exergy losses for every step in both the systems are given.

A significant amount of gas goes to the gas turbine, this explains the high exergy losses in the gas turbine. In Table 3-4 the performance of both the processes is shown.

The efficiency for the Blaue Turm HTGC system is higher than for the system with the LTGC. This is caused by the extra conversion of methane in the HTGC step. This leads to a higher amount of hydrogen. In the Blaue Turm LTGC, none of the methane is converted and is combusted in the gas turbine. This is why the electricity production is higher for the Blaue Turm LTGC process.

3.5.6. Comparison of the processes

The main goal was to produce 99.99% pure hydrogen, which is achieved with all the gasification processes except for the processes based on the Värnamo gasifier. This is caused by the high amount of nitrogen in the producer gas, which is hard to remove. Therefore, these two processes are seen as not suitable for this application. The larger energy consumption and the high losses of the air separation unit in the processes based on the IGT gasifier are reasons to reject these processes.

As can be seen from Table 3-4 the LTGC processes based on the Battelle and the FICFB gasifier, are performing better than the HTGC processes. And for the Blaue Turm it is the HTGC process, which performs better. The Blaue Turm HTGC process has the highest hydrogen yield, but the Battelle LTGC has the highest exergy efficiency.

The comparison of the processes is difficult, since moisture content of the biomass used in the process differs. A moisture content of 10% is used in the Battelle process, 25.2% in the FICFB process and 30% in the Blaue Turm process. The lower moisture content has a positive influence on the performance of the system. If the fuel moisture fraction of the FICB LTGC process is reduced from 25.2 to 10%, the exergy efficiency increases from 45.95 to 48.10%.

3.6. Conclusions

In order to produce 99.99% pure hydrogen from biomass, there are 10 processes developed based on five different gasifiers. For each gasifier, two processes were developed, one with low temperature gas cleaning and one with high temperature gas cleaning. These processes are base on a biomass thermal input of 10 MW. For all processes Cycle-Tempo models are build, and exergy analyses were performed. An important characteristic of the processes is the output of the gasifier. Large amounts of CO_2 and N_2 will complicate the gas processing. For that reason the Värnamo process, because of the high nitrogen fraction, was excluded for further consideration. By using oxygen instead of air as done in the IGT process these complications can be avoided. But also the separation of air is an energy intensive process. Because of the extra losses of air separation the IGT process is also less suitable for hydrogen production. Then, 6 processes and 3 types of gasifiers are left. It appeared that the Battelle gasifier and FICFB gasifier with low temperature gas cleaning are more effective than the gasifiers with high temperature gas cleaning. This is caused by the fact that reforming will take place easier in the LTGC processes than in HTGC processes. The

exergy efficiency of the systems with Battelle gasifier and FICFB gasifier without heat recovery was calculated to be 50.69% and 45.95%. The exergy efficiency with complete heat recovery (supposing that all heat can be used) is somewhat higher, respectively 62.79% and 64.41%. In the case of heat recovery in a real system, the actual exergy efficiency will be anywhere in between those two values. The Blaue Turm HTGC appeared to be also very efficient, with an exergy efficiency without heat recovery of 50.52% and with complete heat recovery of 66.31%.

The hydrogen yield of these three processes (Battelle LTGC, FICFB LTGC & Blaue Turm HTGC) is in the range of 0.096 kg $(kg_{(dry\ biomass)})^{-1}$ to 0.106 kg $(kg_{(dry\ biomass)})^{-1}$. High temperature gas cleaning is preferred since the exergy losses in the equipment are lower for the processes with high temperature gas cleaning. However the hydrogen yield for most of these processes appeared to be lower, which reduces the exergy efficiency. It is supposed that hydrogen should be supplied to the hydrogen transport system at low temperature. Then, the generated hydrogen has to be cooled to near environmental temperatures. Therefore, low temperature gas cleaning is more convenient. Besides, the technology of low temperature gas cleaning is more mature than the high temperature gas cleaning technology.

As the development of the Blaue Turm process is far behind that of the other two processes, the Battelle LTGC process and the FICFB LTGC process are supposed to be the preferred processes for the generation of highly pure hydrogen gas.

3.7. References

1.   Cycle-Tempo, 5.0. TU Delft, 2009.
2.   Paisley M. A., Farris M. C., Black J. W., Irving J. M., Overend R. P. Preliminary Operating Results from the Battell / FERCO Gasification Demonstration Plant in Burlington, Vermont, U.S.A. In: 1st World Conference and Exhibition on Biomass for Energy and Industry, Sevile, Spain 2000.
3.   Paisley M. A., Irving J. M., Overend R. P. A Promising Power Option -- The FERCO SILVAGAS Biomass Gasification Process - Operating Experience at the Burlington Gasifier In: ASME Turbo Expo, New Orleans, 2001.
4.   Paisley M. A., Overend R. P. The SilvaGas (r) Process from Future Energy Resources -- A Commercialization Success In: 12th European Conference and Technology Exhibition on Biomass for Energy, Industry and Climate Protection, Amsterdam, Netherlands, 2002.
5.   Paisley M. A., Welch M. J. Biomass Gasification Combined Cycle Opportunities Using the Future Energy Silvagas(r) Gasifier Coupled to Alstom's Industrial Gas Turbines. In: ASME Turbo Expo 2003, Georgia, 2003.
6.   Stahl K., Neergaard M. IGCC Power Plant for Biomass Utilisation, Värnamo, Sweden. Biomass Bioenergy 1998; 15 (3): 205-211.
7.   Stahl K., Waldheim L., Morris M., Johnsson U., Gardmark L. Biomass IGCC at Värnamo, Sweden - Past and Future. In: GCEP Energy Workshop, California, USA, 2004.
8.   Bolhar-Nordenkampf M., Bosch K., Rauch R., Kaiser S., Tremmel H., Aichernig C., Hofbauer H. Scale-up of a 100kWth pilot FICFB-gasifier to a 8 MWth FICFB-gasifier demonstration plant in Güssing (Austria). In: 1st International Ukrainian Conference on BIOMASS FOR ENERGY, Kiev, Ukraine, 2002.
9.   Hofbauer H., Rauch R., Bosch K., Kock R., Aichernig C. Biomass CHP Plant Güssing - A Success Story. In: Expert Meeting on Pyrolysis and Gasification of Biomass and Waste, Strasbourg, 2002.

10.   Hofbauer H., Rauch R., Foscolo P., Matera D. Hydrogen-rich Gas from Biomass Steam Gasification. In: 1st World Conference and Exhibition on Biomass for Energy and Industry, Sevilla, Spain, 2000.

11.   Hofbauer H., Rauch R., Loeffler G., Kaiser S., Fercher E., Tremmel H. Six Years Experience with the FICFB-Gasification Process. In: 12th European Conference and Technology Exhibition on Biomass for Energy, Industry and Climate Protection, Amsterdam, The Netherlands, 2002.

12.   Hamelinck C. N., Faaij A. P. C. Future prospects for production of methanol and hydrogen from biomass. University Utrecht: Copernicus Institute, 2001.

13.   Schmid C., Mayer M., Meuhlen H. J. Hydrogen from Bio-Mass. In: Hyforum 2003 Beijing 2003.

14.   Bridgwater A. V. The technical and economic feasibility of biomass gasification for power generation. Fuel 1995; 74(5): 631-653.

15.   Cummer K. R., Brown R. C. Ancillary equipment for biomass gasification. Biomass Bioenergy 2002; 23(2): 113-128.

16.   Twigg M. V. Catalyst Handbook. London: Wolfe Publishing Ltd., 1989.

17.   Corella J., Aznar M. P., Caballero M. A., Molina G., Toledo J. M. 140 g H_2/kg biomass d.a.f. by a CO-shift reactor downstream from a FB biomass gasifier and a catalytic steam reformer. Int J Hydrogen Energy 2008; 33(7): 1820-1826.

18.   Kasper S. Clean-up and processing of coal-derived gas for hydrogen applications. Int J Hydrogen Energy 1983; 8(3): 183-190.

19.   Balthasar W., Hambleton D. J. Industrial scale production of hydrogen from natural gas, naphtha and coal. Int J Hydrogen Energy 1980; 5(1): 21-33.

20.   Mahishi M. R., Goswami D. Y. Thermodynamic optimization of biomass gasifier for hydrogen production. Int J Hydrogen Energy 2007; 32(16): 3831-3840.

21.   Hamelinck C. N., Faaij A. P. C. Future prospects for production of methanol and hydrogen from biomass. J Power Sources 2002; 111(1): 1-22.

4. Reference system for a power plant based on biomass gasification and SOFC

This chapter is published and presented at the 8th European Solid Oxide Fuel Cell Forum at Luzern, Switzerland in 2008, titled: Reference System for a Power Plant Based on Biomass Gasification and SOFC, by R. Toonssen, N. Woudstra, A. H. M. Verkooijen.

Abstract: The fossil fuel reserves are declining leading to a search for more efficient ways to produce electricity from these fossil fuels. One of the promising options is the solid oxide fuel cell gas turbine (SOFC-GT) hybrid system. A recent study has shown that it is possible to achieve exergy efficiencies of around 80% with a natural gas fuelled SOFC-GT hybrid system. Although there are still many problems to solve before such systems can be build, this technique appears to be promising. The SOFC-GT hybrid system is also considered for application with biomass as the primary fuel. As the SOFC-GT requires a gaseous fuel, the biomass has to be gasified first. The generated bio syn-gas contains mainly hydrogen, carbon monoxide, methane, water and carbon dioxide. Biomass gasification is considered to be carbon dioxide neutral, due to the short CO$_2$ cycle of biomass. In that case the combined biomass gasification SOFC-GT system appears to be an attractive option for the application of renewable sources of primary energy.

Combining biomass gasification and a SOFC-GT system introduces additional uncertainties, because the gas produced by biomass gasification will contain a variety of impurities like particulates, tars, alkali metals, halogens and sulphur compounds. These impurities will have an adverse effect on the efficiency and the lifespan of the SOFC-GT hybrid system. Appropriate gas cleaning will be necessary to remove these impurities almost completely. Gas cleaning is possible at different temperature levels. In general low temperature gas cleaning and high temperature gas cleaning are distinguished. Low temperature gas cleaning is more close to maturity then the high temperature one. However in the field of gas cleaning there are still many uncertainties, especially with regard to high temperature gas cleaning. An important uncertainty is that insufficient information is available about the tolerance of the fuel cell for the various impurities. In spite of all these uncertainties, the combination of a SOFC-GT hybrid system with biomass gasification is expected to be a challenging option for future energy conversion.

In this chapter, a system design will be presented, that combines biomass gasification with a SOFC-GT hybrid system. The purpose of this system is to serve as a reference for future design evaluations of full scale power systems. The reference design consists of a gasification unit, a gas cleaning system, a SOFC-GT hybrid system and a heat recovery system. The Fast Internal Circulating Fluidized Bed (FICFB) gasification system is selected for the conversion of biomass (wood) into bio syn-gas since the development of this technology has made significant progress. The generated bio syn-gas will be cleaned in a low temperature gas cleaning system. The cleaned gas will be converted in the SOFC-GT hybrid system; residual heat will be used in a steam bottoming cycle.

An exergy analysis is made to evaluate the thermodynamic performance of the designed system. The results of this analysis are used to improve the system performance. The system is designed for a gross electrical output of 30MW.

4.1. Introduction

Due to growing concerns about global warming and climate chances, the search for more sustainable ways of electricity production is increasing. This does not only involve the search for more sustainable sources of energy, but also the search for more efficient ways to convert available fuels into the demanded energy. One of the most promising fuels for electricity production is biomass, due to its short carbon cycle. Therefore biomass is considered to be CO_2 neutral. Since most biomass sources are in a solid state, it is difficult to convert biomass directly into electricity. Therefore, the biomass has to be converted first into a more convenient energy carrier. One option is the gasification of biomass, which converts biomass into bio syn-gas. This bio syn-gas can be applied in a variety of energy conversion processes.

One energy conversion process, which seems very attractive, is the solid oxide fuel cell gas turbine (SOFC-GT) hybrid system. Earlier system studies have shown that exergy efficiencies over 80% are possible with natural gas fuelled SOFC-GT hybrid systems [1]. By combining biomass gasification with a SOFC-GT hybrid system can lead to an efficient power production plant.

This chapter presents a system design for a power plant based on biomass gasification and a SOFC-GT hybrid system. The plant is fuelled with A-quality wood and the gross electricity production is around 30 MW_e. This system design is based on existing technology as far as possible, so it can serve as a reference system for future design studies. By performing an exergy analysis, a clear picture is obtained of the losses and the true thermodynamic efficiency can be determined.

4.2. System configuration

The system consists of four subsystems; the gasifier, gas cleaning, SOFC-GT hybrid system, and the heat recovery. These components are connected in the order as shown in Figure 4-1.
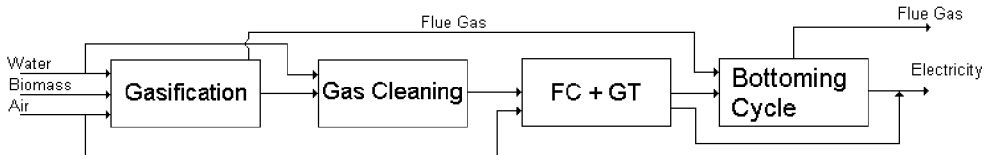
Figure 4-1 block scheme of the system design

In the following sections each of the subsystems will be discussed separately, starting with the gasifier.

4.2.1. The gasifier

For the gasification process the Fast Internal Circulating Fluidized Bed (FICFB) is used. This gasifier is developed by the Institute of Chemical Engineering and AE Energietechnik [2-4]. It is an indirect gasifier, which produces a medium caloric value gas (±12-14 MJ kg^{-1}). The gasification process contains a combustor, which operates at 1000°C and a pressure of 1.5 bar, and a gasifier operating at 800-900°C and a pressure of 1.5 bar. Heat is transferred from the combustor to the gasifier by circulating the bed material between the gasifier and the combustor. Such a gasifier of 8 MW_{th} input has been operated for many years in Güssing Austria [2].

4.2.2. The gas cleaning

The gas coming from the gasification unit cannot directly be used in a SOFC-GT hybrid system, because it contains several impurities, which are harmful to the fuel cell and or gas turbine. Therefore gas cleaning is necessary. The impurities in the bio syn-gas and the assumed tolerances of the fuel cell are listed in Table 4-1.

Table 4-1 impurities in the producer gas and the assumed tolerance of the SOFC-GT

Impurity	Amount in gas	Tolerance of the SOFC-GT
Particulates	10-20 g Nm^{-3} [2]	< 1ppm (10-20 μm) [5]
Tars	0.5-15 g Nm^{-3} [2]	< 1ppm
Alkalis	No Data Available	< 0.1ppm [5]
Sulphur	20-50 ppm [2]	< 1ppm[5-7]
Chlorine	No Data Available	< 1ppm[6, 7]

Gas cleaning will be performed at low temperature, since high temperature gas cleaning is not yet proven [8]. The gas needs to be cooled prior to the cleaning. The gas is cooled in a heat exchanger; the discharged heat can be used in a bottoming cycle. During the cooling a large part of the alkali metals will possibly condense onto the particles entrained in the gas [5]. Also some of the tars will condense. The temperature is chosen well below the dew point of the alkalis, around 120°C. The particles and the condensed alkalis are removed by filtering the cooled gas. Then the gas is scrubbed with water in order to remove the halogens, tars and residual alkalis from the gas. During the scrubbing the gas cools down further, the temperature of the gas leaving the scrubber is approximately 65°C. After scrubbing the gas is compressed to 8 bar, in order to meet the requirements for the SOFC-GT. The compressed gas is led through a packed bed with ZnO. This is supposed to be necessary to remove any sulphur compounds from the gas. To make sure that also the last particles in the gas will be removed, the gas is finally passed through a ceramic filter.

4.2.3. The SOFC-GT hybrid system

The SOFC-GT hybrid system consists of solid oxide fuel cell (SOFC), which partly replaces the combustor of the gas turbine (GT). The cleaned gas is fed to the anode, and compressed air is fed to the cathode. In the fuel cell the clean gaseous fuel is converted directly into electricity. Part of the anode off-gas is recycled to the anode feed; also part of the cathode off-gas is recycled to the cathode feed to preheat the fresh air supplied to the stack. The anode recycle is used to increase the steam to carbon ratio in the cell, since a high steam to carbon ratio prevents carbon deposition [9].

The fuel cell is a direct internal reforming SOFC, which enables the conversion of the methane in the syn-gas into hydrogen and carbon monoxide. The off-gasses are passed to a combustor, where the residual combustible components are burnt using the cathode off-gas flow. The flue gasses are expanded in a turbine for additional power generation. The expanded flue gas is used to recuperate the incoming air after compression. The turbine is connected to a compressor, which is used to compress the air needed for SOFC-GT hybrid system, and a generator. In this way extra electricity is produced.

4.2.4. Heat Recovery

Since the SOFC-GT hybrid system generates more heat than necessary for the various heating purposes, a considerable amount of excess heat is available for application in a bottoming cycle. Heat can be transferred from the system during the cooling of the producer gas before gas cleaning and from the hot flue gas coming from both the gasifier

and the SOFC-GT hybrid system. For these sources two separate boilers are added, which generate high pressure steam for a bottoming cycle. All the steam is expanded in a single turbine, which is coupled to a generator, for additional electricity production.

4.3. System Modelling

For the described system, a steady state model is created using the program Cycle Tempo [10], an in house developed flow sheeting program for the evaluation of energy conversion systems. Actually two models are developed one for the biomass gasification with gas cleaning and the SOFC-GT hybrid system and one for the bottoming steam cycle. This is done to ensure convergence of the models. Some general assumptions have been made:

- The whole system operates at steady state.
- The system is assumed to be adiabatic.
- All heat exchangers are supposed to operate in counter flow.
- Pressure drop in the equipment is 2% of the inlet pressure.
- Fouling of the equipment by tars, alkali metals and other fouling components is neglected. Also the formation of tars, alkali metals and other fouling components in the gas is not taken into account in the models.
- The isentropic efficiency for pumps is set to 75%.
- The isentropic efficiency for compressors is set to 80%, except for compressor of the gas turbine ($\eta_{i, turb.}$= 84.15%).
- The mechanical efficiency for all the rotary equipment is set to 99%.

The FICFB gasifier is modelled as a black box, since detailed models for biomass gasification are not available for this purpose and the exact specifications of the FICFB are not known. The output composition of the gasifier is modelled to be comparable to the composition found in literature [2, 3, 11, 12].

Biomass is fed to the system at a temperature of 15°C and a pressure of 1.5 bar. The other components entering the system, water and air, are at 15°C and a pressure of 1.01325 bar. The flow diagram of the combined gasification SOFC-GT hybrid system is shown in Figure 4-2. The operational temperature of the fuel cell is 750°C and the pressure is 8 bar. The pressure ratio in the SOFC-GT hybrid system is 8 bar. The fuel cell area is supposed to be 11780 m^2 and the fuel cell resistance 0.7 Ω cm^2. The efficiency of the DC/AC converter is 97%.

The recycle of the anode stream is 60%, in order to keep the steam to carbon ratio sufficiently high; the cathode recycle is 80%.

The residual heat, available from the sinks 8, and 23 in Figure 4-2, is used for the generation of high pressure steam. The generated steam is used for power production in a simple steam turbine cycle. A separate model is made for this steam cycle (see Figure 4-3), and the input values of the heat transfer fluids in this system model are adopted from the results of the system model of Figure 4-2. The hot gas flows are cooled in two different boilers consisting each of a economizer, an evaporator and a superheater. The steam generated by these boilers is expanded in a single turbine. Several assumptions have been regarding the heat recovery system.

- The turbine has an isentropic efficiency of 84.96% and a mechanical efficiency of 99%.
- The pumps have an isentropic efficiency of 75% and a mechanical efficiency of 99%.
- The pressure of the deaerator is set to 1 bar.
- The condenser pressure is set to 0.03 bar (assuming a water cooled condenser).
- The pressure of the superheated steam at steam turbine inlet is 38.58 bar and the temperature is 530°C.
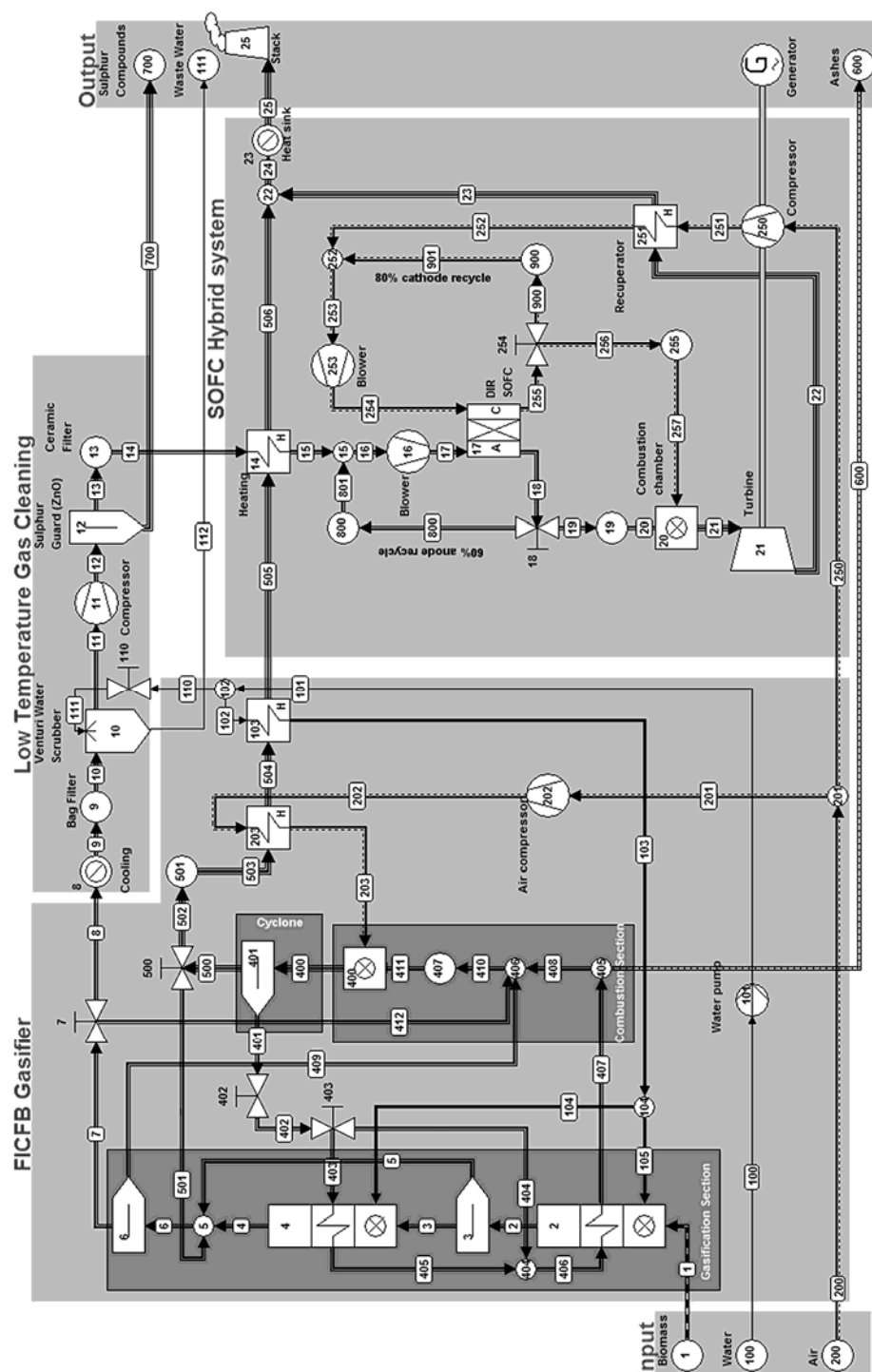
Figure 4-2 flow diagram of the gasification SOFC-GT hybrid system

A flow scheme of the steam bottoming cycle is given in Figure 4-3.
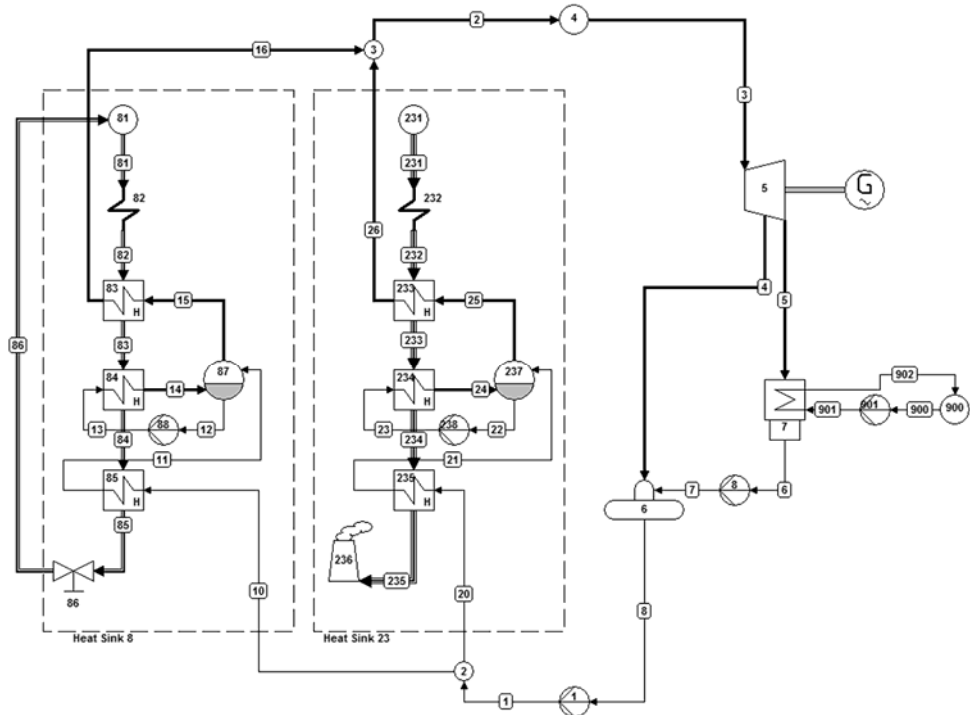
Figure 4-3 flow diagram of the steam bottoming cycle

The dry composition of the biomass used in the system calculations is given in Table 4-2. The assumed moisture content of the biomass is set to 25.2 wt%.

The environmental conditions, as used for the calculation of exergy values, are set to a pressure of 1.01325 bar and a temperature of 15°C, the composition of the environment is defined as presented in Table 4-3.

Table 4-2 dry composition of the used biomass in the model

	Amount	Unit
Carbon (C)	49.97	wt%
Hydrogen (H)	6.12	wt%
Nitrogen (N)	0.55	wt%
Oxygen (O)	42.49	wt%
Sulphur (S)	0.06	wt%
Ash (SiO_2)	0.80	wt%
Lower Heating Value (dry)	18620	kJ kg^{-1}
Exergy (dry)	20611	kJ/kg^{-1}

Table 4-3 chemical composition of the environment

Component	Mole fraction [%]	Component	Mole fraction [%]
$Al_2O_{3(s)}$	0.01	O_2	20.60
Ar	0.91	$SiO_{2(s)}$	0.01
CO_2	0.03	SO_2	0.01
H_2O	1.68	Cl_2	0.01
N_2	76.73	F_2	0.01

4.4. Results

It is assumed that a biomass fuel flow of 4.12 kg s^{-1} is fed to the gasifier at a pressure of 1.5 bar and a temperature of 15°C. This resulted in a gross power of the gasification SOFC-GT hybrid system (without bottoming cycle) of 28.78 MW$_e$. Water and air are fed to the system at environmental conditions; the amounts are calculated by the model. The amount of water needed for the gasification process is 1.302 kg s^{-1}, and the air flow to the gasifier is 7.952 kg s^{-1}. This results in a producer gas with the dry composition as shown in Table 4-4, at a temperature of 817°C and a pressure of 1.48 bar.

Table 4-4 main dry composition of the producer compared with the literature [2]

Component	Output model [vol%]	Literature data [vol%]
Hydrogen (H_2)	35.22	30-40
Carbon monoxide (CO)	22.63	20-30
Carbon dioxide (CO_2)	20.86	15-25
Methane (CH_4)	17.18	8-12
Nitrogen (N_2)	3.93	1-5

In addition to the produces gas, the gasifier produces also 0.026 kg s^{-1} ash and 9.087 kg s^{-1} flue gas. The temperature of the flue gas from the combustor is 1364°C. This hot flue gas is used for pre-heating the air to the combustor and to produce steam for the gasification process. The temperature of the flue gas after air pre-heating and steam production is 789°C. Then the flue gas is used to preheat the producer gas coming from the gas cleaning section. The flue gas leaves the producer gas preheater at a temperature of 689°C. Then the flue gas is mixed with the flue gas from the gas turbine outlet; the mixed gas has a temperature of 617°C. The flue gas mixture is cooled further in the heat recovery boiler to generated steam for the bottoming cycle. The flue gas is transferred to the stack at a temperature of 162°C.

After gasification the producer gas enters the gas cleaning subsystem where it is cooled to 110°C and cleaned in a bag filter before scrubbing. During cooling 6032.28 kW of heat is extracted. The producer gas is scrubbed with 8.95 kg s^{-1} water in the venturi water scrubber. Because of the scrubbing the water content of the gas drops from 34.4 mole% to 21.5 mole%. After scrubbing the gas is compressed to 8.3 bar, this results in a temperature rise from 65°C to 309°C. The power necessary to drive the compressor is 1575.8 kW. After compression the gas is fed to the sulphur removal unit, where all the sulphur is removed (about 0.02 mole%). Then the gas is ready for conversion in the SOFC-GT hybrid system. The gas is heated first to 475°C by the flue gas from the gasifier, before it is mixed with the anode recycle stream. The anode recycle stream is 60% of the flow leaving the anode of the fuel cell. This is done to make sure that the water content of the fuel gas is high enough for the internal reforming processes. Also carbon deposition at the anode, which can deteriorate the performance of the fuel cell [13], can be avoided by doing so. Two recycle blowers one at the inlet of the anode and the other at the inlet of the cathode are installed to overcome

the pressure drop of the fuel cell. The anode recycle blower requires 116.64 kW$_e$ and the cathode recycle blower 640.87 kW$_e$.

The power consumption of the cathode recycle blower is higher since the cathode flow is much larger then the anode flow. The large cathode flow is necessary to cool the stack. The cathode recycle blower only compensates for the pressure drop of the SOFC stack. The compression of air from environmental pressure to the fuel cell stack pressure occurs in a compressor coupled to the gas expansion turbine. After compression the air is heated by the flue gas from the gas turbine exhaust. The calculated flow of fresh air is 19.24 kg s^{-1}. The heated air is mixed with the cathode recycle flow before it enters the recycle blower and the fuel cell. The cathode recycle is assumed to be 80% of the flow leaving the cathode of the fuel cell. The fuel cell operating at 750°C produces 24307.14 kW of electrical energy. Not all fuel is converted in the SOFC stack; the fuel utilization is 80%. The anode and cathode outlet flows are passed to a combustor, where the residual fuel is combusted. The resulting flue gas has a temperature of 940°C, which is also the inlet temperature of the gas turbine. The gas turbine is coupled to the air compressor and a generator through a shaft. The generator produces 4471.28 kW of electrical energy.

Both flue gas flows, the flue gas flows from the gasifier and from the SOFC-GT hybrid system, contain a significant amount of heat. The heat extracted from the flue gasses in the heat recovery boiler is 17272.89 kW.

In Table 4-5 the energy and exergy inputs, consumptions and efficiencies of the system for the conversion of biomass into electricity are presented.

The gross efficiency is calculated by dividing the total delivered gross electrical power by the total absorbed heat power. The net efficiency is calculated by dividing the total delivered net electrical power by the total absorbed heat power.

Table 4-5 energy and exergy input, consumption and efficiency of the biomass gasifier and SOFC-GT hybrid system (without bottoming cycle)

	No.	Source	Energy [kW]	Exergy [kW]
Absorbed power	1	Biomass	61261.93	69812.73
		Total absorbed	**612961.93**	**69812.73**
Delivered gross power	G	Generator (GT)	4471.28	4471.28
	17	Fuel Cell	24307.14	24307.14
		Total delivered	**28778.41**	**28778.41**
Aux power consumption	11	Compressor	1575.80	1575.80
	16	Compressor	116.64	116.64
	101	Pump	0.67	0.67
	201	Compressor	344.87	344.87
	253	Compressor	640.87	640.87
		Total Aux	**2678.85**	**2678.85**
Delivered net power			**26099.56**	**26099.56**
Delivered heat	8	Heat Sink	6032.28	3637.28
	23	Heat Sink	17272.89	10192.88
		Total heat	**23305.16**	**13830.17**
Total delivered			**49404.73**	**39929.73**
Efficiencies		Gross	46.98%	41.22%
		Net	42.60%	37.39%

The residual heat (from the sinks 8 and 23 in Figure 4-2) is used to generate steam in the boilers of the bottoming steam cycle. The heat transfer of each of these sinks corresponds to

the heat transfer in the boilers as modelled in Figure 4-3. The boilers generate steam of 530°C at a pressure of 38.58 bar. The total amount of steam produced in these boilers is 7.54 kg s^{-1}. The steam is expanded in a turbine, which is coupled to a generator through a shaft. This results in an electricity production of 8113.00 kW. The power consumption of the pumps in the heat recovery system is 65.34 kW$_e$. The net electricity production of the steam bottoming cycle is 8047.66 kW. The combined results of the bottoming cycle and the energy conversion system are presented in Table 4-6. The efficiency is calculated by dividing the total delivered power by the total absorbed power (= biomass fuel power to the system).

Table 4-6 energetic and exergetic efficiency of the total system including bottoming cycle

	Source	Energy [kW]	Exergy [kW]
Absorbed power	Biomass	61261.93	69812.73
Delivered net power	SOFC-GT	26099.56	26099.56
	Bottoming cycle	8047.66	8047.66
Total delivered power		**34147.22**	**34147.22**
Efficiency	Total	55.74%	48.91%

The exergy flow diagram of the total system (gasification SOFC-GT hybrid system with bottoming cycle) is depicted in Figure 4-4. The grey blocks in this diagram indicate the process subsystems, in which exergy is lost. The white blocks indicate the exergy transfer between the process subsystems. The bottoming cycle is indicated in the diagram by HR. The losses caused by the heat transfer from the producer gas and flue gas to the steam are included in the losses of the bottoming cycle.
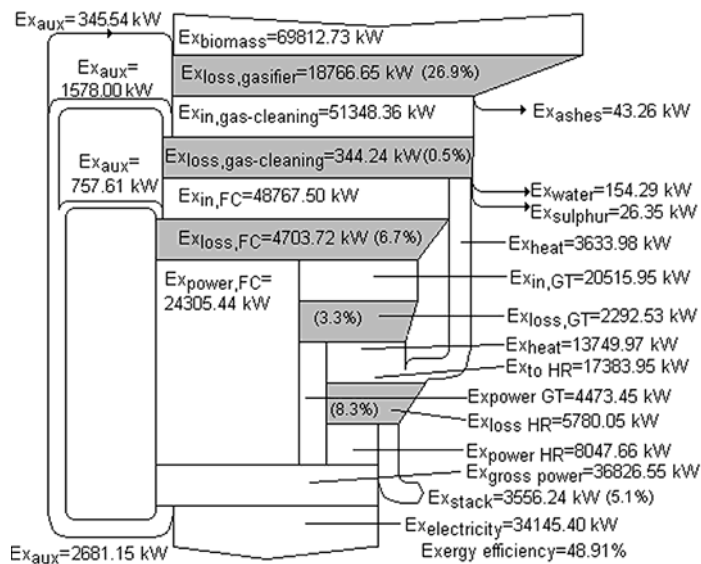
Figure 4-4 Exergy flow diagram of the total system

4.5. Discussion

From Figure 4-4 it becomes clear that the gasification subsystem has the highest exergy losses. These losses are caused by the large irreversibilities of the combustion of the char in the combustor. The losses of the steam production and air preheat are also taken into account. The exergy losses during heat transfer are significant, because of the large temperature differences between the fluids which exchange heat. The system is designed such, that the gasifier can operate independently from the gas cleaning and/or SOFC-GT hybrid system. The exergy losses in the gas cleaning subsystem do not seem to be very large, because the losses due to the heat transfer from the producer gas are not included here as they have been allocated to the bottoming cycle.

Table 4-6 clearly shows the difference between the energy efficiencies and the exergy efficiencies of the total system. This difference is actually caused by the difference between the lower heating value and the exergy value of the biomass.

The biomass gasification combined with SOFC-GT hybrid system is intended to be the reference system for future system design studies. The gasification technique used is chosen because of its relative high hydrogen content of the producer gas. Alternative gasification processes can be considered, for instance pressurized air gasification. Pressurized air gasification generates a producer gas diluted with a significant amount of nitrogen, but has the advantage that the gas is already pressurized; a hot gas cleaning system is easier to implement. On the other hand the nitrogen rich producer gas will affect the performance of the SOFC-GT hybrid system. Further system studies are necessary to show how this affects the overall efficiency. (See chapter 6)

The fuel cell temperature used here (750°C) is relatively low. Most current SOFC's operate at 900-1000°C, but the general trend is to lower the operating temperature of the fuel cell. The lower operating temperature will simplify the construction of the SOFC; they will reduce thermal expansion and corresponding stresses in the materials and will allow the application of more and cheaper materials. The gas turbine can be relatively simple because of the intermediate operating conditions. The low fuel cell temperature has only a limited effect on the overall efficiency of the system [1].

Further optimization the SOFC-GT hybrid system is conceivable of course. A more detailed evaluation of the anode and cathode recirculation, considering other ways to recirculate the gasses as well as the amounts of recirculation. By doing so, the overall efficiency of the process can be improved.

In this system is a relative simple steam cycle used as bottoming cycle. Further reductions of the exergy losses are conceivable but the optimization of the bottoming cycle is not the purpose of this project.

4.6. References

1.   Bosch K. J., Woudstra N., van der Nat K. V. Designing Solid Oxide Fuel Cell Gas Turbine Hybrid Systems Using Exergy Analysis. In: Fourth International Conference on Fuel Cell Science, Engineering and Technology, Irvine (USA), 2006.
2.   Hofbauer H., Rauch R., Loeffler G., Kaiser S., Fercher E., Tremmel H. Six Years Experience with the FICFB-Gasification Process. In: 12th European Conference and Technology Exhibition on Biomass for Energy, Industry and Climate Protection, Amsterdam, The Netherlands, 2002.

3.   Bolhar-Nordenkampf M., Bosch K., Rauch R., Kaiser S., Tremmel H., Aichernig C., Hofbauer H. Scale-up of a 100kWth pilot FICFB-gasifier to a 8 MWth FICFB-gasifier demonstration plant in Güssing (Austria). In: 1st International Ukrainian Conference on BIOMASS FOR ENERGY, Kiev, Ukraine, 2002.
4.   Bolhar-Nordenkampf M., Hofbauer H. Gasification Demonstration Plants in Austria. In: International Slovak Biomass Forum, Bratislava, 2004.
5.   Bridgwater A. V. The technical and economic feasibility of biomass gasification for power generation. Fuel 1995; 74(5): 631-653.
6.   Singhal S. C. Advances in solid oxide fuel cell technology. Solid State Ionics 2000; 135(1-4): 305-313.
7.   EG&G Techincal Services. Fuel Cell Handbook. Morgantown: Nation Energy Technology Laboratory, 2004.
8.   Hamelinck C. N., Faaij A. P. C. Future prospects for production of methanol and hydrogen from biomass. J Power Sources 2002; 111(1): 1-22.
9.   Twigg M. V. Catalyst Handbook. London: Wolfe Publishing Ltd., 1989.
10.   Cycle-Tempo, 5.0. TU Delft, 2009.
11.   Hofbauer H., Rauch R., Bosch K., Kock R., Aichernig C. Biomass CHP Plant Güssing - A Success Story. In: Expert Meeting on Pyrolysis and Gasification of Biomass and Waste, Strasbourg, 2002.
12.   Hofbauer H., Rauch R., Foscolo P., Matera D. Hydrogen-rich Gas from Biomass Steam Gasification. In: 1st World Conference and Exhibition on Biomass for Energy and Industry, Sevilla, Spain, 2000.
13.   Walters K. M., Dean A. M., Zhu H., Kee R. J. Homogeneous kinetics and equilibrium predictions of coking propensity in the anode channels of direct oxidation solid-oxide fuel cells using dry natural gas. J Power Sources 2003; 123(2): 182-189.

5. Hydrothermal gasification combined with a hybrid SOFC-GT

Abstract: *The application of wet biomass in energy conversion systems is challenging, since in most conventional systems the biomass has to be dried. Drying is very energy intensive especially when the biomass has a moisture content above 50 wt% on a wet basis. The combination of hydrothermal biomass gasification and a solid oxide fuel cell (SOFC) gas turbine (GT) hybrid system could be an efficient way to convert very wet biomass into electricity. Therefore, thermodynamic evaluation of combined systems with hydrothermal gasification units and SOFC-GT hybrid units has been performed. Three hydrothermal gasification cases have been evaluated; one producing mainly methane, a second one producing a mixture of hydrogen and methane and the last one producing mainly hydrogen. These three gasification cases have been coupled to the same SOFC-GT hybrid system. Every case has an overall electrical exergy efficiency of around 50%, therefore the combination of hydrothermal gasification and SOFC-GT hybrid systems seems promising. The overall system performance depends for a large part on the liquid gas separation. Further research is required for finding out the optimal separation conditions.*

5.1. Introduction

Increasing concerns about the environmental impacts of fossil fuel consumption and their depletion lead to a rising attention towards more sustainable sources of energy. Biomass is one of the considered sustainable energy sources, due to its carbon dioxide neutrality. Especially, biomass waste and residual biomass streams can be used for energy conversion processes. Many of the modern energy conversion systems convert the biomass first into a secondary energy carrier, before it is converted into electricity. This is because the biomass is usually in a form, which is hard to convert into electricity directly. For instance, manure or algae are usually very wet and cannot be combusted without being dried first. In hydrothermal gasifiers, it is possible to convert wet biomass into a methane or hydrogen rich gas. The gas produced in hydrothermal gasification is relatively clean compared to gas coming from conventional gasification processes. Therefore, simple gas cleaning is sufficient when compared with conventional gasification systems. The methane or hydrogen rich gas produced in hydrothermal gasifiers can be used to produce electricity. The solid oxide fuel cell (SOFC) is an electrochemical device, which can convert the chemical energy in fuel into electricity in an efficient manner. Common fuels for solid oxide fuel cells are hydrogen, methane, or synthesis gas. When operated at elevated pressures, the SOFC can be combined with a gas turbine (GT), to obtain a very efficient power plant.

The combination of biomass gasification with SOFC-GT hybrid systems is getting significant attention from the scientific community [1-11]. All these studies focus on the gasification of relatively dry biomass combined with either SOFCs or SOFC-GT hybrid systems. The combination of super critical water gasification and fuel cells is a new concept.

There is one study performed by Li et al. [12], where a tubular SOFC is tested with simulated syn-gas assumed to be coming from supercritical water gasification.

In this paper, results from thermodynamic evaluations of power plants with hydrothermal gasification systems coupled with SOFC-GT systems are presented. Three different hydrothermal gasification options have been evaluated; one operates at a temperature of 673 K for the production of mainly methane, the second operates at 773 K for the production of a mixture of methane and hydrogen and the last one operates at 873 K for the production of mainly hydrogen. The three types of gasifiers have been coupled to a solid oxide fuel cell- gas turbine hybrid system. Exergy analyses of the complete systems were performed.

5.2. Description of subsystems

The considered systems are divided into three sub-systems, the hydrothermal gasification system, the solid oxide fuel cell system and the gas turbine system. The sub-systems are described in the following sections, respectively.

5.2.1. Hydrothermal gasification

Hydrothermal gasification is also known as subcritical or supercritical water gasification. With this technique, a primary fuel is converted into a secondary fuel in an aqueous medium at temperatures above or around 473 K and a sufficient high pressure to keep the water in a liquid or super critical state (T_c=647 K, p_c=22 MPa) [13]. This gasification technique has several advantages over conventional gasification techniques:
1. Ability to use very wet biomass sources (>80%), like manure or algae
2. High gasification efficiency at relative low temperatures
3. Low formation of tars and chars

Hydrothermal biomass gasification can be divided into three main types [14, 15]:
1. Aqueous phase reforming, compounds originating from biomass (for instance, glucose, sorbitol, glycerol) are gasified at around 488-543 K to mainly hydrogen and carbon dioxide in the presence of a heterogeneous catalyst.
2. Catalyzed (near)-critical gasification, biomass is gasified in the presence of a catalyst to mainly methane and carbon dioxide at either around 623 K in the liquid phase or around 673 K in the supercritical state.
3. Super critical water gasification, biomass compounds are gasified to mainly hydrogen and carbon dioxide with or without a catalyst at temperatures around 873-973K.

In hydrothermal gasification, the special properties of near critical or supercritical water are used [14]. Water changes its character from a solvent for ionic species at ambient conditions to a solvent for non-ionic species at supercritical conditions [16]. Also the electrochemical properties of water change from ambient conditions. The pH values decreases by three units, providing more hydronium ions for acid catalyzed reactions [16]. The reactivity of water increases near the critical point with and without catalyst [16]. At near critical and supercritical conditions water and gasses like O_2, N_2, NH_3, CO, CO_2 are completely miscible and the solubility for inorganic compounds in water decreases [15]. In hydrothermal gasification, water is not only used as a solvent, but also as a reaction agent. Biomass is relatively fast hydrolysed in near or supercritical water resulting in a rapid degradation of the polymeric structure of the biomass into a mixture of sugars [14]. The sugars are further converted as indicated in reactions (5.1) and (5.2).

$$C_6H_{12}O_6 + 6H_2O \rightarrow 6CO_2 + 12H_2 \tag{5.1}$$

$$C_6H_{12}O_6 \rightarrow 3CH_4 + 3CO_2 \tag{5.2}$$
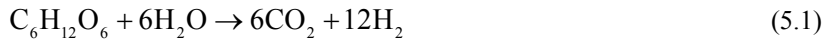
In these reactions, the sugars are represented as glucose. The reactions (5.1) and (5.2) are also relatively fast resulting in a gas at relatively low temperature compared to the "dry process" [14, 15]. The high solubility of the intermediates in the reaction medium significantly inhibits tar and coke formation [14, 15]. After the reaction and cooling carbon dioxide is mainly dissolved in the water, due to its high solubility at elevated pressures. The pressurized gas separated from the liquid phase has a relatively low CO_2 content, hence, a high heating value [14].

A major disadvantage of hydrothermal gasification is the large amount of water which needs to be heated. The heat required to reach e.g. 873 K can exceed the energy content of the applied biomass [14]. Therefore, the application of a heat recovery heat exchanger is required and the efficiency of the heat exchanger is very important.

Supercritical water gasification (SCWG) has special material requirements for the reactor, since in super critical water gasification both the temperature and pressure are high [14]. One of the important problems in hydrothermal gasification is reactor plugging [14, 17, 18]. This is caused by the formation of inorganic salts, which precipitate during the gasification process. The salts can also have deteriorating effect on catalysts [16].

In this paper three cases are considered; the main difference between these cases is the type of hydrothermal gasification employed.

- Case 1, the hydrothermal gasification operates at a temperature of around 700 K, a pressure of 34 MPa and uses a catalyst (activated carbon). This system produces mainly methane and carbon dioxide using mainly reaction (5.2)
- Case 2, operates at a temperature of approximately 800 K, a pressure of 34 MPa and without a catalyst. The product of this system is a mixture of hydrogen, methane and carbon dioxide using both reaction (5.1) and (5.2)
- Case 3, operates at 900 K, a pressure of 24 MPa and also without catalyst. This system produces mainly hydrogen and carbon dioxide using mainly reaction (5.1).

The gas produced during the SCWG is separated from the water by flashing. The produced gas contains some impurities, like hydrochloric acid and hydrogen sulphide. These compounds need to be removed before the gas is fed to the SOFC-GT hybrid system. The SOFC-GT is considered as sensitive towards poisoning by hydrochloric acid and hydrogen sulphide when they are present in excessive quantities, which results in performance deterioration of the systems. Before the removal of hydrochloric acid and hydrogen sulphide, superheated steam is added to the gas to increase the moisture content of the gas and to prevent carbon deposition in the acid gas removal units. Hydrochloric acid is removed by adsorption on sodium carbonate and hydrogen sulphide is removed by adsorption on zinc oxide. Both adsorption processes are performed in packed beds.

The technology of hydrothermal biomass gasification is still in its development stage. There is some experimental data available, but the results are not compared to experimental results. Most of the experimental data available is based on model compounds, like glucose, and very limited data on actual biomass or in this case manure.

5.2.2. Solid oxide fuel cell system

As well as the hydrothermal gasification the SOFC technology is still in a development stage. The solid oxide fuel cell considered in this work is based on Ni/GDC anodes and lanthanum strontium manganite (LSM) cathodes at temperatures above 1173K. No relevant

data is available about stack performance using bio-syngas. Some reports on cell performance using bio-syngas are available [1, 19]. Based on these reports, data necessary for system calculations have been assumed. These assumptions are for the values of different parameters, like fuel cell resistance and current density.

5.2.3. Gas turbine and heat recovery system

The systems do not represent any commercial available gas turbine. The isentropic and mechanical efficiencies are chosen such, that they could represent a well matched gas turbine. The anode gas and cathode gas coming from the fuel cell are partially recycled to the inlet of the fuel cell. The residual gasses are fed to the combustion chamber of the gas turbine. All these units operate at elevated pressure. The flue gasses from the combustion are expanded in the turbine. The turbine exhaust gasses are used to pre-heat the air for the fuel cell.

The flue gasses coming from the gas turbine are mixed with the flue gasses coming form the gasification part. After the mixing of the flue gasses it is still possible to extract heat from the flue gasses. This is included as a heat sink which represents a heat consumer. The recovered heat can be applied for various purposes. The flue gasses are released in the atmosphere through a stack at a temperature of 383 K.

5.3. Modeling

For the modeling of this hydrothermal gasification system combined with SOFC-GT hybrid system the flow sheeting program Cycle-Tempo [20] is used. This flow sheeting program is especially designed for the evaluation of energy conversion systems. In this section, a description given of the model and of the modeling principles is applied. First the gasification model will be discussed and then the SOFC-GT hybrid system. Finally, the used assumptions and model input will be presented.

5.3.1. Hydrothermal gasification of manure

The manure used in this system study is assumed to be a mixture of cow manure and pig manure. The dry ash free (daf) composition of the manure is taken from Phyllis [21], a database of compositions of biomass and waste. The used values are given in Table 5-1.

Table 5-1 composition mixture of cow and pig manure[21]

Component	wt% daf	mol% wet
C	47.4	8.83
H	6.7	7.43
O	35.3	2.47
N	4.2	0.34
S	0.8	0.05
Cl	1.5	0.10
Ash	0	2.31
H_2O	0	78.48
LHV [kJ kg^{-1}]	19859	3960

With these values in the wet composition are based on the assumption of a moisture content of 80 wt% on wet basis. The calculated values of the wet manure can also be found in Table 5-1.

In Figure 5-1, the flow sheet of the hydrothermal gasification of manure is given. For modeling purposes the manure is put into the model as a gas stream.
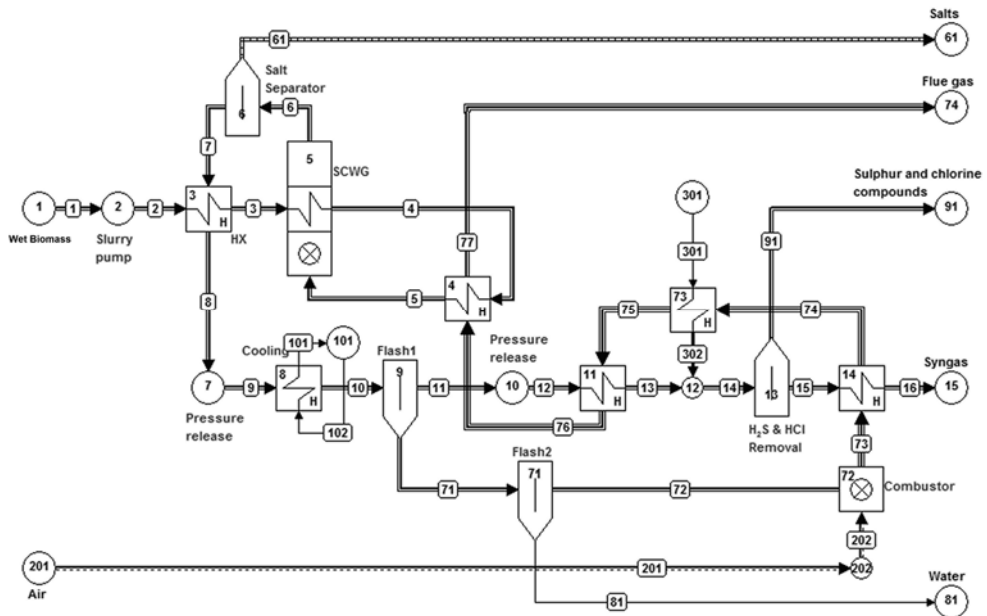
Figure 5-1 flow sheet of super critical water gasification

The compression of the manure is modeled as a sink (no. 2). The output pressure and output temperature are set to the values calculated for the compression of liquid water with an isentropic efficiency of 60% and a mechanical efficiency of 90%. The required power input for the pump is also included in the calculations. This approach is used since the fluid is not a gas but liquid.

The hydrothermal gasification is modeled with single gasifier unit (no. 5); this unit calculates the outgoing gas composition via minimization of the Gibbs energy. For a first estimation of the gas composition coming from the SCWG, Gibbs energy minimization has shown to give good overall predictions for the gas composition [22, 23].

The salts which are formed during the gasification are removed in a separator (no. 6). Some of the heat is then recuperated in heat exchanger (no. 3).

To separate the product gas from the water the pressure is released to flash pressure (sink no. 7) and the fluid is cooled to 298 K with cooling water (heat exchanger no. 8). The mixture is flashed separating the gas from the liquid. The liquid stream is flashed to atmospheric pressure (separator no. 71), to release the dissolved gasses from the liquid water. These released gasses are combusted in a combustor (no. 72) to provide additional heat to the process (heat exchangers no. 4 and 11).

For the flash calculations is a separate Aspen model used, since in Cycle-Tempo it is not possible to do this type of flash calculations. The thermodynamic model used for these flash calculations is Redlich-Kwong-Soave model with modified Huron-Vidal mixing rules [24]. From the flash calculations the separation ratios are determined for the two separators which represent the flashes (no.9 & 71) in the Cycle-Tempo model. The separation factors for hydrochloric acid are not calculated by Aspen, since Aspen is no able to de calculations on ioninc compounds with the Redlich-Kwong-Soave with modified Huron-Vidal mixing rules equations of state model. The solubility of hydrochloric acid is expected to be high, so the separation factors of 95% for the first flash and 75% for the second flash are chosen.

The gas released by the first flash (separator no. 9) is the product which is used later as fuel for the fuel cell. This gas still contains small amounts of hydrochloric acid and hydrogen sulphide. These small amounts need to be removed, since they will have a deteriorating effect on the SOFC-GT hybrid system. Before the hydrogen sulphide and hydrochloric acid is removed, steam is added to the gas in order to prevent carbon formation in the removal system. The superheated steam is produced in a boiler (no. 73) using the hot flue gasses coming from the combustor.

The hydrochloric acid is removed in packed bed with sodium carbonate and hydrogen sulphide is removed from the gas in a packed bed with zinc oxide. This is modelled as a separator (no. 13) with a pressure drop which is assumed to remove all the hydrochloric acid and hydrogen sulphide from the gas. Next the gas is heated in a heat exchanger (no. 14) with the hot flue gas coming from the combustor (no 72).

5.3.2. Solid Oxide Fuel Cell Gas Turbine Hybrid System

In Figure 5-2 the flow sheet for the SOFC-GT hybrid system is given. The fuel gas coming from the gasification section is mixed with a recycle stream from the fuel cell anode before it enters the fuel cell (no. 16). The fuel cell is modeled as a direct internal reforming (DIR) solid oxide fuel cell. The anode gas entering the fuel cell is brought to its chemical equilibrium by means of Gibbs minimization calculations. Then the cell voltage V, active cell area, the current flow I and the electrical power output P_e are calculated by the model. The fuel mass flow into the fuel cell is related to the current flow as indicated in equation (5.3).

$$I = \frac{\phi_{m,a,in}}{M_a} 2F(y_{H_2}^0 + y_{CO}^0 + 4y_{CH_4}^0)U_f \tag{5.3}$$

Here, y_i^0 are the concentrations of the different components at the inlet, M_a is the molar mass of the anode gas, F is the Faraday constant and U_f is the fuel utilization.

The temperature and pressure are supposed to be constant during the process. The mass flow of oxygen from the cathode to the anode is calculated based on the current flow. An energy balance is used to calculate the air flow through the fuel cell, since the temperature at the outlet is given. For the calculation of the cell voltage, the current density and power output a one dimensional model is used. This means that the temperature, pressure and composition are supposed to be constant in a cross-section, perpendicular to the flow of fuel through the fuel cell. The local reversible cell voltage $V_{rev,x}$, the local current density i_x and the local concentrations y_x(H_2, CO, CO_2, CH_4 and H_2O) are calculated. For the cross-section the reversible cell voltage $V_{rev,x}$ is determined with the Nernst equation assuming ideal gas:

$$V_{rev,x} = V_{rev}^0 + \frac{RT}{2F} \ln\left(\frac{y_{O_2,c}^{0.5} y_{H_2,a}}{y_{H_2O,a}} \times p_{cell}^{0.5} \right) \tag{5.4}$$

Where V_{rev}^0 is the standard reversible voltage for hydrogen, R the universal gas constant, T is the temperature, y is the mole fraction at the cross-section and p_{cell} is the pressure. It is assumed that the voltage losses on the level of the electrodes are negligible in the x-direction. This means that the cell voltage is supposed to be constant over the fuel cell. So, the voltage loss ΔV_x can be calculated using the following equation:

$$\Delta V_x = V_{rev,x} - V \tag{5.5}$$

Where ΔV_x is the voltage loss. The current density can then be calculated with:

$$i_x = \frac{\Delta V_x}{R_{eq}} \tag{5.6}$$

Here R_{eq} is the equivalent fuel cell resistance.
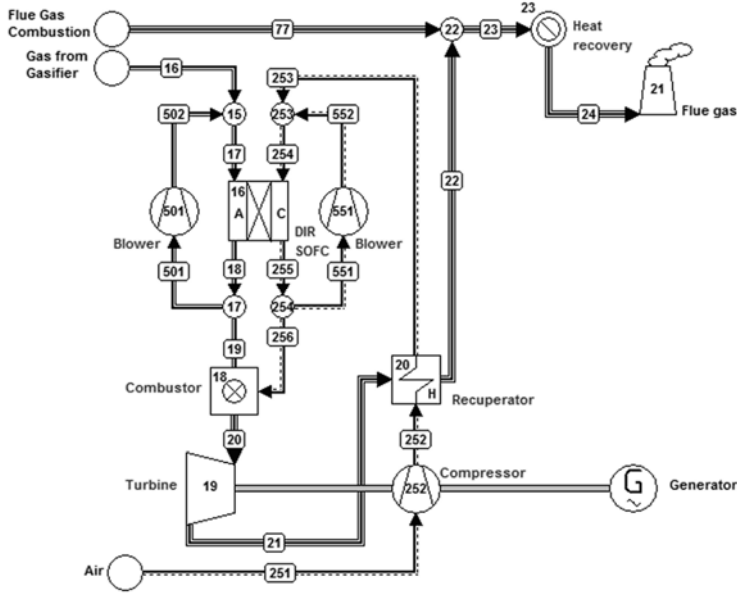
Figure 5-2 flow sheet of the solid oxide fuel cell gas turbine hybrid system

Over the whole fuel cell these quantities are connected with the following equation:

$$\frac{I}{A} = \frac{U_f}{R_{eq} \int_0^{U_F} \frac{d\xi}{(V_{rev,x} - V)}} \tag{5.7}$$

Here, I is the total current, A is the fuel cell area and ξ is the dimensionless reaction coordinate. With the current and voltage known the power output can be calculated.
 The residual fuel leaving the fuel cell is combusted in a combustor (no. 18). The hot flue gasses are then expanded in a turbine (no. 19) which is connected to a generator through a shaft. The enthalpy of the outlet is calculated using equation (5.8), for the compressor equation (5.9) is used.

$$h_{out} = h_{in} - \eta_i (h_{in} - h_{out,s}) \tag{5.8}$$

$$h_{out} = h_{in} + \frac{(h_{out,s} - h_{in})}{\eta_i} \tag{5.9}$$

In these equations, h_{out} is the specific enthalpy of the outlet, h_{in} the specific enthalpy of the inlet, η_i the isentropic efficiency and $h_{out,s}$ is the specific enthalpy of the gas when

isentropically expanded. When the enthalpy change is known, the power output can be determined with the mass flow. The flue gasses are used in a recuperator (no. 20) to pre-heat the air. Finally the flue gasses are mixed with the flue gas from the gasification plant and some heat is recovered in a heat sink (no. 23). This heat could be used to produce even more electricity with for example an organic rankine cycle. After this, the gas is released to the environment in a stack (no. 21).

5.3.3. Assumptions and model input

Several general assumptions have been made for the models:
- Steady state
- No fouling in the equipment
- No catalyst deactivation
- All processes are adiabatic
- The heat exchangers are operated in counter current flow

The input values for the hydrothermal gasification of the different systems are given in Table 5-2. In Table 5-3, the input values for the SOFC-GT hybrid system are given. For both tables, the temperatures (T) are given in °C, the pressures (p) in bar, the mass flow (ϕ_m) in kg s^{-1}, the equivalent fuel cell resistance (R_{cell}) in Ω m^2 and the current density (i) in A m^{-2}.

Cycle Tempo can perform exergy calculations. The exergy of all flows considered in the flow sheet is calculated based on previous calculated temperatures, pressures and chemical composition. The thermo-mechanical (physical) exergy and chemical exergy are calculated separately. The thermo-mechanical exergy Ex_{tm} is calculated using equation (5.10).

$$Ex_{tm} = (h - h_0) - T_0(s - s_0) \tag{5.10}$$

Here, h is the enthalpy of a stream, s is the entropy of a stream, h_0 is the enthalpy of a stream at reference conditions, s_0 is the entropy of a stream at reference conditions and T_0 is the temperature at reference conditions.

For the calculation of the chemical exergy a definition of the environment is required. The composition of the environment in the calculation is given in Table 5-4, which is the composition of air saturated with water vapour as specified Baehr [25], but at an environmental temperature of 288 K and pressure of 101325 Pa. The chemical exergy Ex_{ch} is calculated using equation (5.11).

$$Ex_{ch} = \sum_i y_i ex_{0,i} + RT_0 \sum_i y_i \ln y_i \tag{5.11}$$

Here, y_i is the molar fraction of component i, $ex_{0,i}$ is the standard chemical exergy of component i which is based on the reference environment and T_0 is the reference temperature,

The overall exergy Ex is calculated using the following relation:

$$Ex = \phi_{mol}(Ex_{tm} + Ex_{ch}) \tag{5.12}$$

Where, ϕ_{mol} is the molar flow.

Chlorine, sulphur and the elements in the ash are not defined in the chemical composition of the environment. Therefore, the components containing these elements are assumed to have zero exergy. Since the concentrations of these elements in the biomass are very low this assumption would result only in a negligible error.

Energy efficiencies are based on the Lower Heating Value (LHV) of the fuel. The exergy efficiency is generally defined as follows.

$$\eta_{Ex} = \frac{\sum Ex_{products}}{\sum Ex_{source}} \tag{5.13}$$

Table 5-2 input values for hydrothermal gasification of the different systems

Unit	Name	Case 1	Case 2	Case 3
1	Source	p_{out}=1.01325, T_{out}=15, ϕ_m=0.2778	p_{out}=1.01325, T_{out}=15, ϕ_m=0.2778	p_{out}=1.01325, T_{out}=15, ϕ_m=0.2778
2	Sink/Source	p_{out}=350, T_{out}=21.1	p_{out}=350, T_{out}=21.1	p_{out}=250, T_{out}=19.32
3	Heat Exchanger	Δp_h=6, Δp_l=6.1, $T_{out,h}$=195	Δp_h=6, Δp_l=6.1, $T_{out,h}$=195	Δp_h=5, Δp_l=5.1, $T_{out,h}$=140
4	Heat Exchanger	Δp=0	Δp=0	Δp=0
5	Gasifier	Δp_l=0, $T_{in,2}$=400, p_{react}=343.9, T_{react}=408.49, $p_{out,2}$=343.9, $T_{out,2}$=408.49	Δp_l=0, $T_{in,2}$=500, p_{react}=343.9, T_{react}=500, $p_{out,2}$=343.9, $T_{out,2}$=500	Δp_l=0, $T_{in,2}$=600, p_{react}=343.9, T_{react}=600, $p_{out,2}$=343.9, $T_{out,2}$=600
6	Separator	Δp_1=6, Δp_2=6, ΔT_1=0, ΔT_2=0	Δp_1=6, Δp_2=6, ΔT_1=0, ΔT_2=0	Δp_1=5, Δp_2=5, ΔT_1=0, ΔT_2=0
7	Sink/Source	Δp=178.9, ΔH_{out}=0, $T_{out,est}$=187.5	Δp=178.9, ΔH_{out}=0, $T_{out,est}$=187.5	Δp=80.9, ΔH_{out}=0, $T_{out,est}$=150
8	Heat Exchanger	Δp_h=3, Δp_l=0.01, $T_{out,h}$=25	Δp_h=3, Δp_l=0.01, $T_{out,h}$=25	Δp_h=3, Δp_l=0.01, $T_{out,h}$=25
9	Separator	Δp_1=100, Δp_2=100, ΔT_1=0, ΔT_2=0	Δp_1=100, Δp_2=100, ΔT_1=0, ΔT_2=0	Δp_1=50, Δp_2=50, ΔT_1=0, ΔT_2=0
10	Sink/Source	Δp=43, ΔH_{out}=0	Δp=43, ΔH_{out}=0	Δp=93.1, ΔH_{out}=0
11	Heat Exchanger	Δp_h=0.001, Δp_l=0.1, $T_{out,l}$=400	Δp_h=0.001, Δp_l=0.1, $T_{out,l}$=400	Δp_h=0.001, Δp_l=0.1, $T_{out,l}$=404
12	Node			
13	Separator	Δp_1=0.2, Δp_2=0.2, ΔT_1=0, ΔT_2=0	Δp_1=0.2, Δp_2=0.2, ΔT_1=0, ΔT_2=0	Δp_1=0.2, Δp_2=0.2, ΔT_1=0, ΔT_2=0
14	Heat Exchanger	Δp_h=0.01, Δp_l=0.042, $T_{out,h}$=859	Δp_h=0.001, Δp_l=0.042, $T_{out,h}$=862.5	Δp_h=0.001, Δp_l=0.1042, $T_{out,l}$=835.5
61	Sink/Source			
71	Separator	p_1=1.01325, p_2=1.01325, ΔT_1=24.4, ΔT_2=24.4	p_1=1.01325, p_2=1.01325, ΔT_1=24.4, ΔT_2=24.4	p_1=1.01325, p_2=1.01325, ΔT_1=24.4, ΔT_2=24.4
72	Combustor	p_{out}=1.016, λ=1.3, T_{react}=1000, p_{react}=1.01325	p_{out}=1.016, λ=1.3, T_{react}=1000, p_{react}=1.01325	p_{out}=1.016, λ=1.3, T_{react}=1000, p_{react}=1.01325
73	Heat Exchanger	Δp_h=0.001, Δp_l=0, $T_{out,l}$=400	Δp_h=0.001, Δp_l=0, $T_{out,l}$=400	Δp_h=0.001, Δp_l=0, $T_{out,l}$=404
81	Sink/Source			
91	Sink/Source			
101	Sink/Source	p_{out}=1.01325, T_{in}=20, T_{out}=15	p_{out}=1.01325, T_{in}=20, T_{out}=15	p_{out}=1.01325, T_{in}=20, T_{out}=15
201	Sink/Source	p_{out}=1.01325, T_{out}=15	p_{out}=1.01325, T_{out}=15	p_{out}=1.01325, T_{out}=15
202	Node	ΔP=0	Δp=0	Δp=0
301	Sink/Source	p_{out}=6.8, T_{out}=15, ϕ_m=0.0078	p_{out}=6.8, T_{out}=15, ϕ_m=0.005	p_{out}=6.8, T_{out}=15, ϕ_m=0.005

Where $Ex_{products}$ is the exergy of the flows which are considered to be products going out of the systems, Ex_{source} is the exergy of the flows which are considered to be necessary for making the product going into the system. Further specification of the $Ex_{product}$ and Ex_{source} is necessary in order to calculate system efficiencies. In this paper the electrical exergy efficiency ($\eta_{ex,el}$) is defined as:

$$\eta_{ex,el} = \frac{\sum P_{el,out} - \sum P_{el,in}}{Ex_{fuel,in}} \tag{5.14}$$

Here is $P_{el,out}$ the gross electrical output of the system, $P_{el,in}$ the electrical power input in the system (auxiliary power) and $Ex_{fuel,in}$ is the exergy of the fuel put into the system.

Table 5-3 input for the SOFC-GT hybrid system coupled to the hydrothermal gasification

Unit	Name	All cases
15	Node	Δp=0
16	Fuel Cell	Δp_{an}=0.2, Δp_{cat}=0.2, $T_{in,an}$=900, $T_{in,cat}$=900, T_{out}=1000, p_{fc}=6.5, T_{fc}=950, p_{react}=6.5, T_{react}=950, U_f=0.85, DCAC=0.97, R_{cell}=5e-5, i=2500
17	Node	
18	Combustor	Δp=0.5, T_{react}=1000, p_{react}=6.4
19	Turbine	η_i=0.80
20	Heat Exchanger	Δp_h=0.001, Δp_l=0.2, ΔT_h=30
21	Stack	p_{in}=1.01325
22	Node	Δp=0
23	Heat Sink	Δp=0, T_{out}=110
252	Compressor	PR=6.67, η_i=0.80
253	Node	Δp=0
254	Node	
501	Compressor	η_i=0.70
551	Compressor	η_i=0.70
G	Generator	η=0.97

Table 5-4 chemical composition of the environment [25]

Component	Molar fraction [%]
Ar	0.91
CO_2	0.03
H_2O	1.68
N_2	76.78
O_2	20.60

5.4. Results and discussion

The wet biomass enters the system with a mass flow of 0.28 kg s^{-1} at environmental conditions. This stream is pressurized to a pressure of 35 MPa for cases 1 and 2. For case 3 the manure is pressurized to a pressure of 25 MPa. The pressurization results in power consumption of the pump of 17.83 kW for cases 1 and 2, for case 3 this is 12.75 kW. After the pressurization, the gas is heated in heat exchangers to process conditions and then gasified. The precipitated solid salts are removed and the fluid is cooled by heat exchanging with the pressurized feed. Then some pressure is released and the fluid is further cooled. In Table 5-5, the composition of the resulting fluid (pipe 10) for the different systems is given.

Table 5-5 composition in mole% of the fluid in different pipes of the system

Component	Case 1			Case 2			Case 3		
Pipe number (Figure 1)	10	11	16	10	11	16	10	11	16
Mass flow [kg s^{-1}]	0.26	0.02	0.03	0.26	0.03	0.03	0.26	0.02	0.03
Temperature [K]	298	298	1132	298	298	1136	298	298	1109
Pressure [bar]	150.0	50.0	6.6	150.0	50.0	6.6	150.0	100.0	6.6
H_2	0.95	10.69	7.62	2.39	23.02	18.95	5.86	44.99	38.12
CH_4	5.60	59.57	42.49	5.19	47.89	39.40	4.19	30.57	25.90
CO	0.02	0.06	0.04	0.03	0.26	0.22	0.15	1.17	0.99
CO_2	4.79	25.07	17.88	5.10	24.92	20.51	5.79	20.18	17.10
H_2S	0.07	0.17	0.00	0.07	0.17	0.00	0.07	0.12	0.00
HCl	0.09	0.06	0.00	0.09	0.05	0.00	0.09	0.04	0.00
N_2	0.37	4.26	3.03	0.37	3.59	2.96	0.36	2.84	2.41
NH_3	0.02	0.01	0.00	0.02	0.01	0.01	0.03	0.01	0.01
H_2O	88.09	0.11	28.94	86.74	0.09	17.95	83.46	0.08	15.46

The composition of pipe 10 is entered into the Aspen flash model to determine the separation factors. These separation factors are given in Table 5-6 for every case. The chosen separation factors for hydrochloric acid will hardly influence the calculations since the concentrations are low. In this model it is not important for determining the system performance, since it is assumed that the chlorine removal bed will adsorb all the residual chlorine. When designing an actual system to be build; it is important to know how much chlorine will be in the gas after the flash. Especially, when dimensioning the chlorine removal system. Hydrochloric acid can have a detrimental effect on the solid oxide fuel cell. For case 3, a higher pressure is used in the first flash. This is done to increase the amount of combustibles dissolved in the water. These combustibles are used after the second flash for the generation of heat for the process. When the same pressure was used as in cases 1 & 2, the heat generation was not sufficient for the process.

Table 5-6 separation factors for the two flashes in the different systems

	Case 1		Case 2		Case 3	
	Flash 1	Flash 2	Flash 1	Flash 2	Flash 1	Flash 2
Pressure [bar]	50	1.01	50	1.01	100	1.01
Temperature [K]	298	298	298	298	298	298
CH_4 [mole%]	15.17	0.68	12.84	0.72	19.04	0.44
CO [mole%]	0.00	0.00	8.73	0.00	14.35	1.09
CO_2 [mole%]	58.26	6.52	53.83	6.66	61.36	4.48
H_2 [mole%]	10.72	0.24	8.86	0.34	14.83	0.22
H_2O [mole%]	99.99	99.86	99.99	99.87	99.99	99.80
H_2S [mole%]	78.93	17.52	75.95	17.87	79.93	12.55
HCl [mole%]	95.00	75.00	95.00	75.00	95.00	75.00
N_2 [mole%]	9.33	0.71	7.79	0.00	12.53	0.00
NH_3 [mole%]	97.90	74.54	97.32	75.23	97.66	66.40

The resulting gas composition for pipe 11 can be found in Table 5-5. The gas is further expanded to 6.9 bar and then heated in the following heat exchanger to 673 K before steam is added. In case 1, 0.008 kg s^{-1} steam is added with a temperature of 673 K and a pressure of 6.8 bar. In cases 2 and 3, 0.005 kg s^{-1} steam is added at the same conditions as in case 1.

Since the gas in case 1 is methane rich, more steam is required. This steam is also used in the reforming process in the SOFC downstream. The steam is added to prevent carbon formation in the sulphur and chlorine removal as well as in the SOFC. The composition of the gas send to the SOFC-GT hybrid system (pipe 16) is given in Table 5-5.

Before the gas enters the anode of the fuel cell, it is mixed with the anode recycle stream. The mixture enters the fuel cell at 1173K. Air extracted from the environment is compressed in the compressor of the gas turbine and heated in the recuperator, before it is mixed with the cathode recycle stream. The air mixture enters the cathode of the fuel cell at a temperature of 1173 K. Part of the anode off-gas is recycled as well as a part of the cathode off-gas is recycled, the recycle ratios can be found in Table 5-7.
The residual off-gasses enter a combustor where the residual fuel in the anode off-gas is combusted. The hot flue gas is expanded in the turbine. In Table 5-7, results can be found of the SOFC-GT hybrid system for the different cases.

In Table 5-8, an overview is given of the power production and the efficiencies of the different systems

Table 5-7 results of the SOFC-GT for the different cases

	Case 1	Case 2	Case 3
Air input [kg s^{-1}]	0.31	0.33	0.37
Cell Voltage [V]	0.816	0.821	0.810
Active cell area [m^2]	180.4	185.3	176.5
Anode recycle ratio [%]	19.8	18.8	29.0
Cathode recycle ratio [%]	53.7	54.7	60.6
Turbine inlet temperature [K]	1462	1458	1414
Turbine outlet temperature [K]	1084	1079	1042
Pressure ratio	6.7	6.7	6.7

.

Table 5-8 overview of the performance of the different systems

	System 1		System 2		System 3	
	Energy [kW]	Exergy [kW]	Energy [kW]	Exergy [kW]	Energy [kW]	Exergy [kW]
Fuel input	830.72	841.85	830.72	841.85	830.72	841.85
Delivered power						
Fuel cell	356.94	356.94	368.88	368.88	346.58	346.58
Generator	87.63	87.63	92.81	92.81	94.58	94.58
Gross power	**444.57**	**444.57**	**461.68**	**461.68**	**441.16**	**441.16**
Auxiliary power consumption						
Aux power	25.00	25.00	25.80	25.80	23.90	23.90
Delivered power						
Net power	**419.57**	**419.57**	**435.88**	**435.88**	**417.26**	**417.26**
Total power	**543.78**	**473.55**	**556.20**	**487.00**	**575.01**	**487.31**
Efficiencies						
Gross el. eff. [%]	53.52	52.81	55.58	54.84	53.11	52.40
Net el. eff. [%]	50.51	49.84	52.47	51.78	50.23	49.57

As can be seen in Table 5-8, the net electrical performances of the three cases do not deviate much from each other. The electrical exergy efficiency is around 50%, which is comparable to the efficiency of conversion systems based on dry biomass, like in refs. [2,

11]. When wet biomass is applied in systems for dry biomass, the biomass needs to be dried first. The drying will reduce the performance of the systems based on dry biomass.

In order to get an overview where the exergy losses within the system occur, a exergy flow diagram has been created for each case. In these diagrams, the losses are indicated by the gray areas. In Figure 5-3, the exergy flow diagrams for the three cases are given.
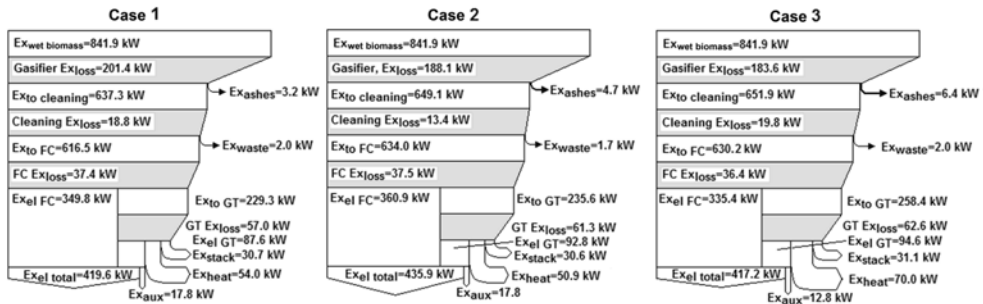
Figure 5-3 exergy flow diagrams for the three different systems

The unit numbers which are included in the different system sections as indicated in Figure 5-3 are given in Table 5-9.

Table 5-9 the units included in the different system sections as indicated in Figure 5-3

System section	Unit number in Figure 5-1 or Figure 5-2
Gasifier	2, 3, 4, 5, 6, 7, 8, 9, 10, 71, 72, 101, 202
Cleaning	11, 12, 13, 14, 73
Fuel cell (FC)	15, 16, 17, 253, 254, 501, 551
Gas turbine (GT)	18, 19, 20, 22, 23, 252

From Figure 5-3 can be seen that the gasification section has the largest losses in the whole system. The losses for the gasification are in case 1 larger than for cases 2 &3. The losses are mainly caused by the irreversibilities in the gasifier (unit 5). The chemical exergy of the stream leaving the gasifier is smaller for case 1 than for the other two cases and the chemical exergy of the input stream is for the three cases the same. This chemical exergy is lost for a large part. Since the loss of exergy should be minimized, cases 2 & 3 are preferred. Other larger contributors in losses of the gasification section are the heat exchangers (unit 3 & 8) and the combustor (unit 72).

The losses in the gas cleaning section of case 2 are significantly smaller then for the other two systems. The losses in this section are dominated by the heat exchangers and the boiler. The cause of these losses can be clearly shown by a heat-temperature diagram of the heat exchangers (units 11 & 14) and the boiler (unit 73) for every case. In Figure 5-4, the heat-temperature diagrams of units 11, 14 and 73 for the different cases have been given.

The slope of the hot fluid temperature line is steeper in case 2 (14.1 K kW^{-1}) than for the other two cases (for case 1: 12.7 K kW^{-1} and for case 3: 9.6 K kW^{-1}). In the other two cases more flue gas is formed in combustor (unit 72), resulting in a larger mass flow. The amount of combustibles going to the combustor is determined by the flash conditions, and that determines the amount of flue gas that is produced. The air factor is for every system the

same. Also, the temperature differences between the hot fluid and the cold fluid are smaller for case 2 than for the other cases. This is represented by the shaded area in Figure 5-4.
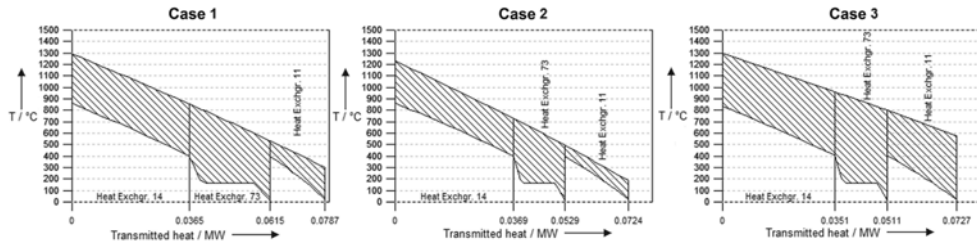
Figure 5-4 heat-temperature diagrams for units 11, 14 & 73 for the different systems

The power output of the fuel cell in case 3 is lower than in the other cases. This is partly caused by the fact that more anode gas is recycled than in the other cases. The recycling has a diluting effect on the fuel, resulting in a lower fuel cell power output. The lower performance of the fuel cell is partly compensated by the higher output of the gas turbine. The air flow through the fuel cell is higher than in the other cases, because the fuel cell requires more cooling due to lower methane fraction and higher hydrogen fraction in the fuel.

For case 1, the losses for the gas turbine are smaller than in the other cases. This is partly caused by the amount of air required in the SOFC-GT hybrid system. The fuel cell is cooled by the cathode air flow. If the amount of hydrogen in fuel increases, the fuel cell requires more cooling, because less heat is extracted by the internal reforming. The increased mass flow of air causes an increase of the losses in the air compressor, air recycle blower, turbine and mixing points.
Case 3 has a larger heat production than the cases 1 &2. Since case 3 has the largest mass flow of flue gas coming from the combustor.
The two flue gas streams coming from the gasification section and from the gas turbine are mixed to make it easier to extract heat from it. The heat is extracted by a heat consumer, which cools the flue gas to a temperature of 383 K. This values is chosen to prevent condensation of the water is the flue gas. The type of heat consumer is not further researched, many options are available, for instance, an organic rankine cycle for the production of additional electricity, steam production for other processes, production of hot water for district heating, etc.

The most determining factor for the performance of the whole system is the flash conditions of the first flash vessel. The flash conditions determine the amount of gas and the composition of the gas. The solubility of the different components in water depends on the pressure. The secondary flash is used to release the dissolved compounds from the water, which results in a combustible gas. It is possible to optimize the flash conditions in such a way that the maximal amount of gas for the fuel cell is produced and still enough heat can be produced from the gas released in the second flash to support the process. This optimization is not performed, and is considered as a future research topic. The current flash conditions deliver almost similar mass flows of gas towards the gas cleaning section and SOFC-GT system.

5.5. Conclusions

The coupling of hydrothermal biomass gasification and a SOFC-GT hybrid system has been thermodynamically evaluated by modeling several systems in Cycle Tempo. The biomass used in this study is a mixture of pig and cow manure with a moisture content of 80 wt% on a wet basis. Three different types of hydrothermal gasification have been modeled and combined with a SOFC-GT hybrid system. Case 1 is based on catalytic gasification at a temperature of around 673K and a pressure of 34 MPa; this results in a producer gas of mainly methane, carbon dioxide and a relatively small amount of hydrogen. Case 2 is based on non-catalytic gasification at a temperature of 773K and a pressure of 34 MPa resulting in a mixture of hydrogen, methane and carbon dioxide. Case 3 is based on non-catalytic hydrothermal gasification at a temperature of 873K and a pressure of 25 MPa resulting in a hydrogen rich gas. The coupled SOFC-GT hybrid is kept identical for every system. The electrical exergy efficiency for the cases 1, 2 and 3 are 49.8%, 51.8% and 49.6%, respectively.

These efficiency values are reasonably comparable with previously reported efficiencies for SOFC-GT systems combined with conventional gasification techniques based on dry biomass. The combination of hydrothermal gasification and SOFC-GT hybrid systems seems very promising especially for wet biomass streams.

The non-catalytic hydrothermal gasification process of cases 2 & 3 are preferred, since these processes have lower chemical exergy losses in the gasification than case 1.

The conditions of the flash used for separating the gas from the liquid have a large influence on the performance of the system because it influences the amount of combustibles dissolved in the liquid. Further study into the flash conditions is required to optimize the system.

5.6. References

1.   Aravind P. V. Studies on High Efficiency Energy Systems Based on Biomass Gasifiers and Solid Oxide Fuel Cells with Ni/GDC Anodes. PhD Thesis, University of Technology Delft, 2007.
2.   Aravind P. V., Woudstra T., Woudstra N., Spliethoff H. Thermodynamic Evaluation of Small Scale Systems with Biomass Gasifiers, Solid Oxide Fuel Cells with Ni/GDC Anodes and Gas Turbines. J Power Sources 2009; 190(2): 461-475.
3.   Panopoulos K. D., Fryda L. E., Karl J., Poulou S., Kakaras E. High temperature solid oxide fuel cell integrated with novel allothermal biomass gasification: Part I: Modelling and feasibility study. J Power Sources 2006; 159(1): 570-585.
4.   Athanasiou C., Coutelieris F., Vakouftsi E., Skoulou V., Antonakou E., Marnellos G., Zabaniotou A. From biomass to electricity through integrated gasification/SOFC system-optimization and energy balance. Int J Hydrogen Energy 2007; 32(3): 337-342.
5.   Athanasiou C., Vakouftsi E., Coutelieris F. A., Marnellos G., Zabaniotou A. Efficiencies of olive kernel gasification combined cycle with solid oxide fuel cells (SOFCs). Chem Eng J 2009; 149(1-3): 183-190.
6.   Seitarides T., Athanasiou C., Zabaniotou A. Modular biomass gasification-based solid oxide fuel cells (SOFC) for sustainable development. Renew Sustain Energy Rev 2008; 12(5): 1251-1276.
7.   Omosun A. O., Bauen A., Brandon N. P., Adjiman C. S., Hart D. Modelling system efficiencies and costs of two biomass-fuelled SOFC systems. J Power Sources 2004; 131(1-2): 96-106.

8.   Fryda L., Panopoulos K. D., Kakaras E. Integrated CHP with autothermal biomass
       gasification and SOFC-MGT. Energy Convers Manage 2008; 49(2): 281-290.
9.   Proell T., Aichernig C., Rauch R., Hofbauer H. Coupling of Biomass Steam
       Gasification and an SOFC - Gas Turbine Hybrid System for Highly Efficient
       Electricity Generation. In: ASME Turbo Expo 2004: Power for Land, Sea, and Air,
       Vienna, Austria, 2004.
10.   Sucipta M., Kimijima S., Suzuki K. Performance analysis of the SOFC-MGT
       hybrid system with gasified biomass fuel. J Power Sources 2007; 174(1): 124-135.
11.   Toonssen R., Woudstra N., Verkooijen A. H. M. Reference System for a Power
       Plant Based on Biomass Gasification and SOFC. In: 8th European Solid Oxide
       Fuel Cell Forum, Luzerne, Switserland, 2008.
12.   Li C.-X., Li C.-J., Guo L.-J. Performance of a Ni/Al2O3 cermet-supported tubular
       solid oxide fuel cell operating with biomass-based syngas through supercritical
       water. Int J Hydrogen Energy doi:10.1016/j.ijhydene.2009.05.033
13.   Peterson A. A., Vogel F., Lachance R. P., Fröling M., Antal M. J., Tester J. W.
       Thermochemical biofuel production in hydrothermal media: A review of sub- and
       supercritical water technologies. Energy Environ Sci 2008; 1(1): 32-65.
14.   Kruse A. Hydrothermal biomass gasification. J Supercrit Fluids 2009; 47(3): 391-
       399.
15.   Kruse A. Supercritical water gasification. Biofuels, Bioprod Biorefin 2008; 2(5):
       415-437.
16.   Brunner G. Near critical and supercritical water. Part I. Hydrolytic and
       hydrothermal processes. J Supercrit Fluids 2009; 47(3): 373-381.
17.   Lu Y. J., Guo L. J., Ji C. M., Zhang X. M., Hao X. H., Yan Q. H. Hydrogen
       production by biomass gasification in supercritical water: A parametric study. Int J
       Hydrogen Energy 2006; 31(7): 822-831.
18.   Antal M. J., Allen S. G., Schulman D., Xu X., Divilio R. J. Biomass Gasification
       in Supercritical Water. Industrial & Engineering Chemistry Research 2000; 39(11):
       4040-4053.
19.   Ouweltjes J. P., Aravind P. V., Woudstra N., Rietveld G. Biosyngas Utilization in
       Solid Oxide Fuel Cells With Ni/GDC Anodes. J Fuel Cell Sci Technol 2006; 3(4):
       495-498.
20.   Cycle-Tempo, 5.0. TU Delft, 2009. www.cycle-tempo.nl
21.   Phyllis, database for biomass and waste. http://www.ecn.nl/phyllis/. ECN
22.   Calzavara Y., Joussot-Dubien C., Boissonnet G., Sarrade S. Evaluation of biomass
       gasification in supercritical water process for hydrogen production. Energy
       Convers Manage 2005; 46(4): 615-631.
23.   Tang H., Kitagawa K. Supercritical water gasification of biomass: thermodynamic
       analysis with direct Gibbs free energy minimization. Chem Eng J 2005; 106(3):
       261-267.
24.   Lu Y., Guo L., Zhang X., Yan Q. Thermodynamic modeling and analysis of
       biomass gasification for hydrogen production in supercritical water. Chem Eng J
       2007; 131(1-3): 233-244.
25.   Baehr H. D. THERMODYNAMIK; eine Einführung in die Grundlagen und ihre
       technischen Anwendungen. Berlin: Springer, 1984.

6. Alternative system designs of biomass gasification SOFC-GT hybrid systems

Abstract: *Biomass represents a worldwide distributed renewable energy source, which can offer an important contribution to the transition from fossil fuels to renewable sources. Hybrid energy systems of fuel cells and gas turbine plants are expected to be the most efficient conversion technology for the future. Plant configurations that combine biomass gasification, high temperature fuel cells and a gas turbine are worthwhile to consider because of their high conversion efficiency and low environmental impact. For the design of such systems a variety of options can be considered. In this chapter four system alternatives are presented in order to evaluate the effects of gasification technique, gas cleaning technology and power level.*
One system is a large scale system (30 MW$_e$) using steam gasification and low temperature gas cleaning. The other is small scale system (100 kW$_e$) based on air gasification and high temperature gas cleaning. Two more systems designs have been established to evaluate step by step the effects of the different gasification and gas cleaning technologies and the power level on the system performance of the hybrid SOFC-GT plant: a large scale system (30 MW$_e$) based on air gasification combined with low temperature gas cleaning and a large scale system (30 MW$_e$) based on air gasification combined with high temperature gas cleaning.
The system performances have been analysed by means of models developed with the thermodynamic flow-sheeting program Cycle-Tempo. The system alternatives are compared using the results from the different models and the exergy analysis made for each system design. It appears that the gasification technology has hardly any influence on the systems performance. High temperature gas cleaning give a slightly higher performance compared to low temperature gas cleaning. The large scale systems are more efficient than the small scale system. The highest electrical exergy efficiency (49.9%) was found for the large scale system based on air gasification with high temperature gas cleaning.

6.1. Introduction

Biomass is a term with which all the organic material from vegetation (like wood or agricultural residues), organic wastes and other biological sources in general are defined. Biomass is a world-wide available renewable energy resource which, when produced by sustainable means, emits approximately the same amount of carbon dioxide during its energy conversion as that adsorbed by photosynthesis during plant life [1]. Therefore, the use of biomass does not contribute to increase CO_2 in the atmosphere, and this makes it an interesting energy source in the present context of environmental attention towards emission levels of greenhouse gases. As biomass is a solid, its conversion to a gaseous or liquid energy carrier is generally preferred and has many advantages in handling and application. A number of different processes is available for converting biomass, essentially based on a thermo-chemical conversion (combustion, pyrolysis, gasification and liquefaction) or biological conversion (digestion and fermentation) [2]. The gasification technology is a well developed conversion technique for the conversion of biomass to a so-called biosyngas essentially made up of methane, hydrogen, carbon oxides and nitrogen,

plus impurities. The biosyngas must be treated in a subsequent gas cleanup section [3]. The composition of syngas from gasifiers strongly depends on the technology (and therefore gasification method) involved, and obviously also on the applied gas cleaning technologies. At present, the main destination for biogas generated by gasifiers is its combustion in engines or turbine plants for power generation. High temperature fuel cells can also use syngas as a fuel if it is sufficiently clean. Fuel cells are energy conversion devices which are not "Carnot limited" and are characterized by potentially high overall efficiency, especially high temperature fuel cells. In fuel cells the energy conversion takes place with a direct electrochemical reaction of fuel oxidation, where the exergy losses are very small with respect to conventional combustion systems [4]. Power generation systems based on fuel cells are therefore a promising method in the outlook of a clean and efficient energy economy, thanks to their high energy conversion rates, flexible fuel utilization and very low pollutant emissions (this being due to fuel cell requirement of very clean fuel). High temperature fuel cells, such as the SOFC (Solid Oxide Fuel Cell), are still in the development stage, but can be integrated into small and large power plants and cogeneration units. Many system designs with SOFC's are conceivable, but due to their high operating temperatures, integration of a SOFC with a gas turbine seems to be very attractive [5, 6].

A reasonable number of studies are available in the literature about integrated biomass gasification and solid oxide fuel cell systems. One of the early studies is performed by Alderucci et al. [7]. In this study a thermodynamic evaluation of an integrated catalytic biomass gasifier and a solid oxide fuel cell is made. In this study an electrical efficiency is reported of 47-51%. In the paper of Zhu et al. [8] some experimental results are given for an intermediate temperature solid oxide fuel cell fuelled by syngas coming from biomass gasification. Omosun et al. [9] evaluated two biomass fuelled SOFC systems thermodynamically. They modelled one system with cold gas cleaning and another system with hot gas cleaning. They found an electrical efficiency for the system with cold gas cleaning of 21% and for the system with hot gas cleaning an electrical efficiency of 23%. The overall system efficiencies are 32% and 60%, respectively. In a study performed by Fryda et al. [10], a gasifier is coupled to a SOFC through heat pipes. The heat pipes supply the surplus heat extracted from the SOFC to the gasification system. On this system, they performed an exergy analysis and found an exergetic electrical efficiency of 34% for a net electrical power production of 170 kW [10]. Sucipta et al. [11] studied the influence of the fuel on the electrical performance of a SOFC micro-GT system. They evaluated different fuels for the SOFC-GT system. The considered fuels are methane, and syngas coming from air gasification, oxygen gasification and steam gasification. The actual performance of the gasification and gas cleaning systems were not included in this study. The fuel coming from steam gasification resulted in the highest electrical efficiency [11].
Jin et al. [12] performed a study on several biomass gasification based systems. One of those systems is a large scale integrated biomass gasification SOFC system (463 MW$_e$). The system included also a Rankine bottoming cycle. A net electrical efficiency of 47.1% was calculated, based on the lower heating value (LHV) of the fuel [12]. Nagel et al. [13, 14] compared in total seven systems based on biomass gasification and SOFC; all of these systems have a power output of approximately 1 MW$_e$. These systems include four different fuel cell designs and three different biomasss gasification designs. It was concluded that a fixed bed updraft gasifier combined with a SOFC is the most efficient option.

Proell et al. [15] combined biomass gasification with a SOFC-GT hybrid system and found an electrical efficiency of around 43% for a plant with a fuel input of 8 MW$_{th}$. The considered SOFC in the system is an internal reforming solid oxide fuel cell. Fryda et al. [16] performed an exergy analysis on an integrated combined heat and power system with autothermal biomass gasification and SOFC micro gas turbine. An exergetic electrical efficiency of 35.6% was found for a system producing 350 kW$_e$. Athanasiou et al. [17] also combined biomass gasification with a SOFC-GT system. They reported that the combination fuelled with olive kernel could reach ideally an electric efficiency of 62%.

In this chapter, four different energy systems, based on solid oxide fuel cell/gas turbine (SOFC-GT) hybrid power plants with integrated biomass gasification have been investigated. The configuration, which combines gasifier, high-temperature fuel cell and gas turbine, permits to produce highly efficient, ultraclean and cost-effective power from biomass. The differences between the four systems can be indicated with three main characterizing factors: the gasification technology, the syngas cleaning technology and the power size. The following systems are distinguished:

S1.   Large scale power plant (30 MW$_e$), with indirect atmospheric steam gasification and low temperature gas cleaning [18]

S2.   Large scale power plant (30 MW$_e$), with direct pressurized air gasification and low temperature gas cleaning

S3.   Large scale power plant (30 MW$_e$), with direct pressurized air gasification and high temperature gas cleaning

S4.   Small scale power plant (100 kW$_e$), with direct pressurized air gasification and high temperature gas cleaning [19].

These four systems have been evaluated by means of modelling with the thermodynamic flow-sheeting program Cycle-Tempo [20], with particular focus on the thermodynamic performance. The influence of the gasification technology, the gas cleaning technology and the scale of the process on the overall system performance has been evaluated.

6.2. System configurations

The four different systems in this chapter do consist of three main parts: the gasification, the gas cleaning and the SOFC-GT hybrid system. A schematic representation of the systems S1, S2, S3 and S4 is given in the Figure 6-1, Figure 6-2, Figure 6-3 and Figure 6-4. In the following sections a description of the different system parts is given, starting with the gasification followed by the gas cleaning and finally the SOFC-GT hybrid system.

6.2.1. Biomass gasification

Three different gasification technologies have been evaluated; indirect atmospheric steam gasification in a fast internal circulating fluidized bed (FICFB) in system S1, direct pressurized air gasification in a circulating fluidized bed (CFB) in systems S2 & S3 and direct pressurized air gasification in a downdraft fixed bed gasifier in system S4.
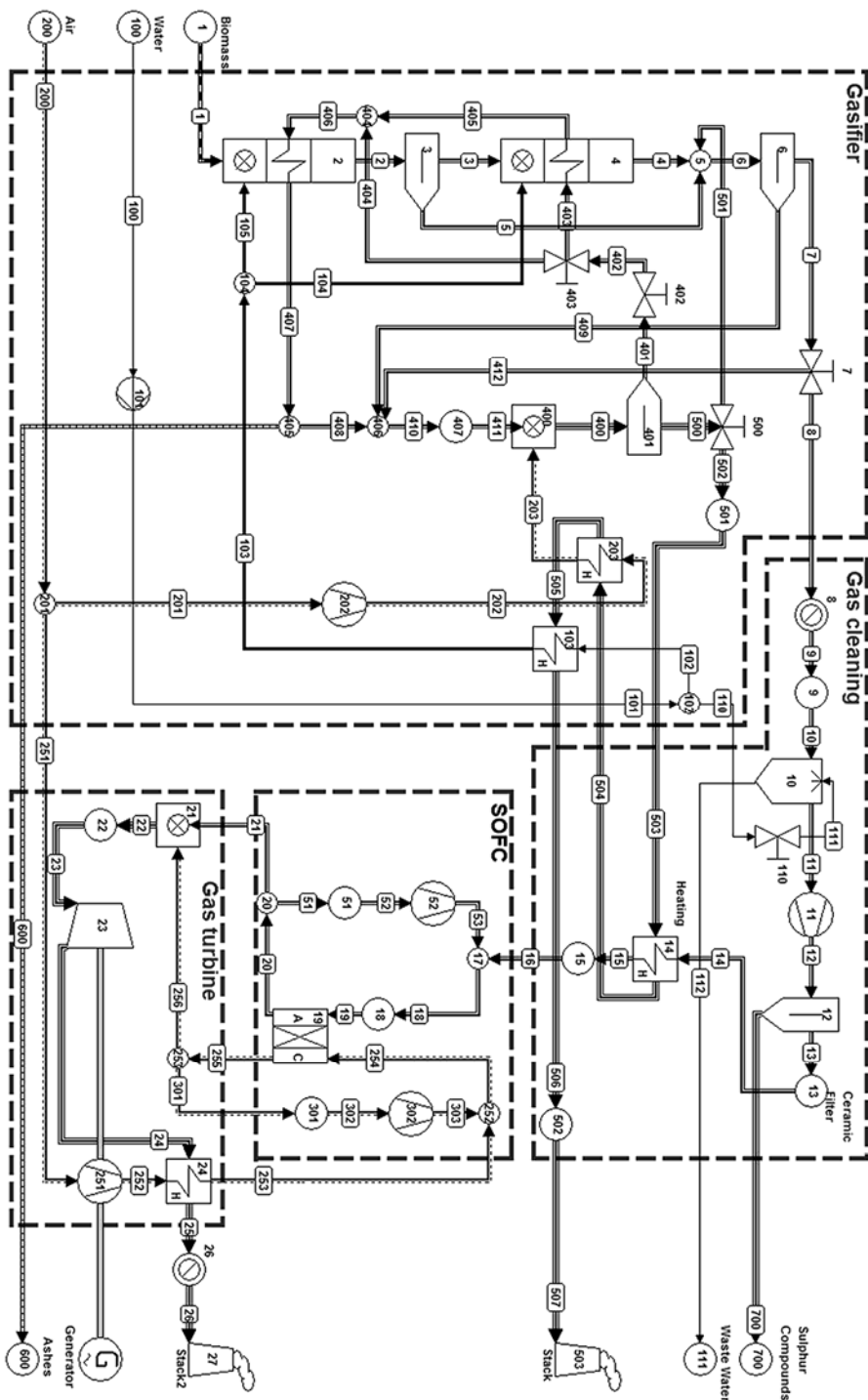
Figure 6-1 flow sheet of system S1(large scale, atmospheric steam gasification, low temperature gas cleaning)
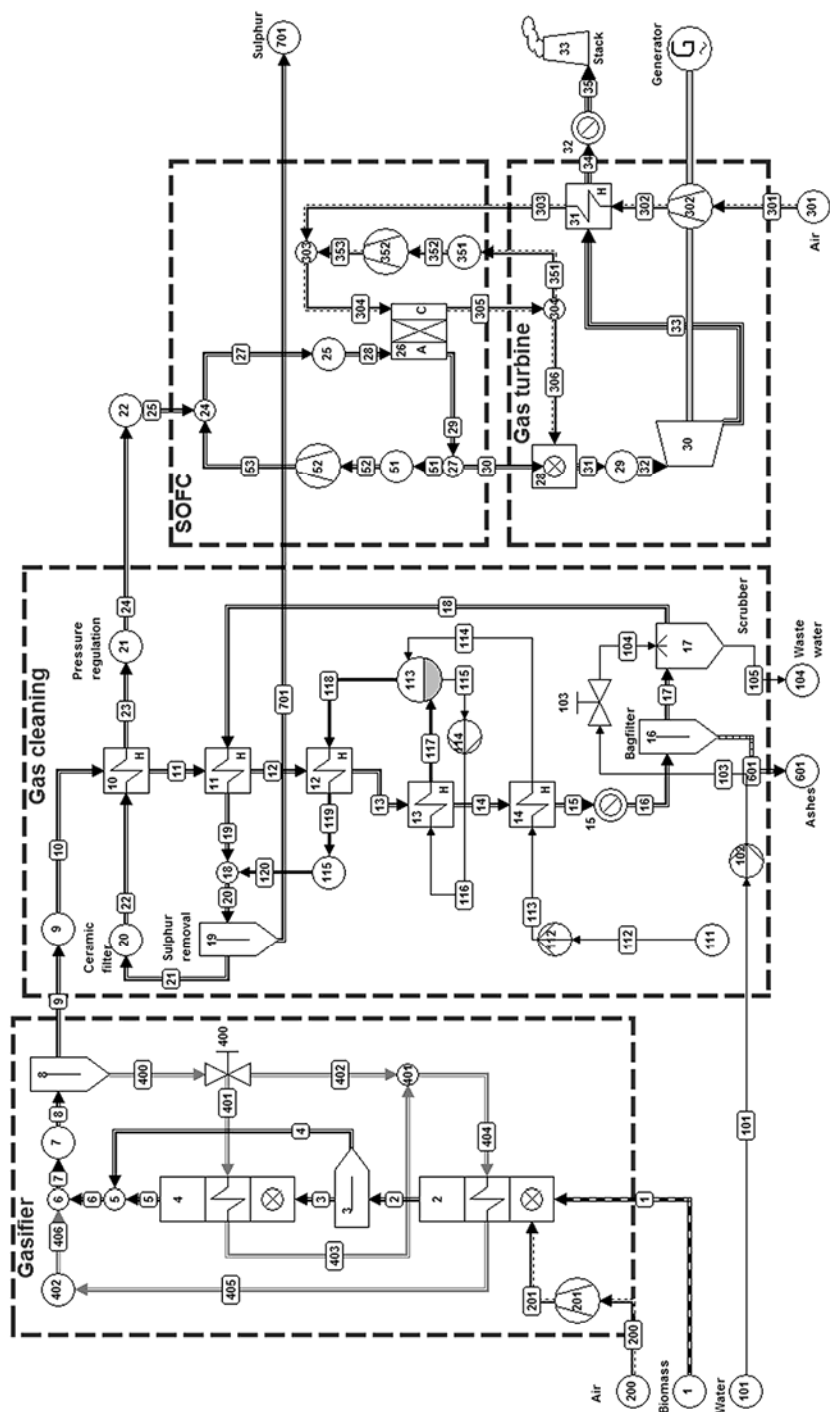
Figure 6-2 flow sheet of system S2 (large scale, pressurized air gasification, low temperature gas cleaning)
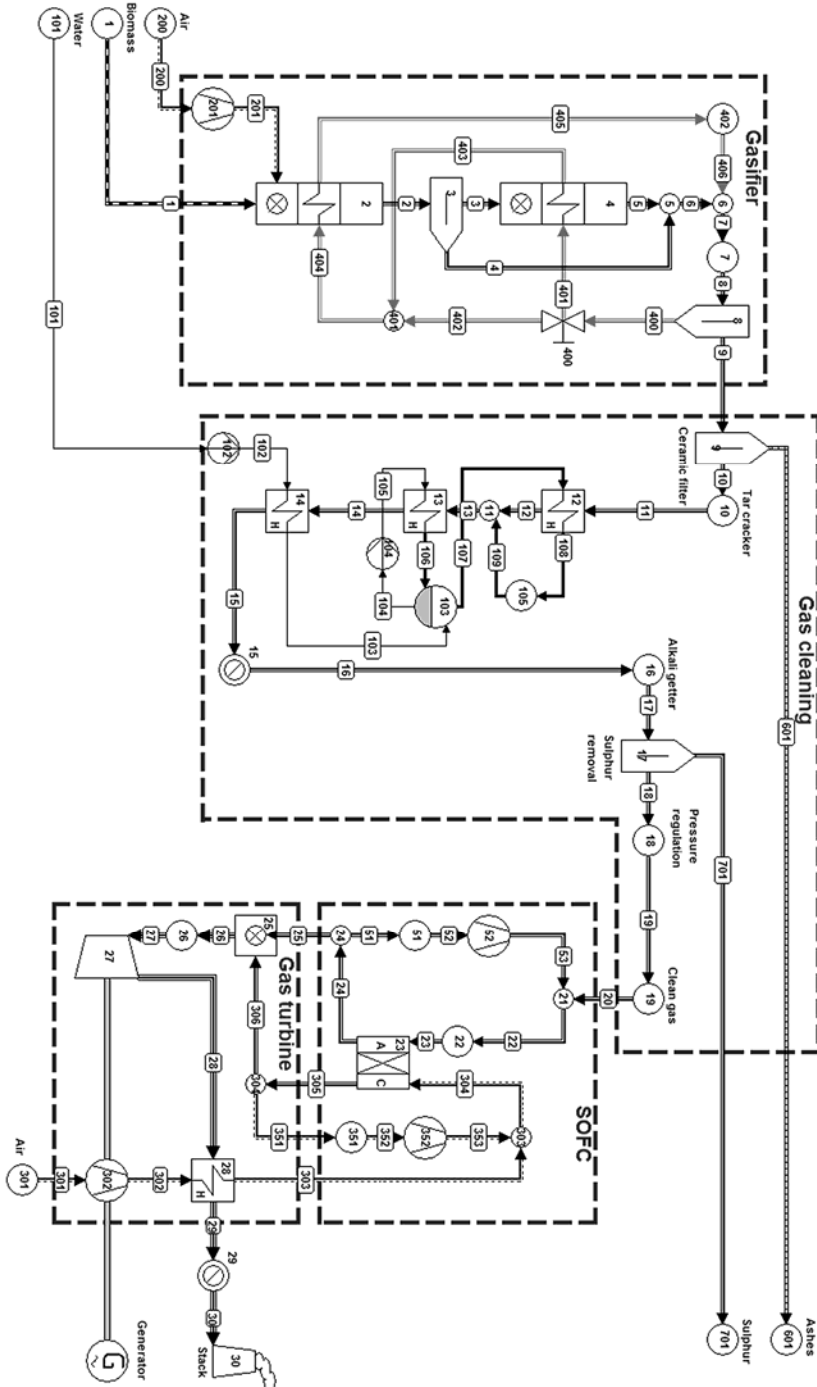
Figure 6-3 flow sheet of system S3 (large scale, pressurized air gasification, high temperature gas cleaning)
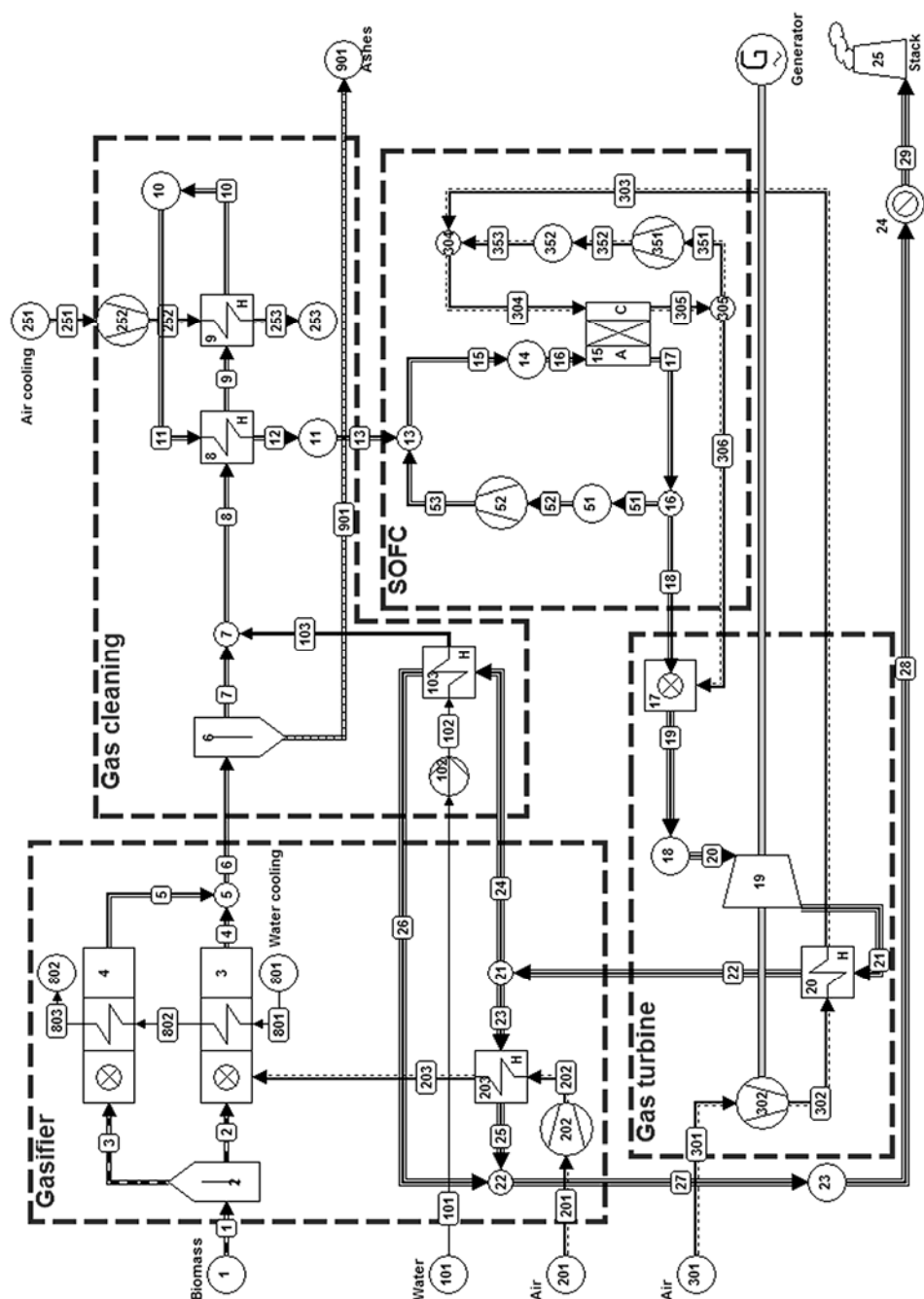
Figure 6-4 flow sheet of system S4 (small scale, pressurized air gasification, high temperature gas cleaning)

Fast internal circulating fluidized bed gasifier

This gasification technology is developed by the Institute of Chemical Engineering and AE Energietechnik. In Figure 2-7, a schematic representation is given of the FICFB. The gasification technology produces a medium calorific value gas (±12-14 MJ kg^{-1}) by means of indirect gasification. The gasifier consists of two fluidized beds: one is a bubbling fluidized bed where the gasification takes place, the other is a circulating fluidized bed in which char and a small amount of syngas is combusted. Circulating the bed material between the gasifier and the combustor provides the heat transfer from the combustor to the gasifier. The gasifier operates at a temperature of about 800-900°C and the combustor at approximately 1000-1100°C. The pressure in both reactors is near atmospheric. For more information see Refs. [21-24].

Circulating fluidized bed gasifier

For the circulating fluidized bed gasifier, the pressurized air gasification unit as used in Värnamo is considered. In Figure 2-5, a schematic representation is given of the CFB. This circulating fluidized bed gasifier operates at a temperature of 950-1000°C and a pressure of 18 bar. Biomass reacts in the gasifier with the air, which enters the gasifier at 220-250°C and a pressure of 18 bar. At the top of the gasifier, the produced gas is separated from the bed material and char. The bed material and char is recycled to the bottom of the gasifier. The char is combusted, thus supplying the heat necessary for the endothermic gasification reactions. More information about the gasifier can be found in Refs. [25, 26].

Fixed bed downdraft gasifier

The fixed bed downdraft gasifier is based on the design as described by Mukunda et al.[27] and by Aravind et al.[19]. In Figure 2-1, a schematic representation is given of the fixed bed downdraft gasifier.
This type of gasifier is currently only available commercially as an atmospheric gasification unit. The pressurized version is currently being developed, but no additional information is available about this high pressure gasification system.

6.2.2. Gas cleaning

The gas produced during the gasification process contains several impurities, like particulates, sulphur compounds, halogen compounds, nitrogen compounds, tars and alkali metals. These impurities need to be removed from the gas before it can be applied in a SOFC-GT, since the impurities have a deteriorating effect on the performance of the SOFC-GT. For instance, the particulates in the gas can cause blockages in the SOFC and these particulates have an abrasive effect on the turbine blades of the gas turbine. The tars can be cracked in the SOFC probably causing carbon formation in the fuel cell. It is also possible that the tars will condense on the turbine blades. Alkali metals can alter the structure of the ceramics in the fuel cell or condense on the turbine blades and have a corrosive effect on the turbine blades. Sulphur and chlorine compounds have a poisoning effect on the catalyst in the fuel cell.
Reported amounts of the different impurities for different gasification technologies are given in Table 6-1.

Table 6-1 Amount of impurities in the producer gas of the different gasification technologies

Impurity	FICFB [22]	CFB [28]	Downdraft gasifier [29]
Particulates [mg Nm^{-3}]	5,000-10,000	Unknown	100-200
Tars [mg Nm^{-3}]	1,500-4,500	<5,000	500-1,500
Alkali metals	Unknown	<0.1 ppm (w)	Unknown
Sulphur compounds	20-50 ppm	Unknown	Unknown
Nitrogen compounds	1,000-2,000 mg Nm^{-3}	<700 ppm (v)	Unknown
Chlorine compounds	Unknown	Unknown	Unknown

Two different gas cleaning approaches have been evaluated: low temperature gas cleaning in the systems S1 & S2 and high temperature gas cleaning in the systems S3 & S4.

In the low temperature gas cleaning system, the gas coming from the gasifier is first cooled to approximately 120°C. The extracted heat can be utilized in a bottoming cycle or to reheat the cleaned gas. During cooling down the alkali metal compounds condense on the entrained particulates [3]. The cooled gas is passed through a bag filter to remove the particulates from the gas. The next step in the gas cleaning process is the water scrubber, which is used to quench the gas and remove halogens, tars and residual alkalis from the gas. In the scrubber the temperature of the gas will decrease to approximately 65°C. The water to gas ratio is set to 2.1 kg water per kg gas.

In system S1, the relatively cool gas is compressed in a compressor to 8.5 bar. Then, the compressed gas is fed to a packed bed with zinc oxide, in order to remove hydrogen sulphide. After sulphur removal, the gas is filtered by a ceramic filter to remove the residual particulates. The temperature of the gas is raised to 700°C in a heat exchanger, using the hot flue gasses coming from the combustion section of the FICFB.

In system S2, the relative cool gas coming from the scrubber is heated to 220°C using the heat from the hot syngas coming from the gasifier. Then, 1 kg s^{-1} steam (220°C; 15.7 bar) is added to the gas, to prevent carbon deposition in the sulphur removal process. After the steam addition, the gas is fed to a packed bed with zinc oxide for the removal of hydrogen sulphide. Next, the gas is filtered by a ceramic filter to remove any residual particulates. Before the gas enters the SOFC-GT hybrid system the temperature of the gas is raised to 700°C using the hot syngas coming from the gasifier; the pressure is reduced to 8 bar.

The hot gas cleaning systems (S3 and S4) start with the removal of particulates by means of a ceramic filter. After the filter, the gas enters a catalytic tar cracking unit operating at 950°C for system S3. The tar cracker of system S4 operates at 800°C. The temperature is determined by the gasification technology. The catalyst used is based on nickel. Then, some superheated steam is produced using part of the heat of gas. This steam is injected into the gas stream to prevent carbon deposition and to quench the gas. After that, the gas is cooled further to 700°C, before it enters a sorbent bed loaded with an alkali getter (bauxite) [30]. Hydrogen sulphide is removed at the same temperature by means of adsorption in a packed bed of zinc titanate [31]. In system S3, the pressure of the gas is reduced to 8 bar before it enters the SOFC-GT hybrid system.

6.2.3. SOFC-GT hybrid system

The design of the SOFC-GT hybrid system is in principle similar for each of the four different systems. The only difference between the systems is the pressure: for the small scale system S4 the pressure is around 6 bar. The large scale systems (S1, S2 & S3) will

operate at 8 bar. The gas coming from the gas cleaning is heated in a heat exchanger to 900°C using the hot recycle from the anode of the SOFC. Then the gas is mixed with the anode recycle stream. The mixed gas enters the anode side of the SOFC. The SOFC is a direct internal reforming fuel cell operating at 950°C on average. So most of the methane is directly converted into hydrogen and carbon monoxide at the anode surface. The fuel cell is based on Nickel/Gadolinia Doped Ceria (Ni/GDC) anodes and Lanthanum Strontium Manganite (LSM) cathodes [19].

At the cathode side of the SOFC, pre-heated and pressurized air is mixed with the hot recycle stream from the cathode before it enters the cathode of the fuel cell. In the fuel cell the fuel is converted into electricity (DC).

The gas which leaves the anode is partly recycled; the other part goes to a combustion chamber. The cathode off-gas is also partly recycled and the remainder goes to the combustion chamber. In the combustion chamber the unconverted fuel is combusted. The hot flue gasses resulting from the combustion are expanded in a turbine, which is connected through a shaft with an air compressor and a generator. The expanded flue gas is used to pre-heat the pressurized air coming from the air compressor. In systems S1, S2 & S3, the residual heat from the flue gas can be utilized further. Utilization of this heat is not investigated. In system S4, the flue gas is also used to produce steam for the steam injection and to pre-heat the air for the gasifier.

6.3. Modelling

The designs of the four different systems have been modelled with the flow sheeting program Cycle-Tempo [20]. This program is especially designed for the thermodynamic evaluation of energy conversion systems. For each system, a model has been created. Some general assumptions have been made regarding the models:

- The systems are operated at steady state
- The heat exchangers are operating in counter current flow
- The processes are adiabatic
- There is no fouling caused by tars and/or alkali metal compounds
- The gas cleaning systems are able to achieve the required gas purity.

The biomass used in the calculation is A-quality wood with a moisture content of 25.2 wt%; the dry composition of the biomass in given in Table 6-2.

Table 6-2 dry composition of the biomass used in the models

	Amount	Unit
Carbon (C)	49.97	wt%
Hydrogen (H)	6.12	wt%
Oxygen (O)	42.49	wt%
Nitrogen (N)	0.55	wt%
Sulphur (S)	0.06	wt%
Ash (SiO_2)	0.80	wt%
Lower heating value (dry)	18,620.00	kJ kg^{-1}
Exergy (dry)	20,611.00	kJ kg^{-1}

The model for the FICFB gasifier (S1) is based on models published earlier [18, 32, 33]. The model of the CFB gasifier (S2 & S3) is based on the model for the Värnamo gasifier as described in Ref. [32]. The model for the downdraft gasification (S4) is based on two

equilibrium gasifiers in parallel. Before the biomass enters the gasifier some carbon and hydrogen are separated from the main biomass stream. The main biomass stream enters the first equilibrium gasifier (unit 3 in Figure 6-4), where the composition of the outgoing gas is determined by minimization of the Gibbs free energy at predefined temperature and pressure. The stream of carbon and hydrogen is fed to the second equilibrium gasifier. The temperature and pressure in this second gasifier (unit 4 in Figure 6-4) is set in such a way that only methane is produced. The products of both gasifiers are mixed to get the final syngas composition.

In Table 6-3 some input parameters for the gasification systems are given.

Table 6-3 input parameters for the gasification in the different systems

	System S1	System S2	System S3	System S4
Mass flow biomass [kg s^{-1}]	4.12	4.12	4.12	0.011
Steam to fuel ratio gasifier	0.32	-	-	-
Air to fuel ratio gasifier	-	1.50	1.50	1.07
Gasification temperature	800	950	950	800
Air to fuel ratio combustor	1.10	-	-	-

In Table 6-4, the input parameters are given for the SOFC-GT hybrid system.

Table 6-4 input parameters SOFC-GT hybrid system

Current density	2500 A m^{-2}
Fuel cell resistance	5e-5 Ω m^2
Fuel cell temperature range	900-1000°C
Fuel utilization	80%
DC/AC conversion efficiency	97%
Turbine inlet temperature	1060-1120°C
Pressure ratio (small scale)	6
Pressure ratio (large scale)	8
Isentropic efficiency compressors (small scale)	75.0%
Isentropic efficiency compressors (large scale)	80.0%
Isentropic efficiency compressor GT (small scale)	78.0%
Isentropic efficiency compressor GT (large scale)	84.2%
Isentropic efficiency turbine (small scale)	78.0%
Isentropic efficiency turbine (large scale)	91.3%

Cycle-Tempo calculates exergy values of all flows in the system diagram in a post processing step. The exergy values are calculated based on previously calculated temperature, pressure and chemical composition. The thermo mechanical exergy and chemical exergy are calculated separately. For the calculation of the chemical exergy a definition of the environment at reference conditions is required. The composition of the environment applied in this study is shown in Table 6-5; this composition is based on the composition of air saturated with water vapour as described by Baehr [34]. The reference temperature and pressure used in the calculation are 15°C and 1.01325 bar, respectively.

Table 6-5 environmental composition

Component	mol%	Component	mol%
Ar	0.91	N$_2$	76.78
CO$_2$	0.03	O$_2$	20.60
H$_2$O	1.68		

Sulphur and the components in the ash are not defined in the chemical composition of the environment. The components containing these elements are assumed to have zero exergy. Since the concentrations of these components in the biomass are very low this assumption would result in a negligible error.

The exergy losses are calculated from the exergy balances of the different system components.

6.4. Results and discussion

For each system, the calculations have been performed. Based on these calculations, the efficiency and performance of the systems have been determined. In Table 6-6, the main results of all systems are presented.

As can be seen from Table 6-6, the performance of the different systems is similar except for the small scale system (S4). The large scale air gasification system with hot gas cleaning (S3) is 0.5 percent point more efficient than the other two large scale systems (S1 & S2).

Table 6-6 performance and exergy efficiency of the considered systems

	System S1	System S2	System S3	System S4
Exergy biomass input [kW]	69813	69813	69813	190.75
Power output fuel cell [kW]	27066	25691	25368	66.71
Power output generator [kW]	10227	12561	13195	27.29
Gross electrical power [kW]	37293	38252	38563	94.00
Auxiliary power consumption [kW]	2866	3785	3740	6.32
Net electrical power [kW]	34427	34468	34823	87.68
Electrical exergy efficiency [%]	49.3	49.4	49.9	46.0

When comparing the large scale systems S1, S2 and S3, it appears that the performance of the fuel cell and the gas turbine are not the same for all. The power generated by the fuel cell is lower in the two systems with air gasification (S2 & S3), than for the system with steam gasification (S1). This lower performance is compensated by a higher power output of the gas turbine. The performance of the fuel cell is determined by the gas composition of the fuel. For systems S2 & S3, the fuel is diluted with nitrogen, as can be seen in Table 6-7. This results in a lower Nernst voltage, therefore in a lower performance than for the case with undiluted gas (S1).

Table 6-7 dry composition of the clean syngas for every system

	S1 [mol%]	S2 [mol%]	S3 [mol%]	S4 [mol%]
Hydrogen (H_2)	35.59	12.93	12.93	26.12
Carbon monoxide (CO)	22.86	17.09	17.09	21.68
Methane (CH_4)	17.36	6.54	6.54	1.78
Carbon dioxide (CO_2)	20.90	15.38	15.38	11.34
Nitrogen (N_2)	3.17	47.31	47.31	34.13
Other	0.12	0.75	0.75	4.95

On the other hand, the mass flow of flue gas through the turbine is larger for the systems with air gasification system (S2 & S3) than for the system with steam gasification S1. The mass flow through the turbine of system S1 is 31.2 kg s^{-1}, for systems S2 & S3 this value is 35.5 kg s^{-1} and 35.9 kg s^{-1} respectively.

To get a better insight in where the losses in the system occur an exergy flow diagram has been created for each system. In Figure 6-5, the exergy flow diagrams for the four different systems are given. To make a comparison between the small scale and large scale systems possible the losses and exergy values are depicted as relative losses. The relative losses are calculated by dividing the losses by the exergy of the biomass input. The relative exergy values are calculated by dividing the exergy values by the exergy of the biomass input.
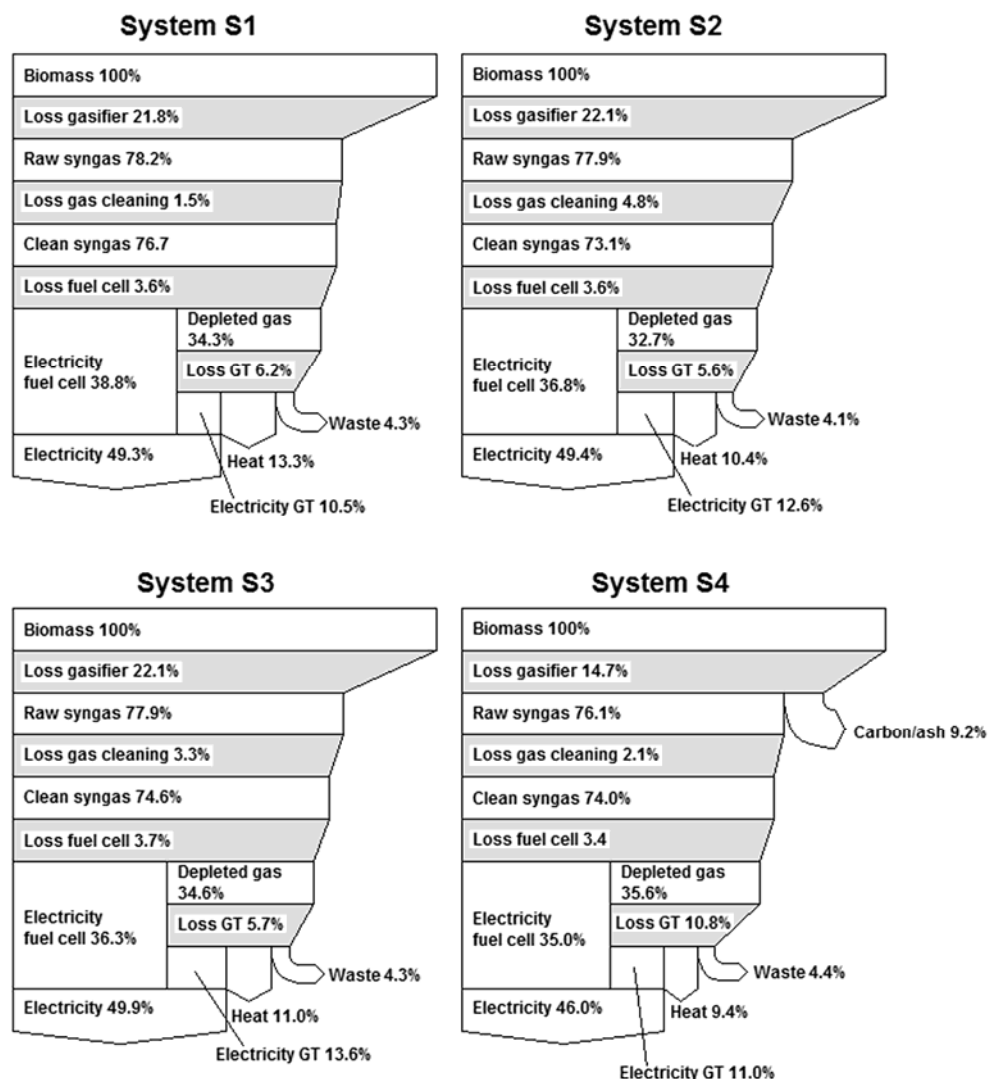
Figure 6-5 exergy flow diagram for the four different systems

The term waste, in Figure 6-5, includes ashes, sulphur compounds, alkalis, waste water and flue gas. From Figure 6-5, it becomes clear that the gasification process causes the largest losses in the system. Although, the losses for the small scale system (S4) are significantly lower than for the large scale systems. The difference between the losses of the small scale

and large scale gasification is caused by unconverted carbon. In the small scale gasification the unconverted carbon (char) is removed together with the ashes from the gasifier. This char still contain as a considerable amount of exergy. When it is accounted for in the gasification losses, the relative exergy losses would be 23.9% instead of 14.7%.

The relative losses of the gas cleaning are lowest for system S1; this is also the only system in which no steam addition in its gas cleaning system is needed. In the other systems, the production of steam causes additional losses. When comparing the gas cleaning systems with steam addition, it becomes clear that the low temperature gas cleaning has the highest losses.

The losses of the fuel cell subsystem are similar for all systems; the exergy losses for system S4 are slightly smaller than for the large scale systems. On the other hand, the losses for the gas turbine are much higher for the small scale system. This is mainly due to the lower isentropic efficiencies for the small scale compressors and turbine.

In the exergy flow diagrams the non-utilized residual heat is indicated as a product. The exergy value is based on the exergy value of the available heat in the process. It is possible to use this heat for additional electricity production by adding for instance an organic rankine cycle. This will improve the net electrical exergy efficiency and is suggested as future work.

6.5. Conclusions

Systems that combine biomass gasification, high temperature fuel cells and gas turbines are widely considered for highly efficient energy conversion processes. When designing such a process a variety of options have to be considered, like what type of gasification, what type of gas cleaning and so on. In this chapter the effect of gasification technique, gas cleaning technology and power level have been evaluated. For this purpose four different systems have been modelled. The first system considered large scale steam gasification coupled with low temperature gas cleaning. The second system considered large scale air gasification coupled with low temperature gas cleaning. The third system is based on air gasification coupled with high temperature gas cleaning. The last system is a small scale system based on air gasification and high temperature gas cleaning. All these systems are coupled to a solid oxide fuel cell gas turbine hybrid system. By means of an exergy analysis the performance of the systems has been evaluated.

It was found that the electrical exergy efficiency of the large scale systems do not deviate much from each other. So the gasification technology has hardly any influence on the overall performance. High temperature gas cleaning should be preferred, since it results in lower exergy losses in the gas cleaning. The system S3 based on pressurized air gasification and hot gas cleaning was the most efficient system. Although the difference with the system based on low temperature gas cleaning was only 0.5%. The electrical exergy efficiency of the small scale system is lower than of the large scale systems, due to the difference in efficiency of the balance of plant components. The amount of residual heat that can be considered for further utilization is the higher for the system based on steam gasification than for the other systems based on air gasification.

6.6. References

1.   McKendry P. Energy production from biomass (part 1): overview of biomass. Bioresource Technol 2002; 83(1): 37-46.
2.   McKendry P. Energy production from biomass (part 2): conversion technologies. Bioresource Technol 2002; 83(1): 47-54.

3.   Bridgwater A. V. The technical and economic feasibility of biomass gasification for power generation. Fuel 1995; 74(5): 631-653.
4.   Standeard F. R. A. M. Analytical Fuel Cell Modelling and Exergy Analysis of Fuel Cells.Mechanical Engineering and Marine Technology, Delft: Delft University of Technology, 1998.
5.   Massardo A. F., Lubelli F. Internal Reforming Solid Oxide Fuel Cell-Gas Turbine Combined Cycles (IRSOFC-GT): Part A---Cell Model and Cycle Thermodynamic Analysis. J Eng Gas Turbines Power 2000; 122(1): 27-35.
6.   Bosch K. J., Woudstra N., van der Nat K. V. Designing Solid Oxide Fuel Cell Gas Turbine Hybrid Systems Using Exergy Analysis. In: Fourth International Conference on Fuel Cell Science, Engineering and Technology, Irvine (USA), 2006.
7.   Alderucci V., Antonucci P. L., Maggio G., Giordano N., Antonucci V. Thermodynamic analysis of SOFC fuelled by biomass-derived gas. Int J Hydrogen Energy 1994; 19(4): 369-376.
8.   Zhu B., Bai X. Y., Chen G. X., Yi W. M., Bursell M. Fundamental study on biomass-fuelled ceramic fuel cell. Int J Energy Res 2002; 26(1): 57-66.
9.   Omosun A. O., Bauen A., Brandon N. P., Adjiman C. S., Hart D. Modelling system efficiencies and costs of two biomass-fuelled SOFC systems. J Power Sources 2004; 131(1-2): 96-106.
10.   Fryda L., Panopoulos K. D., Karl J., Kakaras E. Exergetic analysis of solid oxide fuel cell and biomass gasification integration with heat pipes. Energy 2008; 33(2): 292-299.
11.   Sucipta M., Kimijima S., Suzuki K. Performance analysis of the SOFC-MGT hybrid system with gasified biomass fuel. J Power Sources 2007; 174(1): 124-135.
12.   Jin H., Larson E. D., Celik F. E. Performance and cost analysis of future, commercially mature gasification-based electric power generation from switchgrass. Biofuels, Bioprod Biorefin 2009; 3(2): 142-173.
13.   Nagel F. P., Schildhauer T. J., Biollaz S. M. A. Biomass-integrated gasification fuel cell systems - Part 1: Definition of systems and technical analysis. Int J Hydrogen Energy 2009; 34(16): 6809-6825.
14.   Nagel F. P., Schildhauer T. J., McCaughey N., Biollaz S. M. A. Biomass-integrated gasification fuel cell systems - Part 2: Economic analysis. Int J Hydrogen Energy 2009; 34(16): 6826-6844.
15.   Proell T., Aichernig C., Rauch R., Hofbauer H. Coupling of Biomass Steam Gasification and an SOFC - Gas Turbine Hybrid System for Highly Efficient Electricity Generation. In: ASME Turbo Expo 2004: Power for Land, Sea, and Air, Vienna, Austria, 2004.
16.   Fryda L., Panopoulos K. D., Kakaras E. Integrated CHP with autothermal biomass gasification and SOFC-MGT. Energy Convers Manage 2008; 49(2): 281-290.
17.   Athanasiou C., Vakouftsi E., Coutelieris F. A., Marnellos G., Zabaniotou A. Efficiencies of olive kernel gasification combined cycle with solid oxide fuel cells (SOFCs). Chem Eng J 2009; 149(1-3): 183-190.
18.   Toonssen R., Woudstra N., Verkooijen A. H. M. Reference System for a Power Plant Based on Biomass Gasification and SOFC. In: 8th European Solid Oxide Fuel Cell Forum, Luzerne, Switserland, 2008.
19.   Aravind P. V., Woudstra T., Woudstra N., Spliethoff H. Thermodynamic Evaluation of Small Scale Systems with Biomass Gasifiers, Solid Oxide Fuel Cells with Ni/GDC Anodes and Gas Turbines. J Power Sources 2009; 190(2): 461-475.

20.   Cycle-Tempo, 5.0. TU Delft, 2009.
21.   Bolhar-Nordenkampf M., Bosch K., Rauch R., Kaiser S., Tremmel H., Aichernig
        C., Hofbauer H. Scale-up of a 100kWth pilot FICFB-gasifier to a 8 MWth FICFB-
        gasifier demonstration plant in Güssing (Austria). In: 1st International Ukrainian
        Conference on BIOMASS FOR ENERGY, Kiev, Ukraine, 2002.
22.   Hofbauer H., Rauch R., Bosch K., Kock R., Aichernig C. Biomass CHP Plant
        Güssing - A Success Story. In: Expert Meeting on Pyrolysis and Gasification of
        Biomass and Waste, Strasbourg, 2002.
23.   Hofbauer H., Rauch R., Foscolo P., Matera D. Hydrogen-rich Gas from Biomass
        Steam Gasification. In: 1st World Conference and Exhibition on Biomass for
        Energy and Industry, Sevilla, Spain, 2000.
24.   Hofbauer H., Rauch R., Loeffler G., Kaiser S., Fercher E., Tremmel H. Six Years
        Experience with the FICFB-Gasification Process. In: 12th European Conference
        and Technology Exhibition on Biomass for Energy, Industry and Climate
        Protection, Amsterdam, The Netherlands, 2002.
25.   Stahl K., Neergaard M. IGCC Power Plant for Biomass Utilisation, Värnamo,
        Sweden. Biomass Bioenergy 1998; 15 (3): 205-211.
26.   Stahl K., Waldheim L., Morris M., Johnsson U., Gardmark L. Biomass IGCC at
        Värnamo, Sweden - Past and Future. In: GCEP Energy Workshop, California,
        USA, 2004.
27.   Mukunda H. S., Paul P. J., Dasappa S., Shrinivasa U., Sharan H., Buehler R.,
        Hasler P., Kaufmann H. Results of an Indo-Swiss programme for qualification and
        testing of a 300-kW IISc-Dasag gasifier. Energy for Sustainable Development
        1994; 1(4): 46-49.
28.   Engstrom F. Hot gas clean-up bioflow ceramic filter experience. Biomass
        Bioenergy 1998; 15(3): 259-262.
29.   Stevens D. J. Hot Gas Conditioning: Recent Progress with Large-Scale Biomass
        Gasification Systems. Washington: National Renewable Energy Laboratory
        (NREL), 2001.
30.   Cummer K. R., Brown R. C. Ancillary equipment for biomass gasification.
        Biomass Bioenergy 2002; 23(2): 113-128.
31.   Torres W., Pansare S. S., Goodwin J. G. Hot Gas Removal of Tars, Ammonia, and
        Hydrogen Sulfide from Biomass Gasification Gas. Catal Rev 2007; 49(4): 407 -
        456.
32.   Toonssen R., Woudstra N., Verkooijen A. H. M. Exergy Analysis of Hydrogen
        Production Plants Based on Biomass Gasification. Int J Hydrogen Energy 2008;
        33(15): 4074-4082.
33.   Toonssen R., Woudstra N., Verkooijen A. H. M. Decentralized generation of
        electricity from biomass with proton exchange membrane fuel cell. J Power
        Sources 2009; 194(1): 456-466.
34.   Baehr H. D. THERMODYNAMIK; eine Einführung in die Grundlagen und ihre
        technischen Anwendungen. Berlin: Springer, 1984.

7. Decentralized power generation in a PEM-FC from centralized produced gas

Abstract: *Biomass can be applied as the primary source for the production of hydrogen in the future. The biomass is converted in an atmospheric fluidized bed gasification process using steam as the gasifying agent. The producer gas needs further cleaning and processing before the hydrogen can be converted in a fuel cell; it is assumed that the gas cleaning processes are able to meet the requirements for a PEM-FC. The compressed hydrogen is supplied to a hydrogen grid and can be used in small-scale decentralized CHP units. In this study it is assumed that the CHP units are based on low temperature PEM fuel cells. For the evaluation of alternative technologies the whole chain of centralized hydrogen production from biomass up to and including decentralized electricity production in PEM fuel cells is considered.*
Two models for the production of hydrogen from biomass and three models for the combined production of electricity and heat with PEM fuel cells are built using the computer program Cycle-Tempo. Two different levels of hydrogen purity are considered in this evaluation: 60% and 99.99% pure hydrogen. The purity of the hydrogen affects both the efficiencies of the hydrogen production as well as the PEM-FC systems. The electrical exergy efficiency of the PEM-FC system without additional heat production is calculated to be 31.05% in the case of 60% hydrogen and 32.13% in the case of 99.99% pure hydrogen. The electrical exergy efficiencies of the whole conversion chain appear to be 17.73% and 15.10% respectively. The high losses during purification of the hydrogen gas results in a higher efficiency for the case with low purity hydrogen. The removal of the last impurities strongly increases the overall exergy losses of the conversion chain.

7.1. Introduction

Environmental concerns lead to the search for sustainable energy sources for the future and also more efficient ways to convert fuel into energy. One of the promising primary energy sources is biomass. Due to its short carbon dioxide cycle, it is considered carbon dioxide neutral. Most biomass sources are solid, like wood. These solid biomass sources are hard to handle [1], so they have to be converted into a more convenient secondary energy carrier to enable the conversion of these fuels in advanced conversion systems with gas turbines and/or fuel cells. By biomass gasification hydrogen rich can be produced, which mainly contains hydrogen, carbon monoxide, methane, carbon dioxide and water. The gas contains also small amounts of impurities, like particulates, tars, alkali compounds, sulphur compounds, and halogen compounds. These compounds are often harmful for downstream equipment. Therefore, the gas needs to be cleaned. The needed gas cleaning depends on the application. The application of low temperature fuel cells, as considered in this paper, requires the almost complete removal of harmful components. After gas cleaning the gas can either be directly applied or further processed. When hydrogen is the desired product, as in this chapter, further processing can be performed to increase the amount of hydrogen

in the gas. Methane can be reformed and carbon monoxide can be converted via the water gas shift reaction. Also the further purification of the produced hydrogen is an option. Fuel cells are considered to be highly efficient energy converters. Most fuel cells convert electrochemically hydrogen into water, during this conversion electricity is produced and also some additional heat. There are different types of fuel cells available; they all have their own operating window. The proton exchange membrane fuel cell also known as the PEM fuel cell operates at a temperature of 80°C. This low operating temperature makes it applicable in a domestic setting. Because of the low operating temperature, it generates low temperature heat as a by-product that can be used for space heating.

The combination of biomass gasification and fuel cells is the subject of many studies, like [2-25]. Most of the studies focus on the integration of biomass gasification and high temperature fuel cells, like the studies of Kivisaari et al. [2] and Lobachyov and Richter [6] which focus on biomass gasification and molten carbonate fuel cells (MCFC) for large scale electricity generation. Also studies on small scale electricity generation via biomass gasification and MCFC are presented, like the studies of McIlveen-Wright et al. [3], Donolo et al. [5] and Morita et al.[13].

Many studies are devoted to systems of biomass gasification and solid oxide fuel cells (SOFC). The SOFC is often combined with a gas turbine to form a hybrid system. As in the systems with a MCFC varies the scale from small scale 1 kW$_e$ [9] to large scale 21 MW$_e$[8] or 30 MW$_e$ [20].

Only very few studies are focussing on the application of biomass gasification and PEM fuel cells, like the study of Ersoz et al.[24] and the study of Sordi et al.[25]. In the study of Ersoz et al. [24] a fixed bed gasifier followed by reforming and cleaning units is coupled to a PEM fuel cell. The influence of the hydrocarbon properties, the gasification parameters and the reforming parameters on system efficiency has been tested.

In the study of Sordi et al. [25], the influence of the syn-gas composition on the gas processing and on the electricity generation in a PEM fuel cell is investigated.

The application of fuel cells in micro combined heat and power is widely researched. Most of these micro-CHP systems are fuelled with natural gas. The micro-CHP systems based on PEM fuel cells include desulphurization, reforming, water gas shift reactors and deep carbon monoxide cleaning. An example of such a system can be found in the work of Gigliucci et al. [26].

In this chapter the CHP system is fuelled with hydrogen. There are little studies on CHP systems based on PEM fuel cells fuelled with hydrogen. Saidi et al. [27] performed an exergy analysis on a hydrogen fuelled PEM fuel cell CHP system. They found that high voltage operation reduces the irreversibilities in the system.

In a study of Colella et al. [28] some control strategies for a CHP fuel cell system are evaluated with a special focus on the afterburner sub-system.

In a recent study by Page et al. [29] several energy conversion chains have been evaluated. One of the evaluated chains was the central production of hydrogen via coal gasification, which is distributed in a hydrogen grid and finally used in PEM fuel cell micro-CHPs. They calculated chain efficiencies, on basis of higher heating value of the coal, of 21.8% thermal and 26.2% electrical [29]. However, these efficiencies are not based on detailed system modelling.

In this chapter, two hydrogen production plants based on biomass are designed. One plant is producing a gaseous fuel with 60% hydrogen, and the other plant is producing 99.99% pure hydrogen. The produced hydrogen is assumed to be pumped into a hydrogen

distribution grid, which supplies hydrogen to households. In the household the hydrogen is converted into electrical power and heat. To produce heat and electrical power from hydrogen a micro combined heat and power (μ-CHP) system based on a PEM fuel cell is used. The electrical power demand in an average household is usually not exceeding 1 kW. Therefore, the maximum electrical power output of the μ-CHP system is set to 1 kW. An exergy analysis has been performed on both the hydrogen plants and on the μ-CHP system. The results of this analysis are combined to evaluate the whole conversion chain from biomass into electricity.

The heat production of the PEM fuel cell has a low quality, due to its low operating temperature. The generated heat is not sufficient to fulfil the heat demand of an average dwelling. Therefore, two additional μ-CHP systems based on PEM fuel cells have been considered. These systems produce 1 kW of electrical power and are also able to generate 3 kW of heat. For that purpose one of the additional μ-CHP systems has a fuel by-pass to a boiler to produce additional heat; the other is connected to a ground coupled electrical driven heat pump. Exergy losses are calculated for all system alternatives and a comparison of the losses is presented.

7.2. System configurations

The whole chain from biomass to electricity consists of three main parts; the centralized hydrogen production plant, the hydrogen distribution grid and the μ-CHP system. In Figure 7-1 a schematic representation is given of the chain from biomass to electricity.
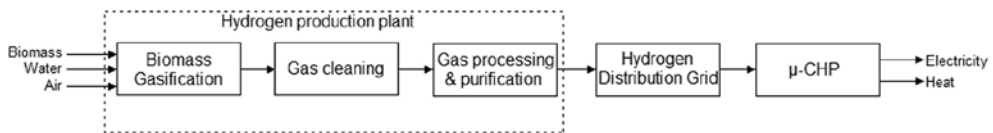
Figure 7-1 schematic overview of the conversion chain

In the next sections each part of the chain will be discussed separately, starting with the hydrogen production plant.

7.2.1.Hydrogen production plant

The hydrogen production plants can be sub-divided into three sections. The first section is the biomass gasification, the second section is the gas cleaning and the final section is the gas processing and purification

Gasification

The hydrogen plants are supposed to be based on the Fast Internal Circulating Fluidized Bed (FICFB) gasifier. The FICFB gasifier is designed by the Institute of Chemical Engineering and AE Energietechnik. This is an indirect steam gasifier, which means the heat required for the endothermic gasification reactions is supplied by a coupled combustor. The gasifier consists of two fluidized beds, one bubbling bed and one circulating fluidized bed. In the bubbling bed the biomass is gasified with steam at a temperature of around 800°C, in the circulating fluidized bed the residual char from the gasification is combusted with air at a temperature of 900-1000°C. The bed material is circulated between the two beds and is used as heat transport medium. The operating pressure is near atmospheric. More information on the FICFB can be found in references [30-34]. This type of gasifier is chosen because it produces a hydrogen rich gas, which results in a high hydrogen yield [35].

Gas cleaning

The gas produced by the gasifier contains several impurities like: particulates (5000-10000 mg Nm^{-3} [33]), tars (1500-4500 mg Nm^{-3} [33]), sulphur compounds (20-50 ppm[1] [33]), nitrogen compounds (ammonia 1000-2000 ppm [33]), halogen compounds and alkali metals [36, 37]. The tars, alkali metals and particulates have the tendency to stick to cold surfaces or cause blockages in al kinds of equipment. These compounds as well as the other impurities have a deteriorating effect on catalytic driven processes as needed for gas processing and final utilisation; therefore the impurities have to be removed in a gas cleaning system.
In the gas cleaning system, the producer gas is cooled in two heat exchangers to a temperature of about 120°C (see Figure 7-2A).

The alkali metal compounds and some of the tars will condense on the entrained particles [1]. When keeping the superficial gas velocity high in the heat exchangers the abrasive nature of the gas will keep the walls of the heat exchangers clean. The cooled gas is filtered in a bag filter before the gas is cleaned in a water scrubber, in which halogen compounds, nitrogen containing compounds, the residual tars and alkali metal compounds are removed. The scrubber has also a quenching effect on the gas, resulting in a temperature drop to 60°C. After scrubbing, the producer gas is compressed to a pressure of 36 bar. The resulting reduction of the gas volume enables smaller equipment downstream. Before the gas is passed through an amount of steam is added, to make sure no carbon will deposit in the heat exchangers. Since carbon can deposit when synthesis gas is cooled or heated, if the water content of the gas is low or the rate of temperature change is low, as illustrated by Aravind et al. [22]. Then the gas is passed through a packed bed filled with zinc titanate, in order to remove traces of hydrogen sulphide in the gas. The regeneration of the sorbent is not considered, because it is an exothermic process that will hardly require any energy. After the sulphur removal, the gas is reheated in a heat exchanger with the heat of the raw producer gas coming from the gasification unit.
There are many uncertainties regarding the gas cleaning, especially the scrubber. The effects of the scrubber on the tar and halogen content are not certain. But due to the low operating temperature it is most likely that only light tar compounds are present in the gas.

Gas processing and purification

The gas processing starts with methane reforming followed by the water gas shift. Methane reforming is supposed to take place in a steam reformer. The hot flue gasses coming from the gasification unit are used to supply heat to the reformer. The steam required for the reforming process is produced with the excess heat from the hydrogen plant. The steam to carbon ratio in the reformer is kept above 2.5. This value is sufficient to prevent carbon deposition [38]. The reformer is operated at a pressure of 35 bar and a temperature of 825°C. The gas coming from the reformer is cooled to 400°C, before it enters the high temperature water gas shift (WGS) reactor. After the high temperature WGS reactor, the gas is cooled to 210°C at this temperature it enters the low temperature WGS reactor. The amount of carbon monoxide in the gas is reduced to 0.5-1 vol% [39, 40].

---

[1] The values are measured after the systems gas cleaning. There is no dedicated sulphur removal in the gas cleaning, so is assumed the values will not deviate much from the measured values.
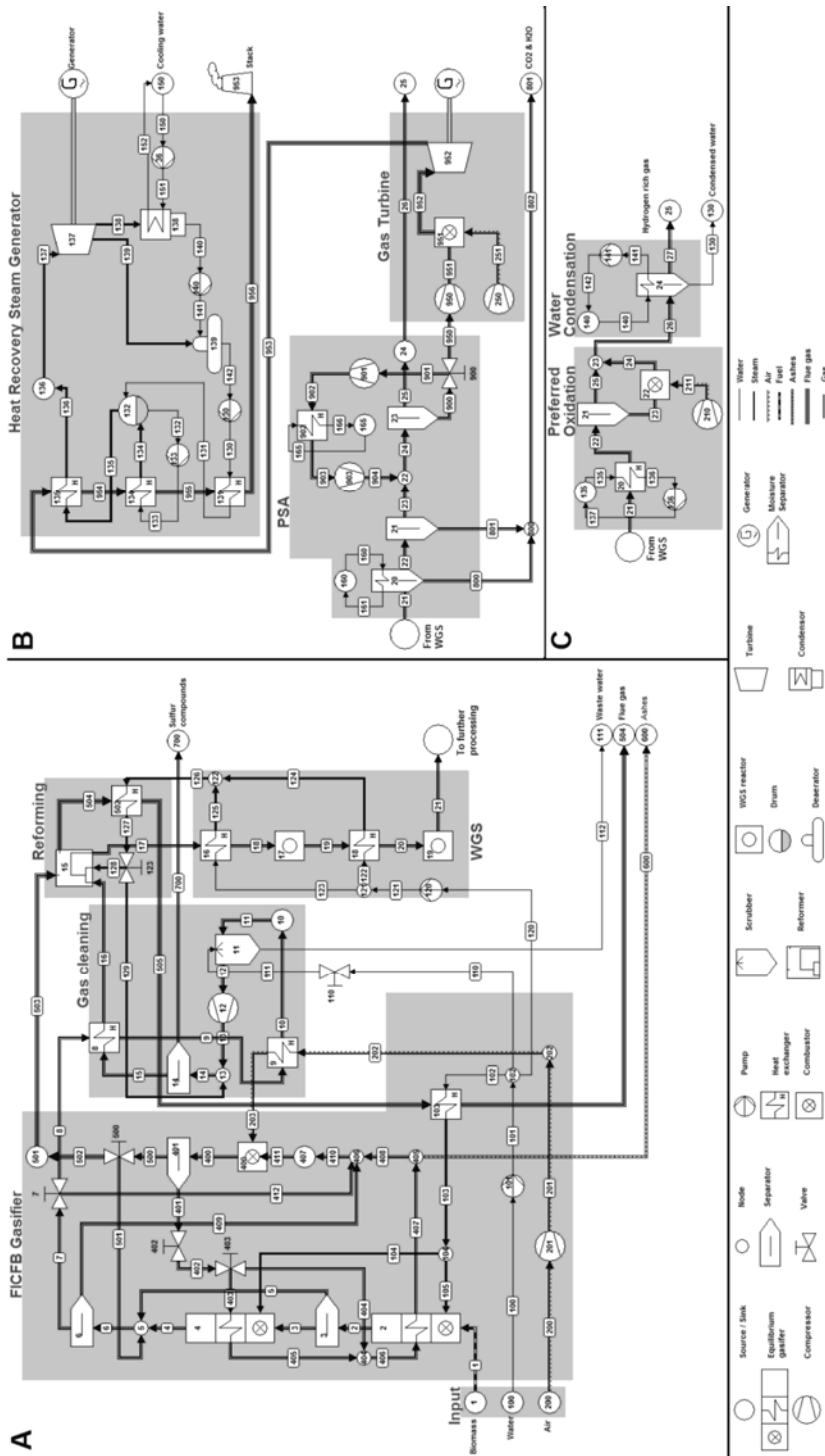
Figure 7-2 flow sheets of the hydrogen plants. The combination of A and C gives hydrogen1 and the combination of A and B gives hydrogen2

After this process step two different gas processing and purification approaches have been considered, leading to two different product qualities and hydrogen production plant designs. In the first approach, called hydrogen1, the gas is further processed in a preferential oxidation unit, in order to remove the residual carbon monoxide from the gas. This unit operates at a temperature of about 135°C. Besides the carbon monoxide also a small amount of hydrogen is combusted. It is assumed that almost all the carbon monoxide is combusted resulting in a CO concentration below 10 ppm. This is currently not the case, but it is expected that with future developments it will be possible.

After the preferential oxidation, the hydrogen gas is cooled to condense the water vapour in the gas. This results in a hydrogen rich gas with a purity of approximately 60%. Other compounds in the gas are carbon dioxide, methane, and nitrogen. It is assumed that the gas from this process is suitable for a PEM fuel cell; most of the compounds in the gas just act as diluents except for carbon dioxide. It is known that carbon dioxide can cause a decrease in the performance of a PEM fuel cell [41-43]. When using a PEM fuel cell specially suited for reformates, the decrease in performance of the fuel cell will be smaller than for a standard PEM fuel cell [44].

In the second approach, called hydrogen2, the gas is further processed in a pressure swing adsorption (PSA) unit (see Figure 10-2B). First, water is condensed by cooling the gas to 30°C. Then the gas is fed to the PSA unit where first CO_2 and residual water is removed, then in a second unit the other substances like nitrogen are removed from the gas. There is chosen for two steps, because for the removal of CO_2 and water a different sorbent is needed than for the other compounds. The waste gas coming from the PSA unit contains significant amounts of hydrogen, CO and CH_4. Therefore, the waste gas is combusted in a gas turbine system connected to a generator that produces electricity. The hot flue gasses coming from the gas turbine are used in a bottoming steam turbine cycle in order to produce additional electricity. In this way most of the electrical power necessary to operate the plant can be generated.

7.2.2. Hydrogen transport and distribution

In this chapter, it is assumed that a hydrogen grid is available. This grid would probably consist of a high pressure part at pressures between 60-80 bar for long distance transport; a medium pressure grid (pressures of approximately 20 bar) for large consumers; and low pressure grid (pressure ±5 bar) for domestic application. It is assumed that the hydrogen production plants should feed into the high pressure grid. Eventually the hydrogen will be available at the domestic level. In this chapter, an energetic efficiency of the gas distribution grid of hydrogen it is assumed to be 94% [29]. The exergetic efficiencies of the distribution grid is assumed to be 1 percentage point lower, so 93%.

The 60% hydrogen will require a larger diameter piping than the 99.99% pure hydrogen for the transport of the same fuel power. Also the compression power required to compress the 60% hydrogen will be higher than for the 99.99% pure hydrogen.

7.2.3. μ-CHP

The μ-CHP is based on a PEM fuel cell with water cooling. The fuel cell is initially designed to generate 1 kW of electrical power. Due to the limited electrical efficiency of the PEM fuel cell unit also an amount of heat is produced at a temperature sufficient to generate hot water for space heating. In this system (see Figure 7-3A) hydrogen is first humidified before it enters the anode of the fuel cell stack.

A blower is used to feed air to the cathode of the fuel cell stack. The off-gasses from the anode contain still some hydrogen and are catalytically combusted in an afterburner using air coming from the cathode. Heat is extracted from the hot flue gasses coming from the combustor as well as from the cooling system of the fuel cell stack. This heat is used for space heating and for humidification. This μ-CHP system alternative without additional heat generation and used for the initial calculations is called PEM1.

The initial μ-CHP system PEM1 only produces about 1.9 kW of heat. However, in a domestic setting the heat demand for space heating is often higher than 1.9 kW. Assuming a maximum heat demand of 3 kW, the μ-CHP system needs to be modified to meet this higher heat demand. Two different design options have been considered. The first uses a hydrogen by-pass of the fuel cell, so additional hydrogen is directly combusted in the catalytic combustor. This enables the production of additional hot water for the space heating system. This system option is called PEM2 (see Figure 7-3B).

The second system option (called PEM3) generates a little more electricity to power an electrical driven ground coupled heat pump, which supplies the extra heat required. The ground coupled heat pump consist of three circuits, the ground coupling circuit; the refrigerant circuit and the space heating circuit (see Figure 7-3C). The cycle that extracts heat from the soil uses a 10% ethylene glycol/water mixture as working fluid. The cycle transfers heat from the ground water to the refrigerant circuit. The working fluid for the refrigerant circuit is R22. Heat extracted from the ground coupled circuit is used to evaporate it. The evaporated R22 is compressed to 26 bar and condensed in a condenser that transfers heat to the space heating circuit. After the condensation of R22, it is throttled to a lower pressure (4.8 bar) and evaporated again. The space heating cycle is similar to the one of the PEM1 system; water of 65°C is used for space heating. The cooled return water (45°C) is heated in the condenser of the refrigerant cycle. The coefficient of performance of the heat pump is 3.21.

In Figure 7-3, the flow sheets of the three μ-CHP system alternatives are given. PEM1 is represented by Figure 7-3A, PEM2 by Figure 7-3B and PEM3 by a combination of Figure 7-3A & Figure 7-3C.

The space heating system uses hot water of 65°C for heating. When the water leaves the space heating system for reheating, it has a temperature of 45°C. The pressure of the water in this system is 1.5 bar.

The electrical power and heat demand of houses are continuously fluctuating; then the μ-CHP system will continuously cycle between full and part load. However, for a first estimate all calculations in this paper are based on design load, and the additional effect of fluctuations in demands are not considered. It is expected that the relative differences between the alternatives are sufficiently represented by the conditions at design load.

7.3. Modelling

The designed systems have been modelled using the computer program Cycle-Tempo [45], a flow sheeting program developed for the evaluation of energy conversion systems. The computer program Cycle Tempo is available for commercial application since 1983. Many universities, research organizations, engineering companies and industries worldwide are using the program.

Figure 7-3 the flow sheet A is of PEM1; B is the flow sheet of PEM2; A and C combined gives the flow sheet of PEM3

A model has been created for both hydrogen production plants. Separate models have been made for the three µ-CHP systems. By combining the results of a hydrogen production plant model and a µ-CHP model a first impression of the performance of the whole chain of power production can be given. Some general assumptions have been made:

- The systems are operated at steady state
- The thermal input of the gasifier is approximately 70 MW
- The heat exchangers are operated in counter current flow
- There is no fouling caused by tars and/or alkali metal compounds
- The gas cleaning systems are able to achieve the required gas purity
- Processes are adiabatic
- The mechanical efficiency of all rotary equipment is 99%

The biomass used in the calculations is A-quality wood with a moisture content 25.2 wt% on dry basis; the dry composition of the biomass is given in Table 7-1.

Table 7-1 dry composition of the used biomass [35, 46]

	Amount	Unit
Carbon (C)	49.97	wt%
Hydrogen (H)	6.12	wt%
Oxygen (O)	42.49	wt%
Nitrogen (N)	0.55	wt%
Sulfur (S)	0.06	wt%
Ash (SiO_2)	0.80	wt%
Lower Heating Value (dry)	18620	kJ kg^{-1}
Exergy (dry)	20611	kJ kg^{-1}

The modelling of the biomass gasification is done in such a way that the mass and energy balances are closed. The composition of the producer gas found in literature is used to tune the gasification model [35]. The model of the gasifier uses two equilibrium gasifiers in series, which calculate the gas composition by Gibbs free energy minimization for different equilibrium temperatures and pressures (See Figure 7-2). The first equilibrium gasifier is mainly used for the production of methane. During the calculation of the equilibrium 22 mole% of carbon is excluded. The separator (nr. 3) behind the first gasifier (nr 2) is used to bypass some of the components resulting from the first gasifier. The remaining mixture is passed to the second gasifier (nr 4). The final composition can be tuned by controlling the operating conditions of the gasifiers and the separated components. Also a small amount (3 vol%) of flue gas from the combustion part of the FICFB is mixed with the gas. The cyclone for the removal of solids is modelled with a separator; it removes the ashes and carbon from the gas. The removed solids are mixed with the bed material and with some (20 wt%) producer gas, this mixture is combusted. The solids are separated in a separator and used to supply heat to the gasifiers.

The calculation of the reforming and water gas shift reactions is also based on the minimization of the Gibbs free energy. It is assumed that these processes reach equilibrium. In Table 7-2 and Table 7-3, the input data for the different model components depicted in Figure 7-2 and Figure 7-3 can be found.

The PEM fuel cell model available in Cycle Tempo is used to calculate the performance of the system. The active cell area and the current flow I are calculated from the specified current density, cell voltage V and electrical power output P_e. It is supposed that the

processes occur at constant temperature and pressure. The fuel flow to the fuel cell $\Phi_{\text{m,a,in}}$ relates to the total current as given by the following equation:

$$I = \frac{\Phi_{\text{m,a,in}}}{M_{\text{a}}} 2F y_{\text{H}_2}^0 U_{\text{F}}$$ (7.1)

Here, $y_{\text{H}_2}^0$ is the hydrogen concentration at the inlet, M_{a} is the molar mass of the anode gas, F is the Faraday constant and U_{F} is the fuel utilization. The mass flow of protons through the membrane is calculated based on the current flow. With the mass flow of protons and the oxygen utilization, the airflow to the fuel cell is calculated. An energy balance is used to calculate the amount of cooling water required to keep the fuel cell at the set outlet temperature.

For the equivalent cell resistance a one-dimensional model is used. The temperatures, pressures and composition are supposed to be constant in a cross section perpendicular to the direction of the fuel flow in the fuel cell. For the cross section, the reversible cell voltage $V_{\text{rev,x}}$ is determined with the Nernst equation assuming ideal gas and gaseous water as a product:

$$V_{\text{rev,x}} = V_{\text{rev}}^0 + \frac{RT}{2F} \ln\left(\frac{y_{\text{H}_2} y_{\text{O}_2,\text{c}}^{1/2}}{y_{\text{H}_2\text{O,c}}} \cdot P_{\text{cell}}^{1/2} \right)$$ (7.2)

where V_{rev}^0 is the standard reversible voltage for hydrogen, R is the universal gas constant, T the temperature, y the mole fraction at the cross-section, and P is the pressure. In the model, it is assumed that the voltage losses on the level of the electrodes are negligible in the x-direction. This means that the cell voltage is supposed to be constant over the fuel cell. So, the voltage loss ΔV_x can be calculated using the following equation:

$$\Delta V_x = V_{\text{rev,x}} - V$$ (7.3)

Then the equivalent fuel cell resistance R_{eq} is

$$R_{\text{eq}} = \frac{\Delta V_x}{i_x}$$ (7.4)

where, i_x is the current density.

The equivalent fuel cell resistance can also be defined using the following equation:

$$R_{\text{eq}} = \frac{i + i_{\text{n}}}{i} \cdot R_{\text{ohm}} + \frac{A}{i} \ln\left(\frac{i + i_{\text{n}}}{i_0} \right) - \frac{B}{i} \ln\left(1 - \frac{i + i_{\text{n}}}{i_{\text{l}}} \right)$$ (7.5)

Here, R_{ohm} is the ohmic resistance of the fuel cell, A is the slope of the Tafel line, B is the constant in the mass transfer overvoltage equation, i_{n} is the internal and fuel crossover equivalent current density, i_0 is the exchange current density and i_{l} is the limiting current density. The used values can be found in Table 7-4.

The fuel utilisation in the model was set to 80% and the oxygen utilisation to 50%. The electrical output of the fuel cell was set in such a way that the net electrical output of the whole μ-CHP system was 1 kW. The conversion of DC to AC is assumed to have an efficiency of 96.5%. The PEM fuel cells are assumed to be suitable for reformate as a fuel, so the CO_2 in the fuel is only considered as a diluent.

Table 7-2 input parameters of the models for hydrogen production.

No.	Description	Input	No.	Description	Input
		Gasifier			PSA (Hydrogen2)
2	Gasifier	P_r=1, T_r=180, S/F=0.2 P_{out}=1.47, T_{out}=800	20	Moisture Separator	ΔP_C=0, ΔP_H=0.62, ΔT_{Cout}=20, ΔT_{Hout}=25
3	Separator	ΔP=0, ΔT=0	21	Separator	ΔP_1=0.62, ΔP_2=30, ΔT=0, CO_2:100%, H_2O:100%
4	Gasifier	P_r=2000, T_r=2000, S/F=0.143 P_{out}=1.47, T_{out}=800	22	Node	ΔP=0
5	Node	ΔP=0	23	Separator	ΔP_1=0.6, ΔP_2=29.6, ΔT=0, other:99.99%, H_2:16%
6	Separator	ΔP=0.01, ΔT=0, C:100%, $SiO2$: 100%	24	Sink/Source	ΔP=0, Est. T_{out}=25
7	Valve	ΔP=0, 20% mass flow pipe 7 to pipe 412	160	Sink/Source	P_{out}=1.01325, T_{out}=15
101	Pump	P_{out}=1.5, η_i=0.75	165	Sink/Source	P_{out}=1.01325, T_{out}=15
102	Node	ΔP=0	800	Node	ΔP=0
104	Node	ΔP=0	900	Valve	ΔP=0, 78% mass flow pipe 900 to pipe 901
201	Compressor	P_{out}=1.49, η_i=0.80	901	Compressor	P_{out}=4.75, η_i=0.80
202	Node	ΔP=0	902	Heat Exchanger	ΔP_C=0, ΔP_H=0.095, ΔT_{Cout}=20, ΔT_{Hout}=30
400	Combustor	P_r=1, T_r=180, λ=1.1	903	Compressor	P_{out}=30.6, η_i=0.80
401	Separator	ΔP=0.01, ΔT=0, SiO2: 100%			Gas Turbine (Hydrogen2)
402	Valve	ΔP=0, mass flow pipe 402 18.3 kg/s	250	Compressor	P_{out}=9, η_i=0.80
403	Valve	ΔP=0, 80% mass flow pipe 402 to pipe 403	950	Compressor	P_{out}=9, η_i=0.80
404	Node		951	Combustor	ΔP=0.18, P_r=9, T_r=1200, λ=2.2
405	Node	ΔP=0.01	952	Turbine	η_i=0.90
406	Node	ΔP=0			Heat Recovery Steam Generator (Hydrogen2)
407	Sink/Source	ΔP=0, Est. T_{out}=1000, WFOT=90	36	Pump	P_{out}=1.21325, η_i=0.75
500	Valve	ΔP=0, 0.3% volume flow pipe 500 to pipe 501	130	Pump	η_i=0.75
501	Sink/Source	ΔP=0, ΔT=0	131	Heat Exchanger	ΔP_C=1, ΔP_H=0.02, ΔT_{pinchC}=10
		Gas cleaning	132	Drum	CRATIO=4
8	Heat Exchanger	ΔP_C=0.72, ΔP_H=00.292, ΔT_{pinchH}=50	133	Pump	η_i=0.75
9	Heat Exchanger	ΔP_C=0.3, ΔP_H=00.286, ΔT_{Cout}=546.81	134	Heat Exchanger	ΔP_C=1, ΔP_H=0.02, ΔT_{pinchC}=20
10	Sink/Source	ΔP=0.028, ΔT=0	135	Heat Exchanger	ΔP_C=1, ΔP_H=0.02, T_{outC}=540
11	Scrubber	ΔP_{gas}=0.0269, T_{ingas}=120,	136	Sink/Source	ΔP=1.2, ΔH=-2
12	Compressor	P_{out}=36.6, η_i=0.80	137	Turbine	P_{in}=80.2, η_i=0.882
13	Node	ΔP=0	138	Condensor	P_{out}=0.03, T_{outC}=19, ΔP_C=0.2
14	Separator	ΔP=0.7164	139	Deaerator	P_{in}=1.01325, ΔP=0
110	Valve	ΔP=0.03, 5X mass flow pipe 12 for pipe 111	140	Pump	η_i=0.75
		Reformer	150	Sink/Source	P_{out}=1.01325, T_{out}=12
15	Reformer	P_r=32.23, T_r=825, S/F=0.333 ΔP_1=0.68, ΔP_1=0.03, T_{out}=800			Preferential oxidation (Hydrogen1)
103	Heat Exchanger	ΔP_C=0.03, ΔP_H=0.282, ΔT_{Cout}=400	20	Heat exchanger	ΔP_C=0. 1, ΔP_H=0.6, T_{outH}=135, T_{outC}=20
123	Valve	ΔP=0, 1.6325 mass flow to pipe 129	21	Separator	ΔP_1=0.62, ΔP_2=0, ΔT=0, CO:100%, H_2:0.7%
502	Heat Exchanger	ΔP_C=0.68, ΔP_H=0.03, ΔT_{Cout}=600	22	Combustor	ΔP=0.62, P_r=30.61, T_r=135, λ=1
		WGS	23	Node	ΔP=0
16	Heat Exchanger	ΔP_C=0.7, ΔP_H=0.66, ΔT_{Hout}=380	135	Sink/Source	P_{out}=1.1325, T_{out}=15, ΔP=0.1
17	Reactor	ΔP=0.64, T_{WGS}=400	136	Pump	η_i=0.75
18	Heat Exchanger	ΔP_C=0.7, ΔP_H=0.66, ΔT_{Hout}=210, T_{Cout}=250	210	Compressor	P_{out}=31.22, η_i=0.80
19	Reactor	ΔP=0.62, T_{WGS}=220			Condensation (Hydrogen1)
120	Pump	P_{out}=38.48, η_i=0.75	24	Moisture separator	ΔP_C=0. 1, ΔP_H=0.6, T_{outH}=25, T_{outC}=20
121	Node	ΔP=0	140	Sink/Source	P_{out}=1.1325, T_{out}=15, ΔP=0.1
122	Node	ΔP=0	141	Pump	η_i=0.75

Table 7-3 input parameters for the models of the μ-CHP systems.

No.	Description	Input	No.	Description	Input
		PEM1			PEM3
1	Sink/Source	P_{out}=1.56, T_{out}=15	1	Sink/Source	P_{out}=1.56, T_{out}=15
3	Humidifier	ΔP_G=0.03, T_{outG}=67, ΔP_W=0.03, T_{outW}=67, RELHUM=1	2	Humidifier	ΔP_G=0.03, T_{outG}=67, ΔP_W=0.03, T_{outW}=67, RELHUM=1
4	Sink/Source	ΔP=0, ΔT=0	3	Sink/Source	ΔP=0, ΔT=0
5	Fuel Cell	SPFC, ΔP_{an}=0.03, ΔP_{cat}=0.03, T_{out}=80, DCAC=0.965, P_{FC}=1.5, T_{FC}=80, U_F=80%, U_{ox}=50%, ΔP_C=0.03	4	Fuel Cell	SPFC, ΔP_{an}=0.03, ΔP_{cat}=0.03, T_{out}=80, DCAC=0.965, P_{FC}=1.5, T_{FC}=80, U_F=80%, U_{ox}=50%, ΔP_C=0.03
6	Node	ΔP=0	5	Combustor	ΔP=0.03, T_r=1200, P_r=1.47
7	Combustor	ΔP=0.03, T_r=750, P_r=1.47	6	Heat Exchanger	ΔP_C=0.031, T_{outC}=65, ΔP_H=0.03
8	Heat Exchanger	ΔP_C=0.031, T_{outC}=80, ΔP_H=0.03	7	Heat Exchanger	ΔP_C=0.031, T_{outC}=80, ΔP_H=0.03
9	Heat Exchanger	ΔP_C=0.031, T_{outC}=65, ΔP_H=0.03	8	Stack	T_{in}=80
10	Stack	T_{in}=80	50	Sink/Source	P_{out}=1.01325, T_{out}=15
100	Sink/Source	P_{out}=1.01325, T_{out}=15	51	Compressor	P_{out}=1.53, η_i=0.8
101	Compressor	P_{out}=1.53, η_i=0.8	52	Node	ΔP=0
104	Node	ΔP=0	70	Heat Sink	P_{out}=1.5, ΔP=0.03, T_{in}=65, T_{out}=45
200	Sink/Source	P_{out}=1.01325, T_{out}=15, ϕ_m=1.1	71	Node	ΔP=0
201	Pump	P_{out}=1.593, η_i=0.75	72	Node	ΔP=0
202	Heat Exchanger	ΔP_C=0.031, ΔT_{pinchC}=5, ΔP_H=0.03	73	Pump	P_{out}=1.593, η_i=0.75
204	Sink/Source		80	Sink/Source	P_{out}=1.01325, T_{out}=15, ϕ_m=1.1
300	Heat Sink	P_{out}=1.5, ΔP=0.03, T_{in}=65, T_{out}=45	81	Pump	P_{out}=1.593, η_i=0.75
301	Node	ΔP=0	82	Heat Exchanger	ΔP_C=0.031, ΔT_{pinchC}=5, ΔP_H=0.03
302	Node	ΔP=0	83	Sink/Source	
303	Pump	P_{out}=1.593, η_i=0.75	101	Compressor	P_{out}=26, η_i=0.8
		PEM2	102	Condenser	ΔP_C=0.03, T_{outH}=60, ΔP_H=0.52
1	Sink/Source	P_{out}=1.56, T_{out}=15	103	Valve	ΔP=20.68, mass flow pipe 104=3.975
2	Valve	ΔP=0.03, 24.8% mass flow pipe 1 to pipe 10	104	Heat Exchanger	ΔP_C=0.096, T_{outC}=3, ΔP_H=0.02, T_{outH}=6.8
3	Humidifier	ΔP_G=0.03, T_{outG}=67, ΔP_W=0.03, T_{outW}=67, RELHUM=1	105	Drum	
4	Sink/Source	ΔP=0, ΔT=0	106	Pump	η_i=0.75
5	Fuel Cell	SPFC, ΔP_{an}=0.03, ΔP_{cat}=0.03, T_{out}=80, DCAC=0.965, P_{FC}=1.5, T_{FC}=80, U_F=80%, U_{ox}=50%, ΔP_C=0.03	110	Pump	P_{out}=1.05325, η_i=0.75
6	Node	ΔP=0	111	Sink/Source	ΔP=0.02, T_{out}=8
7	Combustor	ΔP=0.03, T_r=12000, P_r=1.47, λ=3.5	120	Pump	P_{out}=1.593, η_i=0.75
8	Heat Exchanger	ΔP_C=0.031, T_{outC}=80, ΔP_H=0.03	121	Heat Sink	P_{out}=1.5, ΔP=0.03, T_{in}=65, T_{out}=45
9	Heat Exchanger	ΔP_C=0.031, T_{outC}=65, ΔP_H=0.03	122	Node	ΔP=0
10	Stack	T_{in}=80	123	Node	ΔP=0
11	Sink/Source	ΔP=0.06, ΔT=0			
100	Sink/Source	P_{out}=1.01325, T_{out}=15			
101	Compressor	P_{out}=1.53, η_i=0.8			
104	Node	ΔP=0			
200	Sink/Source	P_{out}=1.01325, T_{out}=15, ϕ_m=1.1			
201	Pump	P_{out}=1.593, η_i=0.75			
202	Heat Exchanger	ΔP_C=0.031, ΔT_{pinchC}=5, ΔP_H=0.03			
204	Sink/Source				
300	Heat Sink	P_{out}=1.5, ΔP=0.03, T_{in}=65, T_{out}=45			
301	Node	ΔP=0			
302	Node	ΔP=0			
303	Pump	P_{out}=1.593, η_i=0.75			

Table 7-4 used values for determining the equivalent fuel cell resistance

Name	Symbol	Value	Unit
Ohmic fuel cell resistance [47]	R_{ohm}	1e-5	$\Omega\ m^2$
Slope Tafel line	A	0.0484	V
Constant in mass transfer overvoltage equation	B	0.05	V
Internal and fuel crossover equivalent current density	i_n	20	$A\ m^{-2}$
Limiting current density	i_l	9000	$A\ m^{-2}$
Exchange current density	i_0	0.67	$A\ m^{-2}$

Temperature and pressure of the fuel entering the μ-CHP systems are fixed to 15°C and 1.56 bar respectively. The air as well as the water used in these μ-CHP systems enters at environmental conditions.

Cycle Tempo can perform exergy calculations. Exergy values of all flows considered in the system flow diagram are calculated based on the previously calculated pressure, temperature and chemical composition. The thermo-mechanical (physical) exergy and the chemical exergy are calculated separately. The calculation of chemical exergies requires the definition of an environment that determines the exergy of any considered component at reference conditions. The environment applied for this study is shown in Table 7-5.

Table 7-5 composition of the environment [35]

Component	Mole fraction	Component	Mole fraction	Component	Mole fraction
$Al_2O_{3(s)}$	0.01	N_2	76.73	SO_2	0.01
Ar	0.91	O_2	20.60	Cl_2	0.01
CO_2	0.03	$SiO_{2(s)}$	0.01	F_2	0.01
H_2O	1.68				

Exergy losses are calculated by the program from the exergy balances of the various processes. A more detailed description of the exergy calculations is presented in the book of Szargut et al. [48]. The environmental temperature is supposed to be 15°C and the environmental pressure 1.01325 bar (1 atm).

The electrical exergy efficiency of the μ-CHP unit is calculated as

$$\eta_{ex,el} = \frac{\sum P_{el,out} - \sum P_{el,in}}{Ex_{fuel,in}} \tag{7.6}$$

Where, $P_{el,out}$ is the electrical output of the system, $P_{el,in}$ the electrical input of the system and $Ex_{fuel,in}$ the exergy of the fuel put in the system.

The overall exergy efficiency is given as

$$\eta_{ex,tot} = \frac{\sum P_{el,out} + \sum Ex_{heat,out} - \sum P_{el,in}}{Ex_{fuel,in}} \tag{7.7}$$

Here, $Ex_{heat,out}$ is the exergy of the usable heat produced by the system.

The overall energy efficiency is calculated as

$$\eta = \frac{\sum P_{el,out} + Q - \sum P_{el,in}}{\phi_{m,fuel} \cdot LHV_{fuel}} \tag{7.8}$$

Here, Q is the usable heat produced by the system, $\Phi_{m,fuel}$ the mass flow of fuel in the system and LHV_{fuel} the lower heating value of the fuel.

7.4. Results

7.4.1. Hydrogen production

The gasification process converts 4.12 kg s^{-1} of wood together with 1.30 kg s^{-1} water into 4.26 kg s^{-1} syn-gas with a composition as given in Table 7-6.

Table 7-6 dry composition of the producer gas compared with literature [32]

Component	Output model [vol%]	Literature data [vol%]
Hydrogen (H$_2$)	35.22	30-40
Carbon monoxide (CO)	22.63	20-30
Methane (CH$_4$)	20.86	15-25
Carbon dioxide (CO$_2$)	17.18	8-12
Nitrogen (N$_2$)	3.93	1-5
Other	0.18	

The residual char from the gasification is combusted to provide the heat required for the endothermic gasification process. For the combustion is 7.97 kg s^{-1} air fed to the combustor; this is an excess of 10%. The temperature of the syn-gas leaving the gasifier is 813°C and the pressure is 1.46 bar. Also a flue gas stream is leaving the gasification unit at a temperature of 1237°C and the same pressure as the producer gas. The flue gas is utilized for a variety of heating purposes like heating the reformer and steam generation for the gasification process.

The generated producer gas is passed to the gas cleaning system. During the gas cleaning process, the composition of the producer gas is not supposed to change. Only the water content of the gas will change. Much water condenses during the scrubbing process and is removed with the waste water. The water fraction changes from 34 mole% to 12 mole%. For the scrubbing process, 16 kg s^{-1} water is used, which enters the scrubber at a temperature of 15°C and a pressure of 1.4 bar. In the pressurization step, gas is compressed to approximately 36 bar. After the compression, 1.6 kg s^{-1} steam is added to increase the water content of the gas. The temperature and pressure of this steam are respectively 600°C and 35 bar. The compressed gas is then desulphurized and transferred to the reformer. In the reformer, the methane is reformed with 1.6 kg s^{-1} steam, which has a temperature of 600°C and a pressure of 35 bar. About 70% of the methane is converted in the reformer. After the reforming, the carbon monoxide in the producer gas is converted into hydrogen in a two stage water gas shift process. The heat extracted during cooling of the gas prior and between the high and low temperature water gas shift is used to produce steam.

Hydrogen1

By combining Figure 7-2A and Figure 7-2C the flow sheet of the hydrogen1 process can be found.

After the WGS process, the gas is cooled to 135°C and then treated in a preferential oxidation reactor to remove the residual carbon monoxide from the gas. As assumed, all the carbon monoxide and 0.7 mole% [49] of hydrogen is converted in the reactor. Finally, the gas is cooled to 25°C in order to condensate large part of the water in the gas. This resulted in a gas composition as given in Table 7-7. The total mass flow of hydrogen rich gas is 4.2 kg s^{-1}. The whole process consumes 3300 kW of electricity, which has to be imported.

Table 7-7 the final composition of 60% pure hydrogen

Component	Molar fraction [mole%]
Hydrogen (H_2)	60.76
Methane (CH_4)	3.16
Carbon dioxide (CO_2)	32.39
Water (H_2O)	0.11
Nitrogen (N_2)	3.54
Argon (Ar)	0.04

Hydrogen2

The flow sheet for the hydrogen2 process can be obtained by combining Figure 7-2A and Figure 7-2B.

In the hydrogen2 process, the gas coming from the WGS system is first cooled before it is transferred to the PSA. During the cooling, a large part of the water in the gas is condensed and removed from the gas. First the residual water and the carbon dioxide are removed from the gas by adsorption. Then in the next step all the other impurities, like methane, carbon monoxide and nitrogen, are removed from the gas. This results in 0.3 kg s^{-1} of 99.99% pure hydrogen, a stream of almost 6 kg s^{-1} containing water and CO_2 and a stream of 0.3 kg s^{-1} with all the impurities. This last stream of impurities contains a reasonable amount of combustibles. Therefore, it is applied in a gas turbine for the generation of additional electric power. The hot flue gasses coming from the gas turbine are cooled in a heat recovery steam generator. The produced steam is used in a bottoming cycle to generate electricity. The overall generated electric power is 6189 kW. The whole process consumes 6427 kW of electricity. A small amount of electrical power (239 kW) has to be supplied from outside the plant.

The two hydrogen production plants

The hydrogen (rich) gas produced in both plants is at a pressure of 30 bar and a temperature of 25°C.

For both hydrogen plants are the exergy efficiencies determined. The exergy efficiency is determined by dividing the exergy of the generated hydrogen (rich) gas flow by the exergy of the biomass plus the imported electrical power input. The exergy efficiency for the hydrogen1 plant is 61.4%. For the hydrogen2 plant the efficiency is 50.5%
In Figure 7-4, the exergy flow diagrams for the two hydrogen production plants are given.

The temperature and pressure of the main streams from biomass to hydrogen in the production plant are given in Table 7-8. The pipe numbers correspond to the pipe numbers in Figure 7-2.

7.4.2.Hydrogen distribution

The hydrogen produced in the hydrogen production plants is produced at a pressure of 30 bar. Therefore, the gas from the gas production plant has to be compressed to 80 bar, before it is fed into the high pressure network. The heat generated during the compression is assumed to be lost. By multiplying the efficiencies of the gas production plants and the gas distribution, the efficiency of the gas production and distribution can be found. For hydrogen1 the exergy efficiency becomes 57.1% and for hydrogen2 47.0%.
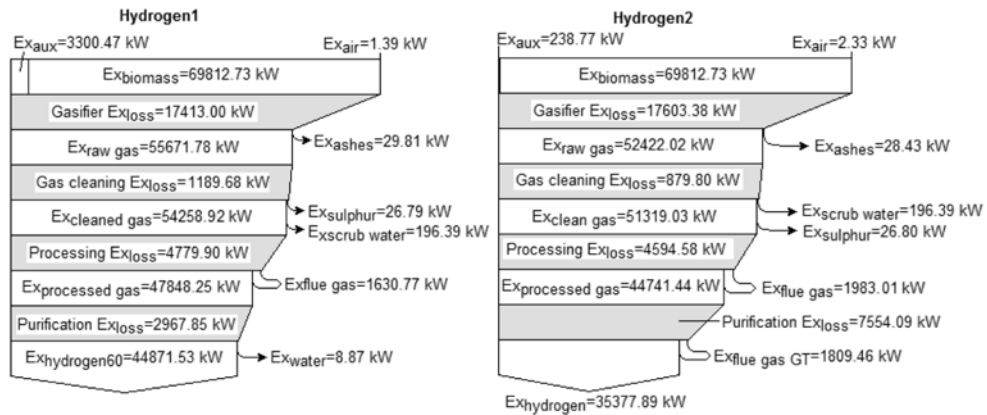
Figure 7-4 exergy flow diagrams of both the hydrogen production plants. The flow diagram on the left is of hydrogen1 and the one on the right is of hydrogen2.

The volume flow of the 60% hydrogen produced by the hydrogen1 plant at 80 bar and a temperature of 15°C is 265 m^3 h^{-1} . The volume flow of the hydrogen2 plant at similar conditions is 156 m^3 h^{-1}.

Table 7-8 temperatures and pressures for several important pipes within the hydrogen production plants

Figure 2 part	Pipe Number	Pressure [bar]	Temperature [°C]	Figure 2 Part	Pipe Number	Pressure [bar]	Temperature [°C]
A	8	1.460	813.08	C	22	31.22	135.00
A	9	1.431	617.76	C	26	30.60	143.81
A	10	1.402	120.00	C	27	30.00	25.00
A	12	1.347	56.30	A	110	1.500	15.01
A	13	36.54	528.38	A	112	1.347	56.30
A	14	36.54	551.46	A	502	1.47	1238.67
A	15	35.82	593.20	A	504	1.44	878.78
A	16	35.10	763.08	A	505	1.41	681.41
A	17	34.42	800.00	A	506	1.382	299.07
A	18	33.76	380.00	B	802	1.22	24.69
A	19	33.12	450.03	B	950	1.000	105.95
A	20	32.46	210.00	B	952	8.82	1371.14
A	21	31.22	225.10	B	953	1.073	805.73
B	22	31.22	30.00	B	956	1.013	111.22
B	25	30.00	105.95	C	130	30.00	25.00

7.4.3.μ-CHP

As mentioned earlier, three different μ-CHP systems have been considered. The first is used as a base case for the calculations, called PEM1. PEM1 will only generate only 1.9 kW of heat. Since it is assumed that the heat demand is 3 kW; additional facilities are necessary to meet this requirement. Two options have been considered for this evaluation: PEM2 and PEM3. Each system is evaluated with two fuels: 60% hydrogen coming from hydrogen1 and 99.99% pure hydrogen coming from hydrogen2. In all the systems the electrical power output of the μ-CHP system is 1 kW.

PEM1

The gross power production of the PEM1 μ-CHP system is 1.07 kW. To produce this amount of power 1.12 kg h^{-1} of 60% hydrogen is required. When using 99.99% pure hydrogen the required amount is 0.09 kg h^{-1}. The calculated cell voltage of the fuel cell using 60% hydrogen is 0.53V, for 99.99% pure hydrogen this is 0.55V. The required fuel cell area also differs with the purity of the fuel. When using 60% pure hydrogen the required fuel cell area is 0.26 m^2 and for pure hydrogen it is 0.25 m^2.
The electrical exergy efficiency for the 60% hydrogen and pure hydrogen are respectively 31.0% and 32.1%. The overall exergy efficiencies are found to be 38.3% and 39.7% respectively. For comparison, the overall thermal efficiencies are 92.4% and 92.8% respectively. These efficiencies are calculated using equations (7.6), (7.7) and (7.8) respectively.

PEM2

The PEM1 unit, as described before, is not able to generate sufficient heat under all circumstances. As the maximum heat demand is set to 3 kW, the unit needs to be modified in order to enable the generation of all the demanded heat. In the PEM2 system, the additional heat is generated by by-passing some fuel and some air to the boiler of the μ-CHP system, as indicated in Figure 7-3B.
For PEM2 some data is given in Table 7-9. The amount of fuel by-passed is dependant of the purity of the fuel. For 60% hydrogen 25.2% needs to be by-passed and for pure hydrogen this amount is 24.8%. The heat production of the fuel cell causes this difference, because the fuel cell operating on 60% hydrogen produces 1.13 kW and the one on pure hydrogen 1.12 kW.

Table 7-9 results for the three μ-CHP systems fuelled with two different fuels

	PEM2		PEM3	
	Hydrogen1	*Hydrogen2*	*Hydrogen1*	*Hydrogen2*
Hydrogen purity [%]	60	99.99	60	99.99
Fuel input [g s^{-1}]	0.439	0.037	0.384	0.032
Air input [g s^{-1}]	2.639	2.530	1.834	1.782
Voltage fuel cell [V]	0.534	0.549	0.534	0.549
Fuel cell area [m^2]	0.273	0.265	0.320	0.309
Auxiliary power [W]	126.48	121.27	317.34	309.07
Electrical exergy efficiency [%]	22.09	23.04	25.27	26.26
Overall energy efficiency [%]	89.96	90.73	102.86	103.28
Overall exergy efficiency [%]	30.14	31.46	34.48	35.84

PEM3

In the PEM3 system, a ground coupled heat pump is used to produce additional heat to meet the requirements. In this system the PEM fuel cell produces a little more electricity to power the heat pump, while the net production of electricity remains at 1 kW. In the case that 60% hydrogen is used the amount of additional power is 0.229 kW, for pure hydrogen this amount is 0.224 kW. Only a small portion of the heat is produced by the heat pump, for 60% hydrogen this amount is 0.735 kW and for pure hydrogen it is 0.718 kW. Some other results for the PEM3 system fuelled with both fuels can be found in Table 7-9.

7.4.4. The whole chain from biomass to heat and power

To determine the exergy efficiency of the whole chain from biomass to electricity, the exergy efficiency of the hydrogen production including the distribution grid needs to be multiplied by the electrical exergy efficiency of the μ-CHP. For the exergy efficiency of the whole chain from biomass to electricity and heat, the calculation is slightly different. The electrical exergy efficiency of the μ-CHP needs to be replaced, in this case, by the overall exergy efficiency of the μ-CHP system. The results are given in Table 7-10.

Table 7-10 efficiencies for the whole chain

	Hydrogen1 (60% pure H_2)		Hydrogen2 (99.99% pure H_2)	
	PEM2	*PEM3*	*PEM2*	*PEM3*
Electric energy efficiency of the chain[%]	14.76	16.88	12.93	14.73
Electric exergy efficiency of the chain[%]	12.61	14.43	10.83	12.34
Total energy efficiency of the chain[%]	59.01	67.48	51.72	58.87
Total exergy efficiency of the chain [%]	17.21	19.69	14.79	16.84
Number of units that could be fueled [-]	9233	10031	7864	8558

In this table also an indication is given for the total number of μ-CHP units that can be fuelled by one single hydrogen plant based on the same amount biomass input. This value is calculated by dividing the output of the hydrogen plant by the fuel input of the μ-CHP.

7.5. Discussion

The calculated carbon dioxide fraction of the producer gas at the exit of the gasifier in the hydrogen production plants is 17 vol%. This is approximately 7 percentage points higher than was found in the literature [32]. As the composition of the biomass was not given in the literature, the difference may result from differences in the biomass. The exergy losses calculated for the hydrogen2 plant are larger than for hydrogen1, as indicated in Figure 7-4. A large problem in the purification is the great loss of valuable hydrogen. In a PSA system some hydrogen is used to purge the adsorber; the used hydrogen is lost. This amount of hydrogen is larger than the amount of hydrogen assumed to be oxidized in the preferential oxidation process.

The purity of the hydrogen is an important factor when used in PEM fuel cells, since these fuel cells are very sensitive towards impurities, especially carbon monoxide. When using pure hydrogen little problems will arise due to impurities. When using less pure fuels like the 60% hydrogen problems seem to be inevitable. Although, the technology is still developing, especially the search for more tolerant electrodes is still ongoing. As well as the research toward improvements in the gas processing techniques, like preferential oxidation. It is likely that the developments in both technologies will meet somewhere midway, with a more tolerant fuel cell and a more effective preferential oxidation. For instance, it could be possible to attain similar performance of the fuel cell operating on 100 ppm CO/H_2 compared to a fuel cell operating on pure hydrogen, according to Kawatsu [50]. The nitrogen, in the 60% hydrogen, act only as a diluent in the PEM fuel cell systems [44]. Platinum is a good catalyst for methane oxidation [51]. However, the methane content is very low and the fuel cell temperature is also low, its effect on the PEM fuel cell performance is negligible.

The size of the fuel cell system as well as the hydrogen distribution grid is influenced by the quality of the fuel. In the case of 60% hydrogen more compression power and also larger pipe diameters are necessary than in the case of pure hydrogen, because of the higher

volume per mole of hydrogen. Despite the higher compression cost and the lower μ-CHP efficiencies the chain efficiencies are higher for the systems fuelled with fuel from hydrogen1 (60% hydrogen). The lower efficiencies of systems with pure hydrogen are caused by the large losses during the purification process of hydrogen2. Also the number of μ-CHP units that can be fuelled by one hydrogen1 plant using the same biomass flow will be larger. This is caused by the large amount of hydrogen which is lost during the purification in hydrogen2.

There is a large difference in the mass flows for the two different hydrogen rich fuels to the μ-CHP system. This is caused by the impurities in the 60% hydrogen. The molecular weight of the impurities is much higher than the molecular weight of hydrogen. When looking at the volume flow, the difference is less. The volumetric flow of the 60% hydrogen is only 31% larger than the pure hydrogen to the μ-CHP system. This larger volume flow results also in an increased required compression power. The lower concentration of hydrogen in the 60% hydrogen results in a lower cell voltage.

The way additional heat is being produced has an influence on the efficiency of the μ-CHP system and on the energy conversion chain. The direct combustion of hydrogen for the production of additional heat leads to large exergy losses. The use of a heat pump can reduce these losses significantly. When the efficiency of the fuel cell increases, the efficiency difference between PEM2 and PEM3 will be larger. Further improvement of the electrical efficiency of the PEM fuel cell as well as the COP of the heat pump can significantly improve the performance of the whole chain.

The heat and electrical power demands of dwellings are strongly fluctuating. A μ-CHP system must be able to manage these fluctuations. High peaks in the heat demand are easier handled by a combustor than by a heat pump. Heat buffers can be helpful to supply the heat also during fluctuating demands. Variations in load are not considered in this study; the response of the system on different heat and power demands is beyond the scope of this work. This study is limited to the systems performance at full load. In actual systems the μ-CHP units will operate at part load for most of the time. This will influence the efficiencies of the μ-CHP systems. The PEM fuel cell unit can in principle have a higher conversion efficiency, because of the higher cell voltage at part load conditions.

7.6. Conclusions

The combination of centralized hydrogen production with decentralized power production with PEM fuel cells has been assessed by modelling the considered system alternatives in Cycle Tempo. The hydrogen production is based on biomass gasification using a FICFB gasifier. PEM fuel cell units are used for the decentralized power production. Two hydrogen production plants have been modelled. The first one is called hydrogen1 and produces 60% hydrogen with an exergy efficiency of 61.4%. The second one is called hydrogen2, produces 99.99% pure hydrogen with an exergy efficiency of 50.5%. The hydrogen produced by these plants is assumed to be fed to a hydrogen distribution grid. Decentralized power production is supposed to occur in μ-CHP units. Each unit generates 1 kW of electricity and 3 kW of heat. The μ-CHP units are connected to the hydrogen distribution grid. By comparing the units fuelled with 60% and 99.99% pure hydrogen, the effect of the purity of hydrogen on the performance of the μ-CHP units is evaluated. Two different ways for the production of all demanded heat by the μ-CHP units are considered. Two alternative designs have been made, PEM2 and PEM3. In PEM2 a fuel by-pass to the boiler is added, so extra fuel can be combusted for heat production. For PEM3, a ground coupled heat pump is supposed to produce additional heat. The total exergy

efficiencies (electricity and heat) for 60% hydrogen to the PEM2 and PEM3 units are respectively 30.3% and 32.9%. The values for 99.99% pure hydrogen are respectively 31.6% and 34.4%. The overall performance of the μ-CHP units fuelled with 60% hydrogen is lower than one fuelled with 99.99% pure hydrogen.

At the end the whole chain of hydrogen production towards the generation of heat and power has to be considered. The total exergy efficiency of this chain, with the PEM2 and 60% hydrogen is 17.2%. In case of 99.99% pure hydrogen the chain exergy efficiency is 14.8%. For PEM3, these values are respectively 19.7% and 16.8%. The use of impure hydrogen results in a better thermodynamic performance. However, it results in larger dimensions (30%) of the equipment because of the higher volume flows of fuel per unit power.

If the whole chain is considered, the PEM3 system with 60% hydrogen gives the highest overall exergy efficiency.

Higher efficiencies of the PEM fuel cell as well as higher COP values of the heat pump will improve the overall exergy efficiency of the whole chain. The calculated exergy efficiencies of the considered conversion chains appear not to be very promising. A search for further improvement or alternative system options seems to be useful. For instance, the centralized conversion of biomass into fuel and the centralized conversion of that fuel into electricity, like is done in an earlier study [20].

7.7. References

1.   Bridgwater A. V. The technical and economic feasibility of biomass gasification for power generation. Fuel 1995; 74(5): 631-653.
2.   Kivisaari T., Bjornbom P., Sylwan C. Studies of biomass fuelled MCFC systems. J Power Sources 2002; 104(1): 115-124.
3.   McIlveen-Wright D. R., McMullan J. T., Guiney D. J. Wood-fired fuel cells in selected buildings. J Power Sources 2003; 118(1-2): 393-404.
4.   Panopoulos K. D., Fryda L. E., Karl J., Poulou S., Kakaras E. High temperature solid oxide fuel cell integrated with novel allothermal biomass gasification: Part I: Modelling and feasibility study. J Power Sources 2006; 159(1): 570-585.
5.   Donolo G., Simon G. D., Fermeglia M. Steady state simulation of energy production from biomass by molten carbonate fuel cells. J Power Sources 2006; 158(2): 1282-1289.
6.   Lobachyov K. V., Richter H. J. An advanced integrated biomass gasification and molten fuel cell power system. Energy Convers Manage 1998; 39(16-18): 1931-1943.
7.   Cordiner S., Feola M., Mulone V., Romanelli F. Analysis of a SOFC energy generation system fuelled with biomass reformate. Appl Therm Eng 2007; 27(4): 738-747.
8.   Ghosh S., De S. Thermodynamic performance study of an integrated gasification fuel cell combined cycle: an exergy analysis. Proc Inst Mech Eng Part A: J Power Energy 2003; 217(6): 575-581.
9.   Hustad J. E., Hofbauer H., Vik A., Byrknes J. BioSOFC - Technology Development for Integrated SOFC, Biomass Gasification and High Temperature Gas Cleaning. In: Biomass Conference, Biomass for Energy, Industry and Climate Protection, Rome, 2004.
10.   Athanasiou C., Coutelieris F., Vakouftsi E., Skoulou V., Antonakou E., Marnellos G., Zabaniotou A. From biomass to electricity through integrated

gasification/SOFC system-optimization and energy balance. Int J Hydrogen Energy 2007; 32(3): 337-342.

11.   Omosun A. O., Bauen A., Brandon N. P., Adjiman C. S., Hart D. Modelling system efficiencies and costs of two biomass-fuelled SOFC systems. J Power Sources 2004; 131(1-2): 96-106.

12.   Monanteras N. C., Frangopoulos C. A. Towards synthesis optimization of a fuel-cell based plant. Energy Convers Manage 1999; 40(15-16): 1733-1742.

13.   Morita H., Yoshiba F., Woudstra N., Hemmes K., Spliethoff H. Feasibility study of wood biomass gasification/molten carbonate fuel cell power system-- comparative characterization of fuel cell and gas turbine systems. J Power Sources 2004; 138(1-2): 31-40.

14.   Ghosh S., De S. Energy analysis of a cogeneration plant using coal gasification and solid oxide fuel cell. Energy 2006; 31(2-3): 345-363.

15.   Seitarides T., Athanasiou C., Zabaniotou A. Modular biomass gasification-based solid oxide fuel cells (SOFC) for sustainable development. Renew Sustain Energy Rev 2008; 12(5): 1251-1276.

16.   Proell T., Aichernig C., Rauch R., Hofbauer H. Coupling of Biomass Steam Gasification and an SOFC - Gas Turbine Hybrid System for Highly Efficient Electricity Generation. In: ASME Turbo Expo 2004: Power for Land, Sea, and Air, Vienna, Austria, 2004.

17.   Fryda L., Panopoulos K. D., Kakaras E. Integrated CHP with autothermal biomass gasification and SOFC-MGT. Energy Convers Manage 2008; 49(2): 281-290.

18.   Fryda L., Panopoulos K. D., Karl J., Kakaras E. Exergetic analysis of solid oxide fuel cell and biomass gasification integration with heat pipes. Energy 2008; 33(2): 292-299.

19.   Karellas S., Karl J., Kakaras E. An innovative biomass gasification process and its coupling with microturbine and fuel cell systems. Energy 2008; 33(2): 284-291.

20.   Toonssen R., Woudstra N., Verkooijen A. H. M. Reference System for a Power Plant Based on Biomass Gasification and SOFC. In: 8th European Solid Oxide Fuel Cell Forum, Luzerne, Switserland, 2008.

21.   Sucipta M., Kimijima S., Song T. W., Suzuki K. Biomass Solid Oxide Fuel Cell-Microgas Turbine Hybrid System: Effect of Fuel Composition. J Fuel Cell Sci Technol 2008; 5(4): 041006.

22.   Aravind P. V., Woudstra T., Woudstra N., Spliethoff H. Thermodynamic Evaluation of Small Scale Systems with Biomass Gasifiers, Solid Oxide Fuel Cells with Ni/GDC Anodes and Gas Turbines. J Power Sources 2009; 190(2): 461-475.

23.   Karl J., Frank N., Karellas S., Saule M., Hohenwarter U. Conversion of Syngas From Biomass in Solid Oxide Fuel Cells. J Fuel Cell Sci Technol 2009; 6(2): 021005.

24.   Ersoz A., Ozdogan S., Caglayan E., Olgun H. Simulation of Biomass and/or Coal Gasification Systems Integrated With Fuel Cells. J Fuel Cell Sci Technol 2006; 3(4): 422-427.

25.   Sordi A., Silva E. P., Milanez L. F., Lobkov D. D., Souza S. N. M. Hydrogen from Biomass Gas Steam Reforming for Low Temperature Fuel Cell: Energy and Exergy Analysis. Braz J Chem Eng 2009; 26(01): 159-169.

26.   Gigliucci G., Petruzzi L., Cerelli E., Garzisi A., La Mendola A. Demonstration of a residential CHP system based on PEM fuel cells. J Power Sources 2004; 131(1-2): 62-68.

27.   Saidi M. H., Ehyaei M. A., Abbasi A. Optimization of a combined heat and power
        PEFC by exergy analysis. J Power Sources 2005; 143(1-2): 179-184.
28.   Colella W. G. Design considerations for effective control of an afterburner sub-
        system in a combined heat and power (CHP) fuel cell system (FCS). J Power
        Sources 2003; 118(1-2): 118-128.
29.   Page S., Krumdieck S. System-level energy efficiency is the greatest barrier to
        development of the hydrogen economy. Energy Policy 2009; 37(9): 3325-3335.
30.   Bolhar-Nordenkampf M., Bosch K., Rauch R., Kaiser S., Tremmel H., Aichernig
        C., Hofbauer H. Scale-up of a 100kWth pilot FICFB-gasifier to a 8 MWth FICFB-
        gasifier demonstration plant in Güssing (Austria). In: 1st International Ukrainian
        Conference on BIOMASS FOR ENERGY, Kiev, Ukraine, 2002.
31.   Bolhar-Nordenkampf M., Hofbauer H. Gasification Demonstration Plants in
        Austria. In: International Slovak Biomass Forum, Bratislava, 2004.
32.   Hofbauer H., Rauch R., Loeffler G., Kaiser S., Fercher E., Tremmel H. Six Years
        Experience with the FICFB-Gasification Process. In: 12th European Conference
        and Technology Exhibition on Biomass for Energy, Industry and Climate
        Protection, Amsterdam, The Netherlands, 2002.
33.   Hofbauer H., Rauch R., Bosch K., Kock R., Aichernig C. Biomass CHP Plant
        Güssing - A Success Story. In: Expert Meeting on Pyrolysis and Gasification of
        Biomass and Waste, Strasbourg, 2002.
34.   Hofbauer H., Rauch R., Foscolo P., Matera D. Hydrogen-rich Gas from Biomass
        Steam Gasification. In: 1st World Conference and Exhibition on Biomass for
        Energy and Industry, Sevilla, Spain, 2000.
35.   Toonssen R., Woudstra N., Verkooijen A. H. M. Exergy Analysis of Hydrogen
        Production Plants Based on Biomass Gasification. Int J Hydrogen Energy 2008;
        33(15): 4074-4082.
36.   Hamelinck C. N., Faaij A. P. C. Future prospects for production of methanol and
        hydrogen from biomass. University Utrecht: Copernicus Institute, 2001.
37.   McKendry P. Energy production from biomass (part 3): gasification technologies.
        Bioresource Technol 2002; 83(1): 55-63.
38.   Twigg M. V. Catalyst Handbook. London: Wolfe Publishing Ltd., 1989.
39.   Wootsch A., Descorme C., Duprez D. Preferential oxidation of carbon monoxide
        in the presence of hydrogen (PROX) over ceria-zirconia and alumina-supported Pt
        catalysts. J Catal 2004; 225(2): 259-266.
40.   Zalc J. M., Löffler D. G. Fuel processing for PEM fuel cells: transport and kinetic
        issues of system design. J Power Sources 2002; 111(1): 58-64.
41.   Cheng X., Shi Z., Glass N., Zhang L., Zhang J., Song D., Liu Z.-S., Wang H.,
        Shen J. A review of PEM hydrogen fuel cell contamination: Impacts, mechanisms,
        and mitigation. J Power Sources 2007; 165(2): 739-756.
42.   Janssen G. J. M. Modelling study of CO_2 poisoning on PEMFC anodes. J Power
        Sources 2004; 136(1): 45-54.
43.   Papageorgopoulos D. C., de Bruijn F. A. Examining a Potential Fuel Cell Poison. J
        Electrochem Soc 2002; 149(2): A140-A145.
44.   EG&G Techincal Services. Fuel Cell Handbook. Morgantown: Nation Energy
        Technology Laboratory, 2004.
45.   Cycle-Tempo, 5.0. TU Delft, 2009. www.cycle-tempo.nl
46.   van der Nat K. V., Woudstr N. N., Spliethoff H. Evaluation of several biomass
        gasification processes for the production of a hydrogen rich synthesis gas In:

International Hydrogen Energy Congress and Exhibition IHEC 2005, Istanbul, 2005.

47.   Ge S.-H., Yi B.-L. A mathematical model for PEMFC in different flow modes. J Power Sources 2003; 124(1): 1-11.

48.   Szargut J., Morris D. R., Steward F. R. Exergy Analysis of Thermal, Chemical, and Metallurgical Processes. Berlin: Springer-Verlag, 1988.

49.   Lee S. H., Han J., Lee K.-Y. Development of 10-kWe preferential oxidation system for fuel cell vehicles. J Power Sources 2002; 109(2): 394-402.

50.   Kawatsu S. Advanced PEFC development for fuel cell powered vehicles. J Power Sources 1998; 71(1-2): 150-155.

51.   Periana R. A., Taube D. J., Gamble S., Taube H., Satoh T., Fujii H. Platinum Catalysts for the High-Yield Oxidation of Methane to a Methanol Derivative. Science 1998; 280(5363): 560-564.

8. Decentralized power generation in a SOFC from centralized produced gas

Abstract: *A thermodynamic evaluation of different energy conversion chains based on centralized biomass gasification and decentralized heat and power production by a solid oxide fuel cell (SOFC) has been performed. Three different chains have been evaluated, the main difference between the chains is the secondary fuel produced via biomass gasification. The secondary fuels considered are hydrogen, synthetic natural gas (SNG) and syngas. These fuels are assumed to be distributed through a transport and distribution grid to the micro-combined heat and power (μ-CHP) systems based on a SOFC and a heat pump. Two systems for the generation of secondary fuels from biomass are modelled using Cycle-Tempo. The hydrogen plant and the syngas plant have been modelled. The efficiency of the synthetic natural gas plant is taken from literature. The μ-CHP systems on the different fuels have also been modelled in Cycle-Tempo. The chain from biomass based centralized gas production towards decentralized heat and power production has been evaluated. The overall exergy efficiency from biomass to heat and power is for the hydrogen route 21.1%, for the SNG route it is 28.4 and for the syngas route it is 30.4%.*

8.1. Introduction

Biomass is considered to be a sustainable and renewable primary fuel, due to its short carbon dioxide cycle. It receives more and more attention because of the increasing awareness towards climate changes and declining fossil fuel reserves. Biomass gasification is considered as one of the promising options for the conversion of biomass into a secondary fuel. This secondary fuel is syngas, a mixture of hydrogen, carbon monoxide, carbon dioxide, methane and water. The syngas produced in gasification can be used directly in combined cycle plants, gas engines or fuel cells. It is also possible to process the produced gas for the production of gaseous and liquid fuels, which can be distributed.
Fuel cells are considered to be highly efficient energy converters. Most fuel cells convert hydrogen electrochemically into water, during this conversion electricity is produced; additionally some heat is produced. High temperature fuel cells are known to be more flexible towards fuels than the lower temperature fuel cells. These high temperature fuel cells can convert besides hydrogen also carbon monoxide and methane and these fuel cells are also less susceptible to contaminants. One type of high temperature fuel cells is the solid oxide fuel cell (SOFC) with an operating temperature between 600°C and 1000°C. This type fuel cell is considered for small scale domestic applications, due to their high electric efficiency and the possibility of co- and poly-generation.
The coupling of biomass gasification and solid oxide fuel cells is subject of many studies, like Refs. [1-16]. Some of these studies focus on large scale systems 30MW$_e$ [14], or 21 MW$_e$ [16]. Other studies focus on small scale systems, like 1 kW$_e$ [4] for testing purposes, or some bigger systems 100 kW [13].
Other studies consider biomass gasification for the production of secondary fuels, like synthetic natural gas (SNG), hydrogen, methanol and Fischer Tropsch fuels. For instance,

Sues et al. [17] evaluated five different biowastes-to-biofuels routes via biomass gasification. The routes included a route towards hydrogen, SNG, Fischer Tropsch fuel, methanol and heat and electricity. Hamelinck and Faaij [18] studied the production of methanol and hydrogen from biomass. In a study of Toonssen et al. [19] an thermodynamic analysis is made on hydrogen production using different gasification technologies. Gassner and Maréchal [20] performed an thermo-economic analysis on the production of SNG from biomass via biomass gasification. Jurascík et al.[21, 22] performed several exergy analyses on the production of SNG from biomass.

The application of SOFC in micro-combine heat and power (μ-CHP) systems receives more attention lately. The influence of fuels on such μ-CHP systems is studied by for instance Braun et al. [23], and Kazempoor et al. [24].

The analysis of the whole chain of gas production, distribution and conversion in a SOFC μ-CHP system, as in this paper, is hardly researched. Page and Krumdieck [25] performed an analysis on different energy chains based on hydrogen, including one chain with coal gasification, hydrogen distribution and a fuel cell μ-CHP system. A previous study [26] is performed on hydrogen production from biomass, hydrogen distribution and proton exchange membrane fuel cell based μ-CHP systems.

In this paper three options of gas production from biomass have been evaluated; the production of hydrogen, the production of SNG and the production of clean dry syngas. The produced gas is assumed to be pumped into a distribution grid, which supplies fuel decentralized conversion. In the dwelling the fuel is converted into electricity and heat. For the production of heat and power a μ-CHP system based on a SOFC is used. The electrical power demand in an average household is usually not exceeding 1 kW. Therefore, the design electrical power output of the μ-CHP system is set to 1 kW. An exergy analysis has been performed on both the gas production as well as on the μ-CHP system. The results of this analysis have been combined to evaluate the whole conversion chain from biomass into electricity. The influence of the fuel production on the whole conversion chain has not been studied before.

The heat production of the SOFC based μ-CHP system is not sufficient to fulfil the heat demand of an average dwelling. Therefore, the SOFC is combined with a ground coupled electrical driven compression heat pump for the production of additional heat. The complete μ-CHP system, SOFC and heat pump, produce net 1 kW of electricity and 3 kW of heat. The influence of the different fuels on the performance the μ-CHP system has been evaluated.

8.2. System configurations

The whole chain from biomass to electricity and heat consists of three parts: the gas production from biomass, the gas distribution grid and the micro-CHP system. In Figure 8-1, a schematic representation is given of the chain from biomass to electricity. In the following sections each part of the chain will be discussed separately, starting with the gas production plants.
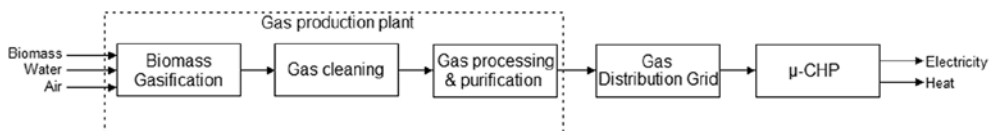
Figure 8-1 schematic overview of the conversion chain

8.2.1.Gas production plants

Three different gas production plants are considered:

GP1   produces pure hydrogen from biomass;

GP2   produces synthetic natural gas (SNG) from biomass;

GP3   produces clean synthesis gas from biomass.

All the three plants are based on the fast internal circulating fluidized bed (FICFB) gasifier followed by low temperature gas cleaning.

The FICFB gasifier is developed by the Institute of Chemcial Engineering and AE Energietechnik. This gasifier consists of two different fluidized beds. One fluidized bed is a bubbling fluidized bed which is used for the gasification of biomass. The other fluidized bed is a circulating fluidized bed which is used for the combustion of unconverted biomass and residual char from the gasification process. The heat produced in the exothermic combustion process is used in the endothermic gasification process. The exchange of heat between the two beds is realized by circulating the hot bed material. The gasification bed is blown with steam of 600°C with a steam to carbon ratio on a dry basis of ±0.5 kg kg^{-1}.The combustion bed is blown with pre heated air and an excess of 10% (λ=1.1). The gasification section operates at a temperature of approximately 800°C and the combustion section at a temperature of approximately 1000°C. More information about the FICFB can be found in Refs. [27-31].

The gas produced by the gasifier contains impurities like particulates (5000-10,000 mg Nm^{-3} [30]), tars (1500-4500 mg Nm^{-3} [30]), sulphur compounds (20-50 ppm [30], these values are measured after the systems gas cleaning without dedicated sulphur removal. Therefore, these values will not deviate much from the measured values.), nitrogen compounds (ammonia 1000-2000 ppm [30]) halogen compounds and alkali metals [32, 33]. It is important to remove these impurities before further processing, since these impurities can have a deteriorating effect on all kinds of processes.

In this study, it is assumed that gas cleaning occurs at low temperature. Therefore, the gas will be cooled to approximately 120°C. During the cooling alkali metal compounds and some of the tar compounds will condense on the entrained particulates [34]. By keeping the superficial gas velocity high in the heat exchangers, the abrasive nature of the gas will keep the walls of the heat exchangers clean. After the cooling, the gas is filtered by means of a bag filter. The virtually particle free syngas is scrubbed in a water scrubber in order to remove halogen compounds, nitrogen containing compounds, the residual alkali metal and tar compounds. Since cold water is used for the scrubbing process, it has a quenching effect on the gas. This quenching effect results in a temperature drop to approximately 40°C. The final step in the gas cleaning is the removal of sulphur compounds, via hydrodesulphurization and a sulphur guard. The hydrodesulphurization is packed bed with Co-Mo/Al$_2$O$_3$ catalyst for the conversion of organic sulphur compounds (thiophene) and COS into hydrogen sulphide. The sulphur guard is a packed bed of zinc oxide, for adsorption of hydrogen sulphide. The operation temperature of the sulphur guard is around 400°C. Therefore, the gas needs to be heated prior to the sulphur guard. The way of heating in the different gas production plants is described in the appropriate sections about the specific gas production plants.

There are many uncertainties regarding the gas cleaning, especially the scrubber. The effect of the scrubber on the tar and halogen content are uncertain. It is assumed the cleaning system is adequate.

Hydrogen production plant (GP1)

The hydrogen plant (GP1) is the same as the plant considered before and is described in Ref. [26]. In the gas cleaning system of this plant, the gas is first compressed to 35 bar and steam (T=600°C; p=35 bar) is added before it is passed through the sulphur removal. After the sulphur guard, the gas is further heated in a heat exchanger using the hot syngas leaving the gasification reactor. For the conversion of methane in the gas, the gas fed to a steam reforming unit. The steam to carbon ratio is kept above 2.5 in order to prevent carbon deposition [35]. The required steam (T=600°C; p=35 bar) is produced with the residual heat from the plant. The operating temperature of the reformer is 825°C and the pressure is 35 bar. After the reforming process, the gas is cooled to 400°C prior to the water gas shift. The water gas shift (WGS) is performed in two steps, first a high temperature WGS step followed by intermediate cooling to 210°C and secondly a low temperature WGS. This reduces the amount of carbon monoxide in the gas to 05-1 vol% [36, 37]. After the WGS processes, the gas is cooled to 30°C in order to condense the water in the gas. Then, the gas is fed to the pressure swing absorption (PSA) unit. The removal of impurities is done in two steps. In the first step, the carbon dioxide and residual water are removed using activated carbon as a sorbent. In the second step the other impurities like nitrogen are removed. In this second step, zeolites are used for the purification. The waste gas coming from the second step contains significant amounts of hydrogen, carbon monoxide and methane. Therefore, the waste gas is combusted; the heat is used to generate additional electricity in a combined cycle. Most of the electrical power necessary to operate the plant can be generated in this way.
The 99.99% pure hydrogen coming from the PSA is further compressed to 50 bar.

SNG production plant (GP2)

The SNG production plant is based on de the plant as described by Gassner and Maréchal [20, 38].
The gas coming from the scrubber is heated by steam, which is produced with the heat produced in the different parts of the plant. The clean syngas coming from the gas cleaning is fed to a methanation unit for the conversion of syngas into methane. The reaction of syngas into methane is given in Equations (8.1) & (8.2).

$$CO + 3H_2 \rightleftarrows CH_4 + H_2O \qquad \Delta H_r^0 = -206 \, kJ \, mol^{-1} \qquad (8.1)$$

$$CO_2 + 4H_2 \rightleftarrows CH_4 + 2H_2O \qquad \Delta H_r^0 = 165 \, kJ \, mol^{-1} \qquad (8.2)$$
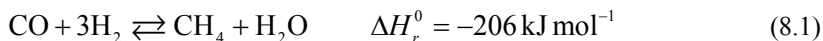
Also the water gas shift reaction is involved in this process; the reaction is given in Equation (8.3).

$$CO + H_2O \rightleftarrows CO_2 + H_2 \qquad \Delta H_r^0 = -41 \, kJ \, mol^{-1} \qquad (8.3)$$
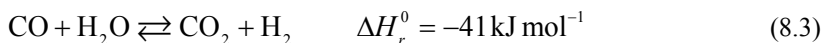
This methanation process is a catalytic process that usually operates in a temperature range of 300-400°C and a pressure above 1 MPa. The most common catalyst used for this process is based on nickel. Therefore, it is important that the syngas is virtually free of sulphur. Sulphur is a known poison for nickel catalysts. To prevent carbon formation/deposition the addition of steam is required. The process is highly exothermic, as can be seen from the reaction enthalpies. Therefore, the process is usually performed in several steps with

intermediate cooling, in order to prevent catalyst deactivation and improve the syngas conversion.

In this system, the methanation process is operated at ambient pressure and at a temperature of 320°C. For the process, an isothermal fluidized bed reactor is used.

After the methanation process the carbon dioxide needs to be removed to improve the quality of the gas suitable for the natural gas grid. For this separation a PSA system is used. There is still a significant amount of hydrogen present in the gas, which needs to be removed. For the removal of the hydrogen, a membrane separator is used. This reactor uses hollow fibre modules made of a polysulfone membrane. The permeate is recycled to the methanation process. The Wobbe index of the gas is 46.1 MJ Nm^{-3} based on the lower heating value (LHV).

Syngas production plant (GP3)

The syngas production plant is the simplest plant of the three gas production plants. Before, the gas coming from the scrubber is passed through to the sulphur removal it is compressed to a pressure of approximately 18.5 bar. This results in a gas temperature of around 400°C. Then the gas is passed through to the sulphur removal. After the complete sulphur removal, the gas is cooled to 30°C in order to condense the water from the gas. The gas is further compressed to 50 bar in two stages with intercooling. During the intercooling, more water is condensed and removed from the gas. After the compression the gas is cooled to 15°C and the condensed water is removed. In Figure 8-2, the flow sheet of the syngas production plant is given.

In Figure 8-2, biomass is fed into the bubbling bed of the gasifier, which is represented by units 2, 3, 4 & 5. The combustor is represented by unit 400. A small amount (3.7 wt%) of flue gas ends up in the syngas this is modelled with valve 500 and stream 501. The raw syngas is cooled in a boiler consisting of economizer (unit 103), an evaporator (unit 106) and a super heater (unit 107). In the boiler steam is produced for the gasification. The cooled syngas is filtered, which is represented by unit 9. Unit 10 is the scrubber. The scrubber gets fresh water extracted from the environment at source 121. The dirty water is removed from the system via sink 125. Before the gas is passed through the sulphur removal (unit 12); it is compressed in unit 13. The clean syngas is then further compressed in units 15 & 17. The water is condensed in units 14, 16 & 18.

The hot flue gas coming from the gasifier (stream 502) is split into two streams. One stream is used to preheat the combustion air in heat exchanger 205. The other stream is used to for the production of steam in a heat recovery steam generator. The steam is produced in a boiler represented by unit 512, 513 & 514. This steam is used to produce electricity with the help of a turbine (unit 155), which is connected to a generator.

8.2.2. Gas transport and distribution grid

The gasses produced in the gas production plants are transported through transport and distribution grid. In the case of the production of SNG the common natural gas distribution network can be used. For the other two cases, it is assumed that a distribution grid is available. In this chapter the assumptions taken for the different grids are similar.

It is assumed that the grid consists of three different pressure levels. The first pressure level is between 60-80 bar for long distance transport, the second level is approximately 20 bar for large consumers the final level is below 1.5 bar for domestic application. In this chapter an energetic efficiency of the gas distribution grid of SNG and syngas is assumed to be 96.5% and for hydrogen it is assumed to be 94% [25]. The exergetic efficiencies of the

distribution grid are assumed to be 1 percentage point lower, so 95.5% for syngas and SNG and 93% for hydrogen.

The efficiency of the hydrogen grid is lower due to the small molecular size of hydrogen; leaks will be greater then for natural gas or syngas.
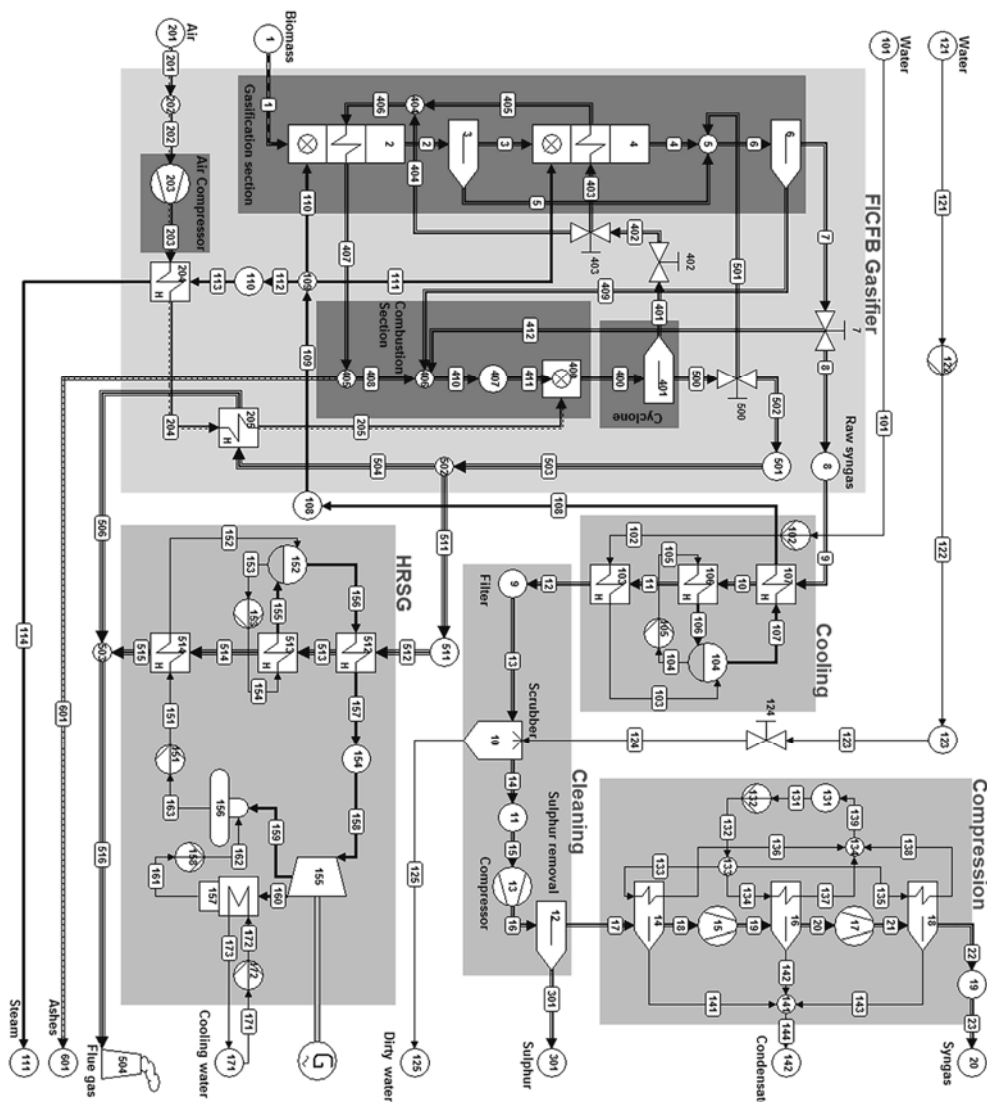
Figure 8-2 flow sheet of syngas production plant (GP3)

8.2.3. μ-CHP

The μ-CHP is based on a SOFC combined with a compression heat pump. The fuel cell is designed to generate approximately 1 kW of electrical power. Due to the limited efficiency and the high operating temperature of the SOFC also an amount of heat is produced. This amount is approximately 1kW and is assumed not to be sufficient for domestic use;

therefore the fuel cell is combined with a heat pump. The heat pump produces additional heat, so the overall heat production is around 3 kW.

The electrical power and heat demand of houses are continuously fluctuating; therefore the μ-CHP system will continuously cycle between full and part load. However, for a first estimate all calculations in this chapter are based on design load, and the additional effect of fluctuations in demands are not considered. It is expected that the relative differences between the alternatives are sufficiently represented by the conditions at design load.

The SOFC operates at 800°C and near atmospheric pressure. The net electrical power output is set to 1 kW and the heat output is determined by the system. In Figure 8-3, a general flow sheet is given for the μ-CHP system. Unit x, pipe x, units and pipes with numbers 201-203 are only in the hydrogen fuelled system. The humidification is added to improve the kinetics of the hydrogen oxidation at the anode of the fuel cell. The other two systems do not have humidification. The hydrogen fuelled system does not have a desulphurizer, since it is assumed no odorizer is added to the hydrogen. Also there is no anode gas recycle in hydrogen fuelled systems.
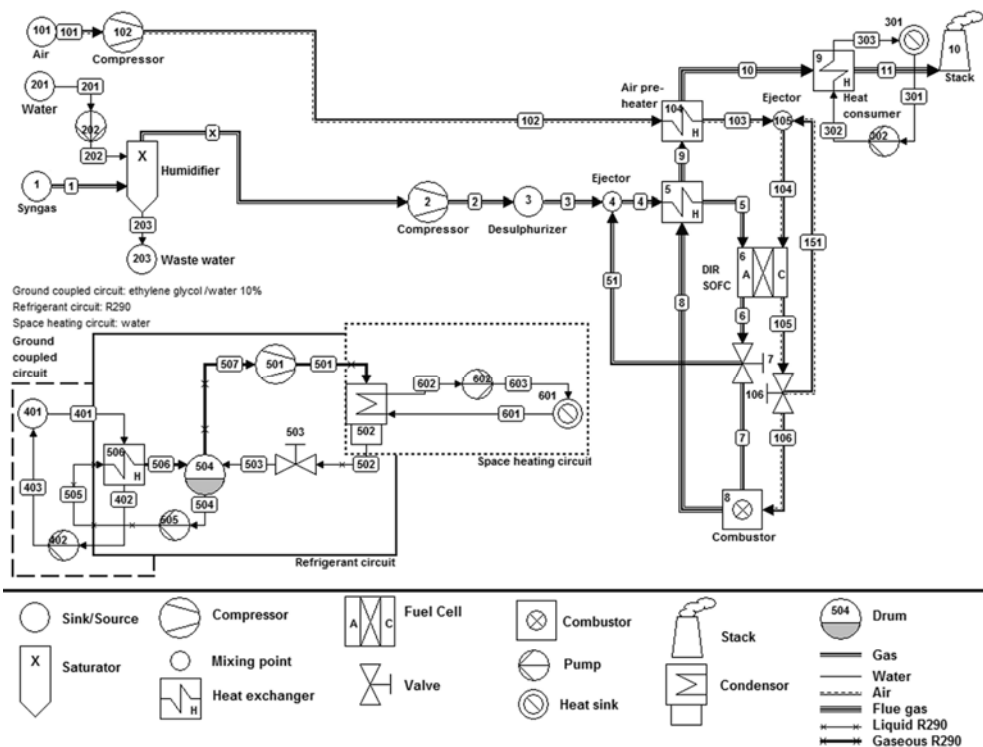
Figure 8-3 general flow sheet of the μ-CHP system

The hydrogen fuelled SOFC system starts with the humidification of the gas (unit x, in Figure 8-3). The moisture content of the gas after humidification is 5 mole%. The residual water leaving the humidifier (stream 203) in removed from the system. A compressor (unit 2) is then used to overcome the pressure drop in the system. The hydrogen is heated in a heat exchanger (unit 5) to 750°C, before it enters the anode of the SOFC. Air (source 101) is blown into the system with the help of a blower (unit 102). This air is also heated in a

heat exchanger (unit 104) to approximately 600°C. Before the air enters the cathode side of the SOFC, it is mixed with a recycle stream with the help of an ejector (unit 105). The SOFC (unit 6) operates at a temperature of 800°C and the off-gas leave the fuel cell at a temperature of 850°C. Part of the air flow (60%) is recycled over the cathode of the fuel cell (stream 151). After the fuel cell, the depleted anode off-gas (stream 7) and the residual air (stream 106) are fed to an afterburner (unit 8), in order to combust the residual hydrogen. The hot flue gasses (±1000°C) are used to heat the fuel and the air coming into the system. A part of the residual heat is used to heat water for the space heating system (unit 301).

The SNG fed μ-CHP system uses a direct internal reforming (DIR) SOFC for the conversion of methane in electricity (see Figure 8-3). As SNG enters the system (source 1), it is compressed to compensate for the pressure drops in the system (unit 2). After the compression the gas is passed through a desulphurizer (unit 3). The desulphurizer is required because it is assumed the SNG is mixed with the natural gas in the grid. This natural gas contains an odorizer, which contains sulphur. After the desulphurizer, the gas is mixed with recycled anode off-gas in order to increase the steam content of the gas stream (unit 4). The resulting gas stream is further heated in a heat exchanger (unit 5) before it is fed to the anode of the DIR-SOFC (unit 6).
Air is taken from the environment (source 101) and blown into the system with the help of a blower (unit 102). The air is heated in a heat exchanger (unit 104) and mixed with a recycle stream from the cathode off-gas (unit 105). The air mixture is fed into the cathode of the fuel cell.
The off-gas from the anode is recycled for 60% (stream 51) and the remainder (stream 7) is fed to a combustor (unit 8). Also the off-gasses of the cathode are partly recycled for 60% (stream 151); the residual off-gasses (stream 106) are used as oxidant in the combustor to combust the anode off-gasses. The hot flue gas from the combustor is used to heat the fuel, the air and some water for the space heating system (unit 301).
The μ-CHP system fuelled with syngas is similar to the SNG fed system.

A ground coupled heat pump is used for the production of additional heat. The heat pump consists of three circuits (see Figure 8-3), the ground coupled circuit, the refrigerant circuit and the space heating circuit. The ground coupled circuit extracts heat from the soil (source 401) using a 10% ethylene glycol/water mixture as a working fluid. This circuit transfers its heat to the refrigerant circuit which uses R290 as a working fluid. The heat extracted from the soil is used to evaporate the refrigerant in unit 506. The evaporated R290 is compressed to 24 bar using a compressor (unit 501). In a condenser (unit 502) the R290 is condensed. The heat released during the condensation process is transferred to the space heating circuit (heat sink 601). After the condensation process the R290 is throttled (valve 503) to a lower pressure of 4.8 bar and evaporated again.
The space heating system uses hot water of 65°C for heating. When the water leaves the space heating system, it has a temperature of 45°C. The pressure in the space heating system is 1.5 bar.

8.3. Modelling
The designed systems have been modelled in the flow sheeting program Cycle-Tempo [39]. This program is especially designed for the thermodynamic evaluation of energy conversion systems.

Models have been created for the hydrogen production plant, the syngas production plant and the μ-CHP systems. The results for the SNG production are taken from the paper of Gassner and Maréchal [38]. The calculated and given gas compositions are used in the models of the μ-CHP systems to determine the efficiency of the μ-CHP systems. By combining these results with the given energetic efficiencies in the paper the overall chain performance has been determined.

Based on the energetic efficiencies given in Ref. [38] and the biomass input the mass flow of produced SNG is determined. With this mass flow a new exergetic efficiency has been determined for the SNG production process. This is done because Cycle-Tempo uses the method of Baehr [40] for the calculations of exergy values and Gassner and Maréchal [38] uses the method of Szargut et al. [41]. In order to compare the results every value is calculated by the method Baehr [40].

The biomass used in the systems is similar for all the systems. It is A-quality wood with a moisture content of 30 wt% on a dry basis; the dry composition of the biomass is given in Table 8-1.

Table 8-1 dry composition of the used biomass [38]

	Amount	Unit
Carbon (C)	50.93	wt%
Hydrogen (H)	6.11	wt%
Oxygen (O)	42.16	wt%
Nitrogen (N)	0.80	wt%
Moisture content	30	wt%
HHV (dry)	19200	kJ kg^{-1}
Exergy (wet)*	13970	kJ kg^{-1}

*) Exergy of the biomass is determined using the method of Baehr [42]

Some general assumptions have been made:
- The systems are operated in steady state.
- The thermal input of the gasifier is 48.5 MW (Lower Heating Value).
- The heat exchangers are operated in counter current flow.
- There is no fouling caused by tars and/or alkali metal compounds.
- The gas cleaning systems are able to achieve the required gas purity.
- Processes are adiabatic.

Table 8-2 comparison of the gas composition in vol% with the literature [43]

Component	Calculated data	Data [38]	Literature data
Hydrogen (H$_2$)	39.7	39.5	37.3
Carbon monoxide (CO)	27.7	28.0	29.4
Methane (CH$_4$)	11.0	9.0	8.8
Carbon dioxide (CO$_2$)	14.5	15.3	16.2
Nitrogen (N$_2$)	2.9	2.9	2.9
Water (H$_2$O)	4.2	3.5	3.6
Ethene (C$_2$H$_4$)	-	1.8	1.8

The model of the hydrogen production plant is similar to the model described in Ref. [26]. The model of the syngas production plant is only based on the gasifier and the gas cleaning of the hydrogen production plant as described in Ref. [26]. The model of the gasification and gas cleaning is validated by comparing the syngas composition with the syngas

composition given in literature (Ref. [43]). In the literature biomass is used with a moisture content of 10 wt%. Therefore, the model is validated on basis of biomass with a moisture content of 10 wt%. The results are given in Table 8-2.

In Table 8-2, the calculated composition of the syngas is compared with literature results. It appears that the calculated composition does not significantly deviate from the literature data. The Cycle-Tempo models do not predict any ethene or higher hydrocarbons. The calculated methane content on other hand is higher than the measured data. This higher value compensates the lack of ethene. The amount of carbon dioxide is slightly underestimated and the amount of water in the gas is somewhat overestimated. The water content of the gas could be further reduced by increasing the water flow through the scrubber. This would reduce the outlet temperature of the scrubber, but this also would result in a lower temperature of the gas leaving the scrubber than indicated in the literature [43].

In Table 8-3, the input parameters for the syngas production plant (GP3) are given. The numbers of the units correspond with the numbers in Figure 8-2.

The SOFC fuel cell model available in Cycle-Tempo is used to calculate the performance of the fuel cell. A short description of the fuel cell model is given in Ref. [13], and can also be found on the Cycle-Tempo website [39]. In Table 8-4, the input parameter for the μ-CHP system are given. The numbers of the equipment correspond with the numbers in Figure 8-3.

Cycle-Tempo can also perform exergy calculations. The exergy values of all flows considered in the system flow diagram are calculated based on previously calculated pressure, temperature and chemical composition. Thermo-mechanical (physical) exergy and chemical exergy are calculated separately. The calculation of the chemical exergy requires the definition of an environment that determines the exergy of any considered component at reference temperature and pressure. In Table 8-5, the environment applied for this study is given. This environmental composition is based on the composition of air saturated with water at the environmental conditions specified in Table 8-5.

The elements in the ash as well as chlorine sulphur and alkali metals are not defined in the chemical composition on the environment. Therefore, components containing these elements are assumed to have zero exergy. Since the concentrations of these elements in the biomass are very low, this assumption would result only in a negligible error.

Table 8-3 input parameters syngas production plant (GP3)

No.	Description	Input	No.	Description	Input
		Gasifier			Gas cleaning
2	Gasifier	p_r=1, T_r=180, S/F=0.2 p_{out}=1.47, T_{out}=800	9	Sink/Source	Δp=005, Δh=0
3	Separator	Δp=0, ΔT=0, CH_4 84%; CO_2 100%	10	Scrubber	Δp_{gas}=0.02, T_{ingas}=120
4	Gasifier	p_r=2000, T_r=2000, S/F=0.143 p_{out}=1.47, T_{out}=800	11	Sink/Source	Δp=0, ΔT=0
5	Node	Δp=0	12	Separator	Δp=0.1, ΔT=0, H_2S:100%
6	Separator	Δp=0.01, ΔT=0, C:100%, SiO2: 100%	13	Compressor	PR=14, η_i=0.80, η_m=0.99
7	Valve	Δp=0, 5% mass flow pipe 7 to pipe 412	122	Pump	p_{out}=1.5, η_i=0.75, η_m=0.99
108	Sink/Source	Δp=0, ΔT=0	123	Sink/Source	Δp=0, ΔT=0
109	Node	Δp=0	124	Valve	6X mass flow pipe 13 for pipe 124
110	Sink/Source	Δp=0, ΔT=0	14	Moisture separator	Δp_C=0.02 , Δp_H=0.1, $T_{out,H}$=30, $T_{out,C}$=20
202	Node	Δp=0	15	Compressor	PR=1.6, η_i=0.80, η_m=0.99
203	Compressor	p_{out}=1.5, η_i=0.80, η_m=0.99	16	Moisture separator	Δp_C=0.02 , Δp_H=0.2, $T_{out,H}$=30, $T_{out,C}$=20
204	Heat exchanger	Δp_C=0.02, Δp_H=0.02, $T_{out,H}$=115	17	Compressor	p_{out}=50.4, η_i=0.80, η_m=0.99
205	Heat exchanger	Δp_C=0.02, Δp_H=0.02, $T_{out,C}$=400, $\Delta T_{pinch,C}$=10	18	Moisture separator	Δp_C=0.02 , Δp_H=0.4, $T_{out,H}$=30, $T_{out,C}$=20
400	Combustor	p_r=1, T_r=180, λ=1.1	19	Sink/Source	Δp=0, T_{out}=15
401	Separator	Δp=0.01, ΔT=0, SiO2: 100%	131	Sink/Source	p_{in}=1.01325, T_{in}=20, T_{out}=15, Δp=0
402	Valve	Δp=0, mass flow pipe 402 18.3 kg/s	132	Pump	η_i=0.75, η_m=0.99
403	Valve	Δp=0, 80% mass flow pipe 402 to pipe 403	133	Node	Δp=0
404	Node	Δp=0	134	Node	Δp=0
405	Node	Δp=0.01			Heat recovery
406	Node	Δp=0	151	Pump	η_i=0.75, η_m=0.99
407	Sink/Source	Δp=0, Est. T_{out}=1000, WFOT=90	152	Drum	CRATIO=4
500	Valve	Δp=0, 0.3% volume flow pipe 500 to pipe 501	153	Pump	η_i=0.75, η_m=0.99
501	Sink/Source	Δp=0, ΔT=0	154	Sink/Source	Δp=1.2, ΔH=-2
		Cooling	155	Turbine	p_{in}=50, η_i=0.88
8	Sink/Source	Δp=0, ΔT=0	156	Deaerator	p_{in}=1.01325, Δp=0
102	Pump	p_{out}=1.5, η_i=0.75, η_m=0.99	157	Condenser	p_{out}=0.03, $T_{out,C}$=19, Δp_C=0.2
103	Heat exchanger	Δp_C=0.02, Δp_H=0.02, $\Delta T_{pinch,H}$=25	158	Pump	η_i=0.75, η_m=0.99
104	Drum	CRATIO=4	171	Sink/Source	p_{out}=1.01325, T_{out}=12
105	Pump	η_i=0.75, η_m=0.99	172	Pump	η_i=0.75, η_m=0.99
106	Heat exchanger	Δp_C=0.02, Δp_H=0.02, $\Delta T_{pinch,C}$=20	502	Node	Δp=0
107	Heat exchanger	Δp_C=0.02, Δp_H=0.02, $T_{out,C}$=600	503	Node	Δp=0
			511	Sink/Source	Δp=0, ΔT=0
			512	Heat exchanger	Δp_C=1, Δp_H=0.02, $T_{out,C}$=540
			513	Heat exchanger	Δp_C=1, Δp_H=0.02, $\Delta T_{pinch,C}$=92
			514	Heat exchanger	Δp_C=1, Δp_H=0.02, $\Delta T_{pinch,C}$=10

Table 8-4 input parameters of the µ-CHP systems

No.	Description	Input
1	Sink/Source	p_{out}=1.01325, T_{out}=15
2	Compressor	η_i=0.68
3	Sink/Source	Δp=0.1
4	Node	Δp=0.09
5	Heat exchanger	$p_{in,C}$=1.23325, Δp_C=0.05, $T_{out,C}$=750, Δp_H=0.03
6	Fuel cell	SOFC-DIR, Δp_{an}=0.04, Δp_{cat}=0.06, T_{out}=850, DCAC=0.92, p_{FC}=1.16325, T_{FC}=800, U_{fuel}=80%
7	Valve (hydrogen) Valve (SNG) Valve (syngas)	0% mass flow pipe 6 to pipe 51 60% mass flow pipe 6 to pipe 51 60% mass flow pipe 6 to pipe 51
8	Combustor	Δp=0.02, T_r=900, p_r=1.13325
9	Heat exchanger	Δp_C=0.04, $T_{in,C}$=45, $T_{out,C}$=65, Δp_H=0.04, $T_{out,H}$=50
10	Stack	
101	Sink/source	p_{out}=1.01325, T_{out}=15
102	Compressor	η_i=0.73
104	Heat exchanger	Δp_C=0.06, Δp_H=0.04
105	Node	Δp=0
106	Valve	60% mass flow pipe 105 to pipe 151
301	Heat sink	p_{out}=1.01325, Δp_C=0
302	Pump	η_i=0.6
401	Sink/Source	Δp=0.02, T_{out}=8
402	Pump	p_{out}=1.05325, η_i=0.6
501	Compressor	p_{out}=24, η_i=0.8
502	Condenser	Δp_C=0.03, $T_{out,H}$=55, Δp_H=0.52
503	Valve (hydrogen) Valve (SNG) Valve (syngas)	Δp=18.68, mass flow pipe 104=4.3 Δp=18.68, mass flow pipe 104=6.335 Δp=18.68, mass flow pipe 104=5.073
504	Drum	
505	Pump	η_i=0.75
506	Heat exchanger	Δp_C=0.096, $T_{out,C}$=3, Δp_H=0.02, $T_{out,H}$=6.8
601	Heat sink	p_{out}=1.5, Δp=0.03, T_{in}=65, T_{out}=45
602	Pump	η_i=0.6
201	Sink/Source	p_{out}=1.01325, T_{out}=20
202	Pump	η_i=0.6
X	Humidifier	Δp_{gas}=0, $T_{out,gas}$=15, Δp_W=0.02, $T_{out,W}$=19, RELHUM=0.03

Table 8-5 environmental composition [40] and conditions

Component	Mole fraction	Component	Mole fraction
Ar	0.91	N_2	76.78
CO_2	0.03	O_2	20.60
H_2O	1.68		
Environmental conditions			
Temperature	15°C	Pressure	1.01325 bar

The thermal efficiencies calculated in this work are based on LHV. The thermal efficiencies for the gas production plants are calculated using Equation (8.4).

$$\eta_{th,gas} = \frac{\phi_{m,product} \cdot LHV_{product} + \sum P_{el,out} - \sum P_{el,in}}{\phi_{m,biomass} \cdot LHV_{biomass}} \tag{8.4}$$

Here, $\phi_{m,product}$ is the mass flow of the product gas, $\phi_{m,biomass}$ is the mass flow of the biomass, $P_{el,out}$ is the electrical output of the system, $P_{el,in}$ is the electrical input of the system, $LHV_{product}$ is the lower heating value of the product gas and $LHV_{biomass}$ is the lower heating value of the biomass.

The electrical and overall thermal efficiency for the μ-CHP systems are calculated using Equations (8.5) & (8.6).

$$\eta_{th,el} = \frac{\sum P_{el,out} - \sum P_{el,in}}{\phi_{m,fuel} \cdot LHV_{fuel}} \tag{8.5}$$

$$\eta_{th,tot} = \frac{\sum P_{el,out} + Q - \sum P_{el,in}}{\phi_{m,fuel} \cdot LHV_{fuel}} \tag{8.6}$$

Here, $\phi_{m,fuel}$ is the mass flow of the fuel into the μ-CHP system, Q is the usable heat produced by the system and LHV_{fuel} is the lower heating value of the fuel.

The exergy efficiency of the gas production plant is given as

$$\eta_{ex,gas} = \frac{Ex_{product,gas} + \sum P_{el,out} - \sum P_{el,in}}{Ex_{biomass}} \tag{8.7}$$

$Ex_{product,gas}$ is the exergy of the produced gas and $Ex_{biomass}$ is the exergy of the used biomass. The electrical and total exergy efficiencies of the μ-CHP systems can be calculated using equations (8.8) & (8.9).

$$\eta_{ex,el} = \frac{\sum P_{el,out} - \sum P_{el,in}}{Ex_{fuel}} \tag{8.8}$$

$$\eta_{ex,tot} = \frac{\sum P_{el,out} + Ex_{heat} - \sum P_{el,in}}{Ex_{fuel}} \tag{8.9}$$

Here, Ex_{heat} is the exergy of the usable heat produced by the system and Ex_{fuel} is the exergy of the fuel put into the system.

8.4. Results

8.4.1. Gas production

The biomass input in all the gas production plants is assumed to be similar. The mass flow of biomass into the gas production plants is set to 4.1 kg s^{-1}, this results in a thermal input of 48.5 MJ kg^{-1} based on the LHV. The steam to biomass ratio on a dry basis is ±0.5 kg kg^{-1}. The steam used in all the systems has a temperature of 600°C. The resulting composition of the syngas at the exit of the gasifier is given in Table 8-6.

Table 8-6 dry composition of syngas leaving the gasifier in vol%

Component	Output model	Data GP2 [38]
Hydrogen (H$_2$)	40.0	41.9
Carbon monoxide (CO)	19.9	22.8
Methane (CH$_4$)	14.4	11.7
Carbon dioxide (CO$_2$)	21.8	20.6
Nitrogen (N$_2$)	3.8	0.5
Other	0.1	2.5

The residual char and a small part of the produced syngas is being combusted to provide the heat required for the endothermic gasification process. For the combustion, a 10% excess air is being used. In GP1, the amount of syngas to the combustion section of the gasifier is much higher then for the other two gas production plants (GP2 & GP3). This is done to increase the flue gas temperature from the combustion section. This extra produced heat is used in the reformer, to perform the endothermic reforming reactions. In this way no additional fuel was required for the reformer.

Hydrogen production (GP1)

In the gasification part of the hydrogen production plant, 16 wt% of the produced syngas is fed to the combustor. For the combustion of this gas and the char, 7.1 kg s^{-1} of air is fed to the combustor. The combustion air is preheated to a temperature of 400°C. This results in a flue gas stream of 8.1 kg s^{-1} with a temperature of 1245°C. The mass flow of syngas is 4.5 kg s^{-1} and it has a temperature of 811°C. The raw syngas is passed to the cleaning process. During the gas cleaning process the composition of the syngas is not supposed to change. Only the water content of the gas will change. The water fraction changes from 41.4 mole% to 7.1 mole%. For the scrubbing process is 34.7 kg s^{-1} water used; the water enters the scrubber at a temperature of 15°C and a pressure of 1.4 bar. After the scrubber the gas is compressed to 36 bar. Before the gas is desulphurized 1.4 kg s^{-1} of steam is added to the gas, in order to increase the water content. The temperature and pressure of the steam are 600°C and 36 bar, respectively. After the desulphurization, the clean syngas is fed into a steam reformer. In the reformer a large part (70%) of the methane is converted. The hot flue gasses coming from the gasification section are being used to supply heat to the reforming process. During the reforming is also 1.4 kg s^{-1} steam added. After the reforming, the carbon monoxide in the syngas is converted into hydrogen in a two stage WGS process. The heat extracted during the cooling prior and between the high and low temperature WGS is used to produce steam. After the WGS, the gas is further cooled before it is transferred to the pressure swing adsorption (PSA) unit. During the cooling, a large part of the water in the gas is condensed and removed. In the first step of the PSA unit, the residual water and carbon dioxide are being removed from the gas. Then in the next step all the other compounds, like nitrogen, are being removed from the gas. This results in 0.3 kg s^{-1} of 99.99% pure hydrogen, a stream of 5.2 kg s^{-1} containing water and CO$_2$ and a stream of 0.3 kg s^{-1} with all the impurities. This last stream of impurities contains a reasonable amount of combustibles. Therefore, it is combusted and the produced heat is used in a combined cycle for the generation of electricity. The overall generated electrical power is 5.7 MW. The whole hydrogen production process consumes 6.0 MW of electricity. Therefore, a small amount of electrical power (0.3 MW) has to be supplied from outside the plant.

SNG production (GP2)

In this chapter, some of the results of Gassner et al. [38] are being used to determine the chain efficiencies. The composition of the product of the SNG plant is given in Table 8-7, as well as the composition of the produced gas for the other gas production processes.

Table 8-7 dry composition of the gasses produced in the different gas production plants

Component	GP1	GP2 [38]	GP3
Hydrogen (H_2)	100	4.8	40.1
Methane (CH_4)	-	92.0	14.4
Carbon monoxide (CO)	-	0.1	21.8
Carbon dioxide (CO_2)	-	1.0	19.9
Nitrogen (N_2)	-	2.1	3.8

The thermal efficiencies given in the paper of Gassner et al. [38] are used for the calculation of the SNG mass flow and electricity production. The mass flow of produced SNG was found to be 0.7 kg s^{-1}. This mass flow is based on a biomass input of 4.1 kg s^{-1}. Besides SNG, there is also an amount of electricity produced. Based on the total thermal efficiency, the amount of electrical power produced is 4.2 MW. This amount of electricity is the net produced electrical power. This produced electricity is considered as a product.

Syngas production (GP3)

In the gasification part of the syngas production plant, 5 wt% of the produced syngas is fed to the combustion part of the gasification process. This gas is combusted together with the residual char from the gasification process. 5.5 kg s^{-1} air is fed to the combustor at a temperature of 400°C. This results in a flue gas stream of 5.9 kg s^{-1} at a temperature of 1048°C. The mass flow of the raw syngas is 5.0 kg s^{-1} at a temperature of 806°C.
In the gas cleaning system, the gas is first cooled to 120°C. The extracted heat is used to produce steam of 600°C. Then the gas is filtered in bag filter. After the filtration, the gas is scrubbed in a water scrubber. Here the water content of the gas drops from 41.3 mole% to 8.1 mole%. The scrubber uses 30.2 kg s^{-1} water with a temperature of 15°C. This causes a temperature drop of the gas. The gas leaving the scrubber has a temperature of 47°C. The gas is compressed to 18.6 bar before it enters the desulphurization system. The compression leads to a temperature increase, so the temperature of the gas entering the desulphurization is 400°C. After the desulphurization, the gas is cooled and further compressed. During the cooling, water is condensed and removed. The composition of the product leaving the syngas plant is given in Table 8-7.
The hot flue gasses coming from the combustion part of the gasifier are used to preheat the combustion air and to produce steam in heat recovery steam generator (HRSG). The generated steam is used in a Rankine cycle to generate some electricity. In the Rankine cycle, 1.9 MW of electricity is generated. The syngas production plant requires 2.9 MW of electricity. Therefore, 1.0 MW of electricity has to be supplied from outside the plant.

The three gas production plants

All the gas production plants produce their gas at a pressure of 50 bar and a temperature of 25°C.
For all the gas production plants, the energy and exergy efficiencies are determined with equations (8.4) and (8.7), respectively. In Table 8-8, the energy and exergy efficiencies of the different gas production plants are given.

Table 8-8 the energy and exergy efficiencies of the different gas production plants

	GP1	GP2	GP3
Energy efficiency	63.5	75.0	85.2
Exergy efficiency	54.9	65.2	75.2

In Figure 8-4, the exergy flow diagrams of GP1 and GP3 are given.
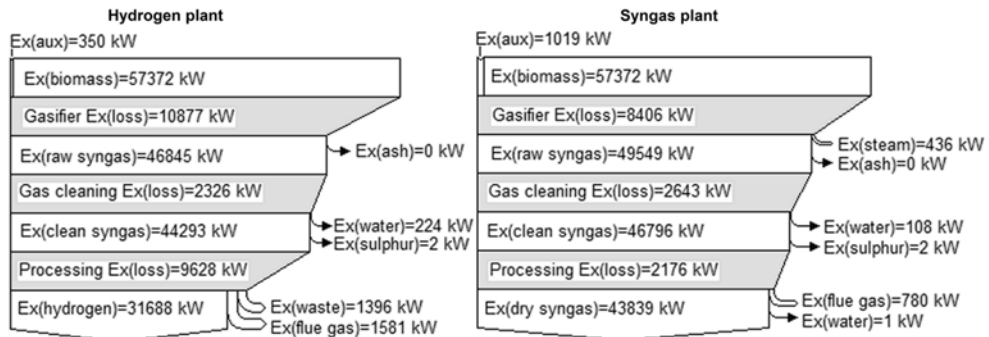
Figure 8-4 exergy flow diagrams of the gas production plants GP1 (left) and GP3 (right)

8.4.2. Gas distribution

The gas coming from the different gas production plants is at a pressure of 50 bar. The high pressure network is assumed to have a pressure of 70 bar. Therefore, the gas from the gas production plant has to be compressed to 70 bar, before it is fed into the high pressure network. The heat generated during the compression is assumed to be lost. By multiplying the efficiencies of the gas production plants and the gas distribution, the efficiency of the gas production and distribution can be found. For the hydrogen production and distribution the exergy efficiency becomes 51.1%; for SNG this is 62.3 and for syngas 71.8%.

Table 8-9 results for the μ-CHP system fuelled with different fuels

Fuel	Hydrogen	SNG	Syngas
Fuel input [g s^{-1}]	0.03	0.06	0.23
Air input [g s^{-1}]	3.73	2.19	3.49
Voltage fuel cell [V]	0.78	0.73	0.72
Fuel cell area [m^2]	0.43	0.50	0.49
Power consumption heat pump [W]	429	629	505
Total auxiliary power [W]	544	699	619
Heat production SOFC [W]	1657	1021	1416
Heat production heat pump [W]	1344	1979	1585
Electrical exergy efficiency [%]	30.3	33.4	31.0
Overall thermal efficiency [%]	118.6	138.4	124.7
Overall exergy efficiency [%]	41.3	45.6	42.3

8.4.3. μ-CHP

As mentioned earlier, two different μ-CHP systems have been considered. The first is fuelled with hydrogen the other system is fuelled with either SNG or syngas. The main difference between the two systems is that the hydrogen fuelled systems does not have an

anode off-gas recycle and the systems fuelled with either SNG or syngas do. It is assumed that the μ-CHP unit generates 1 kW electricity and a heat flow of 3 kW. Since the fuel cell is not able to produce sufficient heat the systems have been coupled with a ground coupled heat pump. Some data is given in Table 8-9 for the μ-CHP systems using different types of fuels.

The calculated coefficient of performance of the compression heat pump is 3.2.
In Figure 8-5, exergy flow diagrams are given for the μ-CHP systems using different types of fuels. The unit numbers which are included in the different system sections as indicated in Figure 8-5 are given in Table 8-10.
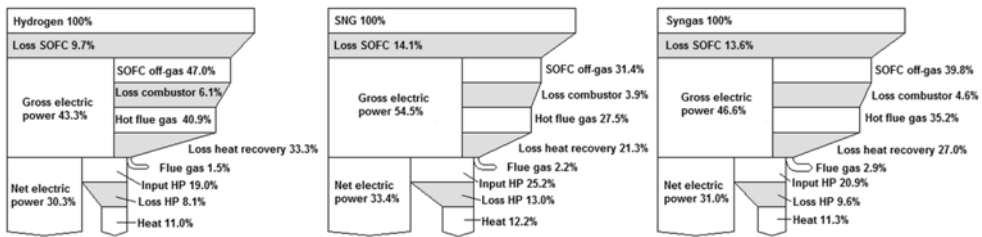
Figure 8-5 exergy flow diagrams of the μ-CHP systems using different types of fuels

Table 8-10 the units included in the different system sections as indicated in Figure 8-5

Fuel	Hydrogen	SNG	Syngas
SOFC	2, x, 6, 102, 105, 106	2, 3, 4, 6, 7, 102, 105, 106	2, 3, 4, 6, 7, 102, 105, 106
Combustor	8	8	8
Heat recovery	5, 9, 104, 301, 302	5, 9, 104, 301, 302	5, 9, 104, 301, 302
Heat pump (HP)	401, 402, 501, 502, 503, 504, 505, 506, 601, 602	401, 402, 501, 502, 503, 504, 505, 506, 601, 602	401, 402, 501, 502, 503, 504, 505, 506, 601, 602

8.4.4. The whole chain from biomass towards heat and power

For the different models in the chain, additional model results and details are supplied in Appendix E, F & G.
To determined the overall chain exergy efficiency from biomass towards electricity, the exergy efficiency of the gas production and distribution needs to be multiplied by the electrical exergy efficiency of the μ-CHP. For the exergy efficiency of the whole chain towards heat and power, the exergy efficiency of the gas production and distribution needs to be multiplied by the overall exergy efficiency of the μ-CHP system. In Table 8-11, the results are given.

Table 8-11 efficiencies for the whole chain

	GP1	GP2	GP3
Fuel	Hydrogen	SNG	Syngas
Electric energy efficiency of the chain [%]	17.8	25.1	25.7
Electric exergy efficiency of the chain [%]	15.5	20.8	22.2
Total energy efficiency of the chain [%]	71.0	100.4	102.7
Total exergy efficiency of the chain [%]	21.1	28.4	30.4
Number of CHP units that could be fuelled	9250	11196	13177

There is also an indication given for the number of μ-CHP units that can be fuelled by one single gas production plant based on the same amount of biomass input. This value is calculated by dividing the output of the gas production plant by the fuel input of the μ-CHP. In Figure 8-6, the exergy flow diagrams of the different chains are given.
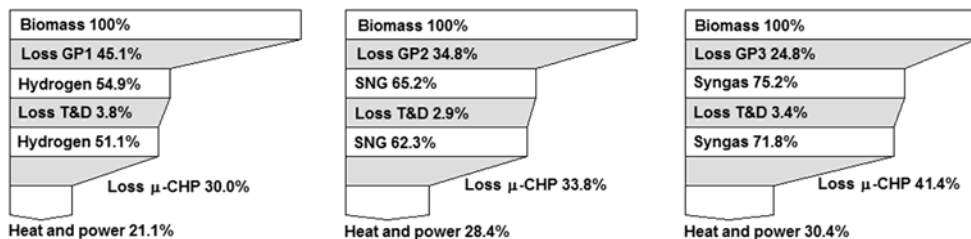
Figure 8-6 exergy flow diagrams of the different chains of biomass towards heat and power

8.5. Discussion

The hydrogen production plant (GP1) has the lowest efficiency, this is caused by the processing and purification. A part of the valuable hydrogen is lost during the purification; also thermodynamic losses occur during the processing and purification. The other two gas production plants (GP2 & GP3) have lower losses resulting in a higher efficiency. This can also be observed from the exergy flow diagrams in Figure 8-4 and Figure 8-6. The SNG plant produces besides SNG also an amount of electricity, which is considered as a product. This also influences the total efficiency. In GP1 and GP3, the syngas is compressed without intercooling. In this way the required temperature for the sulphur removal could be obtained. When the gas was compressed with intercooling, the efficiencies of both plants would be slightly higher, because compression with intercooling is more efficient. On the other hand, the temperature of the gas has to be raised in a different way. For instance, heat of the hot flue gas coming from the FICFB could be used to raise the temperature of the syngas.

There are some differences in the exergy efficiencies calculated and reported for the SNG plant. The main cause is the different method of calculation of the exergy values, in particular for the biomass. In the paper of Gassner and Maréchal [38] the efficiencies and exergy value of the biomass are based on the dry weight of the biomass. The calculations in this paper are based on the 'wet' weight of biomass. Also the method for the calculation of the exergy value for the biomass is different. Gassner and Maréchal[38] based their calculation of the method described by Szargut [41]. In this paper, the method described by Baehr [42] is used. The method described by Szargut [41] is based on an empirically derived equation for the exergy of biomass. Baehr [42] on the other hand describes a method to determine the entropy value for solid fuels (coal), based on the entropy values for other compounds. Based on this entropy value, the chemical exergy of the solid fuel can be determined.

In order to make the results comparable; one single method for the calculation of the exergy has been used. Since most of the models are based on the method described by Baehr [42], this method is used for all the systems.

From Table 8-9, it becomes clear that the use of thermal efficiencies is not appropriate, because of the overall thermal efficiencies being above 100%. These thermal efficiencies ignore the thermodynamic losses that occur in these processes. The exergy efficiencies give

a true indication of the performance. From the same table, it can be seen that the SNG fuelled system has the highest electrical and overall exergy efficiency.

The higher efficiency of the SNG fuelled μ-CHP system is caused by the better integration of heat in the fuel cell. The endothermic reforming gets the heat from the electrochemical conversion of hydrogen. Due to this integration the fuel cell requires less cooling by air, which results in lower auxiliary demand. In Table 8-9, the demanded auxiliary power is for the SNG fuelled system the highest. This higher value is caused by the heat pump and not by the auxiliaries of the fuel cell. Due to the better heat integration in the fuel cell, the amount of heat available for space heating is also smaller. Therefore, the heat pump has to supply more heat in order to meet the 3 kW demand. This can also be observed from Figure 8-5, the losses for the heat recovery are significant lower for the SNG fuelled system than for the other systems.

The losses over the whole chain of biomass towards heat and power are mainly caused by the gas production and the μ-CHP, as can be seen in Figure 8-6. The transport and distribution hardly influences the overall performance.

The heat and electrical power demand in a household are strongly fluctuating. A μ-CHP system must be able to manage these fluctuations. The connection to a grid and the application of heat buffers can help to cope with large fluctuations in demand of electrical power and heat. Variations in the load are not considered in this study; the response of the system on different heat and power demands is beyond the scope of this work. This study is limited to the systems performance at design load. Actual μ-CHP systems will operate at part load for most of the time. This will influence the efficiencies of the μ-CHP system. If comparing different technologies, using systems with almost similar off-design behaviour, a comparison of design load conditions will be decisive (if differences are large enough). The SOFC can in principle have a higher conversion efficiency, because of the higher cell voltage at part load conditions.

8.6. Conclusions

The combination of centralized fuel production with decentralized heat and power production with SOFC has been assessed by modelling the considered system alternatives in Cycle-Tempo. The fuel production is based in biomass gasification using a FICFB gasifier. SOFC units combined with heat pumps are used for the decentralized heat and power production. Three fuel production plants have been considered; a hydrogen production plant, a synthetic natural gas plant and a syngas plant. Two of these plants, the hydrogen plant and the syngas plant, have been modelled in Cycle-Tempo. The SNG plant performance is extracted from Gassner and Maréchal [38].

The hydrogen plant is called GP1 and it produces 99.99% pure hydrogen with an exergy efficiency of 54.9%. The SNG plant is called GP2 and has an exergy efficiency of 65.2%. The syngas plant (GP3) has an exergy efficiency of 75.2%. The gas produced in these plants is assumed to be fed into a gas distribution grid.

The distribution grid is assumed to have an exergy efficiency of 93.0% for hydrogen and 95.5% for SNG and syngas.

Decentralized heat and power production is supposed to occur in μ-CHP units. Each unit generates 1 kW of electricity and 3 kW of heat. The μ-CHP units are connected to the gas distribution grid. By comparing the units fuelled with hydrogen, SNG and syngas, the effect of the fuel on the performance of the μ-CHP units is evaluated. Since the SOFC system is not able to produce all the demanded heat (3 kW), it is coupled with a ground coupled heat pump.

The total exergy efficiencies (electricity and heat) for the hydrogen fuelled µ-CHP system is 41.3%. For the SNG and syngas fuelled units these efficiencies are 45.6% and 42.3%, respectively.

The whole chain of gas production, gas distribution and heat and power production has been considered. The overall exergy efficiency of the chain of hydrogen production towards heat and power is 21.1%. For the chain based on SNG production this overall exergy efficiency is 28.4% and for the chain based on syngas it is 30.4%. The use of either SNG or syngas results in a better thermodynamic performance. The gas processing has a large influence on the performance of the whole chain. The purification of hydrogen results in high losses compared to the other fuel production processes.

When the whole chain is considered the one based on syngas has the highest overall exergy efficiency. Although, the overall exergy efficiency of the SNG chain is only 2.0% lower. This difference is also mainly caused by the losses in the gas production plant. Although, the losses in the µ-CHP system are the lowest for the hydrogen fuelled system, it does not compensate for the high losses in the gas production.

The use of SNG is very interesting, since such a system could also be used with common natural gas. This system could give a significant reduction in the emission of carbon dioxide and improve the efficiency of heat and power production. Besides that, it is easier to apply, because the current infrastructure of gas transport and distribution can be used. Higher efficiencies of the SOFC as well as higher COP values for the heat pump will improved the overall exergy efficiency of the whole chain.

8.7. References

1.   Panopoulos K. D., Fryda L. E., Karl J., Poulou S., Kakaras E. High temperature solid oxide fuel cell integrated with novel allothermal biomass gasification: Part I: Modelling and feasibility study. J Power Sources 2006; 159(1): 570-585.
2.   Aloui T., Halouani K. Analytical modeling of polarizations in a solid oxide fuel cell using biomass syngas product as fuel. Appl Therm Eng 2007; 27(4): 731-737.
3.   Cordiner S., Feola M., Mulone V., Romanelli F. Analysis of a SOFC energy generation system fuelled with biomass reformate. Appl Therm Eng 2007; 27(4): 738-747.
4.   Hustad J. E., Hofbauer H., Vik A., Byrknes J. BioSOFC - Technology Development for Integrated SOFC, Biomass Gasification and High Temperature Gas Cleaning. In: Biomass Conference, Biomass for Energy, Industry and Climate Protection, Rome, 2004.
5.   Athanasiou C., Coutelieris F., Vakouftsi E., Skoulou V., Antonakou E., Marnellos G., Zabaniotou A. From biomass to electricity through integrated gasification/SOFC system-optimization and energy balance. Int J Hydrogen Energy 2007; 32(3): 337-342.
6.   Athanasiou C., Vakouftsi E., Coutelieris F. A., Marnellos G., Zabaniotou A. Efficiencies of olive kernel gasification combined cycle with solid oxide fuel cells (SOFCs). Chem Eng J 2009; 149(1-3): 183-190.
7.   Seitarides T., Athanasiou C., Zabaniotou A. Modular biomass gasification-based solid oxide fuel cells (SOFC) for sustainable development. Renew Sustain Energy Rev 2008; 12(5): 1251-1276.
8.   Omosun A. O., Bauen A., Brandon N. P., Adjiman C. S., Hart D. Modelling system efficiencies and costs of two biomass-fuelled SOFC systems. J Power Sources 2004; 131(1-2): 96-106.

9.   Zhu B., Bai X. Y., Chen G. X., Yi W. M., Bursell M. Fundamental study on biomass-fuelled ceramic fuel cell. Int J Energy Res 2002; 26(1): 57-66.

10.   Fryda L., Panopoulos K. D., Kakaras E. Integrated CHP with autothermal biomass gasification and SOFC-MGT. Energy Convers Manage 2008; 49(2): 281-290.

11.   Fryda L., Panopoulos K. D., Karl J., Kakaras E. Exergetic analysis of solid oxide fuel cell and biomass gasification integration with heat pipes. Energy 2008; 33(2): 292-299.

12.   Sucipta M., Kimijima S., Suzuki K. Performance analysis of the SOFC-MGT hybrid system with gasified biomass fuel. J Power Sources 2007; 174(1): 124-135.

13.   Aravind P. V., Woudstra T., Woudstra N., Spliethoff H. Thermodynamic Evaluation of Small Scale Systems with Biomass Gasifiers, Solid Oxide Fuel Cells with Ni/GDC Anodes and Gas Turbines. J Power Sources 2009; 190(2): 461-475.

14.   Toonssen R., Woudstra N., Verkooijen A. H. M. Reference System for a Power Plant Based on Biomass Gasification and SOFC. In: 8th European Solid Oxide Fuel Cell Forum, Luzerne, Switserland, 2008.

15.   Nagel F. P., Schildhauer T. J., Biollaz S. M. A. Biomass-integrated gasification fuel cell systems - Part 1: Definition of systems and technical analysis. Int J Hydrogen Energy 2009; 34(16): 6809-6825.

16.   Ghosh S., De S. Thermodynamic performance study of an integrated gasification fuel cell combined cycle: an exergy analysis. Proc Inst Mech Eng Part A: J Power Energy 2003; 217(6): 575-581.

17.   Sues A., Jurascík M., Ptasinski K. Exergetic evaluation of 5 biowastes-to-biofuels routes via gasification. Energy 2009; doi:10.1016/j.energy.2009.06.027

18.   Hamelinck C. N., Faaij A. P. C. Future prospects for production of methanol and hydrogen from biomass. J Power Sources 2002; 111(1): 1-22.

19.   Toonssen R., Woudstra N., Verkooijen A. H. M. Exergy Analysis of Hydrogen Production Plants Based on Biomass Gasification. Int J Hydrogen Energy 2008; 33(15): 4074-4082.

20.   Gassner M., Maréchal F. Thermo-economic process model for thermochemical production of Synthetic Natural Gas (SNG) from lignocellulosic biomass. Biomass Bioenergy 2009; 33(11): 1587-1604.

21.   Jurascík M., Sues A., Ptasinski K. J. Exergetic evaluation and improvement of biomass-to-synthetic natural gas conversion. Energy Environ Sci 2009; 2(7): 791-801.

22.   Jurascík M., Sues A., Ptasinski K. J. Exergy analysis of synthetic natural gas production method from biomass. Energy In Press, Corrected Proof

23.   Braun R. J., Klein S. A., Reindl D. T. Evaluation of system configurations for solid oxide fuel cell-based micro-combined heat and power generators in residential applications. J Power Sources 2006; 158(2): 1290-1305.

24.   Kazempoor P., Dorer V., Ommi F. Evaluation of hydrogen and methane-fuelled solid oxide fuel cell systems for residential applications: System design alternative and parameter study. Int J Hydrogen Energy 2009; 34(20): 8630-8644.

25.   Page S., Krumdieck S. System-level energy efficiency is the greatest barrier to development of the hydrogen economy. Energy Policy 2009; 37(9): 3325-3335.

26.   Toonssen R., Woudstra N., Verkooijen A. H. M. Decentralized generation of electricity from biomass with proton exchange membrane fuel cell. J Power Sources 2009; 194(1): 456-466.

27.   Bolhar-Nordenkampf M., Bosch K., Rauch R., Kaiser S., Tremmel H., Aichernig C., Hofbauer H. Scale-up of a 100kWth pilot FICFB-gasifier to a 8 MWth FICFB-

gasifier demonstration plant in Güssing (Austria). In: 1st International Ukrainian Conference on BIOMASS FOR ENERGY, Kiev, Ukraine, 2002.

28.   Bolhar-Nordenkampf M., Hofbauer H. Gasification Demonstration Plants in Austria. In: International Slovak Biomass Forum, Bratislava, 2004.

29.   Hofbauer H., Rauch R., Loeffler G., Kaiser S., Fercher E., Tremmel H. Six Years Experience with the FICFB-Gasification Process. In: 12th European Conference and Technology Exhibition on Biomass for Energy, Industry and Climate Protection, Amsterdam, The Netherlands, 2002.

30.   Hofbauer H., Rauch R., Bosch K., Kock R., Aichernig C. Biomass CHP Plant Güssing - A Success Story. In: Expert Meeting on Pyrolysis and Gasification of Biomass and Waste, Strasbourg, 2002.

31.   Hofbauer H., Rauch R., Foscolo P., Matera D. Hydrogen-rich Gas from Biomass Steam Gasification. In: 1st World Conference and Exhibition on Biomass for Energy and Industry, Sevilla, Spain, 2000.

32.   Hamelinck C. N., Faaij A. P. C. Future prospects for production of methanol and hydrogen from biomass. University Utrecht: Copernicus Institute, 2001.

33.   McKendry P. Energy production from biomass (part 3): gasification technologies. Bioresource Technol 2002; 83(1): 55-63.

34.   Bridgwater A. V. The technical and economic feasibility of biomass gasification for power generation. Fuel 1995; 74(5): 631-653.

35.   Twigg M. V. Catalyst Handbook. London: Wolfe Publishing Ltd., 1989.

36.   Wootsch A., Descorme C., Duprez D. Preferential oxidation of carbon monoxide in the presence of hydrogen (PROX) over ceria-zirconia and alumina-supported Pt catalysts. J Catal 2004; 225(2): 259-266.

37.   Zalc J. M., Löffler D. G. Fuel processing for PEM fuel cells: transport and kinetic issues of system design. J Power Sources 2002; 111(1): 58-64.

38.   Gassner M., Maréchal F. Thermodynamic comparison of the FICFB and Viking gasification concepts. Energy 2009; doi:10.1016/j.energy.2009.05.011

39.   Cycle-Tempo, 5.0. TU Delft, 2009. www.cycle-tempo.nl

40.   Baehr H. D. THERMODYNAMIK; eine Einführung in die Grundlagen und ihre technischen Anwendungen. Berlin: Springer, 1984.

41.   Szargut J., Morris D. R., Steward F. R. Exergy Analysis of Thermal, Chemical, and Metallurgical Processes. Berlin: Springer-Verlag, 1988.

42.   Baehr H. D. Die Exergie von Kohle und Heizöl. Brennstoff-Wärme-Kraft 1987; 39(1/2): 42-45.

43.   Rauch R. Stromerzeugung aus Biomasse durch Wasserdampfvergasung. Wien: TU Wien: Institute fur Verfahrens-, Brennstoff- und Umwelttechnik, 2004.

9. Evaluation of the various systems

The objective of this research is the comparison and selection of suitable conversion technologies for biomass gasification applied in hydrogen based energy systems with fuel cells. These conversion technologies need to be efficient to get the most energy out of the biomass and to assure a CO_2 emissions reduction. In to order to reach this objective, several energy conversion chains from biomass to heat and power in dwellings are compared. For this comparison, the results from the previous chapters are combined and evaluated. The systems of the centralized electricity production are expanded with the transport and distribution of the electricity and heat pumps, in order to get to comparable chains. The energy conversion chains are compared on the basis of their thermodynamic performance, which is mainly focused on the overall and electrical exergy efficiencies. This study shows the preferred options for future applications. The further development of the preferred options needs to be stimulated with priority.

Some key questions can be asked:
1. Centralized or de-centralized power generation?
2. What energy carrier should be distributed? (Hydrogen, SNG, syngas, electricity)
3. What type of gasification?
4. What type of gas cleaning?
5. What type of fuel cell?

In the first section, a short description is given of the systems in the different chapters and an overview is given of results of these systems. In the coming sections, the answers to the questions will be given. The answers to the questions do not appear in the order as they are listed. The order used for answering the questions follows the different chapters in this thesis. In the second section the selection of gasification technology and gas cleaning are discussed. This section gives the answers to questions 3 & 4. In the third section, μ-CHP systems and their fuel are evaluated. This section gives answers to the questions 2 & 5. In the fourth section some considerations will be given about plant scale, also question 1 is answered here. This chapter ends with a view into the future.

9.1. The various systems

In this thesis, several systems for the production of electricity have been evaluated. The focus is on systems from the fuel (biomass) to demanded energy (electricity and heat) of the customer. In this case the customer is a household. Two approaches have been evaluated:
1. The centralized production of electricity, which is transported to the customer through the grid.
   In this approach biomass is gasified to produce syngas. Before this syngas can be used it needs to be cleaned in a gas cleaning system. The clean gas is applied in a SOFC/GT hybrid system for the production of electricity. The produced heat is recovered and also converted into electricity in a steam cycle.
   The power produced in this system is for a large number of customers. The heat required by the customers is produced locally by electrically driven compression heat pumps.
2. The centralized conversion of biomass in gaseous fuel, which is transported and de-centrally converted into heat and power with a μ-CHP system.
   In this approach, biomass is gasified and the produced syngas is cleaned. After the gas cleaning, the gas is further processed into a fuel. This fuel is transported in a distribution grid. The μ-CHP system consists of a fuel cell, for the production of

electricity and some heat. The amount of heat produced is not sufficient to fulfill the required heat demand. Therefore, an electrically driven compression heat pump is used for the additional heat production.

In the following sections, the systems designed in the two approaches will be discussed.

9.1.1. Centralized electricity production

In this thesis, six centralized electricity production plants have been evaluated. In Table 9-1, an overview is given of the exergy efficiencies of the whole chain from biomass (clean wood) to electricity (1 kW$_e$) and heat (3 kW$_e$) for the customer and of the efficiencies of the different steps in the chain. First the different centralized power plants are being discussed. At the end of this section, the transport and distribution and the local heat production are being discussed. The heat production by the ground coupled compression heat pump and the results of the calculations are given here.

Reference plant

In this plant, biomass is converted into electricity via indirect steam gasification and a SOFC/GT hybrid system. For this process, the fast internal circulating fluidized bed (FICFB) is being used. The produced syngas is cleaned by means of low temperature gas cleaning. The low temperature gas cleaning starts with cooling of the producer gas. The particles in the gas are removed by a bag filter. Then the gas is scrubbed in water scrubber, for the removal of tars, alkalis and halogens. The gas is compressed to a pressure of 8 bar, before it is passed through a sulphur guard. The clean gas is heated using residual heat from the process and then it is fed to a SOFC/GT hybrid system for the production of electricity. The SOFC has both an anode and a cathode recycle. The off-gasses of the fuel cell are combusted before they are fed to the turbine. The air used in the fuel cell is compressed in compressor of the gas-turbine. The hot gas leaving the turbine is used to preheat the air in a recuperator. The excess heat in the process is recovered in a heat recovery steam generator and the produced steam is converted in a Rankine cycle into electricity. The net electrical power output of this reference plant is 30 MW. This system is designed as a reference system for other energy conversion systems based on biomass gasification and fuel cells.

The supercritical water gasification (SCWG) plant

In this plant, wet biomass (manure) is converted via super critical water gasification into hydrogen/methane rich gas. The wet biomass is compressed and heated before it is fed to the gasifier. This gasifier operates at 500°C and a pressure of 34 MPa. Most of the reaction products are dissolved in the supercritical water. The mixture is cooled and a large part of the gas is released in a high pressure flash. This gas is cleaned with the help of two guard beds. The clean gas fed to a SOFC/GT hybrid system for the production of electricity. The net electrical power output of this system is 420 kW. For this feasibility study, several plants are designed on the combination of SCWG and fuel cells.

S1 plant

In this plant, biomass is converted via indirect steam gasification and the produced gas is cleaned with low temperature gas cleaning. The clean gas is fed to a SOFC/GT hybrid system for the production of electricity. The plant design is similar to the reference plant. This plant produces net 35 MW$_e$.

S2 plant

Here, the biomass is converted via direct air gasification and the gas is also cleaned with a low temperature gas cleaning system. A SOFC/GT hybrid system is used to produce net 35 MW of electricity from the clean syngas. This plant is similar to S1, except for the gasification technology. The plant is designed to investigate the influence of the gasification technology on the overall plant performance, by comparing it with S1

S3 plant

In the S3 plant, the biomass is also converted into syngas via direct air gasification. The syngas is cleaned with the help of a high temperature gas cleaning system. This plant is similar to S2, except for the gas cleaning system. The gas cleaning consists of a hot gas filter, a tar cracker, an alkali getter and a sulphur guard. Also in this system, a SOFC/GT hybrid system is used for the production of net 35 MW_e. This plant is designed to look into the influence of the gas cleaning on the overall plant performance, by comparing it with S2

S4 plant

In this plant, biomass is converted via direct air gasification and gas is cleaned with the help of a high temperature gas cleaning system. The biomass gasification is based on a pressurized downdraft fixed bed gasifier. Again the gas is fed to a SOFC/GT hybrid system for the production of electricity. The net electrical output of this system is 90 kW. This system was design to research the influence of the plant scale on the overall plant performance, by comparing it with S3.

Annex 9-1

A more conventional approach for the production of energy from biomass is a combustion process combined with steam cycle. Two different options are considered:
1. A 100% biomass fired power plant, like the fluidized bed combustion plant located in Cuijk in The Netherlands. This power plant has a thermal electrical efficiency of 32.1%, when it is only producing electricity[1]
2. A modern coal fired power plant (300MW_e), where 10% of the coal is replaced by biomass. This co-firing power plant could have a thermal electrical efficiency of 45%

Based on these efficiencies, electrical exergy efficiencies can be determined with the help of the exergy factor. The LHV(wet) of the biomass used in most systems is 14.8 MJ kg^{-1}, the exergy of the biomass used in most systems is 16.9 MJ kg^{-1}. This leads to an exergy factor of 1.14. The exergy efficiency can be determined by dividing the thermal efficiency by the exergy factor. This results in an electrical exergy efficiency of 28.2% for the 100% biomass fired power plant. For the co-firing power plants the electrical exergy efficiency is 39.5%. These two systems are added to Table 9-1 under the name "common1" for the 100% biomass fired power plant and "common2" for the co-firing power plant. So, it is possible to compare the more conventional systems with the more advanced fuel cell based systems.

All the centralized plants

The reference plant is evaluated in chapter 4, the SCWG plant in chapter 5 and the plants S1, S2, S3 & S4 are evaluated in chapter 6. The results given in chapters 4, 5 and 6 are only for the centralized electricity production; transport, distribution and local heat production are not included. In this evaluation, the system boundaries are expanded from only the plant

to the plant including distribution network and customer. Losses for transport and distribution (T&D) of electricity are assumed to be approximately 4.6% [2]. This is based on the amount of produced electricity (369.88 PJ) and the losses of the grid (16.84 PJ) in The Netherlands for 2008 [2].

For the determination of the overall chain exergy efficiency, it is assumed that a consumer requires 1 kW of electricity and 3 kW heat. This 3 kW heat is produced de-centrally by a ground coupled electrically driven compression heat pump. In annex 9-2, the description of the used heat pump is given.

Annex 9-2
For the decentralized production of heat, an electrically driven ground coupled compression heat pump is used. This is not a state of the art system; it is designed to be connect to a conventional heating system. This heat pump consists of three closed cycles. The first cycle is the ground coupled cycle, which is used to extract heat from the ground at a temperature of approximately 8°C. The working fluid of this cycle is a 10% ethylene glycol water mixture. The second cycle is the refrigerant cycle. The working fluid of this cycle is R290. The third and last cycle is the space heating circuit. The working fluid is water.
Heat extracted from the ground is used to evaporate the refrigerant in the refrigerant cycle. The evaporated R290 is compressed to 24 bar with a compressor. Then, the compressed R290 is condensed in a condenser and the heat is transferred to the space heating cycle. The condensed R290 is then throttled to a pressure of 4.8 bar. Then the cycle starts again with the evaporation of the R290. The spacing heating cycle uses water of 65°C for space heating. The return temperature of the water in the space heating cycle is 45°C.
To drive the compressor and auxiliary pumps, electricity is taken from the grid.
In Figure 9-1, the flow sheet for the heat pump is given.
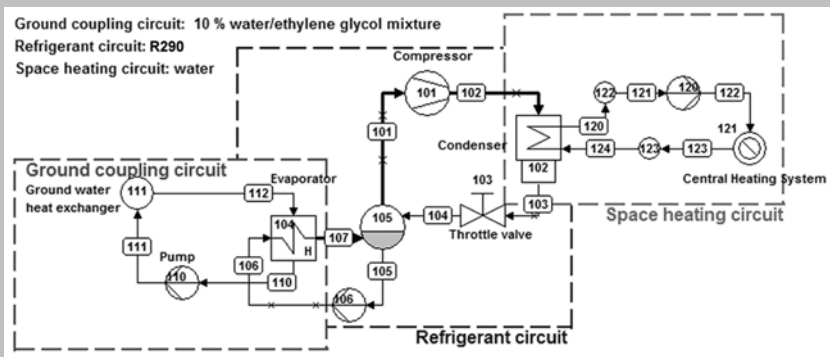
Figure 9-1 flow sheet of electrical driven ground coupled compression heat pump

The coefficient of performance of the heat pump is: COP=3.2.
The electrical input in the heat pump system is 943 W and the heat output is 3 kW. The exergy value of the produced heat is 365W. The exergy efficiency is 38.7%.

The consumer requires 943 W of electric power to obtain 3000 W heat. The total amount of exergy obtained by the consumer is 1365 W; this consists of 1000 W electrical exergy and 365 W exergy of heat. This leads to an exergy efficiency of 70.3%. By multiplying this efficiency with the electrical exergy of the chain, the overall exergy efficiency of the chain is obtained. The exergy efficiency of the de-central heat production is calculated by multiplying the chain efficiency of electricity production with the exergy efficiency of the heat pump.

Table 9-1 overview of the exergy efficiencies for the various systems based on centralized power production

Plant Name	Reference	SCWG	S1	S2	S3	S4	Common1	Common2
Chapter	4	5	6	6	6	6	-	-
Gasification type	Steam	SCWG	Steam	Air	Air	Air	Combustion	Combustion
Gas cleaning	LT	LT	LT	LT	HT	HT	None	None
Plant size [MW$_e$]	30	0.42	35	35	35	0.10	26	300
Central plant	48.9	51.8	49.3	49.4	49.9	46.0	28.2	39.5
T&D	95.4	95.4	95.4	95.4	95.4	95.4	95.4	95.4
Decentral Q Production	18.1	19.1	18.2	18.2	18.4	17.0	10.4	14.6
Chain electrical	46.6	49.4	47.0	47.1	47.6	43.9	26.9	37.7
Chain overall	32.8	34.7	33.1	33.1	33.5	30.9	18.9	26.5

9.1.2. De-centralized electricity production

In this thesis, four different fuel plants have been evaluated. In Table 9-2, an overview is given of the various systems based on centralized gas production and de-centralized conversion in μ-CHP systems. The μ-CHP systems contain a fuel cell and a compression heat pump for the production of additional heat.

Hydrogen1

Hydrogen1 is a hydrogen plant, which produces hydrogen from biomass with a purity of 60%. In this plant, biomass is indirectly gasified with steam in FICFB. The raw syngas is cleaned with a low temperature gas cleaning system. The gas cleaning starts with cooling of the gas to 120°C. Then the gas is passed through a bag filter for the removal of particulates. The gas is scrubbed with water for the removal of tars, alkalis and halogens. Next the gas is compressed and after that passed through a sulphur guard. After the gas cleaning, the syngas is further purified via reforming to remove part of the methane. After the reforming, the gas goes to the water gas shift, for the removal of carbon monoxide. Next, the gas goes through preferential oxidation for the deep removal of carbon monoxide. Finally the gas is dried.

Hydrogen2

Hydrogen2 is a hydrogen plant, which produces highly pure hydrogen (99.99%) from biomass. The biomass is indirectly gasified with steam and the produced syngas is cleaned via low temperature gas cleaning. This is similar to Hydrogen1. In this plant, the clean gas is further processed into hydrogen via reforming, water gas shift and pressure swing adsorption. The pressure swing adsorption is used to purify the hydrogen. The residual heat in the plant is used to produce electricity, which is completely consumed by the auxiliaries of the plant.

GP1

GP1 is similar to Hydrogen2 except for the biomass is input. The biomass input GP1 has a different composition and a different LHV; this composition is similar to the biomass input of GP2 and GP3. The main difference in composition of the biomass is in the fractions of carbon, oxygen and moisture content. This difference leads to a small difference in plant performance.

GP2

GP2 is a gas plant producing synthetic natural gas from biomass. In this plant, biomass is gasified with steam and the produced syngas is cleaned with a low temperature gas cleaning system. The gasification and gas cleaning is similar to the plant of Hydrogen1, Hydrogen2 and GP1. The cleaned gas is further processed into SNG via methanation and purification. In the methanation process the hydrogen and carbon monoxide in the gas are converted into methane. During the purification of the methane, carbon dioxide is removed with the help of a PSA unit and the hydrogen is removed with a membrane separator.

GP3

In GP3, syngas is produced via indirect steam gasification and low temperature gas cleaning. The gasification process and gas cleaning is same as in GP2. The clean syngas is only compressed and dried before it is distributed.

Gas distribution and μ-CHP

The gas produced in the gas production plants is distributed in a transport and distribution system to the end-users (dwellings). The thermal efficiency of the distribution of syngas and SNG is assumed to be 96.5% and for hydrogen it is assumed to be 94% [3]. The exergetic efficiencies of the distribution grid are assumed to be 1 percentage point lower, so 95.5% for syngas and SNG and 93% for hydrogen.

The end-users convert the distributed fuel in an μ-CHP system based on either a PEM-FC or a SOFC into heat and power.

The hydrogen produced in Hydrogen1 or Hydrogen2 is converted in a PEM-FC based μ-CHP system producing net 1 kW_e and 3 kW_{th}. Since the fuel cell is not capable to produce the 3 kW_{th}, a compression heat pump is used for the production of additional heat.

The gas produced in GP1 or GP2 or GP3 is converted in a SOFC based μ-CHP system producing net 1 kW_e and 3 kW_{th}. This type of fuel cell is also not capable to produce all the required heat. So, this μ-CHP system has also a compression heat pump to meet the heat demand.

The two different hydrogen plants together with the PEM-FC based μ-CHP systems have been evaluated in chapter 7. The plants GP1, GP2 and GP3 and the SOFC based μ-CHP system, on the other hand, have been evaluated in chapter 8.

In Table 9-2, Hydrogen 3 is added. This chain contains the hydrogen production as in Hydrogen2 combined with a SOFC based μ-CHP system.

Table 9-2 overview of the exergy efficiencies for the various systems based on de-centralized power production

Plant Name	Hydrogen1	Hydrogen2	Hydrogen3	GP1	GP2	GP3
Chapter	7	7	-	8	8	8
Gasification type	Steam	Steam	Steam	Steam	Steam	Steam
Gas cleaning	LT	LT	LT	LT	LT	LT
Energy carrier	60% H_2	Pure H_2	Pure H_2	Pure H_2	SNG	Syngas
Central plant	61.4	50.5	50.5	54.9	65.2	75.2
T & D	93.0	93.0	93.0	93.0	95.5	95.5
Fuel cell type	PEM-FC	PEM-FC	SOFC	SOFC	SOFC	SOFC
Decentral e production	25.3	26.3	30.3	30.3	33.4	31.0
Decentral Q production	9.2	9.5	11.1	11.1	12.2	11.4
Chain electrical	14.4	12.4	14.2	15.5	20.8	22.2
Chain overall	19.7	16.8	19.4	21.1	28.4	30.4

9.2. What type of gasification and gas cleaning?

The choice of the gasification technology depends on two main factors: the fuel to be gasified and the required product.

Drying of biomass can be energy intensive. If a biomass is very wet, it can be beneficial to use supercritical water gasification for the conversion of biomass. This technology seems very promising [4, 5]. In the SCWG system, the gasification technology is coupled with a SOFC/GT hybrid system (see chapter 5). The expected exergy efficiency is high when it is compared to the reference system (see Table 9-1). In the SCWG system, the excess heat is not utilized. So, the electrical exergy efficiency of this system can be even higher. In Table 9-1, the efficiencies of both the reference system as well as the SCWG system are given. This SCWG technology is relatively new and it is still developing. Most of the experiments are performed at laboratory scale with model compounds. Only a few experiments have been performed with real biomass, which seem very promising. There are still technical difficulties, which need to be solved before this technology can be commercialized.

For the production of hydrogen or other secondary energy carriers from dry biomass indirect steam gasification is the preferred technology, because it results in hydrogen rich producer gas.
In chapter 3, several different biomass gasification technologies have been compared for the production of pure hydrogen. In this comparison, it is shown that for hydrogen production indirect steam gasification is a more suitable technology than for instance direct air gasification. A high hydrogen content of the produced gas is then important, dilution of the hydrogen by other compounds, like nitrogen, is undesired. For the production of bio-fuels, gasification with air producing a fuel gas of 4-7 MJ Nm^{-3} is useless [6]. In the case of the production of secondary energy carriers, the diluents need to be removed, which is energy intensive and reduces the overall exergy efficiency of the fuel production plant.

For the production of electricity, the gasification technology does not have a large influence on the system performance, when using SOFC/GT systems.
The systems S1 and S2, as indicated in Table 9-1, have almost similar electrical exergy efficiencies of 49.3% and 49.4%, respectively. These two systems are similar except for the gasification technology. System S1 is based on indirect atmospheric steam gasification and

system S2 is based on direct pressurized air gasification. So, system S1 produces a syngas virtually free of nitrogen and system S2 produced a syngas which is diluted with nitrogen.

High temperature gas cleaning is more efficient than low temperature gas cleaning, when the clean gas is used at high temperatures.
The systems S2 and S3, as indicated in Table 9-1, are two similar systems. The only difference between the two systems is the gas cleaning. System S2 has low temperature gas cleaning and system S3 has high temperature gas cleaning. The electrical exergy efficiencies are respectively 49.4% and 49.9%. The clean gas in these systems goes to a SOFC/GT and needs to be at a high temperature before it enters the SOFC. The difference in the exergy losses between the two technologies is caused by the heat transfer. In the system S2, the raw gas coming from the gasifier is cooled with cold clean syngas leaving the gas cleaning system. During this heat exchange, exergy is lost due to the temperature difference between the two gas streams.
In chapter 3, the two different gas cleaning technologies have also been evaluated for different gasification technologies. Here, it was also shown that high temperature gas cleaning resulted in lower exergy losses for the gas cleaning section. In these systems the clean gas needed processing at elevated temperatures.
In case the required temperature of the clean syngas is low, then low temperature is more useful to apply.
The high temperature gas cleaning technology is still developing. The low temperature gas cleaning, on the other hand, is a more mature technology. Therefore, the most systems in this study are designed with low temperature gas cleaning, as can be seen in Table 9-1.

9.3. Secondary fuel and µ-CHP

The hydrogen energy economy is considered to be a way to decarbonize the energy supply. In an idyllic vision of a hydrogen energy economy, the energy supply is realized by solely hydrogen and electricity, which are produced from renewable resources [7]. Hydrogen would be used in transport, industrial, commercial and residential applications, where fossil fuels are currently used [7]. The hydrogen energy economy can be seen as a long term project that can be defined as an effort to change the current energy system to one which attempts to combine the cleanliness of hydrogen as an energy carrier with the efficiency of fuel cells [8].
Hydrogen as an energy carrier has its advantages and its disadvantages. The main advantage of hydrogen is the absence of CO_2 when it is combusted or converted, especially when applied in fuel cells. Additionally, hydrogen can be expected to allow the integration of some renewable energy sources, of an intermitting character, in the current energy system. For instance, a photovoltaic solar panel or a windmill linked to a reversible fuel cell, which uses a part of the electricity to produce hydrogen, which is stored, during the day or in windy conditions. At night or in the absence of wind, the hydrogen is consumed to produce electricity.
The main disadvantage of hydrogen is that hydrogen is an energy carrier and not an energy source. Therefore, hydrogen will be as clean as the method employed for its production. Other disadvantages are the low energy density on a volume basis, which makes transport and storage expensive. Furthermore, hydrogen is a highly inflammable and dangerous gas.

9.3.1. Hydrogen production

By comparing the results in Table 9-1 and Table 9-2, it shows that hydrogen is not a suitable energy carrier when looking at chain efficiencies, on the contrary, electricity is.

In this thesis, the production of hydrogen from biomass is evaluated, but also the production of other energy carriers has been considered. The production of hydrogen using different gasification technologies is evaluated in chapter 3. In systems hydrogen1, hydrogen2 and GP1, hydrogen is evaluated as an energy carrier in a chain from biomass towards electricity and heat in a dwelling.

The production of hydrogen from biomass has an exergy efficiency of approximately 50.5%, which is shown in chapter 3. This hydrogen has a purity of 99.99%. Sues et al.[9] found a similar exergy efficiency for the production of hydrogen via biomass gasification. The system hydrogen2 shows that the efficiency of the chain from hydrogen production and distribution to eventually electricity production with a PEM-FC has an overall chain exergy efficiency of 12.4%. This chain from biomass to electricity is based on the production and distribution of pure hydrogen. The system hydrogen1 is used to consider hydrogen with lower purity. When hydrogen with a purity of 60% is applied in a similar chain the overall chain exergy efficiency increases to 14.4%. When comparing hydrogen1 and hydrogen2, it becomes clear that the high purity of the hydrogen reduces the exergy efficiency of the chain; this is also indicated in Table 9-2. The exergy efficiencies are quite low; this means that only a small part of the exergy content of the biomass is converted into electricity and heat.

In system GP1, another chain based on hydrogen production and distribution is evaluated. This chain uses a SOFC for the production of heat and power. The overall chain exergy efficiency is still only 21.1%. Since the exergy efficiency is still low, other energy carrier have been considered. In system GP2, synthetic natural gas produced from biomass has been evaluated and in system GP3 clean and dry syngas from biomass is evaluated. In these two systems, the produced fuel is distributed and de-centrally converted in a SOFC based μ-CHP system. The overall chain exergy efficiencies of these options are 28.4% and 30.4%, respectively. When the losses for electricity transportation and distribution and the decentralized production of heat are included in the results for the reference plant, the overall chain exergy efficiency is 32.8% as indicated in Table 9-1. This efficiency is not much higher than for the decentralized options; the difference is only 4.4% for GP2 and 2.4% for GP3.

When the electrical exergy efficiency is considered then the difference is more significant. The reference system has an electrical exergy efficiency of 46.6% and the μ-CHP systems of GP2 and GP3 have an electrical exergy efficiency of 20.8% and 22.2%, respectively. The way heat is being produced is an important factor in the overall efficiency.

The heat demand of new build dwellings, in the future, will mostly be determined by the hot tap water demand. This is caused by the more and more energy efficient design of dwellings, the demand of hot tap water depends on the behavior of the inhabitants. The demand of hot tap water is only for very short periods of time, so most of the day the electricity demand is more important. So, the production of electricity should be as efficient as possible. Therefore, centralized electricity production should be preferred. On the other hand, buildings are standing for very long time. So even in the future, there will be sufficient houses which have a significant heat demand for space heating. For these dwellings, the heat production remains important. In this case, the centralized power production is still the most efficient option. Although, the exergy efficiency difference between centralized and de-centralized options is not that big. When the heat demand is very large the de-centralized option could even be more efficient than the centralized option.

9.3.2. Comparison SNG and hydrogen

When considering a gaseous fuel as an energy carrier, SNG is a more efficient option than hydrogen. In system GP2, SNG is evaluated as an energy carrier. This is an interesting concept, since it can be applied easily in the current natural gas distribution systems. The process could be operated carbon negative due to the removal of CO_2 during the process. The SNG production process also produces some electricity. The production of SNG from biomass is more efficient than hydrogen production; this is also indicated in Table 9-2. Besides that, SNG is easier to store and transport than hydrogen. The technology for natural gas transport and storage is well established.

9.3.3. Syngas

In system GP3, dry and clean syngas is evaluated as an energy carrier. This is also an interesting concept. In the 1800's and early 1900's, town gas was produced by heating coal without the presence of air. This process led to a gas which mainly consisted of hydrogen, methane, carbon monoxide and some other components. This gas was distributed to dwellings where it was used for heating, lighting and cooking. The gas produced in GP3 also contains these components, although the composition will be different. With the distribution of town gas there is already a lot of experience.

The syngas is also used in the chemical industry as building blocks for all kinds of chemicals.

An important problem is that the stability of the syngas is low. When the syngas is produced it needs to be cooled quickly in order to fix the composition. If the gas comes in contact with catalysts or if the temperature changes slowly, the composition of the syngas can change. This may result in carbon formation, which can lead to blockage and damage to equipment. Another problem is the high hydrogen and carbon monoxide content, which can be very dangerous due to explosion hazards and CO poisoning.

The last points make clear, that SNG is a more attractive energy carrier for the application in dwellings.

9.3.4. Comparison SOFC and PEM-FC

SOFC is the preferred fuel cell type for both centralized and decentralized power generation. The application of the SOFC in the centralized power plants seemed obvious. The SOFC is able to directly convert syngas into electricity, while for the PEM-FC intensive cleaning is required with respect to carbon monoxide. The SOFC is also more tolerant towards other contaminants than the PEM-FC. A study performed by Bosch et al. [10] showed that high conversion efficiencies where possible using a SOFC/GT hybrid system.

The choice of fuel cells for the decentralized power is not that obvious. The PEM-FC has several advantages over the SOFC in decentralized application, especially for μ-CHP applications in dwellings. The PEM-FC has a low operating temperature, which makes fast start-up and shut down possible. The heat generated by the fuel cell has a low temperature, which is ideal for spacing heating applications. The SOFC has very long start-up times because of the high operating temperature and material restrictions. The response time of a SOFC is longer than of a PEM-FC.

In system hydrogen2, a PEM-FC based μ-CHP system fuelled with 99.99% H_2 is evaluated. The performance of this μ-CHP system can be compared with the performance of the μ-CHP system of system GP1. The μ-CHP system of GP1 is based on a SOFC, which is fuelled with 99.99% H_2. The electrical exergy efficiency for both μ-CHP systems are

26.3% and 30.3%, respectively (see also Table 9-2). Based on this difference, the SOFC based µ-CHP system is better option.

In a study performed by Visser [11], the performance of a hydrogen fuelled and a natural gas fuelled µ-CHP based on a PEM-FC has been evaluated. The hydrogen fuelled system is almost similar to the hydrogen1 system, except for the heat pump, which is not included in the system of Visser. The natural gas fuelled system consists of a complete gas processing system which converts the fuel before it enters the PEM-FC; it also lacks a heat pump.

The electrical output of both Visser's systems is 1 KW [11]. The heat output, on the other hand, is determined by the system. The net electrical exergy efficiency for the hydrogen fuelled system is 42% and for the natural gas fuelled system this is 26% [11]. These performances are compared with hydrogen1 for the hydrogen fuelled system and with GP2 for the natural gas fuelled system (see Table 9-2). The electrical efficiency found by Visser is much higher than the efficiency found for hydrogen1. This is caused by the additional heat pump in the hydrogen1 system. On the other hand, the electrical efficiency for the natural gas fuelled system is not higher than the efficiency for GP2. Although, GP2 has a heat pump included the net electrical efficiency is higher. So also in this case the SOFC is preferred.

The µ-CHP systems have been evaluated at the design point, the off-design response of the µ-CHP system has not been evaluated. It is most likely that the µ-CHP system will operate at part-load for most of the time. When the power demand is lower than the design power output, the current density of the cells will be lower. The efficiency of a fuel cell increases when the current density decreases [12].

9.4. Centralized or de-centralized power production?

As indicated in the previous section, the option of centralized fuel production, transport and distribution of that fuel and the decentralized conversion into electricity is not very efficient compared to centralized electricity production. In this section the scale of the centralized power production is discussed.

Large scale biomass based power plants are preferred, when looking at their conversion efficiency.

System S3 is a large scale (30 MW$_e$) plant, which combines biomass gasification with a SOFC/GT hybrid system. The electrical exergy efficiency of this plant is 49.9%. System S4 is a small scale (100 kW$_e$) plant, which also combines biomass gasification with a SOFC/GT hybrid system. The electrical exergy efficiency of the small scale plant is 46.0%. So the large scale plant is more efficient. Equipment, like pumps and compressors, for the small scale plant are less efficient than for large scale plants. This results in relatively larger exergy losses. Therefore, it results in a lower overall performance.

On the other hand, when considering the results of systems S3 & S4, the exergy efficiency of the central plant only differ 3.9 percentage points (see also Table 9-1). So, small scale power plants based on biomass gasification and SOFC/GT systems are very interesting for small communities, which are not connected to the grid. Especially, when these communities use locally collected biomass in this power plant.

Large scale plants are preferred when looking at their individual conversion efficiency. In this thesis, the collection, transport and pre-treatment of biomass are not considered.

Large scale plants required a very large investment at once. The investment costs for a small scale plant are smaller, which makes it easier to realize.

9.5. View into the future

Future energy systems will be characterized by the increasing penetration of strongly fluctuating sources (e.g. wind and solar). The demand of electricity is also fluctuating, but this demand will probably not match with the supply. These fluctuations in demand and supply required a highly flexible energy production chain in which it is possible to manage the difference between supply and demand. Co-production of electricity and fuel in centralized plants could be very interesting to manage the difference in supply and demand. When the wind turbines and solar systems produce a lot of power then the co-production plant can produce fuel (e.g. SNG) instead of electricity. When the production of power from the wind turbine or solar systems is low, the co-production plant could be used to produce power

In this thesis, the co-production concept is not evaluated explicitly. A co-production plant could consist of a biomass gasification system with gas cleaning, a SOFC/GT hybrid system for the production of electricity and syngas processing equipment for the production of fuel. In Figure 9-2, a block diagram of such a system is given.

The advantage of such a system is that it increases the flexibility. The SOFC-GT can be operated at part load, while the gasification keeps operating at full load. The fuel, which is not fed to the SOFC-GT can be used for the production of fuel. In this way it is possible to produce valuable fuel when the electricity prices are low. A disadvantage is that most of the time a part of the plant is not or only partly in use, which can be expensive.
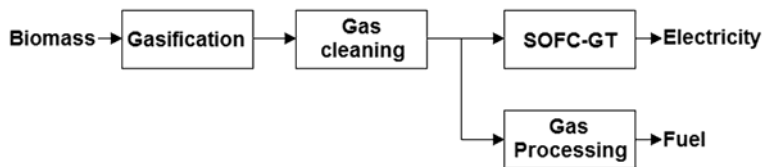
Figure 9-2 block diagram of a co-production system

It is also possible to apply co-production in CHP systems based on SOFC as is done in the work of Hemmes and Patil [13]. In such an application, SNG is produced from biomass in a large centralized plant. The SNG is distributed and locally converted in a co-production system for the production of electricity and hydrogen. The produced hydrogen could be used as a fuel in a fuel cell vehicle. This concept can also be combined with a large scale co-production plant, where electricity and SNG are being produced.

In this way, it is possible to keep the gasification and gas cleaning at full capacity. There are many design and economical aspects to the concept of co-production. For instance, the economics are very tricky with regard to the investment costs of equipment which only operates for a limited time.

9.6. References

1.   Damen K., Faaij A. P. C. A greenhouse gas balance of two existing international biomass import chains. Mitigation and Adaptation Strategies for Global Change 2006; 11 1023-1050.
2.   CBS StatLine - Elektriciteitsbalans; aanbod en verbruik. http://statline.cbs.nl/StatWeb/publication/?DM=SLNL&PA=80324NED&D1=a&

D2=a&D3=220,248-249&HDR=G2,T&STB=G1&VW=T. CBS. Date accessed: 23-3-2010

3. Page S., Krumdieck S. System-level energy efficiency is the greatest barrier to development of the hydrogen economy. Energy Policy 2009; 37(9): 3325-3335.

4. Elliott D. C. Catalytic hydrothermal gasification of biomass. Biofuels, Bioprod Biorefin 2008; 2(3): 254-265.

5. Luterbacher J. S., Fröling M., Vogel F., Maréchal F., Tester J. W. Hydrothermal Gasification of Waste Biomass: Process Design and Life Cycle Asessment. Environmental Science & Technology 2009; 43(5): 1578-1583.

6. Zhang W. Automotive fuels from biomass via gasification. Fuel Process Technol 2009; doi:10.1016/j.fuproc.2009.07.010

7. Florin N. H., Harris A. T. Enhanced hydrogen production from biomass with in situ carbon dioxide capture using calcium oxide sorbents. Chem Eng Sci 2008; 63(2): 287-316.

8. Marban G., Valdes-Solis T. Towards the hydrogen economy? Int J Hydrogen Energy 2007; 32(12): 1625-1637.

9. Sues A., Jurascík M., Ptasinski K. Exergetic evaluation of 5 biowastes-to-biofuels routes via gasification. Energy 2009; doi:10.1016/j.energy.2009.06.027

10. Bosch K. J., Woudstra N., van der Nat K. V. Designing Solid Oxide Fuel Cell Gas Turbine Hybrid Systems Using Exergy Analysis. In: Fourth International Conference on Fuel Cell Science, Engineering and Technology, Irvine (USA), 2006.

11. Visser M. M. C. The design of μ-CHP systems for household use; Modelling of cogeneration systems with fuel cells. MSc Thesis, Delft University of Technology, 2009.

12. EG&G Techincal Services. Fuel Cell Handbook. Morgantown: Nation Energy Technology Laboratory, 2004.

13. Hemmes K., Patil A., Woudstr N. Flexible Coproduction of Hydrogen and Power Using Internal Reforming Solid Oxide Fuel Cells System. J Fuel Cell Sci Technol 2008; 5(4): 041010.

10.Conclusions and recommendations

The objective of this research is the selection of suitable conversion technologies for biomass gasification applied in hydrogen based energy systems with fuel cells. In order to accomplish this objective, several chains from biomass gasification coupled with fuel cells have been evaluated. The application of an exergy analysis to the different conversion chains resulted in an indication of the thermodynamic performance of the different chains. The focus of this thesis is on the thermodynamic performance of the proposed chains. Other aspects, like environmental and economical, are not evaluated. These aspects are beyond the scope of this research.

Some key questions have been asked:
1. Centralized or de-centralized power generation?
2. What energy carrier should be distributed? (Hydrogen, SNG, syngas, electricity)
3. What type of gasification?
4. What type of gas cleaning?
5. What type of fuel cell?

The answers of these questions can be found in the conclusions.

10.1.   Conclusions

The most important findings are:

▪   Centralized power production from biomass is preferred over centralized fuel production and de-centralized power production from that fuel. As it is shown in chapter 9. Although, the differences in the exergy efficiency are not very large. The most import factor in the small difference is the heat production. De-centralized power production is preferred, when the heat demand is much higher.

▪   Large scale biomass based power plants are preferred, when looking at their conversion efficiency. The electrical exergy efficiency is the highest for these systems. This is indicated in chapter 6.

▪   Hydrogen is not a suitable energy carrier, when considering chain efficiencies. On the contrary, electricity is suitable. Other energy carriers, like synthetic natural gas and syngas, are interesting options. From chapter 3, it became clear that the production of pure hydrogen results in high exergy losses. In chapters 7 and 8, hydrogen chains are given. When comparing these results with the results for electricity production as described in chapter 9, it becomes clear that hydrogen gives the least efficient options.

▪   When considering a gaseous fuel as an energy carrier, synthetic natural gas and syngas are a more efficient option than hydrogen. As it is shown in chapter 8. In residential units, synthetic natural gas is more preferred, since the carbon monoxide in syngas is poisonous.

▪   For the production of hydrogen or other secondary energy carriers from dry biomass, indirect steam gasification is the preferred technology. In chapter 3, it is shown that this technology results in a syngas with a high hydrogen content and prevents the dilution of the produced gas with nitrogen.

- For the production of electricity, the gasification technology does not have a large influence on the system performance when using SOFC/GT systems. This is shown in chapter 6. A system based on direct air gasification performed equally to a system based on indirect steam gasification.

- Supercritical water gasification could be useful for the gasification of wet biomass. Especially in power production, the combination of supercritical water gasification and solid oxide fuel cell gas turbine hybrid systems seems very promising, as is shown in chapter 5. This technology is still in a development stage.

- High temperature gas cleaning is more efficient than low temperature gas cleaning, when the clean gas is used at high temperatures. Since it reduces the losses due to heat exchange. This effect is shown in both chapters 3 and 6.

- The solid oxide fuel cell is the preferred fuel cell type for both centralized and decentralized power generation. This type of fuel cell has a higher electrical efficiency and is more tolerant towards contaminations than the proton exchange fuel cell. This can be seen from the comparison between results of chapters 7 and 8 as given in chapter 9.

- Co-production of electricity and fuel in centralized plants could be very interesting. This is shown in chapter 9.

In line with the objective of this study, the suitable conversion technologies for biomass gasification applied in hydrogen based energy systems with fuel cells are:

- For SNG, indirect steam gasification for the production of syngas from biomass.

- For electricity, direct air gasification for the production of electricity with SOFC/GT.

- High temperature gas cleaning.

- Solid oxide fuel cells combined with gas turbines for large scale power production.

- Solid oxide fuel cells for small scale μ-CHP systems fuelled with SNG or syngas.

The answers to the key question are:
1. *Centralized or de-centralized power generation?*
   Centralized power generation
2. *What energy carrier should be distributed? (Hydrogen, SNG, syngas, electricity)*
   Electricity
3. *What type of gasification?*
   For electricity production, direct air gasification;
   For fuel production, indirect steam gasification;
   In case of wet biomass, supercritical water gasification.
4. *What type of gas cleaning?*
   High temperature gas cleaning
5. *What type of fuel cell?*
   Solid oxide fuel cell

10.2.   Recommendations

In this thesis, the fuel used in most studies is clean wood. This fuel is used because it is a reasonably well defined fuel. In the future, it is more likely to use all kinds of biomass waste streams for the production of power. These waste streams are not well defined and will contain more contaminants than clean wood. These contaminants will have a large influence on the design of the gas cleaning systems. Contaminants are not the only problem also the composition will vary widely. Therefore, more studies should be performed on other biomass streams and their influence on the gas cleaning system, as well as on the whole system.
Supercritical water gasification is an interesting technique for the conversion of wet biomass. Since many biomass waste streams are wet, the development of SCWG should be stimulated.

It is recommended to continue the research into the high temperature gas cleaning technologies. A robust cleaning system, which does not require cooling of the raw syngas, is the ultimate goal. Also the research in coupling the SOFC with a gas turbine still needs research, since there are still a lot of technical difficulties. The coupling of the different technologies of biomass gasification, gas cleaning and SOFC/GT and their transient behaviour need further research.

Co-generation can be an interesting option for decoupling the operation of the gasification from the grid demand. This can increase the flexibility of the whole plant. Further research of co-generation plants could be interesting. Especially, the technological and economical implications are very important.

A.   Biomass

Biomass is a name for a wide collection of materials. In the first part of this appendix the properties of biomass and there nature will be discussed. The second part is about the availability of biomass.

A.1.   Different types of biomass

Biomass is a term for all organic material that stems from plants (including algae, trees and crops) [1]. This leads to a wide range of possible sources of biomass each with their own composition. Biomass can be divided into four main categories [1, 2]:

- woody plants;
- herbaceous plants;
- aquatic plants;
- Wastes (like sewage sludge and animal wastes).

The herbaceous plants can be further sub-divided into those with high- and low-moisture content. Important properties for energy conversion processes of woody and herbaceous plants are:

1. the moisture content;
2. calorific value;
3. proportion of fixed carbon & volatiles;
4. the ash/residue content;
5. the alkali metal content;
6. the cellulose/lignin ratio.

In dry biomass conversion processes, the first five properties are important. While for wet biomass conversion processes, the first and the last property are of more importance.

Because of the diverse nature of biomass, properties in these categories can vary widely [2, 3]. In Table A-1 some average values of properties are given for specified biomass groups [4].

A woody plant is a vascular plant that has a perennial stem that is above ground and covered by a layer of thickened bark. Woody plants contain wood, which is composed of structures of tightly bound fibres of cellulose and lignin.

An herbaceous plant is a plant that has leaves and stems that die down at the end of the growing season to the soil level. These plants do not contain wood; therefore their structure is composed of more loosely bound fibres of lignin and cellulose. This also means that the lignin content for herbaceous plants is lower than for woody plants.

Aquatic plants are plants, which grow underwater like kelp and algae. The moisture content of this type of biomass is usually high.

Wastes are all kinds of waste streams, like manure, sewage sludge, refuse-derived fuel (RDF). Most of the wastes are extremely wet, like sewage sludge and most manure.

There are two forms of moisture content, which are of interest in biomass: intrinsic moisture and extrinsic moisture [1]. Intrinsic moisture is the moisture captured within the biomass. This type of moisture is hard to remove. Extrinsic moisture is the moisture which is influenced by the weather condition during harvesting. This type of moisture is easier to remove. The extrinsic moisture content is of special interest, since the intrinsic moisture content is hard to change [1]. The moisture content is one of the important factors for the selection of particular biomass conversion technique. Drying of biomass is energy intensive, so if possible it should be avoided.

The caloric value of biomass represents the heating value when in it is combusted. This heating value can be defined in different two ways: higher heating value (HHV) and lower heating value (LHV).

The fixed carbon is the mass remaining after the release of all the volatiles, excluding the ash and moisture content. The volatile matter is the portion of released gas by heating of the biomass to 1223K for 7 minutes. The fixed carbon together with the volatile matter is measure for the ease of ignition and further gasification or oxidation.

The ash content is the amount of solid residue left over when the biomass is completely combusted. The ash content affects both the handling and the processing costs of the overall biomass energy conversion [1].

The cellulose and lignin are important in biochemical processes, because the biodegradability of cellulose is greater than that of lignin. This is important for the selection of plants for biochemical conversion.

Table A-1 average property values for specified biomass groups [4]

Property	Woody plants	Herbaceous plants	Aquatic plants	Wastes
Example	*Untreated wood*	*Grass/plant*	*Algae*	*Manure*
Moisture content [wt% wet]	18.6	29.8	31.9	44
Lower Heating Value* [kJ kg^{-1}]	18772	18298	23147	18906
Fixed carbon* [wt%]	18.1	17.5	14.8	19.1
Volatile matter* [wt%]	81.9	82.5	85.2	80.9
Ash content** [wt%]	2.2	6.9	6.1	28.5
Cellulose content** [wt%]	39.8	43.9	30	23.1
Hemi-cellulose content** [wt%]	23.3	19.7	35	26.7
Lignin content** [wt%]	24.8	10.9	-	11.3

* **The values are on dry ash free (daf) basis**
****The values are on dry basis**

A.2.   Availability of biomass

The availability of biomass is an important factor for the applicability. A high availability is necessary in order to be able to penetrate the fuel markets [5]. Published research results indicate the global geographical and technical potential of energy crops for the years 2050-2100 [6]. The global geographical potential ranges from 275 to 1115 EJ [6]. This is significant when compared with the world energy consumption today of 410 EJ. There are other researches, which suggest a more cautious approach as indicated in Ref. [7]. When looking into the Dutch setting, there is an energetic potential of about 90 PJ from organic wastes already available [8]. Also studies for the land potential for the production of biomass in the Netherlands have been performed as in Ref. [9]. The expected land potential for energy crop is approximately 50-90 PJ for the year 2015 [9]. Compared to the Dutch energy consumption in 2007 of 3353 PJ, it is a small portion[10].

Transportation of biomass over long distance should not be seen as an obstacle, when biomass can widely be gathered and produced at favourable costs [11]. Densification of the biomass reduces the number of transport moves, since not the volume but the mass becomes restrictive. When wood is pelletized then the density more than doubles [11].

A.3. References

1.   McKendry P. Energy production from biomass (part 1): overview of biomass. Bioresource Technol 2002; 83(1): 37-46.

2.   Williams A., Pourkashanian M., Jones J. M. Combustion of pulverised coal and biomass. Prog Energy Combust Sci 2001; 27(6): 587-610.

3.   Khan A. A. Combustion and Co-Combustion of Biomass in a Bubbling Fluidized Bed Boiler. PhD Thesis, Delft University of Technology, 2007.

4.   Phyllis, database for biomass and waste. http://www.ecn.nl/phyllis/. ECN

5.   Aravind P. V. Studies on High Efficiency Energy Systems Based on Biomass Gasifiers and Solid Oxide Fuel Cells with Ni/GDC Anodes. PhD Thesis, University of Technology Delft, 2007.

6.   Hoogwijk M., Faaij A., Eickhout B., de Vries B., Turkenburg W. Potential of biomass energy out to 2100, for four IPCC SRES land-use scenarios. Biomass Bioenergy 2005; 29(4): 225-257.

7.   Berndes G., Hoogwijk M., van den Broek R. The contribution of biomass in the future global energy supply: a review of 17 studies. Biomass Bioenergy 2003; 25(1): 1-28.

8.   Faaij A., van Doorn J., Curvers T., Waldheim L., Olsson E., van Wijk A., Daey-Ouwens C. Characteristics and availability of biomass waste and residues in The Netherlands for gasification. Biomass Bioenergy 1997; 12(4): 225-240.

9.   Faaij A., Steetskamp I., van Wijk A., Turkenburg W. Exploration of the land potential for the production of biomass for energy in the Netherlands. Biomass Bioenergy 1998; 14(5-6): 439-456.

10.   CBS StatLine - Enerie; verbruik en producentenprijs naar energiebron. http://statline.cbs.nl/StatWeb/publication/?DM=SLNL&PA=80324NED&D1=a&D2=a&D3=220,248-249&HDR=G2,T&STB=G1&VW=T. CBS

11.   Hamelinck C. N., Suurs R. A. A., Faaij A. P. C. International bioenergy transport costs and energy balance. Biomass Bioenergy 2005; 29(2): 114-134.

B.   Biomass pre-treatment

Before biomass can be converted into gas, oil, or sugars, it needs to be pre-treated. The pre-treatment can involve sizing, drying, leaching, torrefaction, and hydrolysis. The type and requirement of pre-treatment depends on the type of biomass used and on the following conversion technique.

In this section some of the pre-treatment processes will be discussed. First the sizing methods for biomass will be discussed, and then some drying methods are treated. This is followed by leaching processes. And finally torrefaction will be discussed. Hydrolysis will not be discussed in this section, but in the section about conversion techniques.

B.1.   Biomass sizing

Every conversion technique has its own demand with regard to size of biomass particles, if solid biomass is used. To prevent for instance clogging of process equipment, sizing of biomass may be required. The two most common devices for sizing biomass are knife chippers and hammer mills [1]. Knife chippers use cutting blades and stationary blades to break the biomass into smaller pieces. Care must be taken to remove any metal and stone that may be mixed with the biomass. The knives can severely be damaged by the stones and metals.

Hammer mills use hammers instead of knives to break the biomass into smaller pieces. The biomass needs to be dry when a hammer mill is used for the size reduction of biomass [2]. In order to ensure the biomass has been properly sized, screens may be used [1].

Pelletizing of biomass as bio-fuels increases energy density, improves storability and eases handling and transport [3]. Cutter shavings and saw dust are preferred materials for the production of wood pellets. The wet material used for pellet production contains about 50-55% water. The material is first ground down to a size of less than 4 mm. Then the material is dried to a water content of 8-12% [3]. Next the biomass compacted and pressed through the holes of a die. The friction created by the passage through the die, increased the temperature of the pellet [4]. This softens the biomass components, which bonds together the material when it is cooled to ambient temperatures.

It is also possible to pelletize other types of biomass, like herbaceous plants.

B.2.   Biomass drying

Some conversion techniques require relatively dry biomass. For instance, most biomass gasification processes require a moisture content between 10 and 20 wt%. Therefore, biomass often needs drying, especially fresh biomass. There are different types of dryers available; some of the techniques are adopted from coal industry. Drying processes require a fairly large energy input to produce the necessary heat. This can reduce the overall plant efficiency. The sequence between sizing and drying depends on the sizing and drying equipment used [1]. Some sizing equipment may require dry biomass and some dryers may require that the biomass is already sized before drying.

The exhaust from drying systems must be monitored for volatile organic compounds (VOC). These compounds can be released by vaporization of volatile compounds or by degradation of the biomass in the dryer. Emissions of VOC during drying usually occur when the feedstock temperature is greater than 373 K [1].

One should also keep in mind the risk for fire and explosions in drying systems. Fire and explosions can result from the ignition of a biomass dust cloud in the dryer or from the ignition of combustible gasses released from the biomass during drying [1, 5].

The type of dryer used depends on several factors: the size of the particles needed drying, the type of biomass, and the capacity of the system [1]. For instance, perforated floor bin dryers are more suitable for small scale biomass plants, while for large scale systems more advanced systems are being used.

Drying technology can be sub-divided into two classes: evaporative drying and mechanical dewatering techniques. Evaporative drying techniques are more common in biomass conversion processes, since mechanical dewatering techniques are usually applied for very wet materials such as slurries and pastes [5]. These mechanical dewatering techniques usually cannot achieve moisture contents below 55 wt% [2]. In evaporative drying techniques heat is supplied to the biomass in order to evaporate moisture from the biomass. Most drying systems operate on basis of heat conduction or heat convection or a combination of heat conduction and convection. Usually, a drying medium is used either directly or indirectly. The drying medium can be a pure vapour (steam), a non-condensable gas (air), or combustion products (flue gas). With the heat supplied by the drying medium, the moisture is evaporated from the biomass. The specific type drier depends on the following: conversion process and the available heat sources. By integrating the drying in the whole plant, the efficiency losses can be reduced. The theoretical energy required for drying of biomass is around 2.5 GJ tonne^{-1} water evaporated assuming an ambient temperature of 288 K [5].

B.3. Leaching

For most processes, especially thermo chemical processes, the inorganic constituents of the biomass can cause problems in the conversion technique or in consecutive equipment. In order to prevent these problems the alkalis and nitrogen compounds need to be removed. This can be done by means of leaching. In the leaching process, biomass is washed in water, followed by a mechanical dewatering. Since alkali compounds in biomass occur as water soluble compounds, washing will release most of the alkalis.

A measure for the amount of alkalis in biomass is the alkali index. This index gives the mass of alkalis in the biomass ($kg\ kg_{biomass}^{-1}$) divided by the heating value ($GJ\ kg_{biomass}^{-1}$) [1]. When the alkali index is below 0.17 kg/GJ then the biomass is considered to have a low severity fouling potential [1]. Is the alkali index above 0.34 kg GJ^{-1} then the biomass is considered to have a high severity fouling potential [1]. Simple leaching over 24 hours can reduce on average the alkali index of biomass by 82% [6]. The amount of potassium and sodium which is removed during leaching can be above 80% [6]. The leaching process can also remove a significant amount of chlorine (>90%) [6]. Smaller fractions of sulphur and phosphorus can be removed as well.

Turn et al. [7] suggests a leaching system which is also used in the sugar industry. It consists of a mechanical dewatering step, followed by rehydration and then again mechanical dewatering. This process can take up a few minutes to hours.

B.4. Torrefaction

Torrefaction is a mild pyrolysis process, which improves the properties of biomass, in particular wood. The temperature in this torrefaction process is in between 500 K and 573 K. These temperatures cause the hemi-cellulose in the biomass to decompose and the structure of the lignin is altered [8]. The products are torrefied wood and some volatiles. The volatiles contain mainly moisture and carbon dioxide [9]. Since these gasses evolve from the torrefaction process, the C/H ratio and the C/O ratio of the biomass will be lowered [9]. The weight is reduced to 70-90% of the original weight. Also, the content of

volatiles is reduced as well as the moisture content. On the other hand, the heating value of the biomass increases. The properties of the end product largely depend on the torrefaction temperature, the residence time and on the type of biomass used [9].

Torrefied biomass is easier to size then fresh biomass. The electricity demand for size reduction can be 50-85% smaller for torrefied biomass compared to fresh biomass [10, 11]. This process is mainly applied before thermo-chemical conversion techniques, especially gasification.

B.5. References

1.   Cummer K. R., Brown R. C. Ancillary equipment for biomass gasification. Biomass Bioenergy 2002; 23(2): 113-128.
2.   Elliott T. C. Standard handbook of powerplant engineering. New York: McGraw-Hill, 1989.
3.   Stahl M., Granstrom K., Berghel J., Renstrom R. Industrial processes for biomass drying and their effects on the quality properties of wood pellets. Biomass Bioenergy 2004; 27(6): 621-628.
4.   Rhén C., Gref R., Sjöström M., Wästerlund I. Effects of raw material moisture content, densification pressure and temperature on some properties of Norway spruce pellets. Fuel Process Technol 2005; 87(1): 11-16.
5.   Brammer J. G., Bridgwater A. V. Drying technologies for an integrated gasification bio-energy plant. Renew Sustain Energy Rev 1999; 3(4): 243-289.
6.   Dayton D. C., Jenkins B. M., Turn S. Q., Bakker R. R., Williams R. B., Belle-Oudry D., Hill L. M. Release of Inorganic Constituents from Leached Biomass during Thermal Conversion. Energy Fuels 1999; 13(4): 860-870.
7.   Turn S. Q., Kinoshita C. M., Ishimura D. M. Removal of inorganic constituents of biomass feedstocks by mechanical dewatering and leaching. Biomass Bioenergy 1997; 12(4): 241-252.
8.   Bourgois J., Guyonnet R. Characterization and analysis of torrefied wood. Wood Sci Technol 1988; 22(2): 143-155.
9.   Prins M. J., Ptasinski K. J., Janssen F. J. J. G. More efficient biomass gasification via torrefaction. Energy 2006; 31(15): 3458-3470.
10.   Bergman P. C. A., Boersma A. R., Kiel J. H. A., Prins M. J., Ptasinski K. J., Janssen F. J. J. G. Torrefaction for entrained-flow gasification of biomass. In: 2nd World Conference and Technology Exhibition of Biomass for Energy, Industry and Climate Protection, Rome, Italy, 2004.
11.   Svoboda K., Pohorelý M., Hartman M., Martinec J. Pretreatment and feeding of biomass for pressurized entrained flow gasification. Fuel Process Technol 2009; 90(5): 629-635.

C.   Biomass conversion techniques

Conversion of biomass into heat and secondary fuels can be divided into three main process technologies: bio-chemical/biological, mechanical extraction and thermo-chemical. Within bio-chemical/biological conversion process two options are available: digestion (production of bio-gas) and fermentation (production of ethanol). Mechanical extraction is a single technology for the production of bio-diesel. The thermo-chemical conversion process encompasses: combustion, liquefaction, pyrolysis and gasification.

The conversion technique largely depends on the type of biomass and on the end-use of the product. Some types of biomass are amenable to nearly all the conversion technologies, while others are suitable for a few methods.

In this section, the different conversion techniques will be discussed except biomass gasification. An indication will be given of which type of biomass can be applied and what is produced. First is started with the bio-chemical/biological methods. Secondly, the mechanical extraction method will be discussed. And finally the thermo-chemical conversion methods will be treated.

C.1. Bio-chemical/biological conversion methods

In bio-chemical/biological conversion several different products can be produced. The products depend on the process and on the micro-organisms used in the process. The following products are most common in bio-chemical/biological conversion of biomass; hydrogen, ethanol and methane. For these processes the biomass needs to be hydrolysed before these processes can be applied.

In the following section, the bio-chemical/biological conversion methods for the specific products will be discussed, starting with the production of hydrogen, followed by the production of ethanol and finally the production of methane.

C.1.1.   Hydrogen production

For the bio-chemical/biological production of hydrogen are several different processes available. All these processes are dependent on the presence of hydrogen producing enzymes [1]. The hydrogen producing enzymes are found to be nitrogenase, Fe-hydrogenase and NiFe hydrogenase [1, 2]. The different processes can be categorized in; fermentative hydrogen production, photolysis process and biological water gas shift. Fermentative hydrogen production can be subdivided into two groups; dark fermentation and light or photo fermentation. In dark fermentation anaerobic bacteria as well as some micro-algae can produce hydrogen at temperatures between 303 and 353K in a dark environment [2, 3]. The substrate for such bacteria and micro-algae is carbohydrate rich, which results in fermentative end products, hydrogen, carbon dioxide and other gasses, like methane or H_2S, depending on the substrate used and the reaction process. When glucose is used as a model substrate the reactions take place as given in equations (C.1) & (C.2).

$$C_6H_{12}O_6 + 2H_2O \rightarrow 2CH_3COOH + 4H_2 + 2CO_2 \qquad (C.1)$$

$$C_6H_{12}O_6 \rightarrow C_3H_7COOH + 2H_2 + 2CO_2 \qquad (C.2)$$
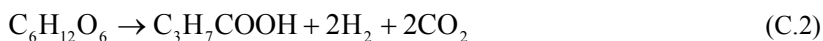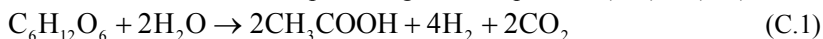
The amount of hydrogen produced by dark fermentation depends on several process parameters, like pH, hydraulic retention time and gas partial pressure [3, 4]. The pH should be between 5 and 6, the hydraulic retention time should be around half a day and the hydrogen concentration should be kept as low as possible [3, 4].

In general the production is around 2 mol of hydrogen per mol of glucose.

In light or photo fermentation are photosynthetic bacteria used to produce hydrogen. The bacteria use the enzyme nitrogenase and solar energy for the conversion of organic acids or biomass into hydrogen. This photo fermentation has three main drawbacks [3]:
1. Low solar energy conversion efficiency
2. Use of nitrogenase enzyme with high energy demand
3. Demand for elaborate anaerobic photo bioreactors covering large areas

Photolysis can be divided into two groups; direct photolysis and indirect photolysis. Direct photolysis is the process of hydrogen production using micro algae, which converts solar energy into chemical energy in the form of hydrogen using a photosynthetic system. Within the photosynthetic systems two processes can be distinguished: photosystem I (PSI) producing reductant for CO_2 reduction and photosystem II (PSII) splitting water and evolving oxygen [3]. Both processes are responsible for the direct photosynthesis process. Electrons are generated when the PSII absorbs light energy. These electrons are transferred to ferredoxin using the solar energy absorbed by PSI. The enzyme hydrogenase accepts the electrons from ferredoxin to produce hydrogen.
Indirect photolysis involves four steps: (1) biomass production by photosynthesis, (2) biomass concentration, (3) aerobic dark fermentation yield 4 mol of hydrogen per mol glucose in the algae cell, along with 2 mol of acetate and (4) conversion of the 2 mol of acetate into hydrogen [3].
The hydrogen production rate is similar to the direct photolysis process, except the indirect photolysis process is less sensitive to oxygen [3].

Biological water gas shift is the water gas shift process performed by bacteria at ambient temperature and pressure [2]. The biological water gas shift is performed in darkness and anaerobic conditions. The feedstock for this process is carbon monoxide, which can be produced by for instance biomass gasification.

C.1.2.   Ethanol production

The production of ethanol is one of the most widely used ways to convert biomass into a fuel. In ethanol production two different feed stocks can be applied. The first one is based on sugar crops (e.g. sugar cane, sugar beet) and starch crops (e.g. maize, wheat). The second one is based ligno-cellulosic biomass. The difference between the two feed stocks is the pre-treatment towards sugars.
The feed stock based on sugar crops and starch crops is ground down and the starch is converted by enzymes to sugars. The sugars are being converted into ethanol by yeast. The resulting ethanol has to be purified by distillation; this is an energy intensive step. There is about 0.450 m^3 of ethanol produced per dry ton of dry corn [5]. The resulting efficiency is 49% (energy content ethanol divided by the energy content of corn). The solid residue from the fermentation process can be used as cattle-feed or in the case of sugar cane, the bagasse can be used as fuel for boilers or for subsequent gasification [5]. This way to produce ethanol is currently applied.
When the feed stock based on ligno-cellulosic biomass is used, the conversion towards ethanol is more complex. The sugars are only available as long polysaccharide chains, which first have to be hydrolysed before the sugars can be fermented into ethanol. The hydrolysis of biomass can be performed in several ways as already described in the liquefaction section.

C.1.3.   Methane production

The biological production of methane from biomass usually occurs via anaerobic digestion of very wet biomass, like manure. The moisture content of the biomass is usually around 80-90%. The wet biomass is converted by bacteria into methane and carbon dioxide. A low percentage of the biomass is converted into gas; sometimes only 1% of the biomass is converted.

There is a specific source for methane rich gas. This gas is landfill gas; the production of methane rich landfill gas from landfill sites makes a significant contribution to the atmospheric methane emissions [6]. When this gas is collected the emission of green house gasses is directly mitigated.

C.2. Mechanical extraction method

Mechanical extraction is the process where oil is produced from various biomass crops, such as oilseed rape, cotton and groundnuts [5]. Oil is not the only product. There is also a residual solid produced, which can be used as cattle fodder. In mechanical extraction the oil is produced by squeezing it out of the biomass. For instance, three tons of rapeseed are required per ton of rapeseed oil produced [5]. The produced oil is further processed by esterification to obtain rapeseed methyl ester (RME) or biodiesel.

C.3. Thermo-chemical conversion methods

C.3.1.   Combustion

The burning of biomass in air, i.e. combustion, is used to convert the chemical energy stored in biomass into heat [5]. The combustion produces hot gasses, mainly carbon dioxide and water, which have a temperature of around 1073-1273K. These temperatures depend on the air factor and on the moisture content of the fuel. The heat in these gasses can be used for various applications, e.g. stoves, furnaces and boilers. In principle, it is possible to combust any type of biomass but in practice it is only feasible for biomass with a moisture content <50%. The scale of combustion plants vary widely, from small scale (domestic application) up to large scale industrial power plants (100-3000MW_{th}). The net electrical efficiency for biomass combustion power plants ranges from 20% to 40% [5]. The higher efficiencies are obtained with systems of over 100 MW_e or when the biomass is co-combusted in coal-fired power plants [5].

C.3.2.   Liquefaction

In liquefaction a number of objectives have to be reconciled: breaking down the macrostructure of biomass, breaking up natural polymers into low molecular weight compounds, stabilizing the reactive species, reducing the oxygen content and increase the C/H ratio [7, 8]. Liquefaction is usually applied to woody plants and herbaceous plants. The liquefaction process can be divided in two different fields: low temperature field (T<533 K) and a high temperature field (T>533 K) [8].
Liquefaction processes in the low temperature field are usually referred to hydrolysis or solvolysis processes. Different media can be applied for the liquefaction process, like acidic aquatic solutions, basic aquatic solutions, and organic solutions [7, 8]. The processes using acid aquatic solution can be sub-divided into processes using low acid concentration and in processes using concentrated acid solutions.
The low acid concentration liquefaction process uses two stages; the first stage is used to break up the hemi- cellulose at a temperature of 400-410 K, the second stage is used to

breakup the cellulose at a temperature of 440-510 K. The acid used is usually sulphuric acid in concentrations of around 0.5-2.5% in water. The resulting product is consisting of dissolved sugars in water. This product is usually further fermented. The residual lignin is used for the production of heat for the process.

The concentrated acid liquefaction process uses three stages; the first stage is used to breakup the hemi-cellulose, the second stage is used for the main hydrolysis of cellulose and the final stage is used for the further hydrolysis of the product coming from the second stage. The decomposition of hemi-cellulose in concentrated acid in the first stage already occurs at a temperature of below 398K. The breakup of cellulose at the second stage occurs at a temperature above 440K. In the last stage the oligosaccharides formed in the second stage are further converted into saccharides. The acid concentration in the reactors of the concentrated acid hydrolysis process is usually around 20-30%. Also here is sulphuric acid most commonly used. After the removal of the acid the product consists of sugar, which can be used for fermentation. The residual lignin is usually used to provide heat for the process.

In basic media, hydrolysis reactions are very slow: but temperature is also an important factor. At temperatures above 410 K the depolymerisation becomes significant. OH- groups contribute to the dissolution of lignin. [8]

In organic media, the chemistry of liquefaction depends on the interaction between the solvent and the substrate. Most efficient solvents are derived from either carbohydrates or lignin. At temperatures above 523 K, it is possible to liquefy and dissolve lignin in simple alcohols, like chloroform, cyclohexanol and phenol [8]. All components of biomass can dissolve in the presence of acidic water and phenol at 513 K [8].

Thermal decomposition of biomass begins at temperatures above 473 K and becomes important at 523 K for carbohydrates and at 553 K for lignin. The overall mechanism of liquefaction is unselective and results in a complex mixture of oils [8]. By using catalysts in a reducing environment the process can be more directed. It also provides the reduction of the C/O ratio in the product. The product is oil.

Hydro thermal upgrading (HTU) is a process where wet biomass is converted into hydrophobic oil. The biomass is treated in liquid water at temperatures of 573-623 K and a pressure of around 12-18 MPa (sub-critical pyrolysis). Besides the oil produced there is also some gas produced, consisting of carbon monoxide, hydrogen, methane and carbon dioxide. The efficiency based on the LHV of both the oil and the biomass is around 60-70%. [9]

C.3.3.   Pyrolysis

Pyrolysis is the heating of biomass at a temperature of 650-800K at a pressure of 0.1-0.5 MPa in the absence of air to convert biomass into liquid oils, solid charcoal and gaseous compounds [3]. There are two different types of pyrolysis: fast pyrolysis and slow pyrolysis. The main product for slow pyrolysis is charcoal; this is usually not of interest in power or gas production. Therefore, the focus in this overview will be on fast pyrolysis.

In fast pyrolysis biomass is heated rapidly in the absence of air. This will result in the formation of a vapour, a solid and subsequently condensed brown bio-liquid. The gaseous products include hydrogen, methane, carbon monoxide, carbon dioxide and other gases depending on the organic nature of the biomass [3]. The liquid products include tars and oils that remain in liquid form at room temperature [3]. Solid products are mainly

composed of char and almost pure carbon plus other inert materials [3]. Pyrolysis is usually used to produce bio-oil or bio-diesel from biomass. In equation (C.3) is the general reaction given.

$$Biomass \rightarrow gasses + oil + char \qquad\qquad (C.3)$$
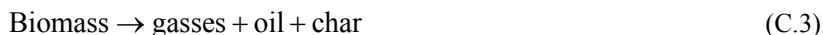
Essential features of fast pyrolysis are [10-12]:
- Very high heating and heat transfer rates, this requires finely ground fuel
- Careful controlled temperature around 700-773K
- Short residence time of the formed vapour
- Rapid cooling of the pyrolysis vapours and aerosols, to produce the bio-oil

These features are required for a high liquid yield. The typical yield of bio-oil from fast pyrolysis is 60-75 wt% of dry biomass [12]. The amount of char is around 15-25 wt% of dry biomass and the amount of non-condensable gas is around 10-20 wt% of dry biomass [12].

There are many different designs available of reactors suitable for biomass fast pyrolysis. The purpose of all the different designs is to provide the essential ingredients for fast pyrolysis; high heating rates, moderate temperatures and short vapour residence time. The most common designs are the fluidized bed and the circulating fluidized bed using pyrolysis gas fluidization agent [11].

The most common sources of biomass used for pyrolysis are woody plants and herbaceous plants. The moisture content is required to be low; otherwise the water will end up in the oil. During the process, some water is formed which cannot be removed by conventional methods, like distillation, from the product. The effect of water is complex in that it affects the stability, viscosity, pH, corrosiveness and other liquid properties [10].

Also the particle size is important in this process. To ensure a good heat transfer to the biomass particle, it needs to be small. Also the heat conductivity of biomass is poor, which also requires the particles to be small. Since these types of biomass are fibrous; it requires a significant amount of energy to reduce the size of these fibrous materials. An optimum has to be found for the particle size required and the energy consumption. Also torrefied biomass is an option worth considering.

C.4. References

1.   Hallenbeck P. C., Benemann J. R. Biological hydrogen production; fundamentals and limiting processes. Int J Hydrogen Energy 2002; 27(11-12): 1185-1193.
2.   Saxena R. C., Adhikari D. K., Goyal H. B. Biomass-based energy fuel through biochemical routes: A review. Renew Sustain Energy Rev 2009; 13(1): 167-178.
3.   Ni M., Leung D. Y. C., Leung M. K. H., Sumathy K. An overview of hydrogen production from biomass. Fuel Process Technol 2006; 87(5): 461-472.
4.   Hawkes F. R., Dinsdale R., Hawkes D. L., Hussy I. Sustainable fermentative hydrogen production: challenges for process optimisation. Int J Hydrogen Energy 2002; 27(11-12): 1339-1347.
5.   McKendry P. Energy production from biomass (part 2): conversion technologies. Bioresource Technol 2002; 83(1): 47-54.
6.   Faaij A. P. C. Bio-energy in Europe: changing technology choices. Energy Policy 2006; 34(3): 322-342.
7.   Behrendt F., Neubauer Y., Oevermann M., Wilmes B., Zobel N. Direct Liquefaction of Biomass. Chem Eng Technol 2008; 31(5): 667-677.

8.   Bouvier J. M., Gelus M., Maugendre S. Wood liquefaction--An overview. Appl
         Energy 1988; 30(2): 85-98.
9.   Goudriaan F., Peferoen D. G. R. Liquid fuels from biomass via a hydrothermal
         process. Chem Eng Sci 1990; 45(8): 2729-2734.
10.   Bridgwater A. V. Principles and practice of biomass fast pyrolysis processes for
         liquids. J Anal Appl Pyrolysis 1999; 51(1-2): 3-22.
11.   Bridgwater A. V., Peacocke G. V. C. Fast pyrolysis processes for biomass. Renew
         Sustain Energy Rev 2000; 4(1): 1-73.
12.   Mohan D., Pittman C. U., Steele P. H. Pyrolysis of Wood/Biomass for Bio-oil: A
         Critical Review. Energy Fuels 2006; 20(3): 848-889.

D.   Thermodynamics of fuel cells and fuel cell modelling

This appendix is divided into two parts; the first part is about the thermodynamics of the fuel cell. The second part discusses the fuel cell model of Cycle-Tempo.

D.1. Fuel cell theory

The performance of a fuel cell can be summarized in graph of its current against the cell voltage characteristics [1]. This is the so-called j-V curve or current voltage curve. In Figure D-1 is an example given of such a curve.
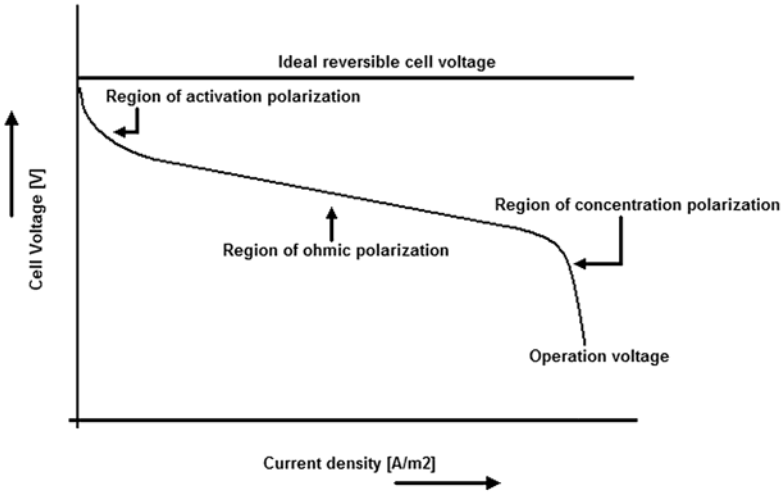
Figure D-1 example of a *j-V* curve with an indication of the three different regions

In Figure D-1, a horizontal line is drawn to indicate the ideal thermodynamically predicted voltage. Since, in reality nothing is behaving ideally, the output voltage of the fuel will be lower. This lowering of the voltage is caused by several effects, which can be indentified in different regions of the j-V curve. In Figure D-1, the three different regions can be indentified. The first region is the region of activation polarization. The second region is the region of ohmic polarization and the final region is the one of concentration polarization. The real fuel cell voltage can be determined with equation (D.1).

$$V = E_{rev} - \eta_{act} - \eta_{ohmic} - \eta_{conc} \tag{D.1}$$

Here is V the real fuel cell voltage, E_{rev} is the ideal thermodynamic cell voltage, η_{act} are the losses caused by the activation polarization, η_{ohmic} the losses caused by the ohmic polarization and η_{conc} are the losses caused by the concentration polarization.
In the following sections each part of equation (D.1) will be explained, starting with ideal thermodynamic cell voltage. This is followed by the activation polarization losses. Next, the ohmic polarization losses will be explained and finally the concentration polarization losses will be discussed.

D.1.1.   Ideal thermodynamic cell voltage

The ideal thermodynamic cell voltage is the voltage a fuel cell would produce when it is operating reversibly. The amount of reversible work a fuel cell can perform can be expressed by equation (D.2).

$$W = E_{rev} \cdot Q \tag{D.2}$$

In this equation is Q the charge. Since electrical work is performed by moving a charge through an electrical potential difference E. In a fuel cell is the charge carried by electrons. In this case the charge can be expressed as indicated in equation (D.3).

$$Q = n \cdot F \tag{D.3}$$

Here is n the number of moles of electrons and F is Faraday's constant. As the reversible work equals the Gibbs free energy of the electrochemical reaction of the fuel cell the relation at standard temperature and pressure can be found as given in equation (D.4).

$$\Delta G_r^0 = -n \cdot F \cdot E_{rev}^0 \Rightarrow E_{rev}^0 = -\frac{\Delta G_r^0}{n \cdot F} \tag{D.4}$$

Often the fuel cell does not operate at standard temperature and pressure. Therefore, some adjustments have to be made to determine the reversible cell voltage at the operational conditions. The reversible voltage of a fuel cell is determined by the temperature, pressure and concentration of the reactants and products. When looking at the influence of the temperature on the reversible cell voltage, the influence of the temperature on the Gibbs free energy has to be understood. In equation (D.5) is the differential expression given for the Gibbs free energy.

$$dG = V \cdot dp - S \cdot dT \tag{D.5}$$

Equation (D.5) can be rewritten for the dependence of temperature at constant pressure as indicated in equation (D.6).

$$\left(\frac{dG}{dT}\right)_p = -S \tag{D.6}$$

When this is applied to equation (D.4) the following result can be obtained.

$$E_{rev}^T = E_{rev}^0 + \frac{\Delta \hat{s}}{n \cdot F}(T - T_0) \tag{D.7}$$

The dependence of pressure can be determined using equation (D.5), this gives:

$$\left(\frac{dG}{dp}\right)_T = V \tag{D.8}$$

When equation (D.8) is combined with equation (D.4) and apply the ideal gas law, the next relation can be obtained.

$$\left(\frac{dE}{dp}\right)_T = -\frac{\Delta n_g \cdot R \cdot T}{n \cdot F \cdot p} \tag{D.9}$$

In this relation is Δn_g the change in total number of moles of gas upon reaction. If n_p is the number of moles in the product and n_r the number of moles of reactant, then $\Delta n_g = n_p - n_r$. The reversible cell voltage also depends on the concentration. To determine the reversible cell voltage the chemical potential is required. The chemical potential is related to concentration through activity (a), as indicated in equation (D.10).

$$\mu_i = \mu_i^0 + R \cdot T \cdot \ln a_i \tag{D.10}$$

The Gibbs free energy for a system of i chemical species is then:

$$dG = \sum_i \mu_i \, dn_i = \sum_i \left(\mu_i^0 + R \cdot T \cdot \ln a_i \right) dn_i \tag{D.11}$$

When an arbitrary chemical reaction is considered, like:

$$1A + bB \rightarrow mM + nN \tag{D.12}$$

The Gibbs free energy of reaction can be determined using equation (D.13).

$$\Delta \hat{g} = (m \cdot \mu_M^0 + n \cdot \mu_N^0) - (\mu_A^0 + b \cdot \mu_B^0) + R \cdot T \cdot \ln \frac{a_M^m \cdot a_N^n}{a_A^1 \cdot a_B^b} \tag{D.13}$$

By rewriting the relation the following equation can be obtained:

$$\Delta \hat{g} = \Delta \hat{g}^0 + R \cdot T \cdot \ln \frac{a_M^m \cdot a_N^n}{a_A^1 \cdot a_B^b} \tag{D.14}$$

This can be combined with equation (D.4) resulting in equation 15.

$$E_{rev}^C = E_{rev}^0 - \frac{R \cdot T}{n \cdot F} \cdot \ln \frac{a_M^m \cdot a_N^n}{a_A^1 \cdot a_B^b} \tag{D.15}$$

Equation (D.15) can be written in a more general form with an arbitrary number of products and reactants.

$$E_{rev}^C = E_{rev}^0 - \frac{R \cdot T}{n \cdot F} \cdot \ln \frac{\prod a_{Products}^{\upsilon_i}}{\prod a_{Reactants}^{\upsilon_i}} \tag{D.16}$$

When al the different effect of temperature, pressure and concentration are combined, the equation for determining the reversible cell voltage becomes:

$$E_{rev} = E_{rev}^0 + \frac{\Delta \hat{s}}{n \cdot F} \cdot (T - T_0) - \frac{R \cdot T}{n \cdot F} \cdot \ln \frac{\prod a_{Products}^{\upsilon_i}}{\prod a_{Reactants}^{\upsilon_i}} \tag{D.17}$$

D.1.2. Activation polarization

The activation polarization is caused by the reaction rates of both the anode and cathode reactions. For instance, in a proton exchange membrane fuel cell the following electrochemical half reaction takes places.

$$\text{anode:} \qquad H_2 \rightarrow 2H^+ + 2e^- \tag{D.18}$$

$$\text{cathode:} \qquad \frac{1}{2} O_2 + 2H^+ + 2e^- \rightarrow H_2O \tag{D.19}$$
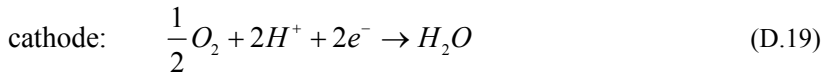
The reaction at the anode has its own reaction rate, as well as the cathode reaction has it own reaction rate. Each reaction can be further divided into more basic reaction steps. The rate of the reaction is determined by the rate of the slowest step. Each reaction and reaction step has to overcome a barrier before a reaction can take place, the so called activation energy barrier as indicated in Figure D-2.
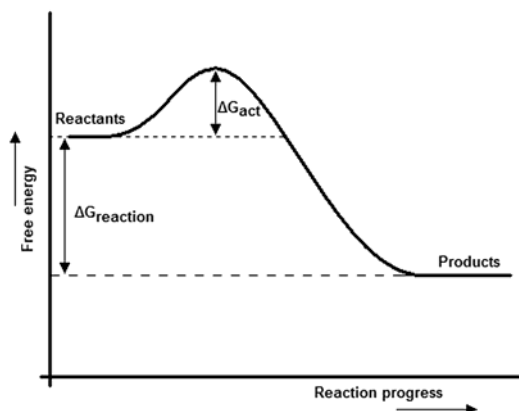
Figure D-2 Activation barrier (ΔG_{act}) impedes the conversion of reactants into products

Looking into the oxidation of hydrogen, this reaction consists of a series of basic steps. These steps could be as follows:

1. Mass transport of hydrogen gas to the electrode (see also Figure D-3):

   $H_{2,bulk} \rightarrow H_{2,gas\ electrode\ interface}$

2. Adsorption of hydrogen onto the electrode surface:

   $H_{2,gas\ electrode\ interface} + M \rightarrow M^{\cdots}H_2$

3. Separation of the hydrogen molecule into two chemisorbed hydrogen atoms on the catalyst surface:

   $M^{\cdots}H_2 + M \rightarrow 2(M^{\cdots}H)$

4. Transfer of electrons from the chemisorbed hydrogen to the electrode, releasing the resulting proton into the electrolyte:

   $2(M^{\cdots}H) \rightarrow 2(M + e^-) + 2H^+_{gas\ electrode\ interface}$

5. Mass transport of the proton away from the electrode:

   $2H^+_{gas\ electrode\ interface} \rightarrow 2H^+_{bulk\text{-}electrolyte}$
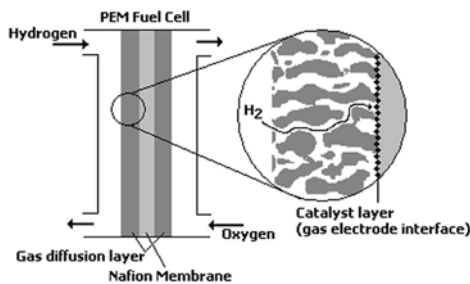
Figure D-3: Details of the gas diffusion layer of a PEM fuel cell

The reaction rate is determined by the slowest step in the reaction, the slowest step is assumed to be the transfer of electrons from the chemisorbed atomic hydrogen to the metal (step 4). The chemisorbed hydrogen is depicted as $M^{\cdots}H$ and the liberated metal site with free electron by $(M + e^-)$. In the following figure, curve 1 depicts the free energy of the chemisorbed atomic hydrogen, which increases with the distance from the metal surface. Curve 2 depicts the free energy of a proton in the electrolyte.
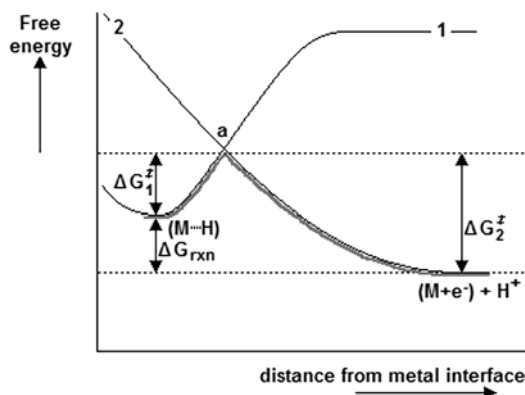
Figure D-4: Schematic illustration of the energies of the chemisorbed hydrogen charge transfer reaction. Curve 1: Shows the energy of the reactant state (M···H). Curve 2: Shows the energy of the product state (M + e⁻). Both as function of the hydrogen atom/ion distance from the metal surface. The solid grey line denotes the minimum energy path for the conversion, and "a" denotes the activated state.[1]

The dark solid line gives the minimum energy path for reaction step 4 and the point "a" indicates the activated state. Species in the activated state have overcome the free energy barrier, so they can either be converted into products or reactants without further impediment. The lower free energy state of product compared to the free energy state of the reactant leads to different activation barriers for the forward and backward reactions. Therefore the forward reaction rate is expected to be faster than the backward reaction rate. These unequal reaction rates lead to a build up of charge, electrons in the metal electrode and protons accumulating in the electrode. The charge accumulation continues until the resultant potential difference ($\Delta\varphi$), the so-called Galvani potential, across the reaction interface counterbalances the free energy difference between the reactant and product state. This effect is depicted in the Figure D-5.
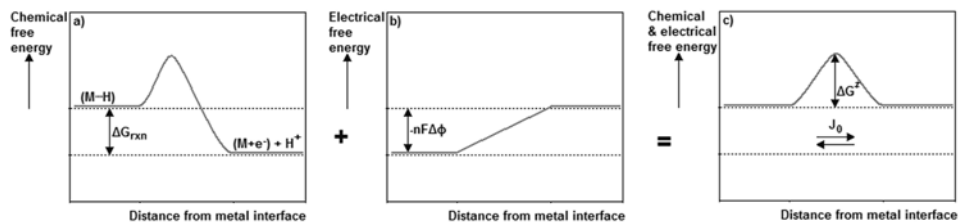
Figure D-5: At equilibrium, the chemical free energy difference (a) across a reaction interface is balanced by an electrical potential difference (b), resulting in a zero net reaction rate (c).[1]

This effect is also found at the cathode of a fuel cell. By adding the up the Galvani potential of the anode and the Galvani potential of the cathode the thermodynamic ideal voltage can be found.

A distinguishing feature of electrochemical reactions is the ability to manipulate the size of the activation barrier by varying the cell potential. The free energy of charged species is sensitive to voltage, so changing the cell voltage change the free energy of the charged species taking part in the reaction. Therefore, the size of the activation barrier can be

influenced. If a part of the Galvani potential is sacrificed, the system energetics can be biased in such a way that the forward reaction is favoured. See the following figure.
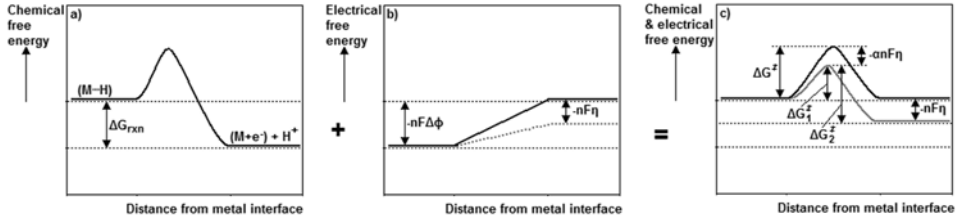
Figure D-6: The chemical energy (a) of the reaction, changing the electrical potential (b) upsets the balance between the foward and reverse activation barriers (c). In this diagram, reducing the Galvani potential by η reduces the foward activation barrier ($\Delta G^{\ddagger}_1 < \Delta G^{\ddagger}_2$) and increases the reverse activation barrier ($\Delta G^{\ddagger}_2 > \Delta G^{\ddagger}_1$).[1]

The galvanic potential at both the anode and cathode have to be reduced to extract a current from the fuel cell. The reduction of the galvanic potentials results in a smaller net fuel cell voltage, as shown in the next figure.
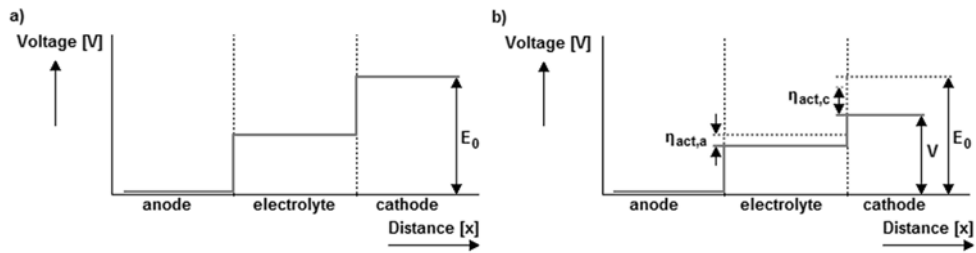
Figure D-7: a) Contributions of the Galvani potentials to the overall cell potential. b) The influence of the losses by lowering the activation energy for the reaction on the net cell potential.[1]

The exchange current density is the equilibrium current density; both forward and backward together give then a net zero current density. The exchange current density is an indication for the rate an equation is given below.

$$j_0 = n \cdot F \cdot c_R^* \cdot f_1 \cdot e^{\frac{-\Delta G^{\ddagger}_1}{R \cdot T}}$$

(D.20)

In this equation is c_R^* the surface concentration of the reactant, f_1 is the decay rate to the products and $\Delta G_1^{\ddagger}$ is the activation energy.

This is a simplified description of the activation polarization losses, because it only considers the sluggish electrode kinetics. But the processes involving the adsorption of the reaction species, the transfer of electrons, the desorption of the species and the electrode structure all contribute to the activation polarization losses [2].

Simplified Activation kinetics: The tafel equation

Tafel observed and reported in 1905, that the overvoltage at the surface of an electrode followed a similar pattern in a great variety of electrochemical reactions [3]. This pattern is shown in Figure D-8, a so called 'Tafel Plot'. The overvoltage is plotted against the logarithm of the current density. For most values of the overvoltage the plot approximates a

straight line. For most values of the overvoltage its value can be calculated by the following equation:

$$\eta_{act} = A^T \cdot \log\left(\frac{i}{i_0}\right)$$ (D.21)

This equation can be rewriten in a linear from as indicated in Equation (D.22).

$$\eta_{act} = -A^T \cdot \ln j_0 + A^T \cdot \ln j$$ (D.22)

In Figure D-8, the line representing this equation is indicated in grey. The slope of the line is represented by the constant A. If the value of constant A is high this means the electrochemical reaction is slow. The value for the exchange current density i_0 is indicated at the intercept of the current density axis.
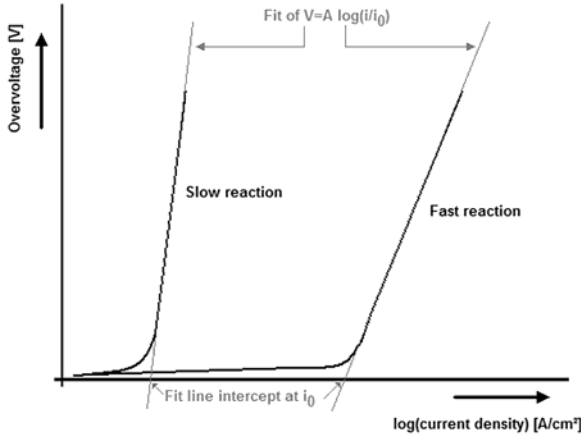
Figure D-8 Tafel plot for slow and fast electrochemical reactions

The activation losses occur at both the anode and cathode. The overall activation losses can be caluclated by determining the activation losses for the anode and cathode separately and putting the results together.

$$\eta_{act} = \eta_{act,anode} + \eta_{act,cathode}$$ (D.23)

D.1.3.   Ohmic polarization

The charge transport inside fuel cells results in a voltage loss for fuel cells. There are two kinds of charges being transported in a fuel cell. The first are the electrons and the second are ions. In most fuel cells, ion charge transport is far more difficult then electron charge transport [1]. There are three main driving forces involved in the charge transport, these forces are:

- electrical driving forces, this can be represented by a electrical potential gradient;
- chemical driving forces, which can be represented by a chemical potential gradient;
- mechanical driving forces, which can be represented by a pressure gradient

The conductors in a fuel cell have an intrinsic resistance to charge flow, this results in a voltage loss. The charge flux can be writen as indicated in equation (D.24), when the charge tranport is dominanted by electrical driving forces.

$$j = \sigma \frac{dV}{dx} \tag{D.24}$$

In this relation, j is the charge flux, σ is the conductivity and dV/dx is the electric field providing the driving force for the charge transport. When this relation is applied for a conductor with a constant cross sectional area A and length L; the equation becomes:

$$j = \sigma \frac{V}{L} \tag{D.25}$$

By solving equation (D.25) for V and applying the relation between charge flux and current (I), a relation similar to Ohms law can be found.

$$V = I \cdot \left(\frac{L}{A \cdot \sigma} \right) = I \cdot R \tag{D.26}$$

Therefore, the ohmic losses can be written as:

$$\eta_{\text{ohmic}} = I \cdot R_{\text{ohmic}} = I \cdot \left(R_{\text{elec}} + R_{\text{ionic}} \right) \tag{D.27}$$

In this equation, R_{elec} is the resistance caused by the electron transport and R_{ionic} the ionic contribution.

The resistance of a fuel cell is geometry dependent, it scales with area. To normalize this effect, the area specific resistance is used. This leads to the equation (D.28).

$$\eta_{\text{ohmic}} = i \cdot ASR_{\text{ohmic}} \quad \text{with} \quad ASR_{\text{ohmic}} = A_{\text{fuel cell}} \cdot R_{\text{ohmic}} \tag{D.28}$$

The resistance of a fuel cell does not only scale with area, but also with thickness. A thinner fuel cell has a lower resistance. This especially applies to the electrolyte of the fuel cell. There is a practical limit to the thickness of a fuel cell. The most important limitations are:

- Mechanical integrity; an electrolyte membrane cannot be to thin that it risks breaking (in case of SOFC) or develops pinholes.
- Non-uniformities; the electrolyte layer has to be uniform in thickness. A non-uniform electrolyte could form hot-spots where the layer is thin; these hot-spots can lead to rapid deteriorating and failure.
- Shorting; extremely thin electrolyte layers can lead to electrical shorting.
- Fuel crossover; when the thickness of the electrolyte decreases the crossover of reactants could increase. This leads undesirable parasitic losses.
- Contact resistance; part of the resistance of the electrolyte is associated with the interface between the electrolyte and the electrode.

Each part of the fuel cell contributes to the fuel cell resistance, but the electrolyte yields the biggest resistance loss for most fuel cells. There three major electrolyte classes used in fuel cells: liquid electrolytes, polymer electrolytes and ceramic electrolytes.

Liquid electrolytes

Liquid electrolytes are used in AFC, PAFC, DCFC and MCFC. There are two types of liquid electrolytes; the first are aqueous electrolytes and the second are ionic electrolytes. In an aqueous electrolyte the charge transport takes place by in water dissolved ions. Ionic electrolytes are ionic liquids which are simultaneously liquid and ionic. The charge transport is here also performed by the ions. The liquid is in most fuel cells immobilized by a matrix material. The matrix material provides mechanical strength, prevents shorting and prevent crossover of reactants.

The different types of fuel cells use different types of electrolytes. The alkaline fuel cell uses concentrated aqueous KOH electrolytes, the phosphoric acid fuel cell uses either

concentrated aqueous H_3PO_4 electrolyte or pure H_3PO_4 as an ionic liquid. Direct carbon and molten carbonate fuel cells use $(K/Li)_2CO_3$ melts at around 450°C as a molten electrolyte. The ionic conductivity depends on the mobility of the ions and the concentration of the ions. The mobility of the ions depends on the ion size and the viscosity of the liquid. When the solution becomes more concentrated, the electrical interaction of the ions on each other becomes more important and influences the mobility of the ions.

Polymer electrolytes

Polymer electrolytes are used in PEM-FC. The most commonly used electrolyte in PEM-FC is Nafion®. Other types of electrolyte are also available, but the working principle is similar. The polymer should posses fixed charged sited in the polymer and it should have free volume or open space. The fixed charged sited should have an opposite charge compared to the moving ions, in order to maintain the net charge balance.
The free volume or open space is important for the ability of ion to move through the polymer. Increasing the polymer free volume increase the range of small structural vibrations and motions within the polymer. Also provides the free volume another phenomenon the vehicle mechanism. In the vehicle mechanism the ion hitching a ride on a certain species (the vehicles) as these vehicles pass by. Water is a common vehicle species in the PEM-FC.

Ceramic electrolytes

Ceramic electrolytes are used in SOFC. These solid materials are crystalline oxide materials that can conduct ions. These materials have a high concentration of oxygen vacancies, which allows the material to have a high ion conductivity. The conductivity of the material depends on the concentration of vacancies and the mobility of the ions.

D.1.4.   Concentration polarization

Concentration polarization or concentartion losses are caused by the depletion of the reactants at the electrode surface causing a concentration difference. Several processes are responsible for the concentration losses: slow diffusion of the reactants in the electrode, solution/desolution of the reactants or production in the electrolyte or diffusion of the reactants or production through the electrolyte. The slow transport of reactant to the electrode and the slow transport of products from the electrode are the main contributors to the concentration losses. The concentration polarization can be described by equation (D.29).

$$\eta_{conc} = \frac{R \cdot T}{n \cdot F} \cdot \ln \frac{i_l}{i_l - i} \tag{D.29}$$

In this equation is i_l the limiting current density. The limiting current density is a measure of the maximum rate at which a reactant can be supplied to the electrode [2].

D.2. Fuel cell Modelling in Cycle-Tempo

Cycle-Tempo [4] is flow sheeting program specially designed for energy conversion system. The uses standard building blocks for the construction of a flow sheet. One of those building blocks is a fuel cell. This building block uses a set of equations for the determining the performance of the fuel cell, which can be in design as well as in off-design. In this chapter the model used for this building block is discussed.

The fuel cell building block can represent many different types of fuel cells, as given in the following list:

- Proton exchange membrane fuel cell; in the program, it is called solid polymer fuel cell (SPFC)
- Phosphoric acid fuel cell (PAFC)
- Alkaline fuel cell (AFC)
- Molten carbonate fuel cell (MCFC); there are three kinds available in Cycle-Tempo (CT). The standard one, one with indirect internal reforming (IIR) and one with direct internal reforming (DIR)
- Solid oxide fuel cell (SOFC); for this fuel cell are also three kinds available in CT. The standard one, one with IIR and one with DIR.
- Direct carbon fuel cell (DCFC)

For each of these fuel cell types it is possible to perform design calculations as well as off-design calculations.

In the fuel cell calculations several steps are taken, as indicated in Figure D-9. Some steps are dependant on the fuel cell type. For instance, the calculation of fuel composition at active area of the fuel cell is only calculated when the fuel is fist reformed. The fuel is only reformed when internal reforming is being applied. In Figure D-9, EEQCOD stands for energy equation code; this determines whether a mass-flow or a temperature needs to be calculated with the help of an additional energy balance.

Figure D-9 calculation steps for the fuel cell model in Cycle-Tempo

In the following sections, the different steps, as indicated Figure D-9, will be discussed; starting at the top of the figure working the way down.

D.2.1.   Calculation of the fuel composition

In the case of an indirect reforming or direct reforming fuel cell, the fuel composition at active cell surface has to be determined. If there is no indirect or direct reforming taking place then the composition is similar to inlet composition.

The following substances can be converted in the reforming step: methane (CH_4) and carbon monoxide (CO). The reactions given in equations (D.30) & (D.31) are assumed to be responsible for this.

$$CO + H_2O \rightleftarrows CO_2 + H_2 \tag{D.30}$$

$$CH_4 + 2H_2O \rightleftarrows CO_2 + 4H_2 \tag{D.31}$$

The reforming calculations are based on the minimization of the Gibbs free energy. In the minimization calculation is a list of possible reaction products required. The list of products in the fuel cell model includes: H_2, CH_4, H_2S, H_2O, CO, CO_2, N_2, Ar, HCl, $C_{(s)}$, SO_2 and O_2. In case of indirect internal reforming a reaction temperature and reaction pressure is required. For the case of direct internal reforming, the reaction temperature equals the fuel operation temperature and the reaction pressure equals the fuel cell pressure.
The calculated composition is being used as inlet composition for the fuel cell calculations.

D.2.2.   Calculation of the anode and cathode outlet compositions

The outlet composition of the anode and cathode of the fuel cell are determined by the type of fuel cell, the fuel utilisation and oxidant utilization. The fuel cell type determines which components are being converted. For instance, the low temperature fuel cells (SPFC, PAFC & AFC) only convert hydrogen, the DCFC only converts carbon, the indirect or external reforming fuel cells only convert hydrogen and carbon monoxide and the direct reforming fuel cells convert hydrogen, carbon monoxide and methane.
The anode outlet composition for the different types of fuel cells is calculated with the help of the inlet composition and the fuel utilization of the fuel cell. In Table D-1, the formulae are given for the different fuel cell types.

For the calculation of cathode outlet composition, the amout of hydrogen equivalents at the anode inlet is required as well as the fuel utilization and the oxidant to fuel ratio. In Equation (D.32), the relation is given for the calculation of the amount of moles of hydrogen equivalents which are bing converted at the cathode.

$$C_{moles} = \left. y_{H_2}^{eq} \cdot U_F \middle/ OFRAT \right. \tag{D.32}$$

In this equation is $y_{H_2}^{eq}$ the molfraction of hydrogen equivalents at the anode entrance. The value is calculated using the following equation.

$$y_{H_2}^{eq} = 2 \cdot y_C^a + \frac{1}{2} \cdot y_H^a - y_O^a \tag{D.33}$$

The calculation of the fractions at the outlet of cathode is calculated with the equation given in Table D-1.
The outlet fractions calculated with the equations in Table D-1 are normalized in such a way that the sum of all anode outlet fractions or all cathode outlet fractions is 1.

D.2.3.   Calculation of temperatures, pressures and enthalpies

The temperatures, pressures and enthalpies are calculated as fuctions of:
- The temperatures and pressures for the unit as supplied by the user
- The pressure and temperature differences supplied by the user
- Pressures, temperatures and enthalpies defined in apparatuses up- or down stream in the system.

In the calculation for the fuel cell 3 separate circuits are being used. These circuits are for the anode, the cathode and the cooling circuit. For every circuit, the temperatures, pressures and enthalpies are calculated separately.

Table D-1 formulae for the calculation of the outlet composition of the different fuel cell types

Fuel cell	Anode	Cathode
AFC	$y_{H_2O}^{a,out} = y_{H_2O}^a + y_{H_2}^a \cdot 2 \cdot U_F$ $y_{H_2}^{a,out} = y_{H_2}^a \cdot (1 - U_F)$	$y_{O_2}^{c,out} = y_{O_2}^c - {C_{moles}}/{2}$ $y_{H_2O}^{c,out} = y_{H_2O}^c - C_{moles}$
PAFC	$y_{H_2}^{a,out} = y_{H_2}^a \cdot (1 - U_F)$	$y_{O_2}^{c,out} = y_{O_2}^c - {C_{moles}}/{2}$ $y_{H_2O}^{c,out} = y_{H_2O}^c + C_{moles}$
SPFC	$y_{H_2}^{a,out} = y_{H_2}^a \cdot (1 - U_F) \qquad y_{H_2O}^{os} = y_{H_2}^a \cdot 2 \cdot U_F \cdot T_{H_2O}^{os}$ $if \quad y_{H_2O}^{os} > y_{H_2O}^a \Rightarrow T_{H_2O}^{os} = \dfrac{y_{H_2O}^a}{y_{H_2}^a \cdot 2 \cdot U_F}$ $\qquad y_{H_2O}^{a,out} = 0$ $else \quad y_{H_2O}^{a,out} = y_{H_2O}^a - y_{H_2O}^{os}$	$y_{O_2}^{c,out} = y_{O_2}^c - {C_{moles}}/{2}$ $y_{H_2O}^{c,out} = y_{H_2O}^c + C_{moles} + C_{moles} \cdot 2 \cdot T_{H_2O}^{os}$
DCFC	$y_{CO_2}^{a,out} = y_{CO_2}^a + y_C^a \cdot 1.5 \cdot U_F$ $y_C^{a,out} = y_C^a \cdot (1 - 0.5 \cdot U_F)$	$y_{O_2}^{c,out} = y_{O_2}^c - {C_{moles}}/{2}$ $y_{CO_2}^{c,out} = y_{CO_2}^c - C_{moles}$
ER or IIR MCFC	$y_{CO_2}^{a,out} = y_{CO_2}^a + (2 \cdot y_{CO}^a + y_{H_2}^a) \cdot U_F \qquad y_{H_2O}^{a,out} = y_{H_2O}^a + y_{}^{}$ $y_{H_2}^{a,out} = y_{H_2}^a \cdot (1 - U_F) \qquad\qquad y_{CO}^{a,out} = y_{CO}^a \cdot (1 - $	$y_{O_2}^{c,out} = y_{O_2}^c - {C_{moles}}/{2}$ $y_{CO_2}^{c,out} = y_{CO_2}^c - C_{moles}$
DIR MCFC	$y_{CO_2}^{a,out} = y_{CO_2}^a + (2 \cdot y_{CO}^a + y_{H_2}^a + 5 \cdot y_{CH_4}^a) \cdot U_F$ $y_{H_2O}^{a,out} = y_{H_2O}^a + (y_{H_2}^a + 2 \cdot y_{CH_4}^a) \cdot U_F$ $y_{H_2}^{a,out} = y_{H_2}^a \cdot (1 - U_F) \quad y_{CO}^{a,out} = y_{CO}^a \cdot (1 - U_F)$ $y_{CH_4}^{a,out} = y_{CH_4}^a \cdot (1 - U_F)$	$y_{O_2}^{c,out} = y_{O_2}^c - {C_{moles}}/{2}$ $y_{CO_2}^{c,out} = y_{CO_2}^c - C_{moles}$
ER or IIR SOFC	$y_{CO_2}^{a,out} = y_{CO_2}^a + y_{CO}^a \cdot U_F \qquad y_{H_2O}^{a,out} = y_{H_2O}^a + y_{H_2}^a \cdot U_F$ $y_{H_2}^{a,out} = y_{H_2}^a \cdot (1 - U_F) \qquad y_{CO}^{a,out} = y_{CO}^a \cdot (1 - U_F)$	$y_{O_2}^{c,out} = y_{O_2}^c - {C_{moles}}/{2}$
DIR SOFC	$y_{CO_2}^{a,out} = y_{CO_2}^a + (y_{CO}^a + y_{CH_4}^a) \cdot U_F$ $y_{H_2O}^{a,out} = y_{H_2O}^a + (y_{H_2}^a + 2 \cdot y_{CH_4}^a) \cdot U_F$ $y_{H_2}^{a,out} = y_{H_2}^a \cdot (1 - U_F) \quad y_{CO}^{a,out} = y_{CO}^a \cdot (1 - U_F)$ $y_{CH_4}^{a,out} = y_{CH_4}^a \cdot (1 - U_F)$	$y_{O_2}^{c,out} = y_{O_2}^c - {C_{moles}}/{2}$

D.2.4.   Calculation of reversible cell voltage

The calculation of the reversible cell voltage is based on the Nernst equation, as indicated in equation (D.17). In Cycle-Tempo the gasses are assumed to behave ideally, therefore Equation (D.17) can be rewritten into:

$$E_{rev} = E_{rev}^0 + \frac{\Delta \hat{s}}{n \cdot F} \cdot (T - T_0) - \frac{R \cdot T}{n \cdot F} \cdot \ln \frac{\prod p_{Products}^{v_i}}{\prod p_{Reactants}^{v_i}} \tag{D.34}$$

The pressures in this equation are partial pressures of the reactants and products. This equation can be rewritten in amore convenient form, for the calculations in Cycle-Tempo.

$$E_{rev} = \frac{\Delta G_R^T}{n \cdot F} - \frac{R \cdot T}{n \cdot F} \cdot \ln \frac{\prod p_{Products}^{v_i}}{\prod p_{Reactants}^{v_i}} \tag{D.35}$$

In this equation the Gibbs free energy of the reaction is given at temperature T instead of the reference temperature. The different reactions and matching Nernst equations are given in Table D-2.

The calculation of the reversible cell voltage is done in three steps:
1. calculation of the standard reversible cell voltage
2. calculation of the composition of the anode and cathode along the length of the fuel cell
3. calculation of the reversible cell voltage with the Nernst equation

Table D-2 Total reaction and Nernst equation for different fuel cell types

Fuel cell type	Reaction	*Nernst equation*
DCFC	$C + O_2 \rightarrow CO_2$	$E_{rev} = \dfrac{\Delta G_R^T}{2 \cdot F} - \dfrac{R \cdot T_{cell}}{2 \cdot F} \cdot \ln \left(\dfrac{\sqrt{y_{O_2,c}} \cdot y_{CO_2,c}}{\left(y_{CO_2,a} \right)^{1.5}} \cdot \sqrt{p_{cell}} \right)$
MCFC	$H_2 + \frac{1}{2} O_2 \rightarrow H_2O$ $CO + \frac{1}{2} O_2 \rightarrow CO_2$	$E_{rev} = \dfrac{\Delta G_R^T}{2 \cdot F} - \dfrac{R \cdot T_{cell}}{2 \cdot F} \cdot \ln \left(\dfrac{\sqrt{y_{O_2,c}} \cdot y_{H_2,a} \cdot y_{CO_2,c}}{y_{H_2O,a} \cdot y_{CO_2,a}} \cdot \sqrt{p_{cell}} \right)$
SOFC & AFC	$H_2 + \frac{1}{2} O_2 \rightarrow H_2O$	$E_{rev} = \dfrac{\Delta G_R^T}{2 \cdot F} - \dfrac{R \cdot T_{cell}}{2 \cdot F} \cdot \ln \left(\dfrac{\sqrt{y_{O_2,c}} \cdot y_{H_2,a}}{y_{H_2O,a}} \cdot \sqrt{p_{cell}} \right)$
SPFC & PAFC	$H_2 + \frac{1}{2} O_2 \rightarrow H_2O$	$E_{rev} = \dfrac{\Delta G_R^T}{2 \cdot F} - \dfrac{R \cdot T_{cell}}{2 \cdot F} \cdot \ln \left(\dfrac{\sqrt{y_{O_2,c}} \cdot y_{H_2,a}}{y_{H_2O,a}} \cdot \sqrt{p_{cell}} \right)$

D.2.5.   Calculation of electrical parameters and fuel flow

In the calculation of the electrical parameters is the relation between the cell voltage and the current density. This relation can be given with equation (D.36).

$$i = \frac{U_F}{R_{eq} \int_0^{U_F} \frac{dx}{E_{rev}(x) - V}} \tag{D.36}$$

In this equation is the reversible cell voltage at a certain place along length of the fuel cell ($E_{rev}(x)$) is important. The integral in this equation represents the voltage loss of the fuel cell, which is indicated in equation (D.37).

$$\Delta V = \left[\int_0^{U_F} \frac{dx}{E_{rev}(x) - V} \right]^{-1} \tag{D.37}$$

By filling equation (D.37) into equation (D.36), the following equation can be obtained.

$$i = U_F \cdot \frac{\Delta V}{R_{eq}} \tag{D.38}$$

The equation can be rewritten to calculated equivalent fuel cell resistance as indicated in equation (D.39)

$$R_{eq} = U_F \cdot \frac{\Delta V}{i} \tag{D.39}$$

The power of the fuel cell can be calculated with:

$$P = i \cdot V = U_F \cdot \frac{\Delta V}{R_{eq}} \cdot V \tag{D.40}$$

The cell voltage as a function of the equivalent fuel cell resistance is given in equation (D.41).

$$V = E_{rev} - R_{eq} \cdot i \tag{D.41}$$

The fuel flow through the fuel cell can be determined by the current flowing through the fuel cell, which is related to the mass flow as indicated in equation (D.42).

$$I = \frac{\phi_{m,a,in}}{M_a} \cdot 2 \cdot F \cdot y_{H_2}^{eq} \cdot U_F \tag{D.42}$$

D.2.6.   Cooling cycle

The low temperature fuel cells can have a cooling cycle. The high temperature fuel cells do not have a cooling cycle. These fuel cells are cooled with the oxidant flow.
When a cooling cycle is applied the temperature is calculated from the energy balance.
If there is no cooling cycle the energy equation code needs to be defined. By defining an energy equation code (EEQCOD), Cycle-Tempo can determined either a mass-flow (EEQCOD=1) or a temperature (EEQCOD=2) from an energy balance.

D.3. Off-design

It is possible to perform off-design calculations with the fuel cell model. In the design calculations the current density and the cell voltage are required for the calculation. For off-design calculations, the cell area and the equivalent cell resistance are required input parameters also one of the following parameters is required: power or cell voltage or current density. With the given area and equivalent resistance and one of the other parameters the missing parameters can be calculated.

For the solid polymer fuel cell, the off-design calculation includes the Tafel equation for the calculation of the activation losses. The following equation is used for the calculation of the cell voltage.

$$V = E_{\text{rev}} - \left(i + i_{\text{n}} \right) \cdot R_{\text{ohm}} - A^T \cdot \ln\left(\frac{i + i_{\text{n}}}{i_0} \right) + B \cdot \ln\left(1 - \frac{i + i_{\text{n}}}{i_1} \right) \qquad \text{(D.43)}$$

In the off-design calculation applies the following equation:

$$V = E_{\text{rev}} - i \cdot R_{\text{od}} \qquad \text{(D.44)}$$

In this equation is R_{od} the fuel cell resistance for the off-design situation. When the equations (D.43) and (D.44) are combined the next equation is obtained.

$$R_{\text{od}} = \frac{i + i_{\text{n}}}{i} \cdot R_{\text{ohm}} + \frac{A^T}{i} \cdot \ln\left(\frac{i + i_{\text{n}}}{i_0} \right) - \frac{B}{i} \cdot \ln\left(1 - \frac{i + i_{\text{n}}}{i_1} \right) \qquad \text{(D.45)}$$

For the calculation of the current density in the off-design situation equation (D.36) is used, but the equivalent fuel cell resistance (R_{eq}) is replace by the off-design resistance (R_{od}). With the help of the design point of the fuel cell the slope of the Tafel line (A) is determined with the help of equation (D.46).

$$A^T = \frac{i_{\text{des}} \cdot R_{\text{eq}} - \left(i_{\text{des}} + i_{\text{n}} \right) \cdot R_{\text{ohm}} + B \cdot \ln\left(1 - \frac{i_{\text{des}} + i_{\text{n}}}{i_1} \right)}{\ln\left(\frac{i_{\text{des}} + i_{\text{n}}}{i_0} \right)} \qquad \text{(D.46)}$$

In this equation is i_{des} the current density at the design point of the fuel cell. This means the design current density has to be put in the model by the user. The equivalent fuel cell resistance is calculated with the current density at the design point using equation (D.36). For off-design calculation some default values are used, when the user does not specify these values. In Table D-3, the default values for the off-design calculations of the SPFC are given.

Table D-3 Default values for the off-design calculation for the SPFC

Description	Symbol	Value	Unit
Internal and fuel crossover equivalent current density	i_{n}	20	A m^{-2}
Exchange current density	i_0	0.67	A m^{-2}
Limiting current density	i_1	9000	A m^{-2}
Mass transfer over voltage	B	0.05	V
Ohmic cell resistance	R_{ohm}	3e-6	Ω m^2

D.4. Proposal for model improvement

In the off-design calculation of the SPFC the activation losses are included. This is not the case for the other fuel cell types, like the SOFC and MCFC.
The same calculation method for these types of fuel cells could be applied. But other default values are required. In the following sections some suggestions are given for the SOFC and MCFC.

D.4.1. SOFC

The ohmic resistance of an SOFC is dependant on the fuel cell temperature, as can be seen from Table D-4. Since the SOFC can operate at a temperature range of 600°C-1000°C, it hard to fix a single default value. As can be seen from Table D-4, the temperature has a large influence of the value of the ohmic resistance. Therefore, it could be useful to use a temperature dependant equation instead of a single value. When there is no value given for the ohmic resistance by the user, the program calculates the ohmic resistance based on the fuel cell temperature.

Table D-4 Ohmic resistance for an SOFC at different temperatures

Temperature [°C]	R_{ohm} [$\Omega \cdot m^2$]	Reference
800	0.60	[5]
850	0.55	[5]
900	0.50	[5]
950	0.45	[5]

In equation (D.47), a suggestion is given for the temperature dependant ohmic resistance [6].

$$R_{ohm} = \frac{T_{fc}}{-34 + 1.25 \cdot 10^6 \cdot \exp\left(-7185/T_{fc}\right)} + 0.04 \tag{D.47}$$

In Table D-5, suggested values are given for the other parameters required for the off-design calculations.

Table D-5 suggested default values for the off-design calculations of the SOFC [1]

Description	Symbol	Value	Unit
Internal and fuel crossover equivalent current density	i_n	20	A m^{-2}
Exchange current density	i_0	1000	A m^{-2}
Limiting current density	i_l	9000	A m^{-2}
Mass transfer over voltage	B	0.08	V

D.4.2. MCFC

For the MCFC also applies the dependence of the resistance on the temperature. In equation, a relation is given for the ohmic resistance [7, 8].

$$R_{ohm} = 0.5 \cdot 10^4 \cdot \exp\left[3016 \cdot \left(\frac{1}{T} - \frac{1}{923} \right) \right] \tag{D.48}$$

In Table D-6, default values for the MCFC are suggested.

Table D-6 suggested default values for the MCFC

Description	Symbol	Value	Unit
Internal and fuel crossover equivalent current density	i_n	20	A m^{-2}
Exchange current density	i_0	150	A m^{-2}
Limiting current density	i_l	9000	A m^{-2}
Mass transfer over voltage	B	0.065	V

D.5. References

1. O'Hayre R. P. Fuel Cell Fundamentals. Hoboken: Wiley, 2006.
2. EG&G Techical Services. Fuel Cell Handbook. Morgantown: Nation Energy Technology Laboratory, 2004.

3.   Larminie J., Dicks A. Fuel Cell Systems Explained. Chichester: John Wiley & Sons Ltd., 2003.
4.   Cycle-Tempo, 5.0. TU Delft, 2006. www.cycle-tempo.nl
5.   Repetto L., Costamagna P. FEM model of the ohmic resistance of IP-SOFCs. J Appl Electrochem 2008; 38(7): 1005-1010.
6.   Yakabe H., Ogiwara T., Hishinuma M., Yasuda I. 3-D model calculation for planar SOFC. J Power Sources 2001; 102(1-2): 144-154.
7.   Koh J.-H., Kang B. S., Lim H. C. Effect of various stack parameters on temperature rise in molten carbonate fuel cell stack operation. J Power Sources 2000; 91(2): 161-171.
8.   Yu L. J., Ren G. P., Jiang X. M., Yuan J. Q., Cao G. Y. Experiment and numerical simulation on the performance of a kW-scale molten carbonate fuel cell stack. Braz J Chem Eng 2007; 24(4): 523-533.

E.   Output data for GP1

Figure E-1 flow sheet hydrogen plant (GP1)

Table E-1 system efficiencies hydrogen plant (GP1)

Delivered	No.	Apparatus	Type	Energy	Totals	Exergy	Totals
				[kW]	[kW]	[kW]	[kW]
Absorbed power	1	Sink/Source	10	48534.43		57371.6	
					48534.43		57371.6
Delivered gross power	2	Generator	G	1743.93		1743.93	
	1	Generator	G	3933.09		3933.09	
					5677.02		5677.02
Aux. power consumption	26	Compressor	29	221.59		221.59	
	36	Pump	8	2.48		2.48	
	101	Pump	8	2.55		2.55	
	120	Pump	8	14.37		14.37	
	130	Pump	8	16.96		16.96	
	133	Pump	8	1.13		1.13	
	12	Compressor	29	2537.6		2537.6	
	140	Pump	8	0.17		0.17	
	201	Compressor	29	529.29		529.29	
	250	Compressor	29	1488.9		1488.9	
	901	Compressor	29	495.17		495.17	
	903	Compressor	29	503.54		503.54	
	950	Compressor	29	213		213	
					6026.65		6026.65
Delivered net power					-349.63		-349.63
Efficiencies	Gross			11.70		9.90	
	Net			-0.72		-0.61	

Table E-2 data pipes hydrogen plant

Pipe No.	Medium	Mass flow [kg s⁻¹]	Pressure [bar]	Temp. [°C]	Enthalpy [kJ kg⁻¹]	Entropy [kJ kg⁻¹ K⁻¹]	Exergy [kJ kg⁻¹]	Quality [%]
1	Fuel 1	4.12	1.47	15	-9080.73	2.1401	13925.15	
2	GASMIX 2	4.944	1.47	800	-7824.16	10.2236	11838.91	
3	GASMIX 3	3.499	1.47	800	-8383.69	10.575	10705.52	
4	GASMIX 4	3.999	1.47	800	-7322.68	12.8866	10455.85	
5	GASMIX 5	1.445	1.47	800	-6470.17	8.8133	14743.18	
6	GASMIX 6	5.685	1.47	810.94	-6872.75	11.8652	11092.34	
7	GASMIX 7	5.315	1.46	810.94	-7430.98	12.5431	9440.47	
8	GASMIX 7	4.465	1.46	810.94	-7430.98	12.5431	9440.47	
9	GASMIX 7	4.465	1.431	416.68	-8276.78	11.5867	8870.27	
10	GASMIX 7	4.465	1.402	120	-8842.77	10.5282	8609.28	
11	GASMIX 7	4.465	1.374	120	-8842.73	10.5372	8606.73	
12	GASMIX 8	2.887	1.347	45.11	-6561.97	9.6675	13050.49	
13	GASMIX 8	2.887	36.54	512.06	-5691.86	9.9022	13852.96	
14	GASMIX 9	4.331	36.54	540.37	-7892.54	10.467	9685.19	
15	GASMIX 10	4.327	35.82	350.06	-8291.18	9.9294	9457.02	
16	GASMIX 10	4.327	35.1	760.94	-7418.55	11.0086	10018.66	
17	GASMIX 11	5.768	34.42	800	-8012.29	11.7033	8319.35	
18	GASMIX 11	5.768	33.76	380	-8945.22	10.6138	7700.35	
19	GASMIX 12	5.768	33.12	450.92	-8945.22	10.6671	7684.98	

Table E-2 data pipe hydrogen plant (cont.)

Pipe No.	Medium	Mass flow [kg s⁻¹]	Pressure [bar]	Temp. [°C]	Enthalpy [kJ kg⁻¹]	Entropy [kJ kg⁻¹ K⁻¹]	Exergy [kJ kg⁻¹]	Quality [%]
20	GASMIX 12	5.768	32.46	210	-9464.85	9.8042	7414.01	
21	GASMIX 13	5.768	31.84	225.56	-9464.85	9.8262	7407.68	
22	GASMIX 14	3.648	31.22	30	-7748.4	8.3787	11121.51	
23	GASMIX 15	0.552	30.6	30	-1039.61	29.5953	70555.73	
24	GASMIX 16	1.589	30.6	107.27	-1369.19	17.7702	41200.89	
25	GASMIX 17	0.259	30	107.27	1183.29	54.2867	121684.7	
26	GASMIX 17	0.259	30	25	0.44	50.7838	121511.3	
27	GASMIX 17	0.259	30	25	0.44	50.7838	121511.3	
28	GASMIX 17	0.259	50	83.87	845.88	51.2654	122217.9	
29	GASMIX 17	0.259	50	25	0.44	48.6778	122118.1	
100	GASMIX 18	38.856	1.013	15	-15908.4	3.7364	0	
101	GASMIX 18	38.856	1.5	15	-15908.4	3.7364	0.05	
102	GASMIX 18	1.324	1.5	15	-15908.4	3.7364	0.05	
103	GASMIX 18	1.324	1.47	600	-12266.3	12.4335	1136.04	
104	GASMIX 12	0.5	1.47	600	-12266.3	12.4335	1136.04	
105	GASMIX 18	0.824	1.47	600	-12266.3	12.4335	1136.04	
110	GASMIX 18	34.647	1.5	15	-15908.4	3.7364	0.05	
111	GASMIX 18	34.647	1.47	15.01	-15908.4	3.7364	0.05	
112	GASMIX 18	36.224	1.347	45.11	-15782.5	4.1519	6.18	
120	GASMIX 18	2.885	1.5	15	-15908.4	3.7364	0.05	
121	GASMIX 18	2.885	38.48	15.34	-15903.4	3.7407	3.75	
122	GASMIX 18	1.092	38.48	15.34	-15903.4	3.7407	3.75	
123	GASMIX 18	1.793	38.48	15.34	-15903.4	3.7407	3.75	
124	GASMIX 18	1.092	37.78	250	-13158.1	9.6274	1052.83	
125	GASMIX 18	1.793	37.78	338.43	-12901.8	10.0823	1178.07	
126	GASMIX 18	2.885	37.22	300.6	-12998.8	9.9248	1126.43	
127	GASMIX 18	2.885	36.54	600	-12293.9	10.9266	1542.68	
128	GASMIX 18	1.441	36.54	600	-12293.9	10.9266	1542.68	
129	GASMIX 18	1.444	36.54	600	-12293.9	10.9266	1542.68	
130	WATERSTM	1.468	83.4	101.22	430.43	1.3144	53.29	0
131	WATERSTM	1.468	82.4	290.21	1290.28	3.1597	381.41	0
132	WATERSTM	6.028	82.4	297.08	1328.51	3.2271	400.2	0
133	WATERSTM	6.028	83.4	297.13	1328.69	3.2272	400.37	0
134	WATERSTM	6.028	82.4	297.08	1685.13	3.8525	576.62	25
135	WATERSTM	1.468	82.4	297.08	2754.99	5.7287	1105.85	100
136	WATERSTM	1.468	81.4	540	3496.05	6.8408	1526.48	100
137	WATERSTM	1.468	80.2	538.67	3494.05	6.8448	1523.32	100
138	WATERSTM	1.283	0.03	24.08	2202.89	7.426	64.69	86.01
139	WATERSTM	0.184	1.013	99.97	2630.46	7.2336	547.7	98
140	WATERSTM	1.283	0.03	24.08	100.99	0.3543	0.49	0
141	WATERSTM	1.283	1.013	24.09	101.12	0.3544	0.59	0
142	WATERSTM	1.468	1.013	99.97	418.99	1.3067	44.06	0
150	WATERSTM	92.066	1.013	12	50.51	0.1806	0.07	0
151	WATERSTM	92.066	1.213	12	50.53	0.1806	0.09	0
152	WATERSTM	92.066	1.013	19	79.83	0.2822	0.12	0
160	WATERSTM	173.52	1.013	15	63.08	0.2245	0	0

Table E-2 data pipes hydrogen plant (cont.)

Pipe No.	Medium	Mass flow [kg s⁻¹]	Pressure [bar]	Temp. [°C]	Enthalpy [kJ kg⁻¹]	Entropy [kJ kg⁻¹ K⁻¹]	Exergy [kJ kg⁻¹]	Quality [%]
161	WATERSTM	173.52	1.013	25	104.93	0.3672	0.71	0
165	WATERSTM	31.242	1.013	15	63.08	0.2245	0	0
166	WATERSTM	31.242	1.013	20	84.01	0.2965	0.18	0
200	GASMIX 19	12.383	1.013	15	-98.85	6.8652	0.13	
201	GASMIX 19	12.383	1.49	56.86	-56.54	6.8912	34.95	
202	GASMIX 19	7.093	1.49	56.86	-56.54	6.8912	34.95	
203	GASMIX 19	7.093	1.46	400	299.72	7.6345	177.02	
250	GASMIX 19	5.291	1.49	56.86	-56.54	6.8912	34.95	
251	GASMIX 19	5.291	9	327.12	222.06	6.9884	285.56	
400	GASMIX 20	26.614	1.48	1233.79	-9524.01	4.7923	1341.06	
401	GASMIX 21	18.3	1.47	1233.79	-13022.2	3.0128	1468.16	
402	GASMIX 21	18.3	1.47	1233.79	-13022.2	3.0128	1468.16	
403	GASMIX 21	14.64	1.47	1233.79	-13022.2	3.0128	1468.16	
404	GASMIX 21	3.66	1.47	1233.79	-13022.2	3.0128	1468.16	
405	GASMIX 21	14.64	1.47	1130.82	-13444.7	2.7229	1129.22	
406	GASMIX 21	18.3	1.47	1153.73	-13360.2	2.7826	1196.52	
407	GASMIX 21	18.3	1.47	1000.18	-13843.1	2.4258	816.4	
408	GASMIX 21	18.3	1.46	1000.18	-13843.1	2.4258	816.4	
409	GASMIX 22	0.37	1.46	810.94	1136.2	2.1821	34779.19	
410	GASMIX 23	19.521	1.46	989.98	-13279.5	2.8635	1836.17	
411	GASMIX 23	19.521	1.46	1057.73	-13095.9	3.005	1979	
412	GASMIX 7	0.85	1.46	810.94	-7430.98	12.5431	9440.47	
500	GASMIX 24	8.314	1.47	1233.79	-1823.85	8.7113	1060.75	
501	GASMIX 24	0.241	1.47	1233.79	-1823.85	8.7113	1060.75	
502	GASMIX 24	8.073	1.47	1233.79	-1823.85	8.7113	1060.75	
503	GASMIX 24	8.073	1.47	1233.79	-1823.85	8.7113	1060.75	
504	GASMIX 24	8.073	1.44	901.39	-2269.86	8.3831	709.32	
505	GASMIX 24	8.073	1.41	705.92	-2521.74	8.1546	523.27	
506	GASMIX 24	8.073	1.382	203.43	-3119.21	7.3111	168.85	
600	GASMIX 21	0	1.46	1000.18	-13843.1	2.4258	816.4	
700	GASMIX 25	0.004	35.82	540.37	509.19	6.4608	612.31	
800	GASMIX 18	2.12	31.22	30	-15842.9	3.9478	4.6	
801	GASMIX 26	3.096	1.22	30	-8944.63	4.8493	450.76	
802	GASMIX 27	5.216	1.22	24.63	-11748.7	4.4889	267.65	
900	GASMIX 28	1.33	1	107.27	-1867.27	11.987	25108.95	
901	GASMIX 28	1.037	1	107.27	-1867.27	11.987	25108.95	
902	GASMIX 29	1.037	4.75	317.19	-1394.64	12.1524	25532.83	
903	GASMIX 29	1.037	4.655	30	-2025.22	10.7149	25316.44	
904	GASMIX 29	1.037	30.6	253.72	-1544.6	10.9051	25742.28	
950	GASMIX 28	0.293	1	107.27	-1867.27	11.987	25108.95	
951	GASMIX 28	0.293	9	416.94	-1146.47	12.205	25766.93	
952	GASMIX 30	5.583	8.82	1369.82	150.36	8.4958	1265.09	
953	GASMIX 30	5.583	1.073	804.8	-583.23	8.5739	509.03	
954	GASMIX 30	5.583	1.053	646.63	-778.02	8.3841	368.92	
955	GASMIX 30	5.583	1.033	317.13	-1162.84	7.8733	131.3	
956	GASMIX 30	5.583	1.013	111.22	-1388.85	7.4089	39.1	

Table E-3 composition of fluids in the hydrogen plant

Composition number	1	2	3	4	5	6	7	8	9	10
C(S)	0.3855	0.2601	0.3168	0.1199		0.0984				
H2	0.2758	0.0118	0.0143	0.2577		0.2115	0.2346	0.3718	0.2422	0.2423
H2O	0.2163	0.5293	0.6446	0.45		0.373	0.4137	0.0709	0.3948	0.395
N2	0.0026	0.0031	0.0037	0.0032		0.0203	0.0225	0.0357	0.0232	0.0233
O2	0.1198					0.0004	0.0005	0.0008	0.0005	
AR						0.0002	0.0002	0.0004	0.0002	0.0002
CO2		0.0901		0.0411	0.5038	0.1151	0.1277	0.2024	0.1318	0.1319
SIO2(S)										
CH4		0.1056	0.0206	0	0.4962	0.076	0.0843	0.1335	0.087	0.087
CO		0	0	0.1279		0.105	0.1165	0.1846	0.1202	0.1203
H2S										
HCL										
SO2										
HF										
Avg.molemass [kg/kmol]	12.99	18.43	15.88	15.55	30.13	18.15	18.82	19.28	18.84	18.84
LHV [kJ/mol]	153.02	189.95	144.62	145.72	398.03	180.59	157.33	249.22	162.36	162.49
HHV [kJ/mol]	174.67	199.76	147.06	157.05	441.67	196.58	175.07	277.32	180.66	180.81

Table E-3 composition of fluids in the hydrogen plant (cont.)

Composition number	11	12	13	14	15	16	17	18	19	20
C(S)	0	0	0	0	0	0	0			0
H2	0.3133	0.384	0.3997	0.6158	0.911	0.7201	1			
H2O	0.4382	0.3675	0.3518	0.0014				1	0.0101	0.067
N2	0.0159	0.0159	0.0159	0.0245	0.0363	0.1141	0		0.7729	0.325
O2						0			0.2075	0.0079
AR	0.0002	0.0002	0.0002	0.0003	0.0004	0.0012	0		0.0092	0.0039
CO2	0.123	0.1937	0.2094	0.3226					0.0003	0.0779
SIO2(S)										0.5183
CH4	0.0214	0.0214	0.0214	0.0329	0.0487	0.1532	0			
CO	0.088	0.0173	0.0016	0.0024	0.0036	0.0114	0			0
H2S										
HCL										
SO2										
HF										
Avg.molemass [kg/kmol]	17.2	17.2	17.2	16.76	3.75	7.47	2.02	18.02	28.85	45.29
LHV [kJ/mol]	117.83	114.92	114.28	176.08	260.34	300.19	242.26	0	0	0
HHV [kJ/mol]	133.49	133.7	133.74	206.07	304.69	345.33	286.32	0	0	0

Table E-3 composition of fluids in the hydrogen plant (cont.)

Composition number	21	22	23	24	25	26	27	28	29	30
C(S)		1	0.081	0						0
H2			0.0279					0.2917	0.2917	0
H2O			0.0491	0.1392		0.0042	0.6269			0.1085
N2			0.0027	0.6748				0.2889	0.2889	0.7394
O2			0.0001	0.0164	1			0	0	0.1043
AR			0	0.008				0.003	0.003	0.0088
CO2			0.0152	0.1616		0.9958	0.3731			0.039
SIO2(S)	1		0.8002							
CH4			0.01					0.3877	0.3877	
CO			0.0138	0				0.0288	0.0288	0
H2S										
HCL										
SO2										
HF										
Avg.molemass [kg/kmol]	60.08	12.01	51.29	29.37	32	43.9	27.71	15.83	15.83	28.07
LHV [kJ/mol]	0	393.46	50.57	0	0	0	0	389.83	389.82	0
HHV [kJ/mol]	0	393.46	52.67	0	0	0	0	436.78	436.76	0

Table E-4 energy and flows in the hydrogen plant

Pipe	Total Energy flow	Therm. Mec. Energy flow	Chemical energy	Total Exergy flow	Therm Mec. Exergy flow	Chemical Exergy
No.	[kW]	[kW]	[kW]	[kW]	[kW]	[kW]
1	55400.29	0	55400.29	57371.6	0	57371.6
2	67311.91	13724.71	53587.19	58531.57	5250.52	53281.04
3	44165.18	11767.05	32398.13	37453.61	4340.21	33113.39
4	52128.64	11740.77	40387.88	41811.11	4441.82	37369.29
5	23146.33	1957.27	21189.06	21310.78	1113.64	20197.14
6	75687.05	14110.11	61576.94	63064.26	5712.23	57352.03
7	63103.54	13663.27	49440.27	50175.43	5469.12	44706.31
8	53006.97	11477.15	41529.82	42147.36	4594.06	37553.3
9	49230.87	7701.04	41529.82	39601.68	2048.38	37553.3
10	46703.96	5174.13	41529.82	38436.47	883.17	37553.3
11	46704.16	5174.34	41529.82	38425.09	871.79	37553.3
12	42144.7	614.87	41529.82	37680.14	126.84	37553.3
13	44656.91	3127.09	41529.82	39997.08	2443.78	37553.3
14	49874.96	8345.14	41529.82	41945.49	4392.19	37553.3
15	48178.43	6648.6	41529.82	40923.12	3368.05	37555.07
16	51954.53	10424.71	41529.82	43353.46	5798.39	37555.07
17	60759.9	15990.61	44769.29	47988.15	8725.25	39262.9
18	55378.5	10609.2	44769.29	44417.61	5154.71	39262.9
19	55369.31	10531.97	44837.34	44328.95	5487.57	38841.39
20	52371.97	7534.62	44837.34	42765.91	3924.52	38841.39
21	52369.93	7517.51	44852.42	42729.38	3955.18	38774.2
22	44969.16	116.73	44852.42	40570.79	1789.17	38781.62
23	44916.82	64.4	44852.42	38948.98	1203.02	37745.96
24	74063.98	593.84	73470.14	65478.52	1815.5	63663.02

Table E-4 energy and flows in the hydrogen plant (cont.)

Pipe	Total Energy flow	Therm. Mec. Energy flow	Chemical energy	Total Exergy flow	Therm Mec. Exergy flow	Chemical Exergy
No.	[kW]	[kW]	[kW]	[kW]	[kW]	[kW]
25	37123.38	344.03	36779.34	31575.09	1090.01	30485.08
26	36816.45	37.1	36779.34	31530.07	1045	30485.08
27	36816.45	37.1	36779.34	31530.07	1045	30485.08
28	37035.82	256.48	36779.34	31713.44	1228.36	30485.08
29	36816.45	37.1	36779.34	31687.54	1202.46	30485.08
100	0	0	0	0	0	0
101	2.52	2.52	0	1.89	1.89	0
102	0.09	0.09	0	0.06	0.06	0
103	4823.23	4823.23	0	1504.44	1504.44	0
104	1822.12	1822.12	0	568.35	568.35	0
105	3001.11	3001.11	0	936.09	936.09	0
110	2.25	2.25	0	1.69	1.69	0
111	2.25	2.25	0	1.58	1.58	0
112	4561.27	4561.27	0	223.97	223.97	0
120	0.19	0.19	0	0.14	0.14	0
121	14.41	14.41	0	10.81	10.81	0
122	5.45	5.45	0	4.09	4.09	0
123	8.96	8.96	0	6.72	6.72	0
124	3002.8	3002.8	0	1149.47	1149.47	0
125	5390.36	5390.36	0	2112.05	2112.05	0
126	8393.16	8393.16	0	3249.32	3249.32	0
127	10426.52	10426.52	0	4450.02	4450.02	0
128	5208.48	5208.48	0	2222.97	2222.97	0
129	5218.04	5218.04	0	2227.05	2227.05	0
130	539.12	539.12	0	78.21	78.21	0
131	1801.01	1801.01	0	559.75	559.75	0
132	7627.49	7627.49	0	2412.27	2412.27	0
133	7628.61	7628.61	0	2413.25	2413.25	0
134	9777.07	9777.07	0	3475.61	3475.61	0
135	3950.59	3950.59	0	1622.93	1622.93	0
136	5038.15	5038.15	0	2240.23	2240.23	0
137	5035.21	5035.21	0	2235.59	2235.59	0
138	2745.68	2745.68	0	83.01	83.01	0
139	473.51	473.51	0	101.01	101.01	0
140	48.65	48.65	0	0.63	0.63	0
141	48.81	48.81	0	0.75	0.75	0
142	522.33	522.33	0	64.66	64.66	0
150	1157.49	1157.49	0	6.07	6.07	0
151	1155.03	1155.03	0	7.9	7.9	0
152	1542	1542	0	10.6	10.6	0
160	0	0	0	0	0	0
161	7261.87	7261.87	0	123.13	123.13	0
165	0	0	0	0	0	0
166	654.01	654.01	0	5.61	5.61	0
200	192.52	192.52	0	1.59	0	1.59

Table E-4 energy and flows in the hydrogen plant (cont.)

Pipe	Total Energy flow	Therm. Mec. Energy flow	Chemical energy	Total Exergy flow	Therm Mec. Exergy flow	Chemical Exergy
No.	[kW]	[kW]	[kW]	[kW]	[kW]	[kW]
201	716.42	716.42	0	432.82	431.23	1.59
202	410.34	410.34	0	247.91	247	0.91
203	2937.25	2937.25	0	1255.58	1254.67	0.91
250	306.08	306.08	0	184.92	184.24	0.68
251	1780.08	1780.08	0	1510.78	1510.1	0.68
400	53687.71	53687.55	0.15	35690.67	35011.36	679.31
401	39246.18	39246.18	0	26867.31	26867.31	0
402	39246.18	39246.18	0	26867.31	26867.31	0
403	31396.95	31396.95	0	21493.85	21493.85	0
404	7849.24	7849.24	0	5373.46	5373.46	0
405	25211.73	25211.73	0	16531.76	16531.76	0
406	33060.97	33060.97	0	21896.23	21896.23	0
407	24223.55	24223.55	0	14940.12	14940.12	0
408	24223.55	24223.55	0	14940.12	14940.12	0
409	12560.06	423.39	12136.67	12884.21	238.5	12645.72
410	47135.26	27088.14	20047.12	35843.5	16044.78	19798.73
411	50719.52	30672.4	20047.12	38631.82	18833.09	19798.73
412	10096.57	2186.12	7910.44	8028.07	875.06	7153.01
500	14209.9	14209.75	0.15	8818.75	8139.44	679.31
501	412.09	412.08	0	255.74	236.04	19.7
502	13797.82	13797.67	0.15	8563.01	7903.4	659.61
503	13797.82	13797.67	0.15	8563.01	7903.4	659.61
504	10197.36	10197.21	0.15	5726.06	5066.45	659.61
505	8164	8163.85	0.15	4224.18	3564.57	659.61
506	3340.85	3340.71	0.15	1363.09	703.48	659.61
600	0	0	0	0	0	0
700	1.87	1.87	0	2.21	1.79	0.43
800	138.89	138.89	0	9.75	9.75	0
801	52.34	52.34	0	1395.53	32.23	1363.3
802	191.24	191.24	0	1396.1	34.22	1361.88
900	36940.58	249.81	36690.77	33389.06	30.73	33358.33
901	28813.65	194.85	28618.8	26043.47	23.97	26019.5
902	29302.71	684.99	28617.72	26483.13	464.64	26018.49
903	28648.65	30.93	28617.72	26258.68	240.19	26018.49
904	29147.16	529.44	28617.72	26700.37	681.88	26018.49
950	8126.93	54.96	8071.97	7345.59	6.76	7338.83
951	8337.8	265.83	8071.97	7538.09	199.25	7338.83
952	10126.05	10125.95	0.1	7063.19	6978.38	84.82
953	6030.36	6030.26	0.1	2842	2757.18	84.82
954	4942.8	4942.7	0.1	2059.75	1974.94	84.82
955	2794.32	2794.22	0.1	733.07	648.25	84.82
956	1532.43	1532.33	0.1	218.29	133.47	84.82
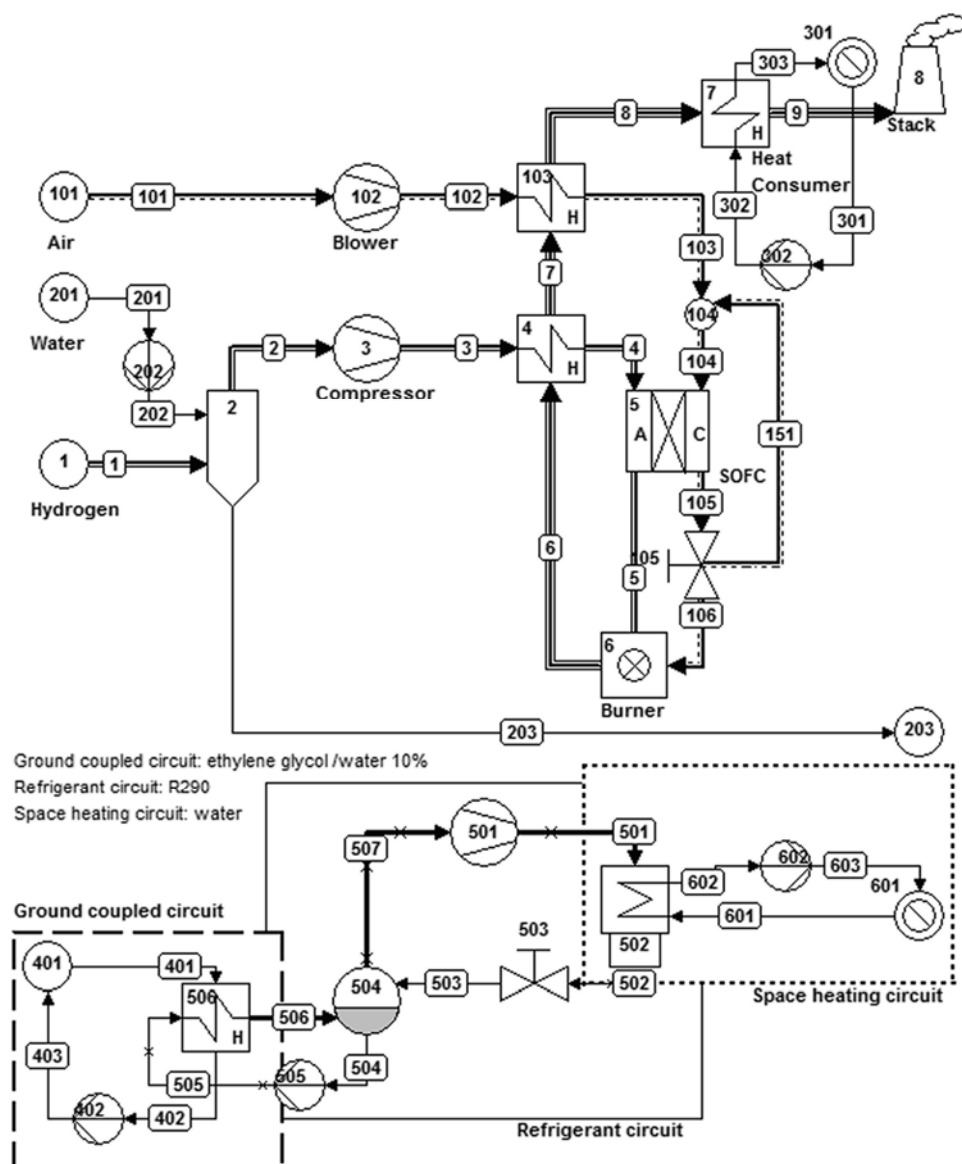
Figure E-2 flow sheet hydrogen fuelled micro-CHP

Table E-5 efficiencies of the hydrogen fuelled micro-CHP

	No.	Apparatus	Type	Energy	Totals	Exergy	Totals
				[kW]	[kW]	[kW]	[kW]
Absorbed	1	Sink/Source	10	3371.96		3303.2	
power					3371.96		3303.2
Delivered	5	Fuel Cell	21	1544.5		1544.5	
gross power					1544.5		1544.5
Aux. power	102	Compressor	29	104.1		104.1	
consumption	3	Compressor	29	10.51		10.51	
	202	Pump	8	0		0	
	302	Pump	8	0.22		0.22	
	402	Pump	8	1.97		1.97	
	501	Compressor	29	426.85		426.85	
	505	Pump	8	0.12		0.12	
	602	Pump	8	0.27		0.27	
					544.06		544.06
Delivered							
net power					1000.45		1000.45
Delivered	301	Heat Sink	10	1656.58		201.49	
heat	601	Heat Sink	10	1343.51		163.45	
					3000.09		364.94
Total							
delivered					4000.54		1365.39
Efficiencies	gross			45.80%		46.76%	
	net			29.67%		30.29%	
	heat			88.97%		11.05%	
	total			118.64%		41.34%	

Table E-6 data pipes hydrogen fuelled micro-CHP

Pipe	Medium	Mass flow	Pressure	Temp.	Enthalpy	Entropy	Exergy	Quality
no.		[kg/s]	[bar]	[°C]	[kJ/kg]	[kJ/kg.K]	[kJ/kg]	[%]
1	GASMIX 1	0.028	1.013	15	-141.57	64.2897	117533.07	
2	GASMIX 2	0.028	1.013	15	-201.37	64.0602	117003.5	
3	GASMIX 2	0.028	1.203	36.5	105.19	64.3805	117217.74	
4	GASMIX 2	0.028	1.183	750	10507.93	81.8112	122597.83	
5	GASMIX 3	0.207	1.143	850	-11045.6	15.3247	4765.78	
6	GASMIX 4	3.754	1.123	995.74	151.74	8.8612	680.34	
7	GASMIX 4	3.754	1.093	934.36	73.5	8.8062	617.95	
8	GASMIX 4	3.754	1.053	447.77	-518.88	8.192	202.55	
9	GASMIX 4	3.754	1.013	50	-960.18	7.3177	13.18	
101	GASMIX 5	3.725	1.013	15	-98.85	6.8652	0.13	
102	GASMIX 5	3.725	1.263	40.63	-72.96	6.8877	19.53	
103	GASMIX 5	3.725	1.203	604	523.91	7.9809	301.41	
104	GASMIX 6	9.046	1.203	750	688.79	8.1604	417.9	
105	GASMIX 7	8.867	1.143	850	804.23	8.2862	499.42	
106	GASMIX 7	3.547	1.143	850	804.23	8.2862	499.42	
151	GASMIX 7	5.32	1.143	850	804.23	8.2862	499.42	
201	GASMIX 8	0.074	1.013	20	-15887.5	3.8084	0.18	
202	GASMIX 8	0.074	1.033	20	-15887.5	3.8084	0.18	

Table E-6 data pipes hydrogen fuelled micro-CHP (cont.)

Pipe	Medium	Mass flow	Pressure	Temp.	Enthalpy	Entropy	Exergy	Quality
no.		[kg/s]	[bar]	[°C]	[kJ/kg]	[kJ/kg.K]	[kJ/kg]	[%]
203	GASMIX 8	0.074	1.013	19	-15891.7	3.7941	0.12	
301	WATERSTM	19.809	1.013	45	188.51	0.6386	6.11	0
302	WATERSTM	19.809	1.053	45	188.52	0.6386	6.11	0
303	WATERSTM	19.809	1.013	65	272.14	0.8935	16.28	0
401	E G/H2O	193.522	1.033	8	32.49	0.1172	0.36	
402	E G/H2O	193.522	1.013	6.8	27.62	0.0999	0.48	
403	E G/H2O	193.522	1.053	6.8	27.62	0.0999	0.49	
501	R290	4.3	24	79.72	38.31	-0.4167	158.95	100
502	R290	4.3	23.48	55	-274.09	-1.338	112.01	0
503	R290	4.3	4.8	0.39	-274.09	-1.2721	93.03	42.07
504	R290	2.463	4.8	0.39	-433.42	-1.8546	101.54	0
505	R290	2.463	4.896	0.41	-433.39	-1.8545	101.55	0
506	R290	2.463	4.8	3	-50.37	-0.4543	81.11	100
507	R290	4.3	4.8	0.39	-54.67	-0.47	81.31	100
601	WATERSTM	16.066	1.5	45	188.56	0.6386	6.16	0
602	WATERSTM	16.066	1.47	65	272.17	0.8935	16.32	0
603	WATERSTM	16.066	1.53	65	272.19	0.8935	16.33	0

Table E-7 composition of fluids of the hydrogen fuelled micro-CHP

Composition number	1	2	3	4	5	6	7	8
H2	1	0.9995	0.1999					
N2				0.7333	0.7729	0.7935	0.8079	
O2				0.1456	0.2075	0.1863	0.1716	
H2O		0.0005	0.8001	0.1121	0.0101	0.0104	0.0106	1
AR				0.0087	0.0092	0.0094	0.0096	
CO2				0.0003	0.0003	0.0003	0.0003	
CH4								
H2S								
CO								
HCL								
C(S)				0				
SO2								
Avg.molemass [kg/kmol]	2.02	2.02	14.82	27.58	28.85	28.77	28.71	18.02
LHV [kJ/mol]	242.36	241.27	48.36	0	0	0	0	0
HHV [kJ/mol]	286.44	285.15	57.15	0	0	0	0	0

Table E-8 energy and exergy flows of the hydrogen fuelled micro-CHP

Pipe	Total Energy flow	Therm.Mec. Energy flow	Chemical energy	Total Exergy flow	Therm.Mec. Exergy flow	Chemical exergy
no.	[kW]	[kW]	[kW]	[kW]	[kW]	[kW]
1	3985.24	0	3985.24	3303.2	0	3303.2
2	3985.55	0.31	3985.24	3303.17	0	3303.17
3	3994.2	8.97	3985.24	3309.22	6.05	3303.17
4	4287.89	302.65	3985.24	3461.1	157.94	3303.17
5	1713.49	916.44	797.05	985.01	324.48	660.53
6	4991.51	4991.45	0.05	2553.66	2551.7	1.96
7	4697.83	4697.77	0.05	2319.51	2317.55	1.96
8	2474.31	2474.25	0.05	760.27	758.3	1.96
9	817.9	817.85	0.05	49.47	47.5	1.96
101	57.92	57.92	0	0.48	0	0.48
102	154.36	154.36	0	72.74	72.26	0.48
103	2377.88	2377.88	0	1122.84	1122.36	0.48
104	7293.51	7293.51	0	3780.14	3778.03	2.11
105	8192.66	8192.66	0	4428.43	4424.45	3.98
106	3277.06	3277.06	0	1771.37	1769.78	1.59
151	4915.6	4915.6	0	2657.06	2654.67	2.39
201	1.55	1.55	0	0.01	0.01	0
202	1.55	1.55	0	0.01	0.01	0
203	1.24	1.24	0	0.01	0.01	0
301	2484.73	2484.73	0	120.97	120.97	0
302	2484.86	2484.86	0	121.05	121.05	0
303	4141.31	4141.31	0	322.46	322.46	0
401	5502.37	5502.37	0	68.75	68.75	0
402	6445.82	6445.82	0	93.48	93.48	0
403	6444.57	6444.57	0	94.1	94.1	0
501	247.35	247.35	0	683.47	683.47	0
502	1096	1096	0	481.66	481.66	0
503	1096	1096	0	400.02	400.02	0
504	1020.26	1020.26	0	250.1	250.1	0
505	1020.19	1020.19	0	250.14	250.14	0
506	76.74	76.74	0	199.78	199.78	0
507	152.47	152.47	0	349.65	349.65	0
601	2015.95	2015.95	0	98.89	98.89	0
602	3359.29	3359.29	0	262.24	262.24	0
603	3359.46	3359.46	0	262.35	262.35	0

F.   Output data for GP2
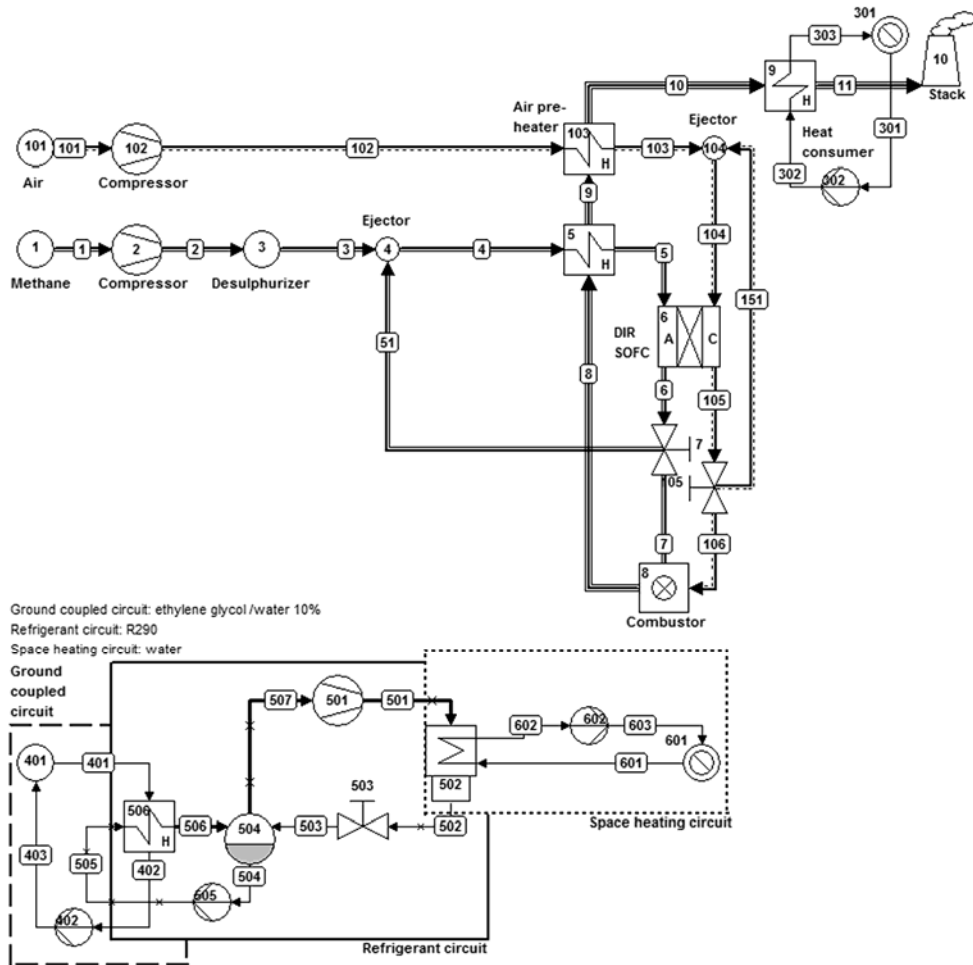
Figure F-1 flow sheet SNG fuelled micro-CHP

Table F-1 efficiencies of the SNG fuelled micro-CHP

	No.	Apparatus	Type	Energy	Totals	Exergy	Totals
				[kW]	[kW]	[kW]	[kW]
Absorbed	1	Sink/Source	10	2890.33		2992.9	
power					2890.33		2992.94
Delivered	6	Fuel Cell	21	1700		1700	
gross power					1700		1700
Aux. power	102	Compressor	29	63.88		63.88	
consumption	302	Pump	8	0.14		0.14	
	402	Pump	8	2.57		2.57	
	501	Compressor	29	626.05		626.05	
	505	Pump	8	0.17		0.17	
	2	Compressor	29	6.2		6.2	
	602	Pump	8	0.4		0.4	
					699.42		699.42
Delivered							
net power					1000.57		1000.57
Delivered	301	Heat Sink	10	1021.13		124.2	
heat	601	Heat Sink	10	1979.33		240.81	
					3000.46		365.01
Total							
delivered					4001.04		1365.58
Efficiencies	gross			58.82%		56.80%	
	net			34.62%		33.43%	
	heat			103.81%		12.20%	
	total			138.43%		45.63%	

Table F-2 data pipes SNG fuelled micro-CHP

Pipe	Medium	Mass flow	Pressure	Temp.	Enthalpy	Entropy	Exergy	Quality
no.		[kg/s]	[bar]	[°C]	[kJ/kg]	[kJ/kg.K]	[kJ/kg]	[%]
1	GASMIX 1	0.061	1.013	15	-4605.3	11.6654	48808.51	
2	GASMIX 1	0.061	1.423	50.19	-4526.91	11.7443	48864.12	
3	GASMIX 1	0.061	1.323	50.19	-4526.91	11.7824	48853.16	
4	GASMIX 2	0.467	1.233	676.58	-8555.01	10.6792	8331.69	
5	GASMIX 2	0.467	1.183	750	-8401.01	10.8503	8436.38	
6	GASMIX 3	0.676	1.143	850	-9164.15	10.1449	2310	
7	GASMIX 3	0.27	1.143	850	-9164.15	10.1449	2310	
8	GASMIX 4	2.249	1.123	969.11	-395.73	8.6946	667.33	
9	GASMIX 4	2.249	1.093	943.98	-427.69	8.6765	640.56	
10	GASMIX 4	2.249	1.053	461.18	-1015.93	8.0743	225.87	
11	GASMIX 4	2.249	1.013	50	-1469.92	7.1847	28.22	
51	GASMIX 3	0.405	1.143	850	-9164.15	10.1449	2310	
101	GASMIX 5	2.188	1.013	15	-98.85	6.8652	0.13	
102	GASMIX 5	2.188	1.263	40.63	-72.96	6.8877	19.53	
103	GASMIX 5	2.188	1.203	610.99	531.76	7.9898	306.7	
104	GASMIX 6	5.156	1.203	750	687.4	8.164	418.97	
105	GASMIX 7	4.947	1.143	850	802.11	8.291	502.1	
106	GASMIX 7	1.979	1.143	850	802.11	8.291	502.1	
151	GASMIX 7	2.968	1.143	850	802.11	8.291	502.1	

Table F-2 data pipes SNG fuelled micro-CHP (cont.)

Pipe	Medium	Mass flow	Pressure	Temp.	Enthalpy	Entropy	Exergy	Quality
no.		[kg/s]	[bar]	[°C]	[kJ/kg]	[kJ/kg.K]	[kJ/kg]	[%]
301	WATERSTM	12.21	1.013	45	188.51	0.6386	6.11	0
302	WATERSTM	12.21	1.053	45	188.52	0.6386	6.11	0
303	WATERSTM	12.21	1.013	65	272.14	0.8935	16.28	0
401	E G/H2O	285.11	1.033	8	32.49	0.1172	0.36	
402	E G/H2O	285.11	1.013	6.8	27.62	0.0999	0.48	
403	E G/H2O	285.11	1.053	6.8	27.62	0.0999	0.49	
501	R290	6.335	24	79.72	38.31	-0.4167	158.95	100
502	R290	6.335	23.48	55	-274.09	-1.338	112.01	0
503	R290	6.335	4.8	0.39	-274.09	-1.2721	93.03	42.07
504	R290	3.629	4.8	0.39	-433.42	-1.8546	101.54	0
505	R290	3.629	4.896	0.41	-433.39	-1.8545	101.55	0
506	R290	3.629	4.8	3	-50.37	-0.4543	81.11	100
507	R290	6.335	4.8	0.39	-54.67	-0.47	81.31	100
601	WATERSTM	23.669	1.5	45	188.56	0.6386	6.16	0
602	WATERSTM	23.669	1.47	65	272.17	0.8935	16.32	0
603	WATERSTM	23.669	1.53	65	272.19	0.8935	16.33	0

Table F-3 composition of fluids of the SNG fuelled micro-CHP

Composition number	1	2	3	4	5	6	7
CH4	0.92	0.1749	0				
CO	0.001	0.0305	0.0374				
CO2	0.01	0.2371	0.2904	0.0454	0.0003	0.0003	0.0003
H2	0.048	0.0755	0.0819				
N2	0.021	0.01	0.0074	0.7374	0.7729	0.815	0.8457
H2O		0.472	0.5828	0.101	0.0101	0.0106	0.0111
O2				0.1075	0.2075	0.1644	0.1329
AR				0.0088	0.0092	0.0097	0.0101
H2S							
HCL							
C(S)		0	0	0			
SO2							
Avg.molemass [kg/kmol]	15.91	23.03	24.7	28.26	28.85	28.68	28.56
LHV [kJ/mol]	749.92	167.22	30.41	0	0	0	0
HHV [kJ/mol]	832.96	185.93	34.01	0	0	0	0

Table F-4 energy and exergy flows of the SNG fuelled micro-CHP

Pipe	Total Energy flow	Therm.Mec. Energy flow	Chemical energy	Total Exergy flow	Therm.Mec. Exergy flow	Chemical exergy
no.	[kW]	[kW]	[kW]	[kW]	[kW]	[kW]
1	3210.37	0	3210.37	2992.94	0	2992.94
2	3215.18	4.8	3210.37	2996.35	3.41	2992.94
3	3215.18	4.8	3210.37	2995.68	2.74	2992.94
4	4745.7	976.96	3768.74	3889.4	344.69	3544.71
5	4817.59	1048.85	3768.74	3938.27	393.56	3544.71
6	2550.97	1620.35	930.61	1561.17	617.17	944
7	1020.39	648.14	372.24	624.47	246.87	377.6

Table F-4 energy and exergy flows of the SNG fuelled micro-CHP (cont.)

Pipe	Total Energy flow	Therm.Mec. Energy flow	Chemical energy	Total Exergy flow	Therm.Mec. Exergy flow	Chemical exergy
no.	[kW]	[kW]	[kW]	[kW]	[kW]	[kW]
8	2856.33	2856.3	0.03	1500.97	1461.27	39.71
9	2784.44	2784.41	0.03	1440.77	1401.06	39.71
10	1461.36	1461.33	0.03	508.03	468.32	39.71
11	440.23	440.19	0.03	63.47	23.77	39.71
51	1530.58	972.21	558.37	936.7	370.3	566.4
101	34.01	34.01	0	0.28	0	0.28
102	90.66	90.66	0	42.72	42.44	0.28
103	1413.74	1413.74	0	671.02	670.74	0.28
104	4167.2	4167.2	0	2160.3	2157.19	3.11
105	4589.13	4589.13	0	2484.02	2475.79	8.23
106	1835.65	1835.65	0	993.61	990.32	3.29
151	2753.48	2753.48	0	1490.41	1485.47	4.94
301	1531.61	1531.61	0	74.57	74.57	0
302	1531.69	1531.69	0	74.62	74.62	0
303	2552.74	2552.74	0	198.76	198.76	0
401	8106.4	8106.4	0	101.29	101.29	0
402	9496.35	9496.35	0	137.73	137.73	0
403	9494.5	9494.5	0	138.63	138.63	0
501	364.4	364.4	0	1006.93	1006.93	0
502	1614.68	1614.68	0	709.6	709.6	0
503	1614.68	1614.68	0	589.34	589.34	0
504	1503.11	1503.11	0	368.46	368.46	0
505	1503.01	1503.01	0	368.52	368.52	0
506	113.06	113.06	0	294.32	294.32	0
507	224.63	224.63	0	515.12	515.12	0
601	2970.01	2970.01	0	145.7	145.7	0
602	4949.1	4949.1	0	386.35	386.35	0
603	4949.34	4949.34	0	386.51	386.51	0

G.   Output data for GP3
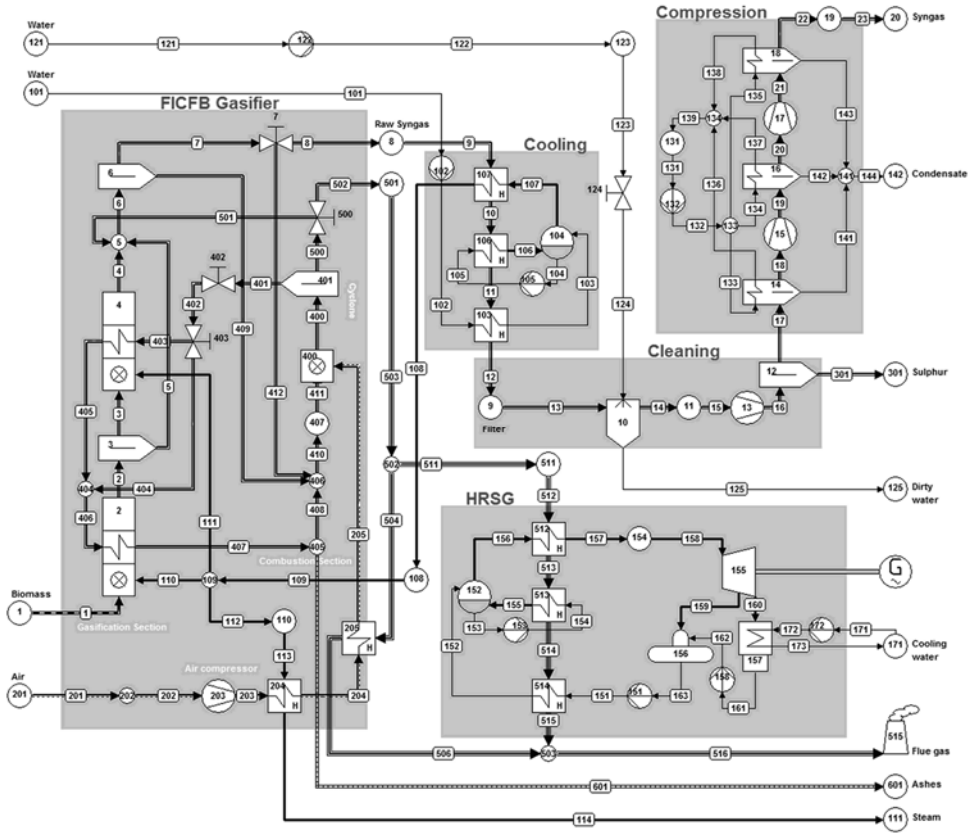
Figure G-1 flow sheet syngas plant (GP3)

Table G-1 system efficiencies syngas plant (GP3)

delivered	No.	Apparatus	Type	Energy	Totals	Exergy	Totals
				[kW]	[kW]	[kW]	[kW]
Absorbed	1	Sink/Source	10	48534.43		57553.4	
power					48534.43		57553.4
Delivered	1	Generator	G	1917.86		1917.86	
gross power					1917.86		1917.86
Aux. power consumption	15	Compressor	29	250.45		250.45	
	17	Compressor	29	292.1		292.1	
	13	Compressor	29	2139.93		2139.93	
	102	Pump	8	0.14		0.14	
	105	Pump	8	0.02		0.02	
	122	Pump	8	1.86		1.86	
	132	Pump	8	0.4		0.4	
	151	Pump	8	12.3		12.3	
	153	Pump	8	1.16		1.16	
	158	Pump	8	0.19		0.19	
	172	Pump	8	0.3		0.3	
	203	Compressor	29	237.63		237.63	
					2936.48		2936.48
Delivered net power					-1018.61		-1018.6
Efficiencies	gross			3.95%		3.33%	
	net			-2.10%		-1.77%	

Table G-2 data pipes syngas plant

Pipe	Medium	Mass flow	Pressure	Temp.	Enthalpy	Entropy	Exergy	Quality
no.		[kg/s]	[bar]	[°C]	[kJ/kg]	[kJ/kg.K]	[kJ/kg]	[%]
1	FUEL 1	4.12	1.47	15	-9080.73	2.1401	13969.27	
2	GASMIX 2	4.944	1.46	800	-7824.16	10.2259	11776.41	
3	GASMIX 3	3.499	1.45	800	-8383.68	10.5799	10637.73	
4	GASMIX 4	3.999	1.46	800	-7322.68	12.8898	10365.29	
5	GASMIX 5	1.445	1.46	800	-6470.17	8.8151	14697.31	
6	GASMIX 6	5.67	1.46	805.55	-6879.22	11.8559	11032.83	
7	GASMIX 7	5.299	1.46	805.55	-7438.85	12.5328	9371.4	
8	GASMIX 7	5.034	1.46	805.55	-7438.85	12.5328	9371.4	
9	GASMIX 7	5.034	1.46	805.55	-7438.85	12.5328	9371.4	
10	GASMIX 7	5.034	1.44	611.48	-7867.43	12.1013	9071.48	
11	GASMIX 7	5.034	1.42	130.95	-8818.88	10.5731	8575.68	
12	GASMIX 7	5.034	1.4	83.64	-8980.16	10.1423	8542.84	
13	GASMIX 7	5.034	1.35	82.75	-8980.16	10.1577	8538.23	
14	GASMIX 8	3.294	1.33	47.36	-6630.35	9.7065	12885.15	
15	GASMIX 8	3.294	1.33	47.36	-6630.35	9.7065	12885.15	
16	GASMIX 8	3.294	18.62	400.34	-5987.12	9.9076	13468.44	
17	GASMIX 9	3.29	18.52	400.34	-5994.87	9.9116	13484.38	
18	GASMIX 10	3.048	18.42	30	-6132.38	8.3029	14255.39	
19	GASMIX 10	3.048	29.47	78.88	-6051.03	8.3498	14322.77	
20	GASMIX 11	3.046	29.27	30	-6126.57	8.101	14326.05	
21	GASMIX 11	3.046	50.4	86.93	-6031.62	8.1546	14405.03	

Table G-2 data pipes syngas plant (cont.)

Pipe no.	Medium	Mass flow [kg/s]	Pressure [bar]	Temp. [°C]	Enthalpy [kJ/kg]	Entropy [kJ/kg.K]	Exergy [kJ/kg]	Quality [%]
22	GASMIX 12	3.044	50	30	-6122.48	7.8689	14402.62	
23	GASMIX 12	3.044	50	15	-6148.17	7.782	14402.84	
101	WATERSTM	2.131	1.013	15	63.08	0.2245	0.72	0
102	WATERSTM	2.131	1.5	15	63.14	0.2245	0.77	0
103	WATERSTM	2.131	1.48	105.95	444.24	1.3737	39.22	0
104	WATERSTM	8.603	1.48	110.95	465.38	1.4291	43.85	0
105	WATERSTM	8.603	1.5	110.95	465.38	1.4291	43.85	0
106	WATERSTM	8.603	1.48	110.95	1022.16	2.8787	168.44	25
107	WATERSTM	2.131	1.48	110.95	2692.5	7.2274	542.21	100
108	WATERSTM	2.131	1.46	600	3705.21	8.9248	1048.85	100
109	GASMIX 13	2.131	1.46	600	-12266.3	12.4367	1048.84	
110	GASMIX 13	0.824	1.46	600	-12266.3	12.4367	1048.84	
111	GASMIX 13	0.5	1.46	600	-12266.3	12.4367	1048.84	
112	GASMIX 13	0.806	1.46	600	-12266.3	12.4367	1048.84	
113	GASMIX 13	0.806	1.46	600	-12266.3	12.4367	1048.84	
114	GASMIX 13	0.806	1.44	115	-13269.97	10.7751	540.57	
121	GASMIX 13	30.206	1.013	15	-15908.43	3.7364	0.72	
122	GASMIX 13	30.206	1.5	15	-15908.37	3.7364	0.77	
123	GASMIX 13	30.206	1.5	15	-15908.37	3.7364	0.77	
124	GASMIX 13	30.206	1.5	15	-15908.37	3.7364	0.77	
125	GASMIX 13	31.947	1.33	47.36	-15773.09	4.1814	3.37	
131	WATERSTM	159.842	1.013	15	63.08	0.2245	0.72	0
132	WATERSTM	159.842	1.033	15	63.08	0.2245	0.72	0
133	WATERSTM	133.702	1.033	15	63.08	0.2245	0.72	0
134	WATERSTM	12.127	1.033	15	63.08	0.2245	0.72	0
135	WATERSTM	14.013	1.033	15	63.08	0.2245	0.72	0
136	WATERSTM	133.702	1.013	20	84.01	0.2965	0.18	0
137	WATERSTM	12.127	1.013	20	84.01	0.2965	0.18	0
138	WATERSTM	14.013	1.013	20	84.01	0.2965	0.18	0
139	WATERSTM	159.842	1.013	20	84.01	0.2965	0.18	0
141	GASMIX 13	0.242	18.42	30	-15844.09	3.9481	1.92	
142	GASMIX 13	0.002	29.27	30	-15843.1	3.9478	3.01	
143	GASMIX 13	0.002	50	30	-15841.21	3.9472	5.08	
144	GASMIX 13	0.246	18.42	30.01	-15844.06	3.9482	1.92	
151	WATERSTM	1.678	53.2	100.77	426.24	1.3116	39.76	0
152	WATERSTM	1.678	52.2	266.65	1177.99	2.9638	298.9	0.61
153	WATERSTM	6.673	52.2	266.65	1168.11	2.9455	294.47	0
154	WATERSTM	6.673	53.2	266.69	1168.28	2.9456	294.62	0
155	WATERSTM	6.673	52.2	266.65	1574.16	3.6977	476.25	25
156	WATERSTM	1.678	52.2	266.65	2792.33	5.9544	1021.58	100
157	WATERSTM	1.678	51.2	540	3526.35	7.0831	1419.08	100
158	WATERSTM	1.678	50	538.63	3524.35	7.0913	1414.66	100
159	WATERSTM	0.23	1.013	120.1	2716.69	7.4618	496.52	100
160	WATERSTM	1.449	0.03	24.08	2273.91	7.6649	-6.82	88.91
161	WATERSTM	1.449	0.03	13	54.6	0.1953	0.94	0
162	WATERSTM	1.449	1.013	13.01	54.74	0.1954	1.04	0

Table G-2 data pipes syngas plant (cont.)

Pipe	Medium	Mass flow	Pressure	Temp.	Enthalpy	Entropy	Exergy	Quality
no.		[kg/s]	[bar]	[°C]	[kJ/kg]	[kJ/kg.K]	[kJ/kg]	[%]
163	WATERSTM	1.678	1.013	99.97	418.99	1.3067	33.95	0
171	WATERSTM	109.67	1.013	12	50.51	0.1806	1.22	0
172	WATERSTM	109.67	1.033	12	50.51	0.1806	1.22	0
173	WATERSTM	109.67	1.013	19	79.83	0.2822	0.26	0
201	GASMIX 14	5.461	1.013	15	-98.85	6.8652	1.02	
202	GASMIX 14	5.461	1.013	15	-98.85	6.8652	1.02	
203	GASMIX 14	5.461	1.5	57.63	-55.77	6.8916	36.24	
204	GASMIX 14	5.461	1.48	202.88	92.43	7.2667	72.61	
205	GASMIX 14	5.461	1.46	400	299.72	7.6345	170.22	
301	GASMIX 15	0.004	18.52	400.34	363.4	6.4356	478.58	
400	GASMIX 16	24.396	1.46	1048.29	-10694.76	3.9535	877.46	
401	GASMIX 17	18.3	1.45	1048.29	-13711.2	2.5274	900.52	
402	GASMIX 17	18.3	1.45	1048.29	-13711.2	2.5274	900.52	
403	GASMIX 17	14.64	1.45	1048.29	-13711.2	2.5274	900.52	
404	GASMIX 17	3.66	1.45	1048.29	-13711.2	2.5274	900.52	
405	GASMIX 17	14.64	1.45	870.46	-14133.69	2.1857	579.92	
406	GASMIX 17	18.3	1.45	912.13	-14049.19	2.2583	642.79	
407	GASMIX 17	18.3	1.45	618.71	-14532.11	1.7953	297.9	
408	GASMIX 17	18.3	1.46	618.71	-14532.11	1.7953	297.9	
409	GASMIX 18	0.37	1.46	805.55	1126.3	2.1729	34799.51	
410	GASMIX 19	18.935	1.46	800	-13865.57	2.2183	1281.68	
411	GASMIX 19	18.935	1.46	800.08	-13865.44	2.2184	1281.78	
412	GASMIX 7	0.265	1.46	805.55	-7438.85	12.5328	9371.4	
500	GASMIX 20	6.096	1.46	1048.29	-1638.54	8.2351	808.23	
501	GASMIX 20	0.226	1.46	1048.29	-1638.54	8.2351	808.23	
502	GASMIX 20	5.87	1.46	1048.29	-1638.54	8.2351	808.23	
503	GASMIX 20	5.87	1.46	1048.29	-1638.54	8.2351	808.23	
504	GASMIX 20	1.141	1.46	1048.29	-1638.54	8.2351	808.23	
506	GASMIX 20	1.141	1.44	212.88	-2630.89	7.0689	163.59	
511	GASMIX 20	4.73	1.46	1048.29	-1638.54	8.2351	808.23	
512	GASMIX 20	4.73	1.46	1048.29	-1638.54	8.2351	808.23	
513	GASMIX 20	4.73	1.44	842.06	-1899.04	8.0246	610.48	
514	GASMIX 20	4.73	1.42	358.69	-2471.7	7.3589	236.32	
515	GASMIX 20	4.73	1.4	110.77	-2738.48	6.8282	127.75	
516	GASMIX 20	5.87	1.4	130.84	-2717.57	6.8813	132.83	
601	GASMIX 17	0	1.46	618.71	-14532.11	1.7953	297.9	

Table G-3 composition of fluids in the syngas plant

Composition number	1	2	3	4	5	6	7	8	9
C(S)	0.3855	0.2601	0.3168	0.1199		0.0987			
H2	0.2758	0.0118	0.0143	0.2577		0.212	0.2353	0.3682	0.3685
H2O	0.2163	0.5293	0.6446	0.45		0.3719	0.4126	0.0806	0.0806
N2	0.0026	0.0031	0.0037	0.0032		0.02	0.0222	0.0347	0.0347
O2	0.1198					0.0004	0.0005	0.0007	
AR						0.0002	0.0002	0.0004	0.0004
CO2		0.0901		0.0411	0.5038	0.1154	0.128	0.2004	0.2005
SIO2(S)									
CH4		0.1056	0.0206	0	0.4962	0.0762	0.0845	0.1323	0.1323
H2S									
SO2									
CO		0	0	0.1279		0.1053	0.1168	0.1828	0.1829
Avg.molemass [kg/kmol]	12.99	18.43	15.88	15.55	30.13	18.14	18.81	19.26	19.25
LHV [kJ/mol]	153.02	189.95	144.62	145.72	398.03	180.98	157.71	246.84	247.01
HHV [kJ/mol]	174.67	199.76	147.06	157.05	441.67	197.01	175.49	274.66	274.86

Table G-3 composition of fluids in the syngas plant (cont.)

Composition number	10	11	12	13	14	15	16	17	18	19	20
C(S)							0		1	0.0882	0
H2	0.3999	0.4002	0.4005							0.0095	
H2O	0.0023	0.0015	0.0008	1	0.0101		0.0265			0.0166	0.0668
N2	0.0377	0.0377	0.0377		0.7729		0.29			0.0009	0.7298
O2				0.2075	1	0.0071				0	0.0178
AR	0.0004	0.0004	0.0004		0.0092		0.0035			0	0.0087
CO2	0.2176	0.2178	0.2179		0.0003		0.0703			0.0052	0.177
SIO2(S)							0.6026	1		0.8715	
CH4	0.1436	0.1437	0.1438							0.0034	
CO											
H2S											
HCL	0.1985	0.1987	0.1988				0			0.0047	0
SO2	19.36	19.36	19.36	18.02	28.85	32	48.27	60.08	12.01	54.18	30.35
HF	268.11	268.33	268.48	0	0	0	0	0	393.46	41.08	0
Avg.molemass [kg/kmol]	298.34	298.57	298.74	0	0	0	0	0	393.46	41.8	0
LHV [kJ/mol]											
HHV [kJ/mol]											

Table G-4 energy and flows in the syngas plant

Pipe	Total Energy flow	Therm.Mec. Energy flow	Chemical energy	Total Exergy flow	Therm.Mec. Exergy flow	Chemical exergy
no.	[kW]	[kW]	[kW]	[kW]	[kW]	[kW]
1	55480.88	80.59	55400.29	57553.4	181.8	57371.6
2	67224.98	13637.79	53587.19	58222.56	4959.28	53263.28
3	44095.62	11697.49	32398.13	37216.45	4081.52	33134.93
4	52026.34	11638.46	40387.88	41448.95	4191.67	37257.29
5	23128.99	1939.93	21189.06	21244.47	1083.85	20160.62
6	75445.11	13868.17	61576.94	62554.39	5359.42	57194.97
7	62847.48	13407.19	49440.29	49662.68	5129.95	44532.73

Table G-4 energy and flows in the syngas plant (cont.)

Pipe	Total Energy flow	Therm.Mec. Energy flow	Chemical energy	Total Exergy flow	Therm.Mec. Exergy flow	Chemical exergy
no.	[kW]	[kW]	[kW]	[kW]	[kW]	[kW]
8	59705.11	12736.84	46968.28	47179.54	4873.45	42306.09
9	59705.11	12736.84	46968.28	47179.54	4873.45	42306.09
10	57547.48	10579.21	46968.28	45669.63	3363.54	42306.09
11	52757.49	5789.21	46968.28	43173.53	867.44	42306.09
12	51945.55	4977.27	46968.28	43008.21	702.12	42306.09
13	51945.55	4977.27	46968.28	42984.99	678.9	42306.09
14	47696.39	727.91	46968.48	42437.76	131.49	42306.27
15	47696.39	727.91	46968.48	42437.76	131.49	42306.27
16	49814.92	2846.44	46968.48	44358.87	2052.6	42306.27
17	49813.45	2844.98	46968.47	44357.21	2048.91	42308.31
18	47009.43	40.95	46968.48	43449.53	1131.2	42318.34
19	47257.38	288.89	46968.48	43654.89	1336.56	42318.34
20	47003.48	35	46968.48	43630.12	1310.9	42319.22
21	47292.66	324.18	46968.48	43870.65	1551.43	42319.22
22	46999.3	30.82	46968.48	43838.75	1518.91	42319.84
23	47015.84	47.36	46968.48	43839.42	1519.58	42319.84
101	89.16	89.16	0	1.53	1.53	0
102	89.03	89.03	0	1.63	1.63	0
103	722.91	722.91	0	83.57	83.57	0
104	3100.96	3100.96	0	377.21	377.21	0
105	3100.98	3100.98	0	377.23	377.23	0
106	7891.01	7891.01	0	1449.07	1449.07	0
107	5512.96	5512.96	0	1155.2	1155.2	0
108	7670.59	7670.59	0	2234.63	2234.63	0
109	7670.57	7670.57	0	2234.61	2234.61	0
110	2966.63	2966.63	0	864.25	864.25	0
111	1801.18	1801.18	0	524.73	524.73	0
112	2902.76	2902.76	0	845.64	845.64	0
113	2902.76	2902.76	0	845.64	845.64	0
114	2093.54	2093.54	0	435.84	435.84	0
121	1264.15	1264.15	0	21.69	21.69	0
122	1262.31	1262.31	0	23.15	23.15	0
123	1262.31	1262.31	0	23.15	23.15	0
124	1262.31	1262.31	0	23.15	23.15	0
125	2986.74	2986.74	0	107.68	107.68	0
131	6689.42	6689.42	0	114.79	114.79	0
132	6689.02	6689.02	0	115.11	115.11	0
133	5595.12	5595.12	0	96.28	96.28	0
134	507.49	507.49	0	8.73	8.73	0
135	586.42	586.42	0	10.09	10.09	0
136	2796.54	2796.54	0	23.72	23.72	0
137	253.65	253.65	0	2.15	2.15	0
138	293.1	293.1	0	2.49	2.49	0
139	3343.29	3343.29	0	28.35	28.35	0
141	5.43	5.43	0	0.46	0.46	0

Table G-4 energy and flows in the syngas plant (cont.)

Pipe	Total Energy flow	Therm.Mec. Energy flow	Chemical energy	Total Exergy flow	Therm.Mec. Exergy flow	Chemical exergy
no.	[kW]	[kW]	[kW]	[kW]	[kW]	[kW]
142	0.06	0.06	0	0.01	0.01	0
143	0.04	0.04	0	0.01	0.01	0
144	5.53	5.53	0	0.47	0.47	0
151	539.32	539.32	0	66.73	66.73	0
152	1801.13	1801.13	0	501.7	501.7	0
153	7094.65	7094.65	0	1965.02	1965.02	0
154	7095.8	7095.8	0	1966.01	1966.01	0
155	9804.28	9804.28	0	3178.03	3178.03	0
156	4510.77	4510.77	0	1714.71	1714.71	0
157	5742.82	5742.82	0	2381.91	2381.91	0
158	5739.47	5739.47	0	2374.49	2374.49	0
159	599.87	599.87	0	114.04	114.04	0
160	3142.44	3142.44	0	-9.89	-9.89	0
161	72.91	72.91	0	1.36	1.36	0
162	72.72	72.72	0	1.5	1.5	0
163	527.15	527.15	0	56.99	56.99	0
171	5968.51	5968.51	0	134.09	134.09	0
172	5968.22	5968.22	0	134.3	134.3	0
173	2752.86	2752.86	0	28.08	28.08	0
201	28.94	28.94	0	5.59	0.95	4.65
202	28.94	28.94	0	5.59	0.95	4.65
203	264.19	264.19	0	197.88	193.23	4.65
204	1073.4	1073.4	0	396.47	391.83	4.65
205	2205.31	2205.31	0	929.5	924.85	4.65
301	1.46	1.46	0	1.92	1.43	0.5
400	34648.87	34648.75	0.11	21406.56	20879.2	527.35
401	26503.07	26503.07	0	16479.59	16479.59	0
402	26503.07	26503.07	0	16479.59	16479.59	0
403	21202.46	21202.46	0	13183.67	13183.67	0
404	5300.61	5300.61	0	3295.92	3295.92	0
405	15017.26	15017.26	0	8490.02	8490.02	0
406	20317.88	20317.88	0	11762.97	11762.97	0
407	11480.45	11480.45	0	5451.52	5451.52	0
408	11480.47	11480.47	0	5451.53	5451.53	0
409	12553.74	417.16	12136.59	12891.65	229.47	12662.18
410	32353.78	17745.18	14608.6	24269.16	9390.62	14878.55
411	32356.4	17747.8	14608.6	24271.06	9392.51	14878.55
412	3142.37	670.36	2472.01	2483.13	256.5	2226.64
500	7831.95	7831.84	0.11	4926.94	4382.18	544.76
501	289.78	289.78	0	182.3	162.14	20.16
502	7542.17	7542.06	0.11	4744.64	4220.03	524.61
503	7542.18	7542.07	0.11	4744.65	4220.04	524.61
504	1465.62	1465.6	0.02	921.99	820.05	101.94
506	333.6	333.57	0.02	186.62	84.68	101.94
511	6076.57	6076.48	0.09	3822.66	3399.99	422.66

Table G-4 energy and flows in the syngas plant (cont.)

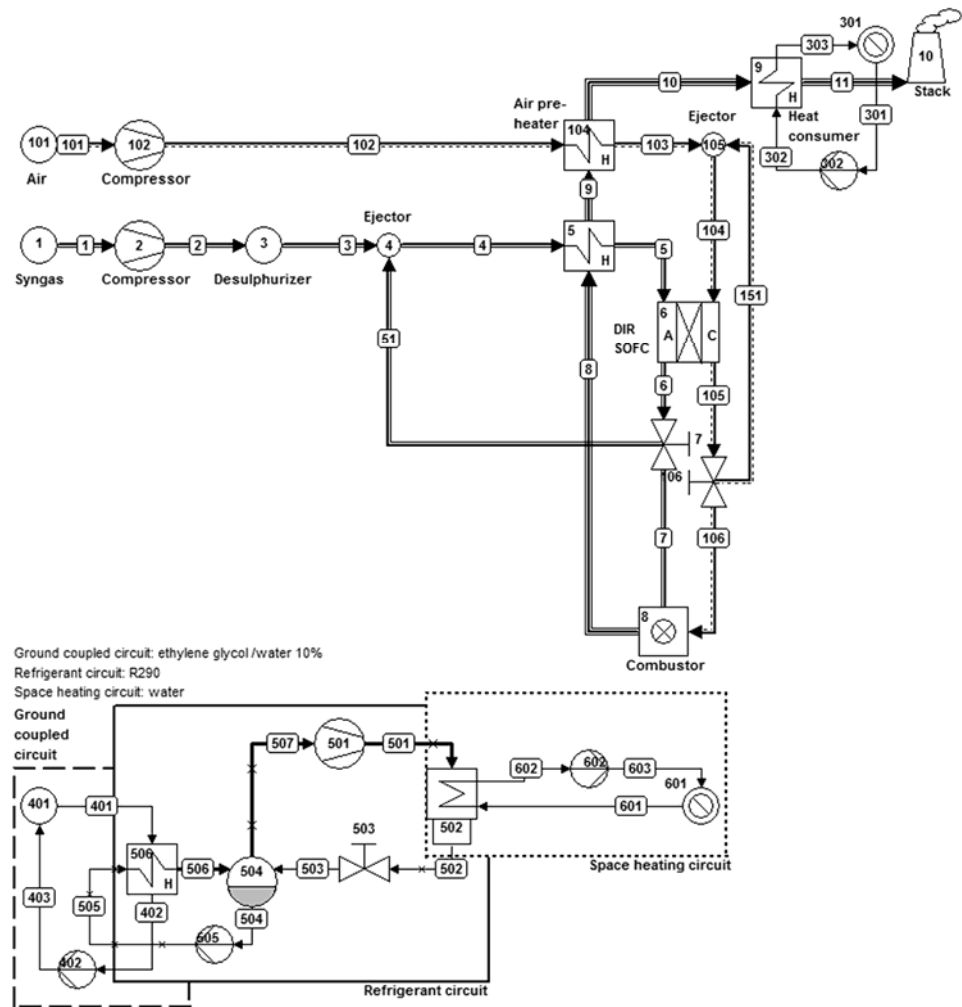| Pipe	Total Energy flow	Therm.Mec. Energy flow	Chemical energy	Total Exergy flow	Therm.Mec. Exergy flow	Chemical exergy
no.	[kW]	[kW]	[kW]	[kW]	[kW]	[kW]
512	6076.57	6076.48	0.09	3822.66	3399.99	422.66
513	4844.51	4844.42	0.09	2887.38	2464.72	422.66
514	2136.02	2135.94	0.09	1117.7	695.04	422.66
515	874.22	874.13	0.09	604.2	181.54	422.66
516	1207.81	1207.7	0.11	779.76	255.15	524.61
601	-0.03	-0.03	0	-0.01	-0.01	0

Figure G-2 flow sheet syngas fuelled micro-CHP

Table G-5 efficiencies of the syngas fuelled micro-CHP

	No.	Apparatus	Type	Energy	Totals	Exergy	Totals
				[kW]	[kW]	[kW]	[kW]
Absorbed	1	Sink/Source	10	3208.67		3229.2	
power					3208.67		3229.18
Delivered	6	Fuel Cell	21	1622		1622	
gross power					1622		1622
Aux. power	102	Compressor	29	98.3		98.3	
consumption	302	Pump	8	0.19		0.19	
	402	Pump	8	2.22		2.22	
	501	Compressor	29	502.73		502.73	
	505	Pump	8	0.14		0.14	
	2	Compressor	29	17.69		17.69	
	602	Pump	8	0.32		0.32	
					621.59		621.59
Delivered							
net power					1000.41		1000.41
Delivered	301	Heat Sink	10	1415.71		172.19	
heat	601	Heat Sink	10	1585.02		192.84	
					3000.73		365.03
Total							
delivered					4001.14		1365.44
Efficiencies	gross			50.55%		50.23%	
	net			31.18%		30.98%	
	heat			93.52%		11.30%	
	total			124.70%		42.28%	

Table G-6 data pipes syngas fuelled micro-CHP

Pipe	Medium	Mass flow	Pressure	Temp.	Enthalpy	Entropy	Exergy	Quality
no.		[kg/s]	[bar]	[°C]	[kJ/kg]	[kJ/kg.K]	[kJ/kg]	[%]
1	GASMIX 1	0.231	1.013	15	-6144.67	9.4583	13962.08	
2	GASMIX 1	0.231	1.423	54.27	-6080.04	9.5227	14008.16	
3	GASMIX 1	0.231	1.323	54.27	-6080.04	9.554	13999.15	
4	GASMIX 2	0.884	1.233	615.06	-7984.59	9.5142	4881.15	
5	GASMIX 2	0.884	1.183	750	-7750.73	9.7728	5040.49	
6	GASMIX 3	1.089	1.143	850	-8658.99	9.0922	1769.86	
7	GASMIX 3	0.435	1.143	850	-8658.99	9.0922	1769.86	
8	GASMIX 4	3.726	1.123	922.94	-301.95	8.5188	608.77	
9	GASMIX 4	3.726	1.093	878.07	-357.45	8.4793	564.64	
10	GASMIX 4	3.726	1.053	402.88	-918.91	7.8638	180.55	
11	GASMIX 4	3.726	1.013	50	-1298.76	7.084	25.38	
51	GASMIX 3	0.653	1.143	850	-8658.99	9.0922	1769.86	
101	GASMIX 5	3.495	1.013	15	-98.85	6.8652	0.13	
102	GASMIX 5	3.495	1.263	40.63	-72.96	6.8877	19.53	
103	GASMIX 5	3.495	1.203	605.55	525.64	7.9828	302.58	
104	GASMIX 6	8.432	1.203	750	688.49	8.1612	418.1	
105	GASMIX 7	8.228	1.143	850	803.79	8.2875	499.91	
106	GASMIX 7	3.291	1.143	850	803.79	8.2875	499.91	
151	GASMIX 7	4.937	1.143	850	803.79	8.2875	499.91	

Table G-6 data pipes syngas fuelled micro-CHP (cont.)

Pipe no.	Medium	Mass flow [kg/s]	Pressure [bar]	Temp. [°C]	Enthalpy [kJ/kg]	Entropy [kJ/kg.K]	Exergy [kJ/kg]	Quality [%]
301	WATERSTM	16.929	1.013	45	188.51	0.6386	6.11	0
302	WATERSTM	16.929	1.053	45	188.52	0.6386	6.11	0
303	WATERSTM	16.929	1.013	65	272.14	0.8935	16.28	0
401	E G/H2O	228.311	1.033	8	32.49	0.1172	0.36	
402	E G/H2O	228.311	1.013	6.8	27.62	0.0999	0.48	
403	E G/H2O	228.311	1.053	6.8	27.62	0.0999	0.49	
501	R290	5.073	24	79.72	38.31	-0.4167	158.95	100
502	R290	5.073	23.48	55	-274.09	-1.338	112.01	0
503	R290	5.073	4.8	0.39	-274.09	-1.2721	93.03	42.07
504	R290	2.906	4.8	0.39	-433.42	-1.8546	101.54	0
505	R290	2.906	4.896	0.41	-433.39	-1.8545	101.55	0
506	R290	2.906	4.8	3	-50.37	-0.4543	81.11	100
507	R290	5.073	4.8	0.39	-54.67	-0.47	81.31	100
601	WATERSTM	18.954	1.5	45	188.56	0.6386	6.16	0
602	WATERSTM	18.954	1.47	65	272.17	0.8935	16.32	0
603	WATERSTM	18.954	1.53	65	272.19	0.8935	16.33	0

Table G-7 composition of fluids of the syngas fuelled micro-CHP

Composition number	1	2	3	4	5	6	7
AR	0.0004	0.0003	0.0003	0.0086	0.0092	0.0095	0.0097
CH4	0.1439	0.0491	0				
CO	0.1989	0.0913	0.0356				
CO2	0.218	0.3378	0.3998	0.052	0.0003	0.0003	0.0003
H2	0.4006	0.1678	0.0473				
H2O	0.0005	0.3215	0.4876	0.073	0.0101	0.0104	0.0107
N2	0.0377	0.0321	0.0293	0.7265	0.7729	0.7981	0.8159
O2				0.1399	0.2075	0.1816	0.1634
H2S							
HCL							
C(S)		0	0	0			
SO2							
Avg.molemass [kg/kmol]	19.36	25.26	28.31	28.78	28.85	28.75	28.68
LHV [kJ/mol]	268.59	105.83	21.53	0	0	0	0
HHV [kJ/mol]	298.87	117.53	23.61	0	0	0	0

Table G-8 energy and exergy flows of the syngas fuelled micro-CHP

Pipe no.	Total Energy flow [kW]	Therm.Mec. Energy flow [kW]	Chemical energy [kW]	Total Exergy flow [kW]	Therm.Mec. Exergy flow [kW]	Chemical exergy [kW]
1	3570.64	0.27	3570.37	3229.18	0	3229.18
2	3585.59	15.21	3570.37	3239.83	10.66	3229.18
3	3585.59	15.21	3570.37	3237.75	8.57	3229.18
4	5424.91	1309.77	4115.14	4317.1	457.05	3860.05
5	5631.75	1516.61	4115.14	4458.02	597.97	3860.05
6	3065.31	2157.36	907.94	1926.67	855.18	1071.49

Table G-8 energy and exergy flows of the syngas fuelled micro-CHP (cont.)

Pipe	Total Energy flow	Therm.Mec. Energy flow	Chemical energy	Total Exergy flow	Therm.Mec. Exergy flow	Chemical exergy
no.	[kW]	[kW]	[kW]	[kW]	[kW]	[kW]
7	1226.12	862.95	363.18	770.67	342.07	428.6
8	4269.62	4269.57	0.05	2268.56	2197.83	70.73
9	4062.78	4062.73	0.05	2104.11	2033.38	70.73
10	1970.55	1970.5	0.05	672.81	602.08	70.73
11	555.04	554.99	0.05	94.58	23.84	70.73
51	1839.19	1294.42	544.77	1156	513.11	642.89
101	54.34	54.34	0	0.45	0	0.45
102	144.82	144.82	0	68.25	67.8	0.45
103	2237.05	2237.05	0	1057.56	1057.11	0.45
104	6801.92	6801.92	0	3525.32	3522.89	2.43
105	7608.1	7608.1	0	4113	4107.86	5.14
106	3043.24	3043.24	0	1645.2	1643.14	2.06
151	4564.86	4564.86	0	2467.8	2464.71	3.09
301	2123.44	2123.44	0	103.38	103.38	0
302	2123.55	2123.55	0	103.45	103.45	0
303	3539.14	3539.14	0	275.57	275.57	0
401	6491.52	6491.52	0	81.11	81.11	0
402	7604.57	7604.57	0	110.29	110.29	0
403	7603.09	7603.09	0	111.01	111.01	0
501	291.81	291.81	0	806.34	806.34	0
502	1293.02	1293.02	0	568.24	568.24	0
503	1293.02	1293.02	0	471.94	471.94	0
504	1203.67	1203.67	0	295.06	295.06	0
505	1203.59	1203.59	0	295.11	295.11	0
506	90.54	90.54	0	235.69	235.69	0
507	179.88	179.88	0	412.5	412.5	0
601	2378.35	2378.35	0	116.67	116.67	0
602	3963.18	3963.18	0	309.38	309.38	0
603	3963.38	3963.38	0	309.51	309.51	0

Nomenclature

A	Slope Tafel line [V]	LHV	Lower Heating value [kJ kg^{-1}]
B	Constant in mass transfer overvoltage equation [V]	Ex	Exergy [W]
P	Power [W]	Q	Heat [W]
p	Pressure [bar]	V	Voltage [V]
h	Enthalpy [kJ mol^{-1}]	T	Temperature [°C]
I	Current [A]	S/F	Steam to fuel ratio [kg kg^{-1}]
i	Current density [A m^{-2}]	PR	Pressure ratio [-]
M	Molecular mass [kg kmole^{-1}]	WFOT	Weight factor old temperature
y	Mole fration [-]	CRATIO	Circulation ratio
R	Ideal gas constant [8.3145 J mole^{-1} K^{-1}]	DCAC	Conversion efficiency of direct current (DC) to alternating current (AC) [%]
R_x	Area specific Resistance [Ω m^2]	U	Utilization [%]
F	Faraday's constant [96485 C mole^{-1}]	RELHUM	Relative humidity

Greek

ϕ	Flow	Δ	Difference
η	Efficiency		

Superscripts

0	At standard temperature (25°C) and pressure (1 atm)

Subscripts

0	Exchange	FC	Fuel Cell
an	Anode	f	Fuel
biomass	Biomass	fuel	Fuel
c	critical	gas	Gas
C	At cold side (of a heat exchanger)	H	At hot side (of a heat exchanger)
cat	Cathode	heat	Heat
e	Electric	i	Isentropic
el	Electric	in	Input
eq	Equivalent	l	limiting
ex	Exergetic	m	Mass
n	Internal & fuel crossover	r	Reaction
ohm	Ohmic	rev	Reversible
out	Output	th	Thermal
pinch	At pinch point	tot	Total
product	Product	W	Water

Abbreviations

AFC	Alkaline Fuel Cell	GDC	Gadolinium Doped Ceria
BFB	Bubling Fluidized Bed	GT	Gas Turbine
CFB	Circulating Fluidized Bed	HHV	Higher Heating Value
COP	Coefficient of Performance	HR	Heat Recovery
daf	dry ash free	HRSG	Heat Recovery Steam Generator
DIR	Direct Internal Reforming	HT	High Temperature
DMFC	Direct Methanol Fuel Cell	HTGC	High Temperature Gas Cleaning
Eff.	Efficiency	HTU	Hydro Thermal Upgrading
ESP	Electrostatic Precipitator	HX	Heat exchanger
FC	Fuel Cell	IGCC	Integrated Gasification Combined Cycle
FICFB	Fast Internal Circulating Fluidized Bed	IGT	Institute of Gas Technology
LHV	Lower Heating Value	PSA	Pressure Swing Adsorption
LMS	Strontium doped Lanthanum Manganite	PSI	Photo System 1
LSF	Lanthanum Ferrite doped with Strontium	PSII	Photo System 2
LT	Low Temperature	PTFE	Polytetrafluoroethylene
LTGC	Low Temperature Gas Cleaning	RDF	Refuse Derived Fuel
MCFC	Molten Carbonate Fuel Cell	RME	Rapeseed Methyl Ester
μ-CHP	Micro Combined Heat and Power	SCWG	Super Critical Water Gasification
MEA	Membrane Electrode Assembly	SDC	Scandium Doped Zirconia
NETL	National Energy Technology Laboratory	SEP	Standard Electrode Potential
PAFC	Phosphoric Acid Fuel Cell	SNG	Synthetic Natural Gas
PBI	Poly Benzimidazole	SOFC	Solid Oxide Fuel Cell
PEDOT	Poly(3,4-ethylenedioxythiophene)	T&D	Transport and Distribution
PEEK	Polyetheretherketones	TSA	Temperature Swing Adsorption
PEM-FC	Proton Exchange Membrane Fuel Cell	U.S.	United States
PFSA	Perfluorosulfonic Acid	VOC	Volatile Organic Compounds
ppm	part per million	WGS	Water Gas Shift
PPO	Polyphenylene Oxide	wt	weight
PPS	Polyphenylene Sulphide	YSZ	Yttria Stabilized Zirconia
PR	Pressure Ratio		

Acknowledgements

Curriculum Vitae

Richard Toonssen was born on 28 March 1978 in The Hague, the Netherlands. He obtained a Bachelor of Science degree in chemical and bio-chemical engineering and a master degree in chemical engineering from Delft University of Technology (TU-Delft) in the Netherlands.

In 2006, he finished his MSc thesis that dealt with the introduction of an organic hydrogen carrier directly into a proton exchange membrane fuel cell.

After finishing his master study in 2006, he commenced his doctoral research at the Energy Technology section of the faculty of Mechanical, Marine and Materials Engineering (3mE) of the TU-Delft. The PhD study focused on system studies of energy conversion systems based on biomass gasification and fuel cells. During this period, he coached several MSc-students and performed some thermodynamic calculations for some compagnies. Most of the results of this doctoral research has been published in various high ranking journals and presented at several conferences.

Publications

1. Toonssen R., Hydrogen production plant based on commercial biomass gasification systems, TU Delft, Technical report, ET-2248, 2007.
2. Toonssen R., Woudstra N., Verkooijen A. H. M., Reference System for a Power Plant Base don Biomass Gasification and SOFC. In: 8th European Solid Oxide Fuel Cell Forum, Luzerne, Switserland, 2008.
3. Toonssen R., Woudstra N., Verkooijen A. H. M., Exergy Analysis of Hydrogen Production Plants Based on Biomass Gasification. Int J Hydrogen Energy 2008; 33(15): 4074-4082.
4. Toonssen R., Woudstra N., Verkooijen A. H. M., Decentralized Generation of Electricity from Biomass with Proton Exchange Membrane Fuel Cell. J Power Sources 2009; 194(1): 456-466.
5. Toonssen R., Woudstra N., Bepaling E-derving bij afname van stoom voor warmtelevering in de nieuw te bouwen stoomturbinecentrale bij AVR Brielselaan te Rotterdam, TU Delft, Technical report, ET-2264, 2009.
6. Toonssen R., Aravind P. V., Smit G., Woudstra N., Verkooijen A. H. M., System Study on Hydrothermal Gasification Combined with a Hybrid Solid Oxide Fuel Cell Gas Turbine, Fuel Cells 2010, doi: 10.1002/fuce.200900188.
7. Toonssen R., Woudstra N., Verkooijen A. H. M., Decentralized Generation of Electricity with Solid Oxide Fuel Cells from Centrally Converted Biomass, Int J Hydrogen Energy 2010, doi: 10.1016/j.ijhydene.2010.05.006.